Vol. 64 April, 1960 No. 4

THE JOURNAL OF PHYSICAL CHEMISTRY

(Registered in U. S. Patent Office)

CONTENTS

NOTES

COMMUNICATION TO THE EDITOR

THE JOURNAL OF PHYSICAL CHEMISTRY

(Registered in U. S. Patent Office)

Published monthly by the American Chemical Society at 20th and Northampton Sts., Easton, Pa.

Second-class mail privileges authorized at Easton, Pa. This publication is authorized to be mailed at the special rates of postage prescribed by Section 131.122.

The *Journal of Physical Chemistry* is devoted to the publication of selected symposia in the broad field of physical chemistry and to other contributed papers.

Manuscripts originating in the British Isles, Europe and Africa should be sent to F. C. Tompkins, The Faraday Society, 6 Gray's Inn Square, London W. C. 1, England.

Manuscripts originating elsewhere should be sent to W. Albert Noyes, Jr., Department of Chemistry, University of Rochester, Rochester 20, N. Y.

Correspondence regarding accepted papers, proofs and reprints should be directed to Assistant Editor, Allen D. Bliss, Department of Chemistry, Simmons College, 300 The Fenway, Boston 15, Mass.

Business Office: Alden H. Emery, Executive Secretary, American Chemical Society, 1155 Sixteenth St., N. W., Washington 6, D. C.

Advertising Office: Reinhold Publishing Corporation, 430 Park Avenue, New York 22, N. Y.

Articles must be submitted in duplicate, typed and double spaced. They should have at the beginning a brief Abstract, in no case exceeding 300 words. Original drawings should accompany the manuscript. Lettering at the sides of graphs (black on white or blue) may be pencilled in and will be typeset. Figures and tables should be held to a minimum consistent with adequate presentation of information. Photographs will not be printed on glossy paper except by special arrangement. All footnotes and references to the literature should be numbered consecutively and placed in the manuscript at the proper places. Initials of authors referred to in citations should be given. Nomenclature should conform to that used in *Chemical Abstracts*, mathematical characters be marked for italic, Greek letters carefully made or annotated, and subscripts and superscripts clearly shown. Articles should be written as briefly as possible consistent with clarity and should avoid historical background unnecessary for specialists.

Notes describe fragmentary or incomplete studies but do not otherwise differ fundamentally from articles and are subjected to the same editorial appraisal as are articles. In their preparation particular attention should be paid to brevity and conciseness. Material included in Notes must be definitive and may not be republished subsequently.

Communications to the Editor are designed to afford prompt preliminary publication of observations or discoveries whose value to science is so great that immediate publication is imperative. The appearance of related work from other laboratories is in itself not considered sufficient justification for the publication of a Communication, which must in addition meet special requirements of timeliness and significance. Their total length may in no case exceed 500 words or their equivalent. They differ from Articles and Notes in that their subject matter may be republished.

Symposium papers should be sent in all cases to Secretaries of Divisions sponsoring the symposium, who will be responsible for their transmittal to the Editor. The Secretary of the Division by agreement with the Editor will specify a time after which symposium papers cannot be accepted. The Editor reserves the right to refuse to publish symposium articles, for valid scientific reasons. Each symposium paper may not exceed four printed pages (about sixteen double spaced typewritten pages) in length except by prior arrangement with the Editor.

Remittances and orders for subscriptions and for single copies, notices of changes of address and new professional connections, and claims for missing numbers should be sent to the American Chemical Society, 1155 Sixteenth St., N. W., Washington 6, D. C. Changes of address for the *Journal of Physical Chemistry* must be received on or before the 30th of the preceding month.

Claims for missing numbers will not be allowed (1) if received more than sixty days from date of issue (because of delivery hazards, no claims can be honored from subscribers in Central Europe, Asia, or Pacific Islands other than Hawaii), (2) if loss was due to failure of notice of change of address to be received before the date specified in the preceding paragraph, or (3) if the reason for the claim is "missing from files."

Subscription Rates (1960): members of American Chemical Society, $12.00 for 1 year; to non-members, $24.00 for 1 year. Postage to countries in the Pan-American Union, $0.80; Canada, $0.40; all other countries, $1.20. Single copies, current volume, $2.50; foreign postage, $0.15; Canadian postage, $0.05; Pan-American Union, $0.05. Back volumes (Vol. 56–59) $25.00 per volume; (starting with Vol. 60) $30.00 per volume; foreign postage per volume $1.20, Canadian, $0.15; Pan-American Union, $0.25. Single copies: back issues, $3.00; for current year, $2.50; postage, single copies: foreign, $0.15; Canadian, $0.05; Pan-American Union, $0.05.

The American Chemical Society also publishes *Journal of the American Chemical Society, Chemical Abstracts, Industrial and Engineering Chemistry*, International Edition of *Industrial and Engineering Chemistry, Chemical and Engineering News, Analytical Chemistry, Journal of Agricultural and Food Chemistry, Journal of Organic Chemistry, Journal of Chemical and Engineering Data* and *Chemical Reviews*. Rates on request.

THE JOURNAL OF PHYSICAL CHEMISTRY

(Registered in U. S. Patent Office)

VOLUME 64 APRIL 22, 1960 NUMBER 4

A DIELECTRIC STUDY OF THE CARBOXYLIC ACID DIMER

BY GRAHAM LOVELUCK[1]

The Edward Davies Chemical Laboratories, University College of Wales, Aberystwyth

Received March 16, 1959

The dielectric constants and loss tangents of pure *n*-caproic acid and of its solutions in xylene and those of cyclohexanecarboxylic acid in tetrachloroethylene have been measured at frequencies up to 10^8 c./sec. The data have been examined in terms of the self-ionization mechanism of Harris and Alder but it is concluded that association beyond the dimer is the more likely basis for the dielectric facts. The latter indicate that the dimer has a small effective dipole moment.

The purpose of this brief account is to assess two particularly interesting aspects of the dipole character of the carboxylic acids.

The well-known dimer of the carboxylic acids is commonly represented as a centro-symmetric structure which, if rigid, would have zero dipole moment. In benzene solutions[2] apparent moments for the dimer of approximately 1.1 *D* have been evaluated on the basis of an atomic polarization term assumed to be the usual small fraction (10–15%) of the electronic polarization. LeFèvre has explicitly characterized this dipole moment as "subject to limitation by the intervention of solvent and atomic polarization effects to unknown extents." Dielectric absorption measurements which we have made allow an estimate of the dipole moment which is independent of the atomic polarization term.

A model of special character has been advanced by Harris and Alder[3] to explain the dielectric constants of the pure carboxylic acids. These dielectric constants are larger than can be accounted for on the basis of the symmetric dimer and they show a significant increase with rising temperature. Harris and Alder advance the formation of a "zwitterionic" structure to account for these facts.

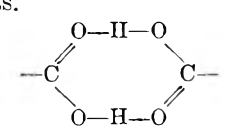

I

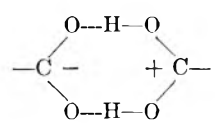

II

The primary aim of this study was to seek evidence for this process.

Results

The dielectric constants and loss factors for two acids, *n*-caproic and cyclohexanecarboxylic, were studied in solution between 10^5 and 10^8 c./sec.: the caproic acid was also measured as the pure liquid. The dielectric relaxation times were evaluated from the generalized Debye relations of Davidson and Cole[4]

$$\epsilon^* = \epsilon_\infty + \frac{\epsilon_0 - \epsilon_\infty}{(1 + j\omega\tau)\beta} \quad (1)$$

$$\epsilon'' = \beta\tau(\epsilon_0 - \epsilon_\infty)\omega \quad (2)$$

ϵ^* is the complex permittivity; ϵ'' the loss factor; ϵ_0 and ϵ_∞ the real components at zero and infinite frequency; ω the angular frequency; τ a mean relaxation time and β an empirical distribution factor which, for a simple Debye relaxation, is unity. Equation 2 is valid only at frequencies far removed from the critical value (*i.e.*, from maximum values of ϵ''). In the first instance it allows of the evaluation of $\beta\tau$, but as Sharbough, Eckstrom and Kraus showed,[5] a plot of log ϵ'' against log (frequency) gives a measure of β in these circumstances. Denney found[6] that data over a limited low frequency region when so treated gave reliable β-values and allowed τ to be determined within 5% of the best value deduced from a complete frequency coverage. The carboxylic acid data all gave $\beta = 1.00 \pm 5\%$.

(1) Metcalf Research Laboratories, Brown University, Providence, R. I.

(2) H. A. Pohl, M. E. Hobbs and P. M. Gross, *J. Chem. Phys.*, **9**, 408 (1941). R. J. W. Le Fèvre and H. Vine, *J. Chem. Soc.*, 1795 (1938).

(3) F. E. Harris and B. J. Alder, *Trans. Faraday Soc.*, **50**, 13 (1954).

(4) D. W. Davidson and R. H. Cole, *J. Chem. Phys.*, **19**, 1484 (1951).

(5) A. H. Sharbough, H. C. Eckstrom and C. A. Kraus, *ibid.*, **15**, 54 (1947).

(6) D. J. Denney, *ibid.*, **25**, 259 (1957).

The relaxation times so obtained are given in Tables I and II. Table III gives the loss tangents ($\tan \delta = \epsilon''/\epsilon'$) at various frequencies for pure *n*-caproic acid.

TABLE I

RELAXATION TIMES AND VISCOSITIES FOR SOLUTIONS OF *n*-CAPROIC ACID IN XYLENE AT 20°

Concn., *M*	$10^{12} \times \tau$, sec.	Viscosity, cp.	$10^{12}(\tau/\eta)$
2.11	7.6 ± 0.1	0.91	8.33
3.15	9.1 ± .5	1.09	8.33
4.43	11.2 ± .5	1.37	8.18
6.09	23.0 ± .1	1.95	11.8
7.62	36.0 ± .1	2.85	12.6
Pure liquid	34.0 ± .2	3.12	10.8

TABLE II

RELAXATION TIMES AND VISCOSITIES FOR SOLUTIONS OF CYCLOHEXANECARBOXYLIC ACID IN TETRACHLOROETHYLENE AT 190°

Concn., *M*	$10^{12} \times \tau$, sec.	Viscosity, cp.	$10^{12}(\tau/\eta)$
2.03	8.0 ± 0.1	1.15	7.0
3.52	8.9 ± .5	2.17	4.1
4.54	10.4 ± .1	2.89	3.6
6.55	47 ± 5	9.42	4.98

TABLE III

LOSS TANGENTS AND PERMITTIVITY FOR PURE *n*-CAPROIC ACID AT 20°

f, Mc./sec.	$10^3 \times \tan \delta$	ϵ'
3.07	0.15	2.62
6.74	.39	2.63
13.78	.81	2.63
28.5	1.64	2.64
54.6	2.91	2.70
69.3	3.75	2.70
89.5	4.87	2.60

Discussion

In the self-ionized dimer of Harris and Alder the effective charge separation is approximately 3.7 Å. which leads to a dipole moment of 18 *D*. If, following Harris and Alder, one assumes that the non-ionized form of the dimer is non-polar and that the monomer and higher multimers are present to a negligible extent, then it is possible to calculate a loss tangent due to the self-ionized form by treating the medium as a mixture of a polar solute in a non-polar solvent. Debye's relation ($\beta = 1.0$) is

$$\tan \delta = \frac{(\epsilon_0 + 2)^2}{\epsilon_0} \times \frac{\pi N c \mu^2}{6750kT} \times \frac{\omega\tau}{1 + \omega^2\tau}$$

c is the concentration in g. mole/l. of the dipoles of moment μ.

The concentration of the self-ionized form can be calculated from Harris and Alder's ΔG^0 for the equilibrium I⇌II. For *n*-caproic acid at 25° their ΔG^0 = 3.35 kcal./mole leads to a ratio of concentrations [II]/[I] of 0.15/100. Taking ϵ_0 = 2.65 for *n*-caproic acid, an appropriate value of τ is needed to complete the calculation of tan δ. This can be obtained from the relations of Hill[7] for the case of a pure liquid, which leaves no uncertainty as to the value of the viscosity which is relevant. The dimensions of the dimer[8] lead to $\tau = 15 \times 10^{-12}$ second. At 90 Mc./sec. the calculated loss tangent is then found to be 0.99×10^{-3} or approximately one-fifth of the experimental value. In making this estimate the data have throughout been taken so as to make the agreement with the observed tan δ as close as possible: for instance, $\mu^2 = (18)^2$ is almost certainly a maximum, as the polarizability of the oxygens in II would significantly reduce the effective moment below that for the rigid zwitterion assumed.

Similarly, assuming ΔG^0 = 3.5 kcal./mole for cyclohexanecarboxylic acid (the ΔG^0 values vary only slightly with the alkyl radical) and $\tau = 22 \times 10^{-12}$ second, one finds for the most concentrated solution in Table II, which contains only one mole per cent. of tetrachloroethylene, that the calculated tan δ's are approximately one quarter the experimental values. This discrepancy is again thought to be beyond the possible range of the calculated value.

According to the Harris and Alder model the zwitterionic form II should, at one temperature, form a constant (small) fraction of the total carboxylic acid concentration. If this were so, the ratio τ/η should be essentially constant for a given solvent. This is certainly not so either for the *n*-caproic acid in xylene or for the cyclohexanecarboxylic acid in tetrachloroethylene.

The most likely interpretation of these results is that the concentrated carboxylic acid solutions (and thus also the pure liquids) contain polar aggregates larger than the dimer. It is well-known that formic acid forms a linear rather than cyclic hydrogen-bond system in the solid, a configuration which gives rise to its large dielectric constant as a liquid (ϵ' = 58.5 at 16°). The same structure is almost certainly formed to some extent in acetic acid (ϵ' = 6.15 at 20°), the study of whose association even in the gas phase suggests that species higher than the dimer are formed.[9] Quantitative assessment shows that the monomer dimer equilibrium is inadequate to account for the state of the acetic acid at concentrations above 2 *M* in benzene, etc.[10]

The higher multimers (trimers, etc.) might well be of an open-chain form having a distinctly polar character relative to the cyclic structures. Such open-chain multimers, including an open-chain dimer, would be of higher energy than the cyclic structures owing to their free terminal carboxylic groups and their proportions would increase with rise in temperature corresponding to the observed rise in dielectric constant. The increased proportion of some larger polar aggregates may be responsible for the rise with concentration of τ/η for caproic acid in xylene.

As the results summarized in Tables I and II emphasize, there is a dielectric absorption of the carboxylic acids at the lower concentrations in

(7) N. E. Hill *Proc. Phys. Soc.*, **67B**, 149 (1954).

(8) "Interatomic Distances," ed. L. E. Sutton, Special Publ. Chem. Soc., London, 1958.

(9) E. W. Johnson and L. K. Nash, *J. Am. Chem. Soc.*, **72**, 547 (1950).

(10) M. Davies and D. M. L. Griffiths, *Z. physik. Chem., Frankfurt*, **2**, 353 (1954).

inert solvents which points consistently to the presence of a polar molecular species. This is certainly not the monomeric carboxylic acid. From the typical data for acetic acid in benzene[10]—and no radical difference would arise from caproic acid in xylene—the fraction of acid as monomer at a concentration of 2 M is close to 0.02. Using this value and μ(monomer) = 1.7 D, $\tau = 10 \times 10^{-12}$ sec., the maximum value of tan δ at 70 Mc./sec. would be 3.0×10^{-5}. The observed value in 2 M caproic acid is 32×10^{-5}.

Accordingly, as the association studies show nearly all the molecules are dimers at this concentration, a mean value for the dimer moment may be calculated from tan δ (observed) neglecting the presence of monomer. The estimate so arrived at is μ(dimer) = 0.7 D.

This moment for the dimer is smaller than that usually quoted. It could be that this is due to the atomic polarization form being significantly larger than the allowance made for it (*e.g.*, 0.15 × the electronic polarization) owing to the flexible dimer bridge.[11] The moment may itself be a consequence of the appreciable distortion of the dimer structure due to interaction with the solvent or the result of its numerous low-frequency vibrations. Alternately, it may merely represent an apparent value arising from a proportion of open-chain (and therefore polar) dimer accompanying the essentially non-polar cyclic form. Insufficient data at present exist to allow an estimate of the extent to which such non-cyclic dimer molecules accompany the normally accepted form.

(11) L. Slutsky and S. H. Bauer, *J. Am. Chem. Soc.*, **76**, 270 (1954).

Experimental

The dielectric measurements were made in an N.P.L. calibrated Hartshorn–Ward apparatus.[12]

n-Caproic acid was stood over anhydrous $MgSO_4$ and fractionally distilled from anhydrous $CaSO_4$. B.D.H. cyclohexanecarboxylic acid melted sharply at the literature m.p. (31°) and was used without further purification. Xylene was purified as by Aihara and Davies[13] and tetrachloroethylene was dried over $CaCl_2$ and carefully distilled.

Acknowledgments.—Thanks are due to Dr. Mansel Davies for his interest in this work and to the D.S.I.R. for a Research Studentship.

(12) L. Hartshorn and W. Ward, *J. Inst. Elect. Engin.*, **79**, 597 (1936).

(13) A. Aihara and M. Davies, *J. Colloid Chem.*, **11**, 671 (1956).

THE AFFINITY OF LEGOGLOBIN AND OTHER HEME PROTEINS FOR GASEOUS NITROGEN, HYDROGEN AND ARGON[1]

BY ROBERT G. MORTIMER[2] AND NORMAN BAUER

Chemistry Department, Utah State University, Logan, Utah

Received April 1, 1959

The affinities of legoglobin from soybean root nodules, of myoglobin and of hemoglobin for gaseous nitrogen, hydrogen and argon were found by determination of gas volumes desorbed from aqueous solutions saturated with gas. The standard free energy changes for the gas uptake processes were found to be in the range of +1.5 to +2.8 kcal./mole, depending on the gas, the protein and the oxidation state of the protein.

Introduction

The first step in biological N_2 fixation is likely to be a sorption of the diatomic molecule at a cationic site on a potential catalyst for reduction.[3] Hemoproteins would seem to offer such a site for the sorption of N_2, by analogy with the behavior of O_2 and from previous evidence[4] that hemoglobin has a small but definite affinity for N_2.

The present study reports our measurements of the amount of gas which can be desorbed from aqueous solutions of legoglobin, of myoglobin and of hemoglobin after saturating these proteins with N_2 or with other relatively inert gases. These measurements are the basis for evaluating the standard free energy of N_2 sorption by legoglobins, which are myoglobin-like proteins extracted from N_2-fixing root nodules of leguminous plants.[5]

(1) Supported by a grant from the Herman Frasch Foundation and presented in part at the joint meeting of the Utah Academy of Sciences, Arts and Letters and the Utah Section of the American Chemical Society, November, 1957.

(2) Woodrow Wilson National Fellow, 1958-1959.

(3) N. Bauer and R. G. Mortimer, *Biochim. Biophys. Acta*, in press.

(4) (a) D. D. Van Slyke, R. T. Dillon and R. Margaria, *J. Biol. Chem.*, **105**, 571 (1934); (b) J. L. Stoddard, *ibid.*, **71**, 629 (1926); (c) J. A. Hawkins and C. W. Schilling, *J. Biol. Chem.*, **113**, 273 (1936).

Experimental Procedure

Materials.—Hemoglobin was prepared from fresh horse blood by the method of Altschul, Sidwell and Hogness.[6] Analysis for heme by the pyridine hemochromogen method[7] indicated a purity of 98%, which was confirmed by an iron content of 0.32 ± 0.01, using the *o*-phenanthroline method. This hemoglobin also was characterized by electrophoretic and sedimentation patterns, using a Spinco Model E and a Spinco Model H apparatus, respectively. The material was electrophoretically homogeneous at *p*H 8.9 after oxidation to Fe^{+3} by $K_3Fe(CN)_6$. The sedimentation constant at 20° and ~ 1 wt. % was 4.4 svedbergs. The material was dialyzed against distilled water at 0°, lyophilized and stored at 0°. This treatment did not denature the protein, as shown by characteristic oxygenation spectra on redissolving just before use.

Myoglobin was prepared from fresh horse heart by the method of George and Stratmann.[8] Spectra of the oxygenated material showed the presence of active heme groups. Analysis for heme groups indicated a purity of 100 ± 5% based on a molecular weight of 17,000; this was confirmed by finding 0.3% iron. The electrophoretic mobilities at *p*H 7.9 and 2° were 1.69×10^{-5} (40%) and 1.10×10^{-5}

(5) N. Ellfolk and A. I. Virtanen, *Acta Chem. Scand.*, **6**, 411 (1952); *cf.* also A. I. Virtanen, J. Jorma, H. Lenkola and A. Linnasolmi, *ibid.*, **1**, 90 (1947).

(6) A. M. Altschul, A. E. Sidwell and T. R. Hogness, *J. Biol. Chem.*, **127**, 123 (1939).

(7) O. Keilin and E. F. Hartree, *Biochem. J.*, **49**, 88 (1951).

(8) P. George and C. J. Stratmann, *ibid.*, **51**, 103 (1952).

(60%) cm./sec./volt/cm. for the two peaks from the material oxidized with potassium ferricyanide. The existence in the myoglobin of two major electrophoretic components not readily separable by ammonium sulfate fractionation is consistent with the observations of Theorell and Åkeson.[9] The sedimentation constant at 20° and ~ 1 wt. % was 1.9 svedbergs. The material was stored at −5° as a paste containing saturated ammonium sulfate.

Legoglobin was prepared from field-grown nodules of Lincoln soybeans, seven weeks after planting. The seed had been inoculated with rhizobia from nodules of greenhouse soybeans. The plants were kept cool during the short interval (15 min.) between uprooting and harvesting the nodules. The excised nodules were immediately dropped on Dry Ice, then stored at −10° until they were ground in a multimixer for extraction of protein. A modification of the methods of Virtanen, *et al.*,[5] and of Little[10] was used for isolating an ammonium sulfate paste of the **legoglobin**. The initial fractionation with ammonium sulfate was carried out in three steps after extracting the minced nodules with 1.6 *M* $(NH_4)_2SO_4$ at *p*H 7 and 0° in air. Fractions precipitating between 1.6–2.1 *M*, 2.1–2.9 *M* and 2.9–4.0 *M* were collected, then the last fraction was dissolved and refractionated until finally at least 90% of the material consisted of the two characteristic electrophoretic components observed by Virtanen and designated here as legoglobin-V. The remaining 10% or less was another protein having a single electrophoretic peak close to that of the fast component of the legoglobin-V. This other protein, which together with legoglobin-V constitutes the bulk of protein from our nodules soluble in the range of 2.1–4.0 *M* ammonium sulfate, has not yet been isolated sufficiently to determine fully its characteristics but it is a heme protein similar to Lb-V. It may be one of the heme proteins reported by Thorogood.[11]

The visible spectrum at *p*H 7 of the Lb-V fraction agreed with that of Sternberg and Virtanen.[12] The sedimentation constant was 1.9 svedbergs at ~1 wt. % and 20°. In agreement with Ellfolk and Virtanen[5] the isoelectric points for the two electrophoretic components were 4.4 and 4.7, as determined from their mobilities in the *p*H range 4.7–7.8; and we use their value of 20,100 for the molecular weight.

The nitrogen, hydrogen and argon gases were obtained in cylinders from the Matheson Co. Typical analyses which were supplied by the company were nitrogen, 0.002% O_2, 0.004% A, 0.002% H_2; hydrogen, 0.002% O_2, 0.05% A, 0.1% N_2; argon, 0.001% O_2, 0.001% H_2, 0.08% N_2. Each gas was passed through aqueous vanadyl sulfate to remove traces of oxygen according to the method of Meites and Meites,[13] and to saturate it with water vapor. The gases were analyzed for oxygen by the method of Silverman and Bradshaw,[14] using a sampling procedure identical with the introduction of gas into the Van Slyke chamber. The oxygen contents of the scrubbed gases were found to be 30 p.p.m. or less, except for the argon, for which 80 p.p.m. were determined after long use of the scrubber without regeneration. This was more than adequate for keeping the oxygenated hemoproteins down to a negligible concentration.

The 0.01 *M* buffer solvent was prepared from sodium barbital and its *p*H adjusted with sodium hydroxide to 7.91. The buffer was protected to prevent carbon dioxide uptake during storage, but a small amount of carbon dioxide could not be excluded during preparation of some solutions. This was desorbed before final measurements were made.

Methods.—The improved procedure of Van Slyke, *et al.*,[4] was modified to allow a more direct comparison of the solubilities of the three gases in a given protein solution, to conserve protein sample, and to more precisely define the state of the protein. The apparatus was a commercial Van Slyke manometric gas solubility unit, modified to pass thermostated water at 20.0° through the chamber jacket and provided with a fitting for gas-filling of the chamber or evacuation of the manifold between chamber and gas source.[15] It was operated in a constant temperature room held at 20.0°.

The protein samples were dissolved in 0.01 *M* sodium barbital buffer, then oxidized with potassium ferricyanide or reduced with sodium dithionite. Finally, the solutions were dialyzed 12 hours against buffer maintained at *p*H 7.91, at 0° and at constant ionic strength by several changes of buffer. The reduced samples were kept under an argon atmosphere during dialysis.

The protein concentration was determined by the cyanmethemoblobin method,using the millimolar extinction coefficient $\epsilon = 11.5$ of Drabkin[16] for hemoglobin and for myoglobin. The corresponing value $k = 0.418$ g.$^{-1}$ l. cm.^{1} for legoglobin-V at $\lambda = 540$ mμ was determined from a lyophilized sample.

Each 4 to 5 ml. sample was extensively degassed within the Van Slyke chamber and then, using the apparatus as a tonometer, the sample was saturated with A, H_2 or N_2 by shaking at barometric pressure with octyl alcoho antifoam. After removal of the gas phase from the chamber, the dissolved and protein-bound gas was desorbed and its pressure P_v measured. Determinations were made successively with all three gases on the same sample without removing it from the chamber, repeating measurements for each gas until agreement of P_v within 0.2% was attained. Gas solubilities in the buffer alone were determined under identical conditions.

Results and Calculations.—We have determined the volumes of N_2, of A and of H_2 gas desorbed from solutions of ferrolegoglobin-V (Lb^{+2}-V), of ferrilegoglobin-V (Lb^{+3}-V), of horse ferromyoglobin (Mb^{+2}), of horse ferrimyoglobin (Mb^{+3}), of horse ferrohemoglobin (Hb^{+2}) and of horse ferrihemoglobin (Hb^{+3}).

Table I gives values of Bunsen's coefficient, α, in cc. of gas per ml. of protein solution per atm. of saturating pressure, based on a Henry's law correction, which is valid for N_2 in Hb^{+2} below 6 atm.,[4] to the corresponding volume v_p for a barometric saturating pressure. The v_p values were calculated from the formula of Van Slyke, *et al.*,[4] except that his empirical correction was not used. Thus our values α depart from the absolute values by a per cent. or so; but this represents a small systematic error that is practically constant for both solvent and solution, hence largely cancels out in calculating the quantity of interest, β, discussed below.

Also given in Table I are values of affinity coefficients β, the volume of gas in cc. (STP) per atm. associated with one gram of protein, calculated under the assumption that the amount of gas taken up by v_s ml. of solution is additively composed of the uptake by $0.75W$ ml. of protein and the uptake by $(v_s - 0.75W)$ ml. of pure solvent, where W = grams of protein per v_s ml. of solution. Likewise, values are given for β', a quantity similar to β except for the assumption that the partial specific volume of the protein is 0.85 instead of 0.75 cc./g., *i.e.*, assuming that part of the solvent capacity of the buffer is immobilized through hydration of the protein in the extent of 10% by weight. Table I includes other quantities necessary for the calculation of β and β' from α.

Our value of β for N_2 gas desorbed from ferrohemoglobin, 0.019_6 cc./g./atm. at 20.0°, checks satisfactorily with that of Van Slyke, *et al.*,[4] (0.0164 to 0.0167 at 25° for crystallized horse Hb; 0.012 to 0.019 for other samples), who used a considerably different but painstaking method. Stoddard[4] obtained $\beta = 0.017 \pm 0.0004$ for N_2 from horse Hb at 20.0°. The expected decrease in β with increasing temperature is probably responsible for some of the difference between this investigation and that of Van Slyke, *et al.* Also, differences arise from the fact that in earlier investigations, neither the *p*H nor the oxidation state of the protein was carefully controlled. The agreement cited above confirms the other evidence that oxygen was satisfactorily excluded from the protein. Thus the absolute value of β is probably correct to within about 5% for 8 wt. % solutions; and to 10% for 3 wt. % solutions. *Differences* in β values are probably significant to 1 or 2% for 8 wt. % solutions, considering that the reproducibility of α was 0.1 to 0.2%. This would imply an uncertainty of 12 to 25% in relative

(9) H. Theorell and A. Akeson, *Ann. Acad. Sci. Fennicae Chem.*, **60**, 303 (1953).

(10) H. N. Little, *J. Am. Chem. Soc.* **71**, 1973 (1949).

(11) E. Thorogood, *Science*, **126**, 1011 (1957).

(12) H. Sternberg and A. I. Virtanen, *Acta Chem. Scand.*, **6**, 1342 (1952).

(13) L. Meites and T. Meites, *Anal. Chem.*, **20**, 984 (1948).

(14) L. Silverman and W. Bradshaw, *Anal. Chim. Acta*, **12**, 526 (1955).

(15) W. Paul and F. J. W. Roughton, *J. Physiol.*, **113**, 23 (1951).

(16) D. Drabkin, *Am. J. Med. Sci.*, **209**, 268 (1945).

β values for the lowest protein concentration used (2.3 wt. %).

TABLE I

BUNSEN COEFFICIENTS α AND AFFINITY COEFFICIENTS β,β' FOR GAS DESORPTION FROM HEME PROTEIN SOLUTIONS IN AQUEOUS BUFFER[e]

Protein[b]	Concn., g./100 ml.	Gas	α	β	β'
Hb^{+3}	8.1	N_2	0.01678	0.0234	0.0251
	8.1	H_2	.01778	.0112	.0131
	8.1	A	.0346	.0352	.0383
Hb^{+2}	8.3	N_2	.01650	.0196	.0213
	8.3	H_2	.01904	.0265	.0282
	8.3	A	.03590	.0506	.0542
Mb^{+3}	4.8	N_2	.01602	.0154	.0171
	4.8	H_2	.01779	.0102	.0119
	4.8	A	.03468	.0417	.0465
Mb^{+2}	7.7	N_2	.01710	.0280	.0299
	7.7	H_2	.02059	.0477	.0483
	7.7	A	.03692	.0649	.0691
$(Mb^{+2})^a$	9.4	N_2	.01636	.0172	.0188
	9.4	H_2	.01839	.0180	.0200
	9.4	A	.0345	.033	.0362
$(Lb^{+3}\text{-}V)^b$	2.3	N_2	.01580	.010	.011
	2.3	H_2	.01792	.012	.014
	2.3	A	.03363	.017	.018
$(Lb^{+3}\text{-}V)^c$	9.7	N_2	.01583	.0117	.0132
	9.7	H_2	.01791	.0129	.0148
	9.7	A	.0337	.0247	.0278
$(Lb^{+2}\text{-}V)^b$	2.3	N_2	.01594	.016	.018
	2.3	H_2	.01804	.017	.019
	2.3	A	.03427	.046	.048
$(Lb^{+2}\text{-}V)^c$	3.5	N_2	.01653	.0317	.0326
	3.5	H_2	.01951	.0577	.0600
	3.5	A	.03526	.0685	.0703
$(Lb^{+2}\text{-}V)^d$	8.1	N_2	.01611	.0149	.0167
	8.1	H_2	.01847	.0198	.0217
	8.1	A	.03421	.0304	.0339

[a] Sample of Mb in presence of 0.005 *M* ascorbic acid. [b] Sample of Lb-V with about 10% other protein (*cf.* Text). [c] Sample of Lb-V after refractionation of (b). [d] Sample of Lb-V separate from (b) or (c), in presence of 0.005 *M* ascorbic acid. [e] Buffer = 0.01 *M* sodium barbital, for which at 20° $\alpha = 0.0158_5$ atm.$^{-1}$ for N_2; 0.0179_6 atm.$^{-1}$ for H_2; and 0.0338_1 atm.$^{-1}$ for A. [f] Hb = Horse hemoglobin; Mb = horse myoglobin; Lb = root nodule legoglobin.

Discussion

Free Energy of Gas Uptake Process.—In order to translate values of β or β' into an expression of the energy and entropy of interaction between hemoprotein Hp and a relatively inert gas G, let us assume the simplest possible reaction between the two, Hp + G → Hp·G, forming a loose addition compound somewhat analogous to the well-known compounds Hb·O_2, Hb·CO.

The fact that only those proteins containing heme groups are known to show affinity for relatively inert gases indicates that each heme protein has only one kind of (secondary) site for attachment of G, closely associated with the (primary) site of oxygenation. Aqueous solutions of plasma proteins exhibit β values very nearly equal to zero[4]; *i.e.*, these non-heme proteins exclude gas from their domain in the solution. Such exclusion would seem to be a general property of proteins except when the molecule contains some group with a concentrated electrostatic charge.

The controversy[4,17] as to whether the N_2 uptake by Hb is a mere solution, or adsorption or a chemical compound formation actually has not been settled by the finding[4] of adherence to Henry's law in the moderate pressure (0 to 6 atm.) region. This follows from the fact that adsorption isotherms tend toward linearity in the region well below saturation pressure and from the fact that the dependence of (Hp·G) on (G) must be practically linear when these species are in chemical equilibrium with Hp, if the equilibrium constant strongly favors decomposition of Hp·G. However, adsorption and chemical reaction become equivalent when there is only one kind of site for adsorption and if there is only one or a definite small number of sites per molecule. In that case, a

TABLE II

EQUILIBRIUM CONSTANTS K_a AND STANDARD FREE ENERGY CHANGES ΔF_u^0 FOR UPTAKE OF GASES BY AQUEOUS[e] HEME PROTEINS AT 20°

Protein[f]	Concn., g./100 ml.	Gas	K_a (atm.$^{-1}$)	ΔF_u^0 (kcal. mole^{-1})	K_a' (atm.$^{-1}$)	$\Delta F_u^{0\prime}$ (kcal. mole^{-1})
Hb^{+3}	8.1	N_2	0.0177	2.34	0.0194	2.30
	8.1	H_2	.0084	2.81	.0100	2.68
	8.1	A	.0272	2.11	.0298	2.04
Hb^{+2}	8.3	N_2	.0151	2.44	.0164	2.40
	8.3	H_2	.0205	2.27	.0218	2.13
	8.3	A	.0399	1.88	.0428	1.84
Mb^{+3}	4.8	N_2	.0125	2.55	.0143	2.48
	4.8	H_2	.0083	2.79	.0098	2.70
	4.8	A	.0353	1.95	.0397	1.88
Mb^{+2}	7.7	N_2	.0236	2.16	.0252	2.14
	7.7	H_2	.0410	1.86	.0409	1.86
	7.7	A	.0562	1.68	.0600	1.64
$(Mb^{+2})^a$	9.4	N_2	.0143	2.49	.0157	2.42
	9.4	H_2	.0150	2.44	.0167	2.38
	9.4	A	.0278	2.09	.0307	2.03
$(Lb^{+3}\text{-}V)^b$	2.3	N_2	.0088	2.76	.010	2.68
	2.3	H_2	.0108	2.64	.013	2.53
	2.3	A	.016	2.41	.017	2.38
$(Lb^{+3}\text{-}V)^c$	9.7	N_2	.0108	2.64	.0122	2.56
	9.7	H_2	.0119	2.58	.0137	2.50
	9.7	A	.0230	2.20	.0262	2.12
$(Lb^{+2}\text{-}V)^b$	2.3	N_2	.015	2.44	.017	2.38
	2.3	H_2	.016	2.41	.018	2.34
	2.3	A	.044	1.82	.046	1.80
$(Lb^{+2}\text{-}V)^c$	3.5	N_2	.0299	2.05	.0308	2.03
	3.5	H_2	.0545	1.70	.0582	1.66
	3.5	A	.0671	1.57	.069	1.56
$(Lb^{+2}\text{-}V)^d$	8.1	N_2	.0139	2.49	.0156	2.42
	8.1	H_2	.0185	2.32	.0203	2.27
	8.1	A	.0286	2.07	.0323	2.00

[a] Sample of Mb in presence of 0.005 *M* ascorbic acid. [b] Sample of Lb-V with about 10% other protein (*cf.* Text). [c] Sample of Lb-V after refractionation of (b). [d] Sample of Lb-V separate from (b) or (c), in presence of 0.005 *M* ascorbic acid. [e] Buffer = 0.01 *M* sodium barbital, for which at 20° $\alpha = 0.0158_5$ atm.$^{-1}$ for N_2; 0.0179_6 atm.$^{-1}$ for H_2; and 0.0338_1 atm.$^{-1}$ for A. [f] Hb = Horse hemoglobin; Mb = horse myoglobin; Lb = root nodule legoglobin.

(17) J. B. Conant and N. D. Scott, *J. Biol. Chem.*, **68**, 107 (1926).

stoichiometric equation such as the one above will characterize the process of gas uptake even if the forces are so weak as to be normally classed with those of "physical adsorption."

Accordingly, we may proceed to calculate the standard free energy change in the gas uptake process from the equilibrium constant $K_a = [a_{Hp\cdot G}]/[a_{Hp}][a_G]$. The ratio of activities $a_{Hp\cdot G}/a_{Hp}$ may be evaluated readily with high accuracy without knowing the absolute values of activity coefficients $\gamma_{Hp\cdot G}$ and γ_{Hp}, since for this kind of reaction these two coefficients must be practically equal at fixed pH and ionic strength. We imply that attachment of G does not substantially alter the formal electric charge on the protein molecule. Also, $a_G = P_G$ to within a per cent. or so when the gas pressure P_G does not exceed 1 atm.

Consequently we have $K_a = C_{Hp\cdot G}/[C_{Hp}P_G]$ atm.$^{-1}$. Also of course, $\Delta F_u^0 = -RT \ln K_a$ for the standard uptake process.

In Table II are given values of K_a and ΔF_u^0 corresponding to the β values in Table I which measure the concentration of Hp·G. Also given are value of K_a' and $\Delta F_u^{0\prime}$ corresponding to β' values, to show the small effect of assuming a 10% hydration of the protein.

Binding Forces.—Some insight into the kind of forces responsible for "inert" gas uptake by heme proteins may be obtained through estimates for N_2 of upper and lower limits, $\Delta H^0_{max.,\,N_2}$ and $\Delta H^0_{min.,\,N_2}$ for the heat of such secondary gasation, based on the mean experimental value of $\Delta F^0_{u,N_2} = +2.4$ kcal./mole and on the limiting entropy changes $\Delta S^0_{max,\,N_2}$, $\Delta S^0_{min,\,N_2}$. The entropy loss for secondary gasation is probably greater than that for primary oxygenation, since the latter involves liberation of a tightly bound water molecule[18]; *i.e.*, $-\Delta S^0_{min,\,N_2} > 22$ e.u. Also, $-\Delta S^0_{max.\,N_2} < 41.7$ e.u. if 3 degrees of translational freedom and one of rotation are lost on N_2-uptake. Accordingly, $-\Delta H^0_{min,\,N_2} \geqslant 4.0$ and $-\Delta H^0_{max.\,N_2} \leqslant 9.7$ kcal./mole. A theoretical estimate[19] of ΔH^0 for argon–water clathrate formation suggests that 3.5 kcal./mole is the upper limit of the van der Waals (dispersion and repulsion) contribution to the $-\Delta H^0$ of trapping of N_2 in aqueous protein, at 273°K. This follows in part from the fact that N_2 is larger than A but has about the same polarizability, and from the fact that the method of estimation leads to agreement with experiment in similar cases only through ignoring the polarization of the clathrated atom by the incompletely screened fields of protons in water. Protonic or other partly screened electrostatic fields such as dipoles must be considered when the trapped atom is asymmetrically located within a cavity, as is argon within water. We conclude that electrostatic as well as dispersion forces are responsible for the uptake of N_2 by aqueous heme proteins.

The implications for biological N_2-fixation will be discussed elsewhere.

Acknowledgments.—We appreciate the assistance of Miss D. I. Christensen and of Mr. A. O. Pulley in preparing and characterizing the legoglobin; and are indebted to Prof. K. Fajans for theoretical discussions.

(18) F. Haurowitz in "Haemoglobin," F. J. W. Roughton and J. C. Kendrew, eds., Interscience Publ., Inc., New York, N. Y., 1949, pp. 53–64; *cf.* also R. L. Berger, Thesis, Pennsylvania State U., 1956.

(19) R. M. Barrer and W. I. Stuart, *Proc. Roy. Soc.* (*London*), **A243**, 172 (1957).

ISOPROPYL RADICAL REACTIONS. III. REACTIONS WITH HYDROGEN ATOMS

BY CARL A. HELLER AND ALVIN S. GORDON

Contribution Branch, Michelson Lab., U. S. Naval Ordnance Test Station, China Lake, Cal.

Received April 30, 1959

The mercury sensitized photolysis of deuterium–diisopropyl ketone and hydrogen–diisopropyl ketone d_2, $(CH_3)_2CDCOCD(CH_3)_2$, mixtures were used to study the hydrogen atom–isopropyl radical reactions at 85°. Of particular interest are $D + \text{iso-}C_3H_7 \rightarrow C_3H_7D^*$, $C_3H_7D^* + M \rightarrow C_3H_7D + M$, $C_3H_7D^* \rightarrow CH_3 + CH_3CHD$. The minimum half-life of the excited propane is calculated from the pressure variation to be 2×10^{-6} sec. The ketone is shown to be a much more efficient quencher of the vibrationally excited propane than is hydrogen or helium. A complete mechanism for this reaction system is proposed and the ratios of some elementary reactions are calculated.

Introduction

Previous studies of the reaction of H atoms and propyl radicals have been either in the low pressure region of the Wood–Bonhoeffer tube[1] or at 50–100 mm., using mercury photosensitization of propane[2] to generate the propyl radicals and H atoms. At low pressures the propane was completely converted to methane by the attack of H atoms. The cracking reactions were proposed

$$C_3H_7 + H \longrightarrow C_2H_5 + CH_3$$
$$C_2H_5 + H \longrightarrow 2CH_3$$

The propyl radicals in the first reaction are a mixture of iso- and *n*-propyl formed by the abstraction of H atoms from propane. At higher pressures the major reaction is the combination of the H atom and the free radical

$$C_3H_7 + H \longrightarrow C_3H_8$$

This change of mechanism with pressure suggests the formation of an activated propane molecule

(1) E. W. R. Steacie, "Atomic and Free Radical Reactions," 2nd Ed., ACS Monograph, Reinhold Publ. Corp., New York, N. Y., 1954.

(2) S. Bywater and E. W. R. Steacie, *J. Chem. Phys.*, **19**, 319 (1951).

which can be deactivated by collisions or can decompose by localization of the energy in the proper vibration mode. Similar mechanisms have been proposed for the methyl–deuterium atom exchange[3] as well as for ethyl–deuterium[3] and hydrogen[4,5] atom exchange and cracking. In principle these reactions are not different from the pressure dependent reaction of methyl–methyl[1] and ethyl–ethyl[5] combination.

This paper reports an investigation of the mercury sensitized reaction of diisopropyl ketone and H_2 in a pressure region where the products depend on the ketone concentration (3 to 40 μ-moles/l.). Diisopropyl ketone was used as a source of isopropyl radicals. Previous papers[6-8] have established the mechanism of the photolysis of diisopropyl ketone well enough to allow its use as an isopropyl radical source.

Experimental

The photolyses were carried out in a cylindrical quartz vessel inside an aluminum block furnace with windows at both ends. Hanovia S2537 lamps built in a flat spiral were used for the Hg sensitized runs. Hanovia S100 lamps which give no resonance line at 2537 Å. were used for a few runs where only the ketone was to be photolyzed.

The purification and deuteration of the ketone has been described.[6] Hydrogen, deuterium and xenon were used directly from the tank after mass spectrometer analysis for purity. The xenon contained impurities of neon, krypton and nitrogen. Helium (main impurity air) was purified by passage through a carbon trap at −196°.

The products of the reaction were analyzed by a double column gas chromatograph and a mass spectrometer, using techniques described in Paper II.[6] For many runs xenon was added to the reactants to serve as an internal standard. Most of the photolyses were carried out at about 85°.

The master mixtures of hydrogen (or deuterium), ketone and xenon could not be checked by our analytical procedures. A mixture made up to an H_2/ketone ratio of 7.4 when mass spectrometrically analyzed, resulted in ratios ranging from 10 to 15. It is thought that this uncertainty is mainly due to absorption of the ketone in the mass spectrometer, and it introduces a doubt as to the actual ketone concentrations in the photolysis runs. For example the position of the lines in Fig. 1 would be shifted to the left if the ketone concentration in the reaction vessel were lower than that in the storage vessel because of the adsorption on the wall. This uncertainty in ketone concentration does not affect the validity of the qualitative effects, but results in a large experimental error for the measured minimum half-lifetime of the excited propane molecule.

Results and Discussion

Only radical–radical and radical–hydrogen atom reactions occur under our experimental conditions (see Appendix at end of this section).

The reactions of D atoms and isopropyl radicals contrasted to the reaction of isopropyl radicals alone show up strikingly in the products of the reaction and their distribution (Table I and ref. 6, 8), and indicate rapid reactions dependent on the presence of D atoms. The propane fraction is much larger than when due only to disproportionation of isopropyl radicals. The excess propane

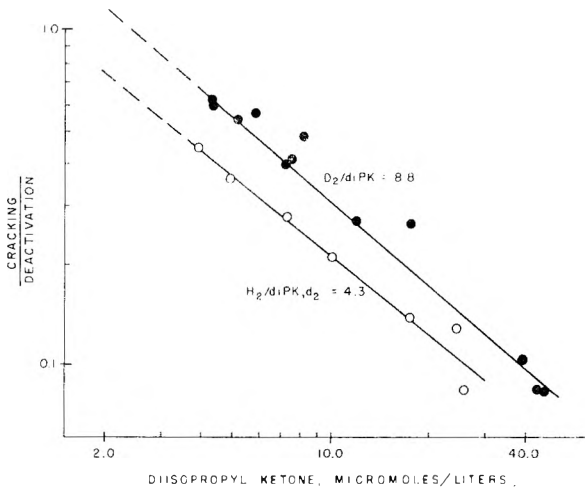

Fig. 1.—Cracking/deactivation ratios for excited propane *vs.* ketone concentration on a log–log graph.

over that from disproportionation contained a deuterium atom, showing that it was formed by a D atom adding to an isopropyl radical. Methane, ethane, isobutane and isopentane are important products, increasing in importance as the ketone pressure is lowered from 4 to 0.10 mm. These results were to be expected from the reactions postulated in previous work involving H atoms and hydrocarbons. In this work the addition of D atoms to isopropyl radicals gives rise to vibrationally excited propane molecules which are stabilized by collision or "crack" to methyl and ethyl radicals.

The behavior of the propylene–dimethylbutane ratio indicates another set of reactions. With constant initial conditions this ratio decreases as the percentage decomposition increases. For small decomposition the ratio exceeded the 0.63 expected from disproportionation of isopropyl radicals. The increase results from the disproportionation reaction of an isopropyl radical and a hydrogen atom to form propene and H_2. Above about 10% decomposition of the diisopropyl ketone the ratio becomes smaller than 0.63, because there is enough propene product so that the addition of an H atom to propene to form an isopropyl radical is important. Previous work has shown that the addition reaction forms isopropyl rather than *n*-propyl; in the present work this is confirmed by the lack of *n*-propyl product such as 2-methylpentane or *n*-hexane in the products.

The quenching/cracking ratio of the excited propane should be affected by any molecular species present. As noted above, the ketone concentration had a marked effect. A series of experiments were made at H_2/ketone ratios of 4.3 (as shown in Fig. 1) and 7.4 (20 runs which are not shown). The lines drawn showed no effect of H_2 within experimental error. If we take experimental error into consideration, H_2 is at most only 1/10 as effective as ketone for removing vibrational energy from excited propane.

The effect of added helium was studied by making eight runs with helium replacing 60% of the H_2. This series falls just below the line for D_2–ketone shown in Fig. 1, with about the same scatter in points. The ineffectiveness of helium as a third

(3) R. Berisford and D. J. LeRoy, *Can. J. Chem.*, **36**, 982 (1958).

(4) Moyra J. Smith, Patricia M. Beatly, J. A. Pinder and D. J. LeRoy, *ibid.*, **33**, 821 (1955).

(5) B. de B. Darwent and E. W. R. Steacie, *J. Chem. Phys.*, **16**, 381 (1948).

(6) C. A. Heller and A. S. Gordon, THIS JOURNAL, **62**, 709 (1958).

(7) S. G. Whiteway and C. R. Masson, *J. Am. Chem. Soc.*, **77**, 1508 (1955).

(8) C. A. Heller and Alvin S. Gordon, THIS JOURNAL, **60**, 1315 (1956).

TABLE I

RATES OF FORMATION OF PRODUCTS FROM MIXTURES OF DiK/D_2 AND DiK-d_2/H_2

Ketone μmoles/l.	4.1	11.6	23.9	3.70	9.9	17.2	4.85	377	393
D_2/ketone	8.8	8.8	8.8	...	...	...	...	2.1	2.1
H_2/ketone-d_2	...	...	....	4.3	4.3	4.3	7.4	2.7	3.6
% decomposition[d]	28	14	5.2	17	7.5	3.0	4.7	2.7	3.6
Rates[a]									
CO	4.57	5.41	4.51	3.30	2.49	2.64	1.17	20.4	28.1
Methane	2.57	1.11	0.48	0.55	0.22	0.22	0.36	0.28	1.06
Ethylene	0.27	0.21	Trace	.09	.09	.11	...	.66	0.84
Ethane	.88	.35	0.39	.39	.08	.15	.29	.21	.32
Propylene	.35	.64	1.08	.45	.45	.61	.12	5.30	11.8
Propane	3.36	4.68	4.59	2.03	2.20	2.73	1.27	11.1	11.9
Isobutane	0.92	0.78	0.35	0.69	0.35	0.21	0.30	0.63	0.56
Isopentane	.17	.19	.16	.12	.14	.05	.022	0.42	.29
2-Methylpentane						.07			.08
2,3-Dimethylbutane	.18	.546	.87	.38	.46	.38	.092	7.55	4.44
Ratio[e]	.63	.27	.158	.45	.21	.14	.34	0.14	0.18

[a] Micromoles $l.^{-1}$ $sec.^{-1}$ × 10^2 at 88 ± 2°. [b] 207°. [c] 306°. [d] 100 × CO/ketone = % decomposition. [e] Cracking/deactivation.

body for removing vibrational energy is to be expected.[9]

The light intensity was varied roughly fourfold by appropriately changing the distance of the lamp from the reaction vessel. The rate of formation of CO increased, and the change in product distribution reflected the higher steady-state concentration of the radicals. The cracking/quenching ratio of the excited propane is not affected by the change in light intensity.

A paper[10] published since our work was finished concerns the cracking of propene to methyl and ethylene by H atoms adding to form hot isopropyl radicals. We repeated the work, and our results indicate that there is no evidence that the "cracking" of hot isopropyl radicals is an important reaction.[11] In addition, we examined three pairs of runs at similar ketone concentration but different per cent. photolysis. In no case was the cracking/quenching ratio ever affected by the differing amounts of product propene even when 15% of the ketone was photolyzed.

The presence of deuterium or hydrogen molecules can have physical effects aside from giving a source of atoms. These gases compete with the ketone in quenching Hg (6^3P_1) atoms. At constant ketone concentration and constant light intensity it was found that increasing D_2 or H_2 decreased per cent. photolysis of the ketone because of the competitive quenching of the excited mercury atoms.

Appendix

To demonstrate that only radical–radical and radical–H atom reactions are of importance in the work reported in this paper, these experiments were carried out:

(1) Two runs were made with added D_2 using the S100 lamp (medium pressure mercury arc) and the product distribution was found to be the same as without D_2 at 85°. These results show that there was no abstraction from the D_2. Our previous work[6,8] indicated that there is no abstraction from the ketone at this temperature and light flux.

(2) Photolyses of the diisopropyl ketone at 85° and pressures much higher than that in this work were made using a 2537 Å. lamp in the presence of Hg but no D_2. Once again the major product distribution was undisturbed, showing the absence of abstraction reactions.

The rate of the mercury sensitized photolysis of the ketone decreases only slowly as the pressure is lowered. Thus at the low pressures of this work the radical, atom and molecule concentrations assure that no abstraction reactions occur.

Mechanism

From the results it is possible to write a mechanism using reactions proposed in previous work. As discussed just above, only radical–radical and radical–atom reactions need be considered.

$$C_3H_7COC_3H_7 + Hg\ (^3P_1) \longrightarrow 2C_3H_7 + CO + Hg(^1S_0) \quad \text{(i) (a)}$$

$$C_3H_7COC_3H_7 + h\nu \longrightarrow 2C_3H_7 + CO \quad \text{(b)}$$

$$D_2 + Hg\ (6^3P_1) \longrightarrow 2D + Hg\ (6^1S_0) \quad \text{(ii)}$$

$$CH_3CHCH_3 + D \longrightarrow C_3H_7D^* \quad (1)$$

$$\text{iso-}C_3H_7 + D \longrightarrow C_3H_6 + HD \quad (2)$$

The excited propane formed in reaction 1 can react as

	Molar bond dissociation energy	
$C_3H_7D^* + M \longrightarrow C_3H_7D + M$	....	(3)
$C_3H_7D^* \longrightarrow CH_3 + CH_3CDH$	84 kcal.	(4)
$C_3H_7D^* \longrightarrow \text{iso-}C_3H_6D + H$	95 kcal.	(5a)
$C_3H_7D^* \longrightarrow \text{iso-}C_3H_7 + D$	>94 kcal.	(5b)
$C_3H_7D^* \longrightarrow n\text{-}C_3H_6D + H$	99 kcal.	(6)

Quantitative Calculations

Reaction volumes and concentrations of intermediary species are unknown in mercury photosensitized reaction. However, the reactions of the excited propane can be followed by considering the ratios of the unimolecular decomposition reactions of the excited propane and its bimolecular quenching reaction, which has the advantage of cancel-

(9) D. E. Hoare and A. D. Walsh, Chm. Soc. Spec. Pub. No. 9, "Reactions of Free Radicals in the Gas Phase," 1957, p. 17–28.

(10) P. J. Boddy and J. C. Robb, *Proc. Roy. Soc. (London)*, **A249**, 518 (1959).

(11) The results will be published in a separate paper.

ling the concentration of excited propane. Since a concentration gradient of radicals may also exist, it is also necessary to use calculations where this will not have any effect. The depletion of ketone in the reaction volume may lead to an error in calculations involving ketone concentration, but the error should be kept small by convection currents.

Reaction of the Vibrationally Excited Propane Molecules. 1. Rupture to Methyl and Ethyl Radicals.—The ratio of reaction 4 to reaction 3 is the easiest to study since (4) is the most rapid of the unimolecular decomposition reactions. The >94 kcal. put into the excited propane by the C–D bond formation plus the 2–3 kcal. internal energy of a thermalized isopropyl radical will give >96–97 kcal. total internal energy. This is easily sufficient to break the C–C bond if localized in the proper vibrational mode.

The C–C break yields one methyl and one ethyl radical; the radicals are measured as the stable products of their reactions. Reactions of methyl and ethyl radicals with themselves or each other are slow because their concentrations are low compared to the isopropyl and D atom concentrations. For instance, the rate of *n*-butane production in all the experiments is below the limits of detection with our gas chromatographic techniques. Methyl radical products are methane and isobutane. The ethyl radical products are ethane, ethylene, isopentane (from the reaction of ethyl and isopropyl), and methyl radicals from the decomposition of the vibrationally excited ethane.[4,12] To correct for the "cracking" reaction of ethyl radicals it is necessary to use the difference between the methyl and ethyl radical products. The difference should be three times the rate of ethyl cracking, since each cracked ethyl yields two methyl radicals.

The deactivation of excited propane is measured by the propane in excess of that produced by isopropyl disproportionation; disproportionation is a constant proportion of combination. The rate of C–C cracking to deactivation is given by the equation

$$r = \frac{\text{methane} + \text{isobutane} - \frac{2}{3}(\text{methane} + \text{isobutane} - \text{ethane} - \text{ethylene} - \text{isopentane})}{\text{propane} - 0.63 \times \text{2,3-dimethylbutane}} \qquad \text{(I)}$$

According to the proposed mechanism

$$r = \frac{k_4}{k_3(\mathrm{M})}$$

where (M) is the concentration of the deactivating molecule. Deactivation is generally not as simple as shown by reaction 3 since there are completely inefficient collisions[13] as well as collisions which remove only a small amount of the excess vibrational energy.[14] Since consideration of stepwise deactivations is mathematically difficult,[15,16] the data are treated as an over-all single step deactivation by ketone molecules.

To test this assumption a plot of log r *vs.* log (ketone) was made. Figure 1 shows this plot for two sets of data, which include some of the runs in Table I. The points fall along a reasonably straight line. However, the slope is -0.8 rather than the value of -1 predicted by the mechanism; the experimental difficulties inherent in low pressure work may account for the discrepancy. For example, ketone adsorption on the surface depends upon the shape of the adsorption isotherm in the pressure region and this isotherm is unknown.

The cracking/quenching ratio is seen to increase continuously with decreasing pressure, and qualitatively shows that quenching of the excited propane molecule by (1) radiating or (2) quenching on the wall, cannot be important processes. Both of these processes would dominate the apparent quenching of excited propane as the pressure is lowered, and the cracking/quenching ratio would asymptotically approach a constant value.

In Fig. 1 the lines for D and H atoms are separated. This separation is outside experimental error. Even though both lines may be displaced due to adsorption, the displacement should be the same for the two mixtures. In addition, both lines were reproduced by two separately prepared mixtures of ketone-D_2 and ketone-D_2-H_2. The propane formed in the two cases was isotopically identical, *i.e.*, CH_3CHDCH_3. Neither H_2 nor D_2 showed enough deactivation efficiency for the separation to be due to the more efficient quenching by H_2 compared with D_2. For example, a mixture of H_2/ketone = 7.4 fell on top of the line shown for a ratio of 4.3, so that the H_2 or (D_2) is not an efficient quencher compared with the ketone. In similar experiments it was demonstrated that helium is also an inefficient quencher for vibrationally excited propane. The separation, therefore, is due to a difference in the bond formed. Formation of a C–D bond makes a less stable excited molecule than the formation of a C–H bond, since the C–D bond is stronger than the C–H bond.

2. Rupture of Excited Propane to Isopropyl Radical and H Atom.—The splitting off of an H or D atom from the center carbon of the excited propane is energetically possible. The rates of these reactions compared with the quenching rate of excited propane can be calculated by examining the deuterium labelling in the propane product. The calculation requires the measuring of a few per cent. of $C_3H_6D_2$ or C_3H_8 in C_3H_7D and is thus fairly inaccurate. The nine runs used to determine reaction 5b were easier to analyze than the four runs for (5a). Reaction 5b produces iso-C_3H_7 which can react with H atoms to give excited C_3H_8. Assuming that the quenching/cracking ratio of this excited propane is the same as for $C_3H_7D^*$, the measured C_3H_8 rate may be multiplied by (r + 1) to get the rate of C_3H_7 formation. If

(12) R. K. Brinton and E. W. R. Steacie, *Can. J. Chem.*, **33**, 1840 (1955).

(13) F. J. Lipscomb, R. G. W. Norrish and B. A. Thrush, *Proc. Roy. Soc.* (*London*), **233A**, 455 (1956).

(14) R. E. Dodd and E. W. R. Steacie, *ibid.*, **A223**, 283 (1954).

(15) H. S. Johnston, *J. Chem. Phys.*, **20**, 1103 (1952).

(16) B. H. Mahon, THIS JOURNAL, **62**, 100 (1958).

this rate is divided by the numerator of eq. I, we get the rate k_{5b}/k_4 which should be pressure independent. This ratio lies between 0 and 0.42 with an average value 0.21 ± 0.10, a reasonable value considering that the excited propane has only 2–3 kcal./mole excess energy over that necessary to break the C–D bond.

3. Rupture of Excited Propane to *n*-Propyl Radical and H Atom.—This process would produce n-C_3H_6D which would appear in the products as 2-methylpentane by combination with isopropyl radicals; no methylpentane was found in the products. Since there is barely enough total vibrational energy to break the primary C–H bonds, it would be expected that this process would be very inefficient.

Disproportionation Reaction of Isopropyl Radical and D Atom.—The results of runs of small decomposition at higher pressures indicate the occurrence of reaction 2. The rate of formation of propene in excess of 0.63 × 2,3-dimethylbutane is a measure of the extent of reaction 2. Unfortunately, the propene can also react with H atoms and as the propene concentration increases it will disappear in part from the products by the reaction

$$C_3H_6 + D \longrightarrow \text{iso-}C_3H_6D$$

The results of runs with larger percentage reaction indicate that this reaction occurs, since the propene is smaller than 0.63 × 2,3-dimethylbutane. The maximum rate of excess propylene formation has been compared to the rate of formation of excited propane; the value for $k_2/k_1 \simeq 0.2$.

Calculation of Minimum Half-life of Excited Propane.—From the plot for D_2–ketone in Fig. 1, it is seen that a short extrapolation gives the ketone concentration for which $k_4 = k_3[M]$. This is the point where, without assumptions as to the efficiency of collisions, the deactivation rate equals the decomposition *via* reaction 4. An average collision interval can be calculated from kinetic gas theory. For this purpose the collision diameters used were 4.0 Å. for ketone and 3.0 Å. for propane. Ketone concentration was taken as 3 micromole $l.^{-1}$ and gave an interval between collisions of 2×10^{-6} sec. This equals the minimum half-life of the excited propane based on the first collision with a probability = 0.5. Since each vibration takes about 10^{-12} sec., the average excited propane molecule undergoes at least 10^6 vibrations before dissociating at the C–C bond. It is of interest to note that excited ethane from methyl–methyl combination has a similarly calculated minimum half-life of 1.6×10^{-5} sec. with acetone as deactivating molecule.[14]

Effect of Temperature.—Runs were made at 98, 200 and 400°. At 98° the apparent increase in cracking may be within experimental error. At 200° there was qualitatively considerable cracking in the presence of H atom; cracking was not found without hydrogen atoms.[6] However, abstraction reactions occur and a quantitative measure of cracking *vs.* deactivation could not be calculated. At 300° the cracking products are only slightly higher in the presence of hydrogen atoms than in their absence.

Deuteration of Products.—The data in Table II show the deuteration of the methane and propane products. The CH_4 at these temperatures results from the disproportionation of CH_3 and C_3H_7 radicals. The deuteration above methane-d_1 results from reaction sequences

$$CH_3 + D \longrightarrow CH_3D^*$$
$$CH_3D^* \longrightarrow CH_2D + H$$
$$CH_2D + D \longrightarrow CH_2D_2,^* \text{ etc.}$$

In the run with 3.70 μmoles $l.^{-1}$ ketone the CH_3D methane formed can be accounted for by the H atom cracking of the CH_3CDH radical. There is good agreement between the number of CH_3D molecules produced and the number of ethyls cracked to methyl.

TABLE II

RATES OF FORMATION OF SOME DEUTERATED PRODUCTS[a]

Ketone, μmoles/l.	25.0	7.02	3.70
D_2/ketone	4.0	8.8	...
H_2/ketone-d_2	...	...	4.3
% Decomposition[b]	14.0	15.0	17.0
CH_4	0.16	0.10	0.42
CH_3D	.43	.19	0.13
CH_2D_2	.16	.24	
CHD_3	.09	.43	
CD_4	.02	.23	
C_3H_8	2.40		
C_3H_7D	5.76		
$C_3H_6D_2$	0.97		
$C_3H_5D_3$	0.24		
$C_3H_4D_4$	Trace		

[a] Experimental conditions as in Table I. [b] 100 × CO/Ketone = % decomposition.

The diisopropyl ketone in the products is marked with D atoms, which shows that ketonyl radicals formed by mercury photosensitization, can combine with D atoms. The combination of hydrocarbon radicals with ketonyl radicals is not an important reaction since no higher ketones are found in the products.

Acknowledgment.—The authors wish to thank Dr. W. H. Urry for discussions of the mechanism, and for suggesting improvements in the manuscript.

INFRARED SPECTRA OF SN_2F_2 AND SNF[1]

By G. A. Gallup and J. L. Koenig

Department of Chemistry, University of Nebraska, Lincoln, Nebraska

Received June 17, 1959

The infrared spectrum of SN_2F_2 has been determined, and frequency assignments have been made on the basis of a planar structure. The fundamentals of SNF have also been assigned.

Introduction

Recently, Glemser, Schroder and Haeseler[2] reported the synthesis of a compound with the molecular formula SN_2F_2. They propose for this compound a resonating structure

which is suggested by the hydrolysis products.[2] Along with the SN_2F_2 a compound with the formula SNF is formed. The latter substance is considerably less stable than the SN_2F_2 and decomposes over a period of a few hours. It is not easy to remove the SNF from SN_2F_2; however, the decrease in intensity with time of some of the bands in the spectrum allows a decision to be made between the bands of SN_2F_2 and those of SNF.

There are no compounds analogous or closely related to SN_2F_2 that have known spectra. This lack makes the present assignment tentative, since it is based on the spectrum of only SN_2F_2.

Experimental

SN_2F_2 was prepared by the method of Glemser, Schroder and Haeseler[2] from S_4N_4 prepared by the method of Arnold, Hugill and Hutson[3] and from AgF_2 purchased from the Harshaw Chemical Co. It was found that a recently purchased product was necessary.

Spectra were taken on both a freshly prepared sample of SN_2F_2 and on one 15 hr. old. The freshly prepared sample showed three bands which had virtually disappeared at the end of 15 hr. These three were attributed to SNF, which would have three fundamentals. The spectra are shown in the figures. They were obtained using a Perkin–Elmer Model 21, double beam spectrometer with NaCl optics for the 2–15 μ region and CsBr optics for the 15–36 μ region. No bands were observed above 1700 or below 380 cm.$^{-1}$.

SN_2F_2 reacts rapidly with mercury. Therefore, the pressures were measured with a "Pyrex" helical manometer having roughly the same sensitivity as a mercury manometer. SN_2F_2 also reacts rapidly with hydrocarbon and silicon stopcock greases. "Kel-F" fluorocarbon grease was found to give fairly satisfactory results and could hold a vacuum if stopcock clamps were used.

SN_2F_2 and/or SNF reacted slightly with the cell windows giving them a cloudy appearance. There were two "window peaks" detected and these are shown in the spectra in the figures. These peaks could be removed only by repolishing the windows. The SN_2F_2 also attacked the window cement ("Pliobond" rubber cement) but apparently did not impair its action.

Discussion and Frequency Assignment

The present frequency assignment is made on the basis of the planar structure for SN_2F_2 proposed by Glemser and Haeseler. This structure is easily seen to have C_{2v} symmetry. Of the nine normal modes four are of type A_1, three of type B_1 and one each of types A_2 and B_2, if the z-axis is taken in the plane of the molecule bisecting the N–S–N angle. The seven A_1 and B_1 motions are in the plane of the molecule, while the A_2 and B_2 are out of plane. The A_2 fundamental is inactive in the infrared. The vibrations will be numbered in order of decreasing frequency using ν_1 to ν_4 for the A_1, ν_5 for the A_2, ν_6 to ν_8 for the B_1 and ν_9 for the B_2 species.

If the x-axis is also taken in the plane of the molecule the moments of inertia are in the order $I_{xx}<I_{zz}<I_{yy}$, therefore, the A_1 fundamentals should give rise to B-type bands and the B_1 fundamentals to A-type bands. The B_2 fundamental should be a C-type band.

Various combinations and overtones are active in the infrared and the direct products of the non-totally symmetric irreducible representations of C_{2v} are $A_2^2 = A_1$, $A_2xB_1 = B_2$, $A_2xB_2 = B_1$, $B_1^2 = A_1$, $B_1xB_2 = A_2$ and $B_2^2 = A_1$. All of the observed bands except the one at 864 cm.$^{-1}$ may be explained in terms of the vibrations of species A_1 and B_1.

The frequencies of the observed bands are listed in Table I with the assignment. Examination of the spectrum shows that there are two relatively strong bands at 1525 and 1330 cm.$^{-1}$. These frequencies are considerably higher than any of the fundamentals in either S_4N_4 or NF_3 which are shown in Table II, and since the bonds in SN_2F_2 would be expected to be weaker than the bonds in these "parent" compounds, the two strong high frequencies are assigned to combinations. The next strong band is at 805 cm.$^{-1}$ and while the band shape is unresolved it is reasonable to assign this to the highest of the B_1 frequencies. The bands at 623 and 421 cm.$^{-1}$ appear to be A-type and are therefore assigned to the other two B_1 frequencies. The bands at 754, 725 and 508 cm.$^{-1}$ appear to have B-type band shapes and are therefore assigned to the upper three A_1 frequencies. The fourth A_1 frequency, corresponding approximately to the N–S–N angle deformation, would be expected to

TABLE I

INFRARED ABSORPTION BANDS OF SN_2F_2

Band, cm.$^{-1}$	Assignment	Band, cm.$^{-1}$	Assignment
1625	$2\nu_6(A_1)$	845	$2\nu_8(A_1)$
1525	$\nu_2 + \nu_6(B_1)$	805	$\nu_6(B_1)$
1405	$\nu_2 + \nu_4 + \nu_7(B_1)$	754	$\nu_1(A_1)$
1330	$\nu_2 + \nu_7(B_1)$	725	$\nu_2(A_1)$
1251	$2\nu_7(A_1)$	623	$\nu_7(B_1)$
1150	$\nu_2 + \nu_8(B_1)$	508	$\nu_3(A_1)$
1080	$\nu_2 + \nu_8 - \nu_4(B_1)$	421	$\nu_8(B_1)$
883	$\nu_4 + \nu_6(B_1)$	70 (calcd.)	$\nu_4(A_1)$
864	?		

(1) Submitted to the Graduate Faculty in the University of Nebraska in partial fulfillment of the requirements for the degree of Master of Science.

(2) O. Glemser, H. Schroder and H. Haeseler, *Z. anorg. allgem. Chem.*, **279**, 28 (1955).

(3) M. H. M. Arnold, J. A. C. Hugill and J. M. Hutson, *J. Chem. Soc.*, 1645 (1936).

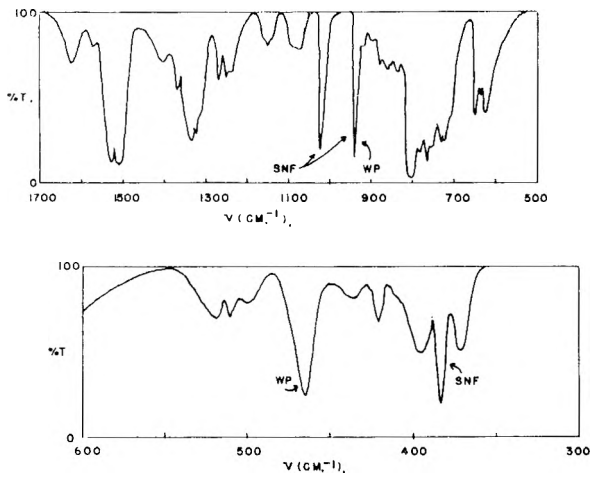

Fig. 1.—The spectrum of the reaction product immediately after preparation. The total gas pressure was *ca.* 20 mm. of Hg in a 10 cm. cell with NaCl windows for the 1700-600 cm.$^{-1}$ region and CsBr windows for the 600-300 cm.$^{-1}$ region. The 600-300 cm.$^{-1}$ region of the spectrum has been redrawn from linear wave length to linear wave number for uniformity. "WP" signifies the window peaks.

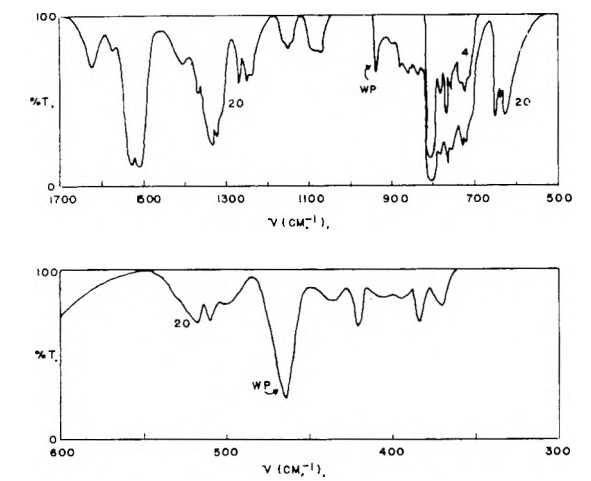

Fig. 2.—The spectrum of the reaction mixture 15 hr. after preparation. The pressure of gas in mm. is given on the spectrum and the cell is the same as was used for Fig. 1. Again, the 600-300 cm.$^{-1}$ region has been redrawn and "WP" signifies the window leaks.

TABLE II

FUNDAMENTALS OF NF_3 AND S_4N_4

NF_3[4]		S_4N_4[5]	
Band, cm.$^{-1}$	Assignment	Band, cm.$^{-1}$	Assignment
1032	$\nu_1(A_1)$	925	B_2
905	$\nu_3(E)$	888	A_1
647	$\nu_2(A_1)$	792	B_1
493	$\nu_4(E)$	696	E
		615	A_1
		557, 552	E
		519	B_2
		460	A_2
		347	E
		213	B_1, E
		177	A_1, B_2
		173	A_2

be very low since the force constant for this type of motion in S_4N_4 is small.[5] The other active fundamental, ν_9, would also be expected to be quite low in frequency.

All but four of the weaker bands can be attributed to binary combinations or first overtones of the observed fundamentals. These four are 1405, 1080, 883 and 864 cm.$^{-1}$. The last one may not be a separate band. The band at 883 cm.$^{-1}$ seems to be a binary combination of ν_6 with one of the low frequency fundamentals. Of these (ν_4, ν_5 or ν_9) only $\nu_4 + \nu_6$ and $\nu_5 + \nu_6$ are active. Similarly the band at 1080 cm.$^{-1}$ could be $\nu_2 + \nu_8 - \nu_4$ or $\nu_2 + \nu_8 - \nu_5$. Here again the combination with ν_9 is inactive. The band at 1405 cm.$^{-1}$ could be $\nu_2 + \nu_7 + \nu_4$ or $\nu_2 + \nu_7 + \nu_9$. In this last case the combination with ν_5 would be inactive.

While there is little direct evidence to aid in choosing among the above possibilities, they all correspond to the addition or subtraction of nearly the same frequency to previously assigned bands. This may indicate that these combinations all contain the same low frequency fundamental. Since ν_4 is the only one possible for all three, it has been chosen. Using this assumption the frequency of ν_4 is calculated to be $(\nu_2 + \nu_8) - (\nu_2 - \nu_4 + \nu_8) = 70$ cm.$^{-1}$. The band at 864 cm.$^{-1}$ if it is separate and due to SN_2F_2 seems to have no explanation in terms of the A_1 and B_1 fundamentals. It may possibly arise through a combination involving ν_5 or ν_9. However, such an assignment appears at the moment to be useless speculation.

While the infrared spectrum cannot be used to prove that the structure for SN_2F_2 proposed by Glemser and Haeseler is correct, it can be seen that the planar form and the spectrum are consistent. Other reasonable structures for SN_2F_2 do not have as high a symmetry as C_{2v}, but chemical rather than spectral evidence must be used to rule these out at the moment.

Fundamentals of SNF

The three bands which decrease in intensity with time are found at 1024, 941 and 391 cm.$^{-1}$ and have been assigned to SNF. There seems to be little doubt that 391 cm.$^{-1}$ is the angle deformation frequency. On the basis of a bent structure, S=N—F, the other two are rather close together for fundamentals of the same symmetry type. Indeed, they are so close that it is impossible to calculate real force constants without assuming the equilibrium S–N–F angle to be less than 91°. If on the other hand the sulfur were the central atom it would be expected that the two stretching frequencies would occur quite widely spaced. It therefore appears that either (1) one of the two frequencies, 1024 or 941, does not correspond to a fundamental or (2) there is a fortuitous cancellation of off diagonal terms in the GF matrix so that the two stretching motions do not interact with one another.

It is interesting to compare these frequencies with those for nitrosyl fluoride, ONF, which have

(4) M. K. Wilson and S. R. Polo, *J. Chem. Phys.*, **20**, 1716 (1952).
(5) E. R. Lippincott and M. C. Tobin, *ibid.*, **21**, 1559 (1953).
(6) P. J. H. Woltz, E. A. Jones and A. H. Nielsen, *ibid.*, **20**, 378 (1952).

been determined by Woltz, Jones and Nielsen.[6] They give 1844.03 cm.$^{-1}$ (N–O), 765.85 cm.$^{-1}$ (N–F) and 521 cm.$^{-1}$ (bending). If either 1024 or 941 cm.$^{-1}$ is the N–F stretching frequency in SNF, it appears that there is a considerable increase in this frequency in replacing oxygen by sulfur. This could be explained either on the basis of (2) above or on the expectation that S=N would be a less electronegative group than O=N and therefore, should form a somewhat stronger bond with fluorine.

The disappearance of SNF appears to result in the formation of a polymeric substance coating the interior of the containers.

Acknowledgment.—The authors wish to acknowledge the many helpful discussions with Dr. R. H. Harris concerning the chemical properties of SN_2F_2 and SNF.

LUMINESCENCE SPECTRA OF NAPHTHOLS AND NAPHTHALENEDIOLS: LOW-TEMPERATURE PHENOMENA[1]

BY DAVID M. HERCULES AND L. B. ROGERS

Department of Chemistry and Laboratory for Nuclear Science, Massachusetts Institute of Technology, Cambridge 39, Mass.

Received June 26, 1959

Low-temperature fluorescence spectra of some molecular and ionic hydroxy-naphthalenes are reported for the first time. Frequencies of fluorescence maxima obtained at 77°K. in rigid glass solvents were higher than those obtained at room temperature in the same solvent. This "blue shift" has been attributed to fluorescence emission from a solute molecule without solvent reorientation at the low temperature. Fine structure appeared in the low-temperature fluorescence spectra of three diols having molecular symmetry. Spacings between the vibrational peaks of the fluorescence spectra have been correlated with the infrared spectra. Phosphorescence for some of the hydroxy-naphthalenes has been reported.

Introduction

Although electronic absorption spectra at the temperature of liquid nitrogen[2] have recently received much attention, comparable investigations of electronic fluorescence spectra generally have been neglected. Bowen and his co-workers have investigated the low-temperature fluorescence of some condensed-ring hydrocarbons[3] and also have studied inter-molecular energy transfer between compounds of this type.[4] The monumental investigations of Lewis and Kasha[5] spurred interest in phosphorescence phenomena and a recent publication[6] summarizes much of the work concerning phosphorescence in rigid media at liquid-nitrogen temperature.

Utilization of rigid media offers two advantages for the correlation of fluorescence spectra with molecular structure. First, the efficiency of luminescence is usually increased over that at room temperature. Second, the spectra often become much sharper in rigid media. Both effects result from decreased thermal motion of the solvent molecules at the lower temperature.

In the present investigation extreme sharpening was found to occur in the fluorescence spectra of three symmetrical diols. In addition, a "blue shift" of the fluorescence spectrum was encountered in going from room temperature to 77°K. in a given solvent. This "blue shift" is thought to arise because the solvent molecules do not orient themselves to the equilibrium excited state of the molecule at 77°K. whereas they do at room temperature. Because of the complexity of systems examined, no attempt has been made to assign the difference in behavior to any particular type of molecular interaction.

Experimental

Materials.—All naphthols and naphthalenediols were purified, and oxygen-free solutions were prepared, as described elsewhere.[7] EPA and EAA, solvents used for low-temperature studies, were prepared as follows.

EPA.—Ether, isopentane and alcohol (8:3:5)—Mallinckrodt reagent-grade ether, absolute alcohol and Eastman Kodak technical-grade isopentane were used without further purification. The mixture showed no residual fluorescence at the level of sensitivity used.

EAA.—Ether, alcohol and ammonia (10:9:1)—Mallinckrodt reagent-grade ether, absolute alcohol and du Pont concentrated, reagent-grade ammonium hydroxide were all used as supplied. No residual fluorescence was found at the level of sensitivity used for measurement.

Apparatus.—The apparatus used to obtain low-temperature fluorescence spectra has been described.[8] In brief, radiation from a high-pressure mercury lamp was passed through a Bausch and Lomb grating monochromator (effective band width of 6.6 mμ/mm.) and into the top of an uncovered 1-cm.^{2} silica cell held by an aluminum block in an unsilvered Pyrex dewar flask. Fluorescence was, in turn, passed through a Beckman DU monochromator to a photomultiplier tube for which the relative sensitivity at different frequencies was known. Before obtaining a spectrum, the response was adjusted using a 10^{-4} *M* solution of 2-naphthol in EPA as a reference standard of intensity. Spectra were recorded using a Beckman spectral energy recording adapter to feed a Leeds and Northrup recording potentiometer.

Low-temperature absorption spectra were obtained using a Beckman DU spectrophotometer with a similarly modified cell compartment which held two Corex cells. Spectra were obtained manually in the fashion used for normal Beckman DU operations. The two major limitations of this method were that only one sample could be run at a time, and the spectral range was limited by the short wave length cut-off of Pyrex glass (approximately 3000 Å.).

Room-temperature absorption spectra were obtained with a Beckman DU spectrophotometer. Infrared spectra were

(1) Work performed at the Massachusetts Institute of Technology.
(2) F. Hoch, *J. Chem. Educ.*, **32**, 469 (1955).
(3) E. J. Bowen and B. Brocklehurst, *J. Chem. Soc.*, 6477 (1955).
(4) E. J. Bowen and B. Brocklehurst, *Trans. Faraday Soc.*, **51**, 390 (1955).
(5) G. N. Lewis and M. Kasha, *J. Am. Chem. Soc.*, **66**, 2100 (1944).
(6) G. Porter and M. W. Windsor in "Molecular Spectroscopy," G. Snell, ed., Inst. of Petroleum, London, 1955; see also M. Kasha and S. P. McGlynn, *Ann. Rev. Phys. Chem.*, **7**, 403 (1956).
(7) D. M. Hercules and L. B. Rogers, *Spectrochim. Acta*, 393 (1959).
(8) W. E. Ohnesorge and L. B. Rogers, *ibid.*, **27** (1959).

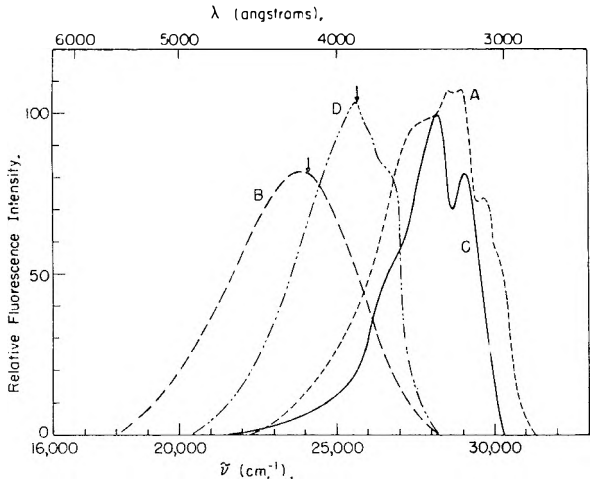

Fig. 1.—Fluorescence spectra of 1- and 2-naphthol in EPA and EAA at the temperature of liquid nitrogen: A, 1-naphthol in EPA glass; B, 1-naphthol in EAA glass; C, 2-naphthol in EPA glass; D, 2-naphthol in EAA glass.

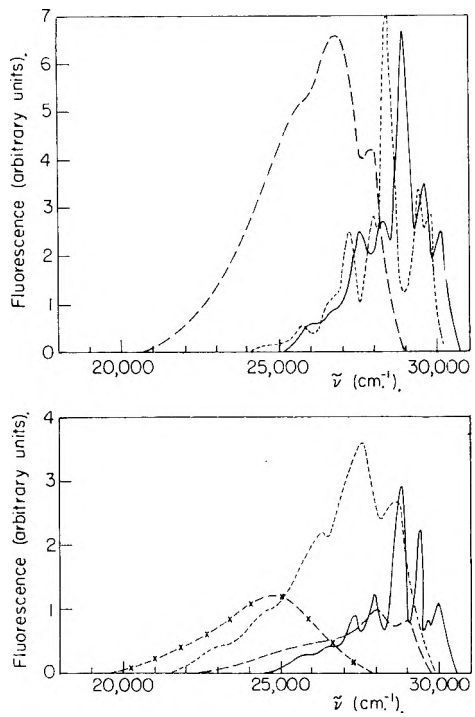

Fig. 2.—Fluorescence spectra for the naphthalenediols dissolved in EPA at the temperature of liquid nitrogen: (Upper curves): ———, 2,3-naphthalenediol; . . . . . , 1,5-naphthalenediol; – – – –, 1,3-naphthalenediol. (Lower curves): ———, 2,7-naphthalenediol; . . . . . , 1,6-naphthalenediol; – – – –, 2,6-naphthalenediol, – x – x, 1,4-naphthalenediol.

obtained in KBr pellets with a Perkin-Elmer model 21 recording spectrophotometer.

Results

Low-temperature Fluorescence Spectra.—Figure 1 shows the fluorescence spectra of 1-naphthol and 2-naphthol in EPA and EAA glasses at liquid nitrogen temperature; Figures 2 and 3 show the corresponding fluorescence spectra of some naphthalenediols. All of these spectra have been corrected for photomultiplier response, so arrows have been used to indicate the original apparent maxima where differences exist. (The room-temperature fluorescence spectra of the above compounds in EPA are not listed because they are the same as those obtained in 95% ethanol.[7]) From the red shift of the spectra in EAA compared to EPA, it is evident that the spectra in EAA arise from hemi-ionic species, while those in EPA are due to molecular species.

There are three noteworthy differences between the fluorescence spectra of the hydroxy-naphthalene compounds at room temperature and those at liquid nitrogen temperature (77°K.). At the lower temperature, general sharpening of the spectra occurred for all of the molecular species and also for certain hemi-ionic species that had broad structureless bands at room temperature. Indeed, the sharpening was extremely high in the cases of the 1,5- 2,3- and 2,7-diols for which the molecular fluorescence spectra were as sharp as the spectrum obtained for anthracene under similar conditions on the same instrument. An investigation is currently under way on an instrument of higher resolution to determine whether the fine structure of these spectra can be resolved further.

Another interesting observation was made in conjunction with fluorescence investigations of diols in EAA. At room temperature, two fluorescence spectra were observed—the molecular spectrum and the hemi-ionic spectrum produced by excited-state dissociation of the molecule.[7] This was confirmed by the fact that the absorption spectrum at room temperature was characteristic of the molecular species. At 77°K., however, only ionic emission was observed. Absorption spectra, in EAA at 77°K., were characteristic of the hemi-ionic form, indicating that the relative basicity of ammonia increased sufficiently on going from 273 to 77°K. to cause ionization of the naphthalenediols.

The last item worthy of note is the "blue shift"[9] of the fluorescence spectra on lowering the temperature to 77°K. All compounds showed a "blue shift," the smallest being about 150 cm.$^{-1}$ and the largest being about 3300 cm.$^{-1}$. In Table I, the frequency shifts for the naphthols and naphthalenediols are tabulated, along with those for anthracene. These shifts are discussed below.

Frequency Shifts and the Franck–Condon Principle.—Recent papers have dealt with the effect on molecular spectra of momentary states formed immediately on absorption of radiation ("Franck–Condon states"). Bayliss and McRae[10] interpreted certain solvent shifts by consideration of a "Franck–Condon state," ("F–C state") while Pimentel[11] considered a similar state when discussing the effect of hydrogen-bonding on molecular spectra.

The nature of the "F–C state" is depicted in Fig. 4. In brief, solvent molecules in the immediate vicinity of a solute molecule are oriented in a configuration which is energetically favorable to the ground state of the solute molecule. When such a solute molecule absorbs radiation, its charge distribution changes from that of its ground state to that of its excited state in a much shorter time than

(9) The term "blue shift" denotes a shift toward higher frequencies.

(10) N. S. Bayliss and E. G. McRae, THIS JOURNAL, **58**, 1002 (1954).

(11) G. C. Pimentel, *J. Am. Chem. Soc.*, **79**, 3323 (1957).

TABLE I

FREQUENCY SHIFTS OF FLUORESCENCE MAXIMA FOR NAPHTHOLS AND NAPHTHALENEDIOLS IN EPA AND EAA ON GOING FROM ROOM TEMPERATURE TO LIQUID NITROGEN TEMPERATURE

Compound	Form	Frequency, cm.$^{-1}$ Room temp.	Low temp.	Difference
Anthracene	Molecular	24,750	24,800	50
		25,900	26,000	100
1-Naphthol	Molecular	27,400	29,000	1600
	Hemi-ionic	20,600	23,900	3300
2-Naphthol	Molecular	27,700	28,200	500
	Hemi-ionic	23,000	25,300	2300
1,3-Naphthalenediol	Molecular	26,400	26,850	450
	Hemi-ionic	23,000	24,100	1100
1,4-Naphthalenediol	Molecular	23,550	23,850	300
1,5-Naphthalenediol	Molecular	29,450	29,600	150
		28,400	28,480	80
	Hemi-ionic	22,750	25,850	3100
1,6-Naphthalenediol	Molecular	27,350	27,550	200
	Hemi-ionic	23,000	25,500	2500
2,3-Naphthalenediol	Molecular	29,500	29,600	100
	Hemi-ionic	25,050	27,250	2200
2,6-Naphthalenediol	Molecular	27,800	27,950	150
	Hemi-ionic	22,550	25,500	2450
2,7-Naphthalenediol	Molecular	28,700	28,800	100
	Hemi-ionic	24,100	26,750	2650

is required for molecular vibration or diffusion (Franck–Condon principle). Therefore, the excited solute-molecule will be surrounded by solvent molecules in a configuration favorable to its ground state. Such a situation is referred to as the "F–C state." At room temperature, the solvent molecules reorient themselves in about 10^{-11} second to a configuration energetically favorable to the excited state of the solute molecule. Reorientation has the effect of lowering the energy of the equilibrium excited state relative to that of the F–C state. The magnitude of this effect will depend to some extent upon the difference in charge distribution between the ground and excited states of the solute molecule. Of course, it will also depend on the polar nature of the solvent. At room temperature, the lifetimes of fluorescent states, which are generally about 10^{-8} second, are much longer than the time required for solvent reorientation, so emission is observed from the equilibrium excited state rather than from the "F–C state." At 77°K., however, the reverse may be true; *i.e.*, the time required for reorientation of the solvent may be longer than the lifetime of the fluorescent excited state, and emission will be observed from the "F–C state." In short, the excited solute molecule in a rigid glass will remain in the "F–C state" until emission occurs.

Molecular electronic selection rules are such that if radiative transitions can occur between the equilibrium excited state and the ground state, transitions will be permitted between the "F–C state" and the ground state. Therefore, the emission occurring for the naphthols and naphthalenediols dissolved in EPA and EAA solvents at 77°K. must be attributed to spectroscopic combination

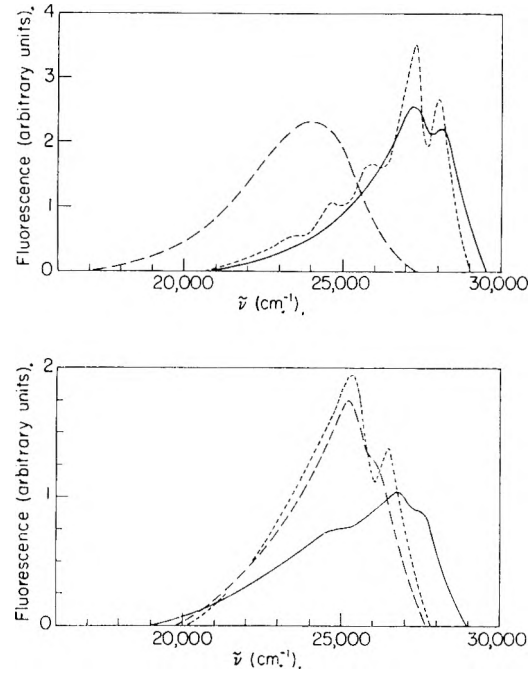

Fig. 3.—Fluorescence spectra for the naphthalenediols dissolved in EAA at the temperature of liquid nitrogen: (Upper curves): ———, 2,3-naphthalenediol; . . . . . , 1,5-naphthalenediol; – – – –, 1,3-naphthalenediol. (Lower curves): ———, 2,7-naphthalenediol; . . . . . , 1,6-naphthalenediol; – – – –, 2,6-naphthalenediol.

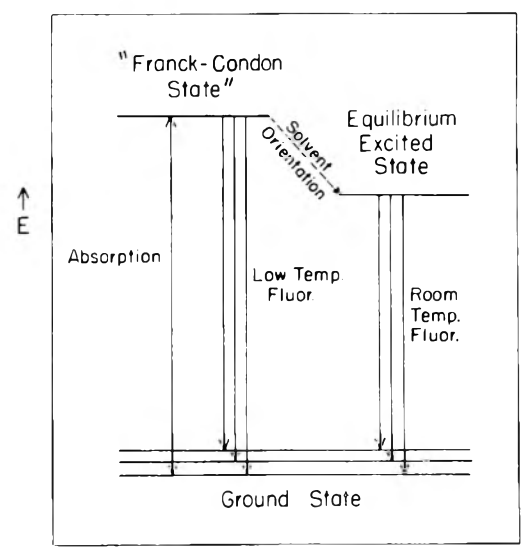

Fig. 4.—Process of luminescent emission from equilibrium excited state and "Franck–Condon state."

of the "F–C state" and the ground state. If such a mechanism is a valid explanation of low-temperature fluorescence emission, the following characteristics should be evident.

1. Because of the greater energy separation of the "F–C" and ground states compared to the equilibrium excited state and the ground state, there should be a "blue shift" of the low temperature fluorescence spectra compared to those at room temperature in the same solvent. The data of Table I support this conclusion.

2. Because the energy differences between the ground state and the F–C state should not depend

upon the rigidity of the medium, there should be no shift in absorption spectra at 77°K., compared to room temperature. Measurements of absorption spectra of a number of diols in EPA and EAA at 77°K. revealed that the spectra were substantially identical to those for the same compounds in ethanol at room temperature.[7] The largest difference observed was 100 cm.$^{-1}$, a change of questionable significance considering that the estimated standard deviation for an absorption peak was about ± 75 cm.$^{-1}$.

3. The "blue shift" should be more pronounced for a highly polar solute than for a non-polar species because the greater the polarity in the ground state, the greater the interaction with polar solvent molecules. Electronic excitation of the solute then necessitates a greater change in the orientation of the solvent "sphere," thereby increasing the energy of the "F-C state" over the equilibrium excited state.

Table I shows that only a small shift is experienced by anthracene, a relatively non-polar molecule. Molecular forms of the diols show larger shifts because they are relatively polar in their ground states and undergo a larger change in charge distribution upon excitation. However, the hemi-ionic forms are even more polar and they experience the largest shifts.

4. Because the energy difference between the "F-C state" and the equilibrium excited state depends only upon rigidity of the medium, there should be no change in frequency of the fluorescence spectra, with temperature, once the medium has become rigid. Fluorescence spectra obtained in EPA and EAA at the temperature of liquid helium (4°K.) showed no frequency shifts with respect to spectra in the same solvents at 77°K. Therefore, the "blue shifts" observed above must be due to the rigidity of the medium rather than solely to temperature differences.

Spectral Fine Structure.—Of the compounds studied in the present investigation, only 1,5-, 2,3-, and 2,7-diols showed considerable fine structure in their low-temperature molecular fluorescence, having structure equivalent to that observed for the spectrum of anthracene under the same conditions. In EAA, the hemi-ionic forms of these diols had spectra showing fine structure equivalent to that shown by other diols in the molecular form. Therefore, the oft-quoted rule that hydroxyl substitution causes smearing of fine structure, necessarily holds only at room temperature.

The reason for the sharper spectra of these three isomers is not readily apparent. It is interesting to note that if OH is treated as a single atom, the three isomers in question possess either C_{2v} or C_{2h} symmetry; the unsymmetrical diols show no degree of fine structure. Indeed, one might expect the symmetrical diols to show sharper spectra because of vibrational forbiddingness between the lowest level of the excited state and the various levels of the ground state. If this were the case, one might expect a correlation between the spacing in the low-temperature fluorescence spectra and the infrared spectra of these molecules. Such a correlation was found between the infrared spectra in KBr pellets at 298°K. and the fluorescence spectra at 77°K., as shown in Table II.

TABLE II

COMPARISON OF SPACINGS (IN CM.$^{-1}$) BETWEEN VIBRATIONAL LEVELS DETERMINED BY INFRARED AND BY FLUORESCENCE

1,5-Naphthalenediol		2,3-Naphthalenediol		2,7-Naphthalenediol	
Fluor.	Infrared	Fluor.	Infrared	Fluor.	Infrared
1425	1370	710	?	680	800
1825	1600	1385	1280	1150	1150
2740	(2 × 1370)	2040	(2 × 1150)	1620	1625
3200	3250	2810	3300	2400	?
				3100	3200

A disturbing factor in the above picture is the failure to observe fine structure in the low-temperature fluorescence spectra of the 1,4- and 2,6-diols, both of which are symmetrical. This indicates that the symmetry argument presented above is not necessarily complete and that other factors affect the appearance of fine structure.

Phosphorescence.—No strong phosphorescence was observed for any of the naphthols or naphthalenediols. (Lewis and Kasha[5] reported phosphorescence for both naphthols, but their instrument was more sensitive than the present one.) An extremely weak phosphorescence band appeared at 18,000 cm.$^{-1}$ for the ionic 1,5-diol in EAA at 77°K. Also, molecular 2,7-diol showed a very weak band in the same region. The compound exhibiting the strongest phosphorescence was the 2,5-diol in EPA and EAA at 77°K. The band was of moderate intensity and occurred in the vicinity of 19,000 cm.$^{-1}$ for both the molecular and ionic forms. The half-life of phosphorescence was about 1.5 sec. at 77°K. and 2 sec. at 4°K. None of the phosphorescence bands could be examined for structure because of the low sensitivity of the IP28 photomultiplier tube in this region of the spectrum.

Conclusions

Fluorescence spectra, in rigid solvents at 77°K., have been attributed to emission from a "Franck–Condon state" of the molecule. The suggestion has been made that fine structure in some of the spectra may be the result of molecular symmetry. Agreement has been established for spacings between corresponding peaks in the fluorescence and infrared spectra of symmetrical diols.

Acknowledgment.—The authors wish to express their appreciation to Dr. Samuel C. Collins and Mr. Robert Cavileer of the M.I.T. Cryogenics Laboratory for assistance in the liquid helium work. This work was supported in part by the Atomic Energy Commission under Contract AT(30-1)-905.

APPLICATION OF GIBBS AND GIBBS-DUHEM EQUATIONS TO TERNARY AND MULTICOMPONENT SYSTEMS

BY NEV A. GOKCEN

Contribution from the University of Pennsylvania, Philadelphia, Penna.

Received June 29, 1959

A simple method of application of the Gibbs equation for the calculation of partial molar properties of components in ternary and multicomponent systems, from the known partial molar property of one component, is presented. It is also shown that Wagner's, McKay's and Schuhmann's equations for the calculation of thermodynamic properties of ternary systems may be rederived in a systematic and concise manner either from the Gibbs free energy function or the Gibbs–Duhem equation, and that Wagner's and Schuhmann's methods consist of the integration of the same cross differential equation along the same path. In addition, these methods are extended to multicomponent systems.

The Gibbs–Duhem equation has been used for deriving the partial molar properties of ternary and multicomponent systems from the *experimental data on the partial molar property of one component.*[1–4] For this purpose, Darken[1] obtained an equation by integration to express the molar property of a multicomponent system from which the unknown partial molar properties can be obtained by differentiation. Wagner,[2] McKay[3] and Schuhmann,[4] however, first differentiated the Gibbs–Duhem equation for a *ternary* system and then integrated it to obtain the appropriate equations for the partial molar properties. The purpose of this paper is (a) to present a simple method of application of the Gibbs and Gibbs–Duhem equations for the calculation of partial molar properties of components from the known partial molar property of one component, (b) to rederive Wagner's, McKay's, and Schuhmann's equations in a simple and concise manner either by using the Gibbs free energy function or the Gibbs–Duhem relation, and to show that their equations are based on the same relationship obtained by cross differentiation, and (c) to extend their equations, as such applicable to the ternary systems, to the multicomponent systems.

Equations.—The equations used in deriving the necessary relationships are based on the following properties of exact differentials. Let u, $\mathfrak{M}$ and $\mathfrak{N}$ be some functions of x and y. An expression such as $\mathfrak{M}dX + \mathfrak{N}\,dy$ is an exact differential if it is equal to the complete differential of a function u; *i.e.*

$$du = \mathfrak{M}dx + \mathfrak{N}dy \qquad (1)$$

Since the sequence of differentiation of u with x and y is immaterial

$$\left[\frac{\partial^2 u}{\partial x \partial y} = \left(\frac{\partial \mathfrak{M}}{\partial y}\right)_x \text{ and } \frac{\partial^2 u}{\partial y \partial x} = \left(\frac{\partial \mathfrak{N}}{\partial x}\right)_y\right]$$

it can be shown readily that

$$\left(\frac{\partial \mathfrak{M}}{\partial y}\right)_x = \left(\frac{\partial \mathfrak{N}}{\partial x}\right)_y \qquad (2)$$

For any explicit function $\mathfrak{M}$ of x and y, *i.e.*, $\mathfrak{M} = f(x,y)$, complete differentiation, ($d\mathfrak{M} = (\partial\mathfrak{M}/\partial x)\,dx + (\partial\mathfrak{M}/\partial y)\,dy$), and then imposing the condition that $\mathfrak{M}$ be constant yields

$$\left(\frac{\partial \mathfrak{M}}{\partial x}\right)_y \left(\frac{\partial x}{\partial y}\right)_{\mathfrak{M}} \left(\frac{\partial y}{\partial \mathfrak{M}}\right)_x = -1 \qquad (3)$$

The preceding relationship is also applicable to the implicit function $(\mathfrak{M}, x, y) = 0$. Substitution of eq. 3 in eq. 2 gives

$$\left(\frac{\partial \mathfrak{N}}{\partial \mathfrak{M}}\right)_y = -\left(\frac{\partial x}{\partial y}\right)_{\mathfrak{M}} \qquad (4)$$

The usefulness of eq. 2 and 4 may be illustrated as follows. If $\mathfrak{N}$ is a property that cannot be as conveniently measurable as $\mathfrak{M}$, x and y, it can be obtained by integrating either eq. 2 or 4, whichever is best suited to the available data.

Equations 2 and 4, usually called cross differentials, are very useful in deriving numerous thermodynamic relations. As a classical example the derivation of the well-known Maxwell relations may be cited.

Application to Ternary Systems.—Let n_1, n_2, n_3 represent the numbers of moles of components 1, 2 and 3 in a ternary system; F the corresponding Gibbs free energy; μ_1, μ_2 and μ_3 the chemical potentials of components. The complete differential of the Gibbs free energy at constant pressure and temperature is

$$dF = \mu_1\,dn_1 + \mu_2\,dn_2 + \mu_3\,dn_3 \qquad (5)$$

where $\mu_i = \partial F/\partial n_i$ at constant pressure, temperature and $n_1, n_2, \ldots\ldots n_{i-1}$. *If the experimental values of μ_1 at various compositions are known,* and the evaluation of μ_2 and μ_3 from μ_1 is desired, then a suitable cross differential can be used. Thus imposing the restriction that n_3 be constant in eq. 5 and then applying eq. 2 yields

$$\left(\frac{\partial \mu_2}{\partial n_1}\right)_{n_2,n_3} = \left(\frac{\partial \mu_1}{\partial n_2}\right)_{n_1,n_3} \qquad (6)$$

It is important to note the symmetry of subscripts in eq. 5 and 6, and to remember that in obtaining eq. 6 for the other chemical potentials, e.g., $\partial\mu_3/\partial n_1$, all the subscripts 2 and 3 must be interchanged so that eq. 5 remains unchanged. This generalization is also applicable to all the succeeding relationships and, further, it simplifies the derivation of any equation for multicomponent systems.

Since it is more convenient to deal with mole fractions or mole ratios than with mole numbers, it is desirable to choose the independent variables

$$x = \frac{n_3}{n_1 + n_3} \qquad (7)$$

and

$$y = \frac{n_3}{n_2 + n_3} \qquad (8)$$

(1) L. S. Darken, *J. Am. Chem. Soc.*, **72**, 2909 (1950).
(2) C. Wagner, "Thermodynamics of Alloys," Addison-Wesley Press, 1952, p. 19.
(3) H. A. C. McKay, *Nature*, **169**, 464 (1952).
(4) R. Schuhmann, Jr., *Acta Met.*, **3**, 219 (1955).

where x and y may also be expressed by substituting the mole fractions for n's. The reasons for choosing x and y in this manner are that they may assume, unlike n_1/n_3 and n_2/n_3, finite values between zero and unity and that the restrictions on the left and the right sides of eq. 6 make y and x, respectively, constant. Expressing $(\partial x)_{n_2, n_3}$ and $(\partial y)_{n_1, n_3}$ by means of eq. 7 and 8, and substituting in eq. 6 and noting that for the intensive properties such as μ_2 and x, $(\partial\mu_2/\partial x)_{n_1, n_3}$ is the same as $(\partial\mu_2/\partial x)_y$, it can be shown readily that

$$\left(\frac{\partial\mu_2}{\partial x}\right)_y = \frac{y^2}{x^2}\left(\frac{\partial\mu_1}{\partial y}\right)_x \qquad (9)$$

The corresponding relation for μ_3 is obtained by interchanging the subscripts 2 and 3 first in eq. 6 and then in eq. 7 and 8 so that $z = n_2/(n_1 + n_2)$ and $(1 - y) = n_2/(n_2 + n_3)$; the result is

$$\left(\frac{\partial\mu_3}{\partial z}\right)_y = -\left(\frac{1-y}{z}\right)^2\left(\frac{\partial\mu_1}{\partial y}\right)_z \qquad (10)$$

Equation 9 or 10 may be integrated to obtain the values of μ_2, or μ_3, *e.g.*

$$\mu_2(x,y) - \mu_2(x \to 0, y) = \int_{x\to 0}^{x} \frac{y^2}{x^2}\left(\frac{\partial\mu_1}{\partial y}\right)_x dx \quad \text{(constant } y\text{)} \qquad (11)$$

In this equation μ_2 $(x\to 0, y)$ can be evaluated from the binary system "1–2," because as x approaches zero the mole fraction of "3" also approaches zero

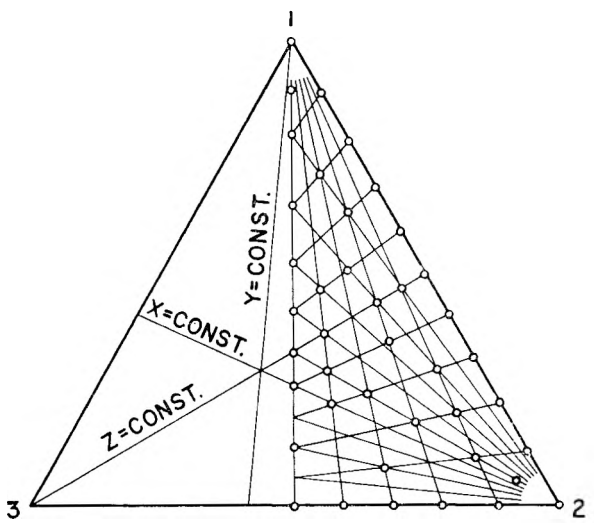

Fig. 1.—Ternary diagram with the lines of constant molar ratios. The circles represent a suggested set of compositions at which the partial molar property of one component may be determined.

and the line representing x in Fig. 1 approaches the edge "1–2." Further, for practical purposes the smallest value of y should be of the order of 0.05, and if the value of x near zero is much less than 0.05, x and y lines intersect each other very close to the apex "1"; hence the mole fraction of "2" also approaches zero. However, μ_2 approaches minus infinity with decreasing concentration of component 2 because $\mu_2 = \mu^0_2 + RT \ln \gamma_2 N_2$ where $\mu^0_2 = \mu_2$ at $\gamma_2 N_2 = 1$, and γ_2 and N_2 are the activity coefficient and mole fraction, respectively, it is preferable to substitute the excess partial molar free energy $\bar{F}_1$ (excess) $= RT \ln \gamma_1$ or merely $\ln \gamma_1$ for μ_1 in eq. 11. In the resulting equation the lower integration limit of right side is finite because of the following reasons: (a) In the range of $y \geq 0.05$, $(\partial \ln\gamma_1/\partial y)_x$ approaches zero faster than x, first, because $\ln \gamma_1$ approaches zero faster than x according to Raoult's law, and second, $\ln \gamma_1$ is a very weak function of y at a small constant value of x, and (b) consequently, $x\to 0$ need not be extremely small; therefore y^2/x^2 is finite. The reader may verify the statements in (a) and (b) by using any set of reliable data for a ternary system. The uncertainty that may be at first attributed to eq. 11 at $y/x = \infty$ and $y/x = 0/0$ really belongs to the integration of Gibbs–Duhem relation for the binary system "1–2," for, at these values of y/x, the mole fraction of component 3 is zero. In order to obviate this difficulty it has been assumed that $\ln \gamma_1 = BN^2_2$ is a well-behaving function for "1–2," *i.e.*, the parameter B is finite. (See for example Wagner for details of integration with this relationship.)

The lower limit of integration in eq. 11 may be chosen as $x = 1$ for some purposes, *e.g.*, when the uncertainty at $x \to 0$ is large, or the data in the vicinity of $N_1 \to 1$ are not adequate.

Integration of eq. 11, wherein $\ln \gamma_1$ is substituted for μ_1, is carried out along each line of constant y in the following manner. Ln γ_1 is plotted *versus* y for the various constant values of x. The slopes of the tangent line at the chosen value of y would then yield $(\partial \ln\gamma_1/\partial y)_x$. Multiplying these values with y^2/x^2 and plotting *versus* x provides another graph from which the integral can be evaluated. Equation 10 also can be evaluated in the same manner.

A considerable amount of labor in calculation can be eliminated if the activity measurements are made at or in the vicinity of the triple intersections, or at the double intersections, which are as uniformly distributed as possible. It appears that a good number of triple intersections may be achieved if all the lines from any corner divide 60° into equal angles, as for example in Fig. 1 where 60° is divided into 10 equal angles. A satisfactory investigation of a system may thus be possible with the alloys having the compositions indicated by the circular points and their symmetrical equivalents on the other half of the triangle. Although some lines may have as few as four experimental points, additional values may be obtained by short interpolation from any adjacent points. Other procedures for a satisfactory distribution of these points also may be devised.

Application to Multicomponent Systems.—Equation 5 for a multicomponent system is

$$dF = \mu_1\, dn_1 + \mu_2\, dn_2 + \mu_3\, dn_3 + \mu_4\, dn_4 \ldots + \mu_i\, dn_i \qquad (12)$$

for which eq. 6 may be written as

$$\left(\frac{\partial\mu_2}{\partial n_1}\right)_{n_2,n_3,n_4\cdots n_i} = \left(\frac{\partial\mu_1}{\partial n_2}\right)_{n_1,n_3,n_4\cdots n_i} \qquad (13)$$

The two satisfactory independent intensive variables for the conversion of eq. 13 are

$$x = \frac{n_i}{n_1 + n_2 + n_4 + \ldots\ldots n_i} \qquad (14)$$

and

$$y = \frac{n_i}{n_2 + n_3 + n_4 + \ldots n_i} \qquad (15)$$

Partial differentials of n_1 and n_2 from these equations can now be expressed in terms of x and y and then substituted into eq. 13. The result is identical with eq. 9.

The independent variables expressed by eq. 14 and 15 are not unique; any other set would yield an equation either identical with or similar to eq. 9. For example

$$x = \frac{n_4}{n_1 + n_3 + n_4 + \ldots n_i} \qquad (16)$$

and

$$y = \frac{n_4}{n_2 + n_3 + n_4 + \ldots n_i} \qquad (17)$$

would yield the same equation as 9. Nevertheless the choice of eq. 14 and 15 has the merit that these variables make the foregoing treatment general, hence also applicable to a binary system. Thus for such a system $i = 2$ and $x = n_2/n_1$; $y = 1$, or y is no longer a variable, and eq. 6 assumes the familiar form

$$d\mu_2 = -d\mu_1/x = -(n_1/n_2)\, d\mu_1$$

Representation of Multicomponent Systems.—Integration of eq. 9 or 11 for the multicomponent systems requires the representation of such systems on appropriate coördinates. In this respect, consideration of quaternary systems is helpful in devising a general method.

The tetrahedron in Fig. 2 represents a quaternary system for which eq. 14 and 15 may be written as

$$x = \frac{1}{\frac{n_1}{n_4} + \frac{n_3}{n_4} + 1} \qquad (18)$$

and

$$y = \frac{1}{\frac{n_2}{n_4} + \frac{n_3}{n_4} + 1} \qquad (19)$$

Hence, n_3/n_4 may be held constant without making x and y constants. Any constant ratio n_3/n_4 is the same as the ratio of mole fractions N_3/N_4, and in the plane 1-2-W this ratio is constant. Along any line 1-V, $(N_3 + N_4)/N_2$, hence N_4/N_2, is also constant; therefore, y is constant. Accordingly, the line 1-V represents the variation of only x along the path of integration. The plane 1-2-W may be represented on ordinary triangular coördinates as shown in Fig. 3. The corner W represents the sum of unity for $N_3 + N_4$ in the same ratio as N_3/N_4 = 4-W/3-W in Fig. 2.

For a multicomponent system, the common constant ratios for x and y are N_3/N_i, N_4/N_i, ...; therefore on the corner W, all the mole fractions other than 1 and 2 must be grouped together in proportions satisfying the constancy of such molar ratios. For each chemical potential μ_3, $\mu_4 \ldots \mu_i$, the appropriate planes of representation may be chosen in a similar manner.

Other Methods for Ternary Systems.—The cross differential of the type represented by eq. 4 may now be applied to eq. 5 to obtain

$$\left(\frac{\partial \mu_2}{\partial \mu_1}\right)_{n_2,n_3} = -\left(\frac{\partial n_1}{\partial n_2}\right)_{\mu_1,n_3} \qquad (20)$$

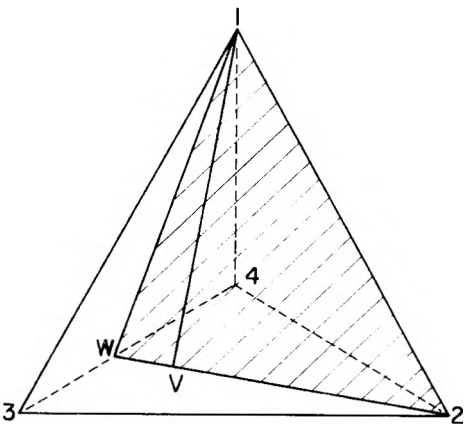

Fig. 2.—Representation of a quaternary system by means of a tetrahedron. On the intersecting plane 1-2-W, n_3/n_4 or N_3/N_4 is a constant.

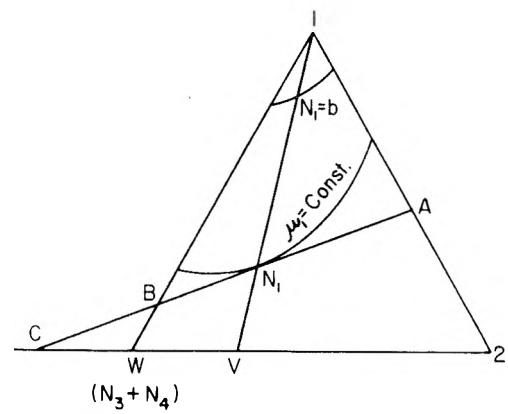

Fig. 3.—Representation of the section 1-2-W in Fig. 2 on triangular coördinates. At W, sum of the mole fractions N_3 and N_4 is unity with a constant value of N_3/N_4 throughout. Straight line A-B-C is tangent to a constant μ_1-curve at N_1.

The chemical potentials are intensive properties; hence they may be written as some functions of two independent composition variables, or any two independent mole ratios such as n_1/n_2 and n_2/n_3. It is therefore evident that the constancy of n_2 and n_3 for the left-hand side of eq. 20 is equivalent to that of n_2/n_3. Further, the elimination of n_1 and n_2 from the right-hand side of eq. 20 by means of $(\partial n_1/\partial n_2)n_3 = [\partial(n_1/n_3)/\partial(n_2/n_3)]_{n_3} = \partial(N_1/N_3)/\partial(N_2/N_3)$ yields

$$\left(\frac{\partial \mu_2}{\partial \mu_1}\right)_{n_2/n_3} = -\left(\frac{\partial \frac{N_1}{N_3}}{\partial \frac{N_2}{N_3}}\right)_{\mu_1} \qquad (21)$$

where the constancy of n_3 on the right side is now redundant since the mole fractions are independent of n_3. Equations 20 and 21 may also be obtained immediately by applying eq. 4 to the Gibbs–Duhem relation arranged in the following exact differential form

$$-d\mu_3 = \frac{n_1}{n_3} d\mu_1 + \frac{n_2}{n_3} d\mu_2 \qquad (22)$$

It is interesting to note that eq. 20 is also applicable to binary systems, since in this case $n_3 = 0$, and μ_1 is a function of either N_1 or N_2; hence when μ_1 is held constant, N_1 and N_2 are also held constant,

and as a result $N_1/N_2 = n_1/n_2$ becomes constant; consequently $(\partial n_1/\partial n_2)_{\mu_1 \text{ or } N_1}$ reduces to N_1/N_2. It will be seen later that eq. 20 is thus completely general, and applicable to any system of any number of components.

In Wagner's treatment the independent variables expressing the chemical potentials are chosen[5] as N_1 and $y = N_3/(N_2 + N_3)$. Elimination of N_2 and N_3 from eq. 21 by using y and $N_1 + N_2 + N_3 = 1$, then noting that the constancy of n_2/n_3 is the same as that of y, and multiplying both sides with $(\partial\mu_1)_y$ gives

$$(\partial\mu_2)_y = \frac{y}{(1-N_1)^2}\left(\frac{\partial N_1}{\partial y}\right)_{\mu_1}(\partial\mu_1)_y - \frac{N_1}{1-N_1}(\partial\mu_1)_y \tag{23}$$

Dividing both sides with $(\partial N_1)_y$ and comparing the first term on the right with eq. 3 shows that

$$\left(\frac{\partial N_1}{\partial y}\right)_{\mu_1}\left(\frac{\partial\mu_1}{\partial N_1}\right)_y = -\left(\frac{\partial\mu_1}{\partial y}\right)_{N_1}$$

Substitution of this relation in eq. 23 yields Wagner's equation; *i.e.*

$$\left(\frac{\partial\mu_2}{\partial N_1}\right)_y = -\frac{y}{(1-N_1)^2}\left(\frac{\partial\mu_1}{\partial y}\right)_{N_1} - \frac{N_1}{1-N_1}\left(\frac{\partial\mu_1}{\partial N_1}\right)_y \tag{24}$$

The corresponding relation for μ_3 may be obtained either by starting with eq. 20 for μ_3, or eliminating $\partial\mu_2$ from eq. 24 by means of eq. 22; *however a much shorter procedure consists of interchanging the subscripts 2 and 3 in eq. 24 and in y, and then observing that y and dy become 1 − y and −dy, and the last term remains unchanged.*

The foregoing method makes quite evident the necessity of choosing y as one of the variables because y must be any function of the mole ratio n_2/n_3 which appears on the left-hand side of eq. 21 so that the constancy of y is the same as that of n_2/n_3. Therefore, any simple variable satisfying this condition may be selected; *e.g.*, N_3/N_2, or $N_2/(N_2 + N_3)$, the latter simply being equal to $1 - y$ used in deriving eq. 24. However it is convenient to use an expression for y which, unlike N_3/N_2, should remain finite for all values of N_2 and N_3. This provides the justification for Wagner's choice of $N_3/(N_2 + N_3)$. Further when $y = 0$, eq. 24 becomes applicable to the binary system 1-2, and when $y = 1$ the relationship for $(\partial\mu_3/\partial N_1)_y$ becomes the expression for the binary system 1-3.

The foregoing treatment shows that eq. 24 may be obtained in a simple and concise manner by applying the cross differential 4 either to eq. 5 or to eq. 22 and then substituting the variables N_1 and y, and utilizing eq. 3. Further it is seen that eq. 20 is also that obtained by Schuhmann[4]; hence both methods are based on the same cross-differential. It is interesting to note that eq. 20 has been presented earlier by McKay[3] but not applied to the ternary systems as shown by Schuhmann.

McKay has applied eq. 6 to the ternary solutions of limited concentrations by using the molar ratios $r_{13} = n_1/n_3$ and $r_{23} = n_2/n_3$, or the corresponding molalities as the independent variables. His integral equation is equivalent to that obtained by substituting $(\partial r_{13})_{n_2, n_3}$ and $(\partial r_{23})_{n_1, n_3}$ for the corresponding partial differentials of n_1 and n_2 in Eq. 6 and integrating from $r_{13} = 0$ to a finite value at constant r_{23}. However, it was pointed out in connection with eq. 7 and 8 that $r_{13} = N_1/N_3$ and $r_{23} = N_2/N_3$ become infinite when the mole fraction of component 3 becomes zero. Nevertheless McKay's equation is simple and very useful for the particular solutions wherein *the molar ratios are finite.*[6] An excellent summary of his method and the correlation of various thermodynamic properties of strong electrolytes are presented by Harned and Owen.[7]

In their succeeding treatments, Wagner used an analytical integration of eq. 24, and Schuhmann, a direct graphical integration of eq. 20; in both methods the integration is along the path of constant y (or N_2/N_3), and from N_1 in the vicinity of unity to any value of N_1.

Multicomponent Systems.—The foregoing relationships may now be extended to the multicomponent systems in the following manner. Imposing the restrictions that n_3, $n_4 \ldots n_i$ be constant, and then applying eq. 4 to eq. 12 yields

$$\left(\frac{\partial\mu_2}{\partial\mu_1}\right)_{n_2,n_3,n_4\ldots n_i} = -\left(\frac{\partial n_1}{\partial n_2}\right)_{\mu_1,n_2,n_4\ldots n_i} \tag{25}$$

The molar restrictions outside the parentheses may be divided by n_3, and, in view of the arguments concerning similar restrictions on eq. 21 concerning the redundancy of n_3, it is seen readily that

$$\left(\frac{\partial\mu_2}{\partial\mu_1}\right)_{\frac{n_2}{n_3},\frac{n_3}{n_4},\ldots\frac{n_{i-1}}{n_i}} = -\left(\frac{\partial\frac{N_1}{N_3}}{\partial\frac{N_2}{N_3}}\right)_{\mu_1,\frac{n_3}{n_4},\ldots\frac{n_{i-1}}{n_i}} \tag{26}$$

This relationship may also be obtained by writing the Gibbs–Duhem equation in the same form as in eq. 22, but grouping all the additional terms with $d\mu_3$ on the left and then applying eq. 4 with the same restrictions.

Integration of eq. 26 may be carried out either by an analytical or a graphical method. Application to a quaternary system is sufficient to illustrate the pertinent methods and extend them to multicomponent systems.

Analytical Method.[8]—Wagner's method of integration *for the ternary systems* may now be extended to the quaternary systems. *The important point in this procedure is the choice of independent variables so that the necessary equation for integration remains as simple as that for a ternary system.* The method by which Wagner's equations are rederived in this paper is valuable in making this choice. Thus, for eq. 26, the variable y, that must be chosen with N_1, should be such that (i) when y and n_3/n_4 are held constant, it must satisfy the restriction that n_2/n_3 is also a constant, that (ii) it should be finite for all values of mole fractions, and that (iii) when $y = 0$ it should preferably

(5) Wagner assumed that μ_2 was known instead of μ_1. Interchanging the subscripts 1 and 2 would make his equations identical with those in this paper.

(6) H. A. C. McKay, *Trans. Faraday Soc.*, **49**, 237 (1953).

(7) H. S. Harned and B. B. Owen, "Physical Chemistry of Electrolytic Solutions," Third Edition, Reinhold Publ. Corp., New York, N. Y., 1958, p. 620.

(8) The term analytical here refers to the general method and the final integral equation, though some of the terms in Wagner's integral may be evaluated either graphically or analytically. In contrast Schuhmann's integration by the method of tangent intercepts is purely graphical.

reduce the system into a binary system so that the resulting equation would assume the simple form. The relationship satisfying these conditions is

$$y = \frac{N_3 + N_4}{N_2 + N_3 + N_4} \qquad (27)$$

It is therefore obvious that for a multicomponent system the numerator in this equation contains i − 2 terms, and the denominator i − 1 terms. In the tetrahedron of Fig. 2, representing a quaternary system, the plane 1-2-W is that on which $n_4/n_3 = N_4/N_3 = a$ is a constant. Along any line from 1 to any point V, the ratio n_2/n_3 is also a constant. Integration of eq. 26 will therefore be carried out along the line 1-V on which there is one independent composition variable, *i.e.*, N_1. From eq. 27, and from $N_4/N_3 = a$, and $\Sigma N_i = 1$, it follows that

$$N_2 = (1 - N_1)(1 - y), \text{ and } N_3 = y\,\frac{1 - N_1}{1 + a}$$

Elimination of N_2 and N_3 from eq. 26 by means of the preceding relations gives

$$\left(\frac{\partial \mu_2}{\partial \mu_1}\right)_{y,\,\frac{n_3}{n_4}} = \frac{y}{(1 - N_1)^2}\left(\frac{\partial N_1}{\partial y}\right)_{\mu_1,\,\frac{n_3}{n_4}} - \frac{N_1}{1 - N_1} \qquad (28)$$

This relationship is the same as eq. 23 except for the additional restriction n_3/n_4 on both sides; hence it may be transformed into the form represented by eq. 24, *i.e.*

$$\left(\frac{\partial \mu_2}{\partial N_1}\right)_{y,\,\frac{n_3}{n_4}} = -\frac{y}{(1 - N_1)^2}\left(\frac{\partial \mu_1}{\partial y}\right)_{N_1,\,\frac{n_3}{n_4}} - \frac{N_1}{1 - N_1}\left(\frac{\partial \mu_1}{\partial N_1}\right)_{y,\,\frac{n_3}{n_4}} \qquad (29)$$

Integration of this equation is then carried out at constant y and n_3/n_4 from $N_1 \rightarrow 1$ to N_1 as outlined by Wagner. It is interesting to note that the integration of the left-hand side of eq. 29, after multiplication by ∂N_1, is

$$\int_{N_1 \rightarrow 1}^{N_1} d\mu_2 = \mu_2\left(y, \frac{n_3}{n_4}, N_1\right) - \mu_2\left(y, \frac{n_3}{n_4}, N_1 \rightarrow 1\right), \quad (\text{constant } y \text{ and } n_3/n_4) \qquad (30)$$

where the lower integration limit μ_2 (y, n_3/n_4, $N_1 \rightarrow 1$) is, in view of vanishing concentrations of all solutes, the same as μ_2 ($N_1 \rightarrow 1$) and may be obtained from the binary system 1-2 as pointed out by Wagner.

For a multicomponent system, obviously there are additional restrictions n_4/n_5, etc. on both sides of eq. 29. The relationships for other chemical potentials can be obtained by interchanging the subscripts in eq. 29 and in the parameter y.

Graphical Method.—Equation 25 may be integrated for a quaternary system by extending the graphical method for the ternary systems described by Schuhmann. The integration path is again represented by the constant ratios n_2/n_3 and n_3/n_4, *i.e.*, along 1-V in Figs. 2 and 3. Thus, the integration from $N_1 = b$ to N_1, for a quaternary system is given by

$$\mu_2\left(y, \frac{n_3}{n_4}, N_1\right) - \mu_2\left(y, \frac{n_3}{n_4}, N_1 = b\right) = -\int_b^{N_1}\left(\frac{\partial n_1}{\partial n_2}\right)_{\mu_1, n_3, n_4} d\mu_1, \left(\text{constant } y, \frac{n_3}{n_4}\right) \qquad (31)$$

In a quaternary system, constant μ_1 is represented by an appropriate surface in the tetrahedron; the intersections of 1-2-W with the constant μ_1-surfaces are represented by the constant μ_1 curves. The intercept of the tangent $N_1 - A$ with the edge 1–2 yields, on the basis of the expansion of the right hand side of eq. 26 and the values of $\partial N_1/\partial N_3$ and $\partial N_2/\partial N_3$ from the triangle, the relations

$$\left(\frac{\partial n_1}{\partial n_2}\right)_{\mu_1, n_3, n_4} = \frac{N_3\,\partial N_1/\partial N_3 - N_1}{N_3\,\partial N_2/\partial N_3 - N_2} = \frac{2 - A}{1 - A} = \left(\frac{N_1}{N_2}\right)_{\text{on } 1-2} \qquad (32)$$

The right-hand side of eq. 31 may thus be evaluated graphically from a plot of the values of eq. 32, *vs.* μ_1 at constant n_2/n_3 and n_3/n_4.

For the chemical potential μ_3, eq. 26 assumes the form

$$\left(\frac{\partial \mu_3}{\partial \mu_1}\right)_{\frac{n_2}{n_3},\,\frac{n_3}{n_4}} = -\left(\frac{\partial \frac{N_1}{N_2}}{\partial \frac{N_3}{N_2}}\right)_{\mu_1,\,\frac{n_3}{n_4}} \qquad (33)$$

Hence the evaluation of $\partial n_1/\partial n_3$ must be made on a plane containing the edge 1–3 and intersecting 2–4, so that the restriction of constant n_2/n_3 and n_3/n_4 on the right side is satisfied.

For a ternary system, *i.e.*, $N_4 = 0$ in Fig. 3, the intercepts A, B and C are such that from the implicit function $f(n_1, n_2, n_3)\mu_1 = 0$ and from eq. 3 they satisfy the relationship

$$\left(\frac{\partial n_1}{\partial n_2}\right)_{\mu_1, n_3}\left(\frac{\partial n_2}{\partial n_3}\right)_{\mu_1, n_1}\left(\frac{\partial n_3}{\partial n_1}\right)_{\mu_1, n_2} = \frac{2 - A}{1 - A}\,\frac{W - C}{2 - C}\,\frac{1 - B}{W - B} = -1 \qquad (34)$$

where all segments, except $W - C$ outside the triangle, are positive. (See also Schuhmann.) Equation 34 constitutes a statement of Menelaus and Ceva theorems in geometry.[9] In a quaternary system the intercepts B and C are of no useful significance since they do not correspond to any relevant partial derivative.[10] The relationships parallel to eq. 34 may be obtained by means of the intercepts of a plane tangent to the constant μ_1-surface in the quaternary tetrahedron. In view of the fact that μ_1 is a homogeneous function of zeroth degree in the number of moles of all components, there are four possible implicit functions, and their derivatives in the form represented by eq. 3, *i.e.*

$f_1(n_1, n_2, n_3)_{\mu_1, n_4} = 0$, (35)

$$\left(\frac{\partial n_1}{\partial n_2}\right)\left(\frac{\partial n_2}{\partial n_3}\right)\left(\frac{\partial n_3}{\partial n_1}\right) = -1 \qquad (35a)$$

$f_2(n_1, n_2, n_4)_{\mu_1, n_3} = 0$, (36)

$$\left(\frac{\partial n_1}{\partial n_2}\right)\left(\frac{\partial n_2}{\partial n_4}\right)\left(\frac{\partial n_4}{\partial n_1}\right) = -1 \qquad (36a)$$

$f_3(n_1, n_3, n_4)_{\mu_1, n_2} = 0$, (37)

$$\left(\frac{\partial n_1}{\partial n_3}\right)\left(\frac{\partial n_3}{\partial n_4}\right)\left(\frac{\partial n_4}{\partial n_1}\right) = -1 \qquad (37a)$$

$f_4(n_2, n_3, n_4)_{\mu_1, n_1} = 0$, (38)

$$\left(\frac{\partial n_2}{\partial n_3}\right)\left(\frac{\partial n_3}{\partial n_4}\right)\left(\frac{\partial n_4}{\partial n_2}\right) = -1 \qquad (38a)$$

(9) O. Veblen and J. W. Young, "Projective Geometry," Ginn and Co., New York, N. Y., 1918, p. 89.

(10) A somewhat parallel situation occurs when a partial molar property $\bar{G}_1$ is obtained from a plot of the molar property G *vs.* N_1. In a binary system the intercepts are G_1 and G_2, in a ternary system when G at a chosen ratio N_2/N_3 is plotted *vs.* N_1, the intercept at $N_1 = 1$ is G_1 but the intercept at $N_1 = 0$ is not a useful thermodynamic property (see eq. 1 in Darken).

In eq. 35a–38a, μ_1 is held constant throughout, and the n's other than those in the parentheses are also held constant. A tetrahedron has six edges, each of which, or its extension in space, is generally intersected by a plane. The intercepts of the tangent plane with six sides must obey these equations. Multiplying eq. 35a–38a and taking the square root gives

$$\left(\frac{\partial n_1}{\partial n_2}\right)\left(\frac{\partial n_2}{\partial n_3}\right)\left(\frac{\partial n_3}{\partial n_4}\right)\left(\frac{\partial n_4}{\partial n_1}\right) = \pm 1 \qquad (39)$$

where the derivatives in parentheses represent the molar ratios at the intercepts on the four edges 1–2, 2–3, 3–4 and 4–1, respectively. Equation 39 represents the extension of Menelaus and Ceva theorems[9] to an equal tetrahedron. Since there are four chemical potentials, there are three more sets of equations similar to eq. 35–38 and three more relations represented by eq. 39.

Another interesting relationship may be derived by the application of eq. 3 to

$$f_6(\mu_1, n_2, n_3)_{n_1, n_4} = 0 \qquad (40)$$
$$f_6(n_1, \mu_2, n_3)_{n_2, n_4} = 0 \qquad (41)$$
$$f_7(n_1, n_2, \mu_3)_{n_3, n_4} = 0 \qquad (42)$$

and multiplying the results side by side and then cancelling out the six derivatives by means of the relationships similar to eq. 13

$$\left(\frac{\partial \mu_1}{\partial n_2}\right)_{n_1, n_3, n_4} = \left(\frac{\partial \mu_2}{\partial n_1}\right)_{n_2, n_3, n_4}$$
$$\left(\frac{\partial n_3}{\partial \mu_1}\right)_{n_1, n_2, n_4} = \left(\frac{\partial n_1}{\partial \mu_3}\right)_{n_2, n_3, n_4}$$
$$\left(\frac{\partial \mu_2}{\partial n_3}\right)_{n_1, n_2, n_4} = \left(\frac{\partial \mu_3}{\partial n_2}\right)_{n_1, n_3, n_4}$$

The result is

$$\left(\frac{\partial n_2}{\partial n_3}\right)_{\mu_1, n_1, n_4}\left(\frac{\partial n_3}{\partial n_1}\right)_{\mu_2, n_2, n_4}\left(\frac{\partial n_1}{\partial n_2}\right)_{\mu_3, n_3, n_4} = -1 \qquad (43)$$

Numerous similar relations may be obtained by following a consistent pattern of sequence in the subscripts of variables as shown in eq. 40–42.

Division of eq. 43 by eq. 35a yields

$$\left[\left(\frac{\partial n_1}{\partial n_2}\right)_{\mu_3}\left(\frac{\partial n_2}{\partial n_1}\right)_{\mu_1}\right]_{n_3, n_4}\left[\left(\frac{\partial n_1}{\partial n_3}\right)_{\mu_2}\left(\frac{\partial n_3}{\partial n_1}\right)_{\mu_2}\right]_{n_2, n_4} = 1 \qquad (44)$$

Again numerous such relations readily may be obtained. The quantities in the first set of brackets in the preceding equation refer to the tangents on the constant n_3/n_4 plane, and the others to those on the constant n_2/n_4 plane.

In eq. 43 and 44 all tangents intersect one another at the point where the constant μ_1, μ_2 and μ_3-surfaces also intersect one another at one point. For a ternary system $n_4 = 0$ and all tangents are on the same plane.

Equations 34–44 are not essential but they are useful in checking the results of the graphical calculations within the accuracy with which the tangents can be drawn.

It should be pointed out that the methods of the author, Wagner, McKay and Schuhmann, are also applicable to any extensive property $G = f(n_1, n_2 \ldots\ldots)$, because the complete differential of such a function has the form represented by eq. 12.

Consistency of Calculations.—Internal consistency of calculations can be tested as follows. For a ternary system the complete differential of the molar free energy, $F_m = \mu_1 N_1 + \mu_2 N_2 + \mu_3 N_3$, is

$$dF_m = (\mu_1 - \mu_3)\,dN_1 + (\mu_2 - \mu_3)dN_2 \qquad (45)$$

Cross differentiation of this equation, as shown by eq. 2, gives

$$\left[\frac{\partial(\mu_1 - \mu_3)}{\partial N_2}\right]_{N_1} = \left[\frac{\partial(\mu_2 - \mu_3)}{\partial N_1}\right]_{N_2} \qquad (46)$$

For the activity coefficients, this equation becomes

$$\left(\frac{\partial \ln \frac{\gamma_1}{\gamma_3}}{\partial N_2}\right)_{N_1} = \left(\frac{\partial \ln \frac{\gamma_2}{\gamma_3}}{\partial N_1}\right)_{N_2} \qquad (47)$$

In all the foregoing methods, the integration was carried out along the lines from the corners intersecting the opposing edge of the triangle. Equation 47, however, represents the partial differentials along the lines parallel to the edges; hence it is a useful relationship in testing the internal consistency of the calculations by plotting $\ln(\gamma_1/\gamma_3)$ *vs.* N_2 along a chosen line of constant N_1, parallel to 2–3, and likewise plotting $\ln(\gamma_2/\gamma_3)$ *vs.* N_1 at constant N_2; at the intersection of constant N_1 and N_2 lines the slopes must be equal. An alternative method consists of the graphical integration of eq. 47 along the entire length of either a constant N_1 or a constant N_2 line.

A relationship similar to eq. 47 for the section of the quaternary system shown in Fig. 3 may be obtained by using the constant ratio $N_4/N_3 = a$, and $\Sigma N_i = 1$ to eliminate N_3 and N_4, and then by expressing the coefficients of dN_1 and dN_2 in eq. 45.

Acknowledgment.—This research has been sponsored by the U. S. Atomic Energy Commission, Contract AT (30-1) 1976.

THE EQUILIBRIUM ADSORPTION OF HETEROGENEOUS POLYMERS

By E. R. Gilliland and Edgar B. Gutoff[1]

Chemical Engineering Department, Massachusetts Institute of Technology, Cambridge, Mass.

Received July 20, 1959

The isotherm for the equilibrium adsorption of heterogeneous polymers for dilute solutions at their theta temperatures has been solved. Depending on the parameters, preferential adsorption of either the high or low molecular weight species is possible. High heats of adsorption and low heats of solution would tend to aid preferential adsorption of the high molecular weight species. Applications to polymer fractionation and determination of molecular weight distribution curves are discussed. On reduction to isotherms of homogeneous polymers, these equations show that at low concentrations the amount adsorbed per unit adsorbent is proportional to solution concentration. At higher concentrations, an asymptote is approached. With higher molecular weights, the asymptote is approached at lower concentrations. Normally, adsorption should decrease with temperature, but the opposite can occur. It is hoped this work will aid in explaining the mechanisms of filler reinforcement, and of adhesion.

The adsorption of polymers onto solid surfaces plays an important role in the reinforcing action of fillers and in the bonding action of adhesives. Any preferential adsorption that takes place would affect the mechanism of these actions, and could also be used as a means of fractionating a polymer or of determining its molecular weight distribution. Now various workers[2-5] studying solution adsorptions offer conflicting evidence as to preferential adsorption. In one case, the adsorption of the higher molecular weights was found to be so preferential that the technique can be used to determine apparently reliable molecular weight distribution curves.[6] It is the purpose of this paper to obtain a theoretical expression for the adsorption of heterogeneous polymers, and thus indicate just what affects preferential adsorption. The general lines of treatment of Simha, *et al.*,[7] for homogeneous polymers have been followed.

Tending to hold an adsorbed polymer molecule on a surface is an attractive energy expressed as a heat of adsorption; however, an entropy effect also acts on the molecule. It is not known, in general, whether or not adsorption leads to an increased number of configurations in the polymer-adsorbent-solvent system. Attractions between polymer and solvent molecules will manifest themselves in reducing the effective heat of adsorption, thus reducing adsorption; interactions between polymer molecules must also be considered.

If the number of adsorbed segments per polymer molecule increases with molecular weight, then it appears that preferential adsorption of the high molecular weight species is favored by high heats of adsorption, low heats of solution, and an increase with molecular weight in the number of configurations of the adsorbed phase relative to the solution phase.

The actual adsorption equation is found by equating partial free energies of the adsorbed and dissolved molecules, which are equal at equilibrium. However, only the two-dimensional case (all the segments of the adsorbed molecule lie on the surface) has been solved, although a crude model is presented for the general case. As will be explained in a later section, Simha's original simplification of the configurational entropy for the three-dimensional case is not used, as it leads to untenable conclusions.

A. Solution Phase

For the solution, the lattice treatment as described by Flory[8] is used. The free energy change upon mixing pure amorphous polymer and pure solvent is

$$\frac{\Delta F_{\text{mix}}}{kT} = N_0 \ln v_0 + \sum_t U_t \ln v_t + K_2 N_0 v_2 \quad (1)$$

where

ΔF_{mix} = the free energy change of mixing pure amorphous polymer with solvent, ergs
k = Boltzmann's constant, 1.37×10^{-16} erg/°K.
T = absolute temp., °K.
N_0 = no. of solvent molecules
v_0 = vol. fraction of solvent
v_t = vol. fraction of polymer of size t
v_2 = total vol. fraction of polymer
U_t = no. of polymer molecules of size t
t = no. of segments per polymer chain, with a segment being equal in vol. to a solvent molecule
K_2 = a measure of nearest neighbor interactions for the solvent with polymer segments, free energy divided by kT

Differentiating with respect to U_t, the number of polymer molecules of size t, yields for the partial free energy of solution

$$\frac{\partial \Delta F_{\text{mix}}}{kT \partial U_t} = \ln v_t - t + 1 + v_2 t - v_t + K_2 t (1 - v_2)^2 \quad (2)$$

B. Partial Free Energy of the Adsorbed Polymer, and the Equilibrium Equation

I. Two-Dimensional Case.—Every segment of an adsorbed molecule lies on the surface.

If A_t molecules of size t are adsorbed, and the heat of adsorption is H ergs per segment, then the change in free energy due only to heat effects from pure amorphous polymer to adsorbed polymer is

$$\frac{\Delta F^{(H)}}{kT} = -\sum_t A_t t H/kT \quad (3)$$

and the partial free energy is

$$\frac{\partial \Delta F^{(H)}}{kT \partial A_t} = -tH/kT \quad (4)$$

(1) Ionics, Incorporated, Cambridge 42, Massachusetts.

(2) (a) M. A. Golub, personal communication (April 13, 1954); (b) *J. Polymer Sci.*, **11**, 583 (1953).

(3) I. M. Kolthoff and A. Kahn, THIS JOURNAL, **54**, 251 (1950).

(4) I. Landler, *Compt. rend.*, **225**, 234 (1947).

(5) A. J. Poynton, Sc.D. Thesis, Chem. Eng. Dept., M.I.T. (Oct. 1952).

(6) E. R. Gillil and E. B. Gutoff, *J. Appl. Polymer Sci.*, in press; also E. B. Gutoff, Sc.D. Thesis, Chem. Eng. Dept., M.I.T. (Sept. 1954).

(7) R. Simha, H. L. Frisch and F. R. Eirich, THIS JOURNAL, **57**, 584 (1953); also *J. Chem. Phys.*, **21**, 365 (1953).

(8) P. J. Flory, "Principles of Polymer Chemistry," Cornell Univ. Press, Ithaca, N. Y., 1953.

Analogously to eq. 1, for the mixing of the adsorbed molecules with the surface

$$\frac{\Delta F^{(a)}}{kT} = N_s(1-\phi)\ln(1-\phi) + \sum_t A_t \ln \phi_t + N_s K_1 \phi(1-\phi) \quad (5)$$

where

N_s = no. of adsorption sites, each site being large enough to accommodate one segment
K_1 = a parameter expressing nearest neighbor interaction free energy, divided by kT, for the adsorbed segments
ϕ = fraction of adsorption sites occupied by polymer
ϕ_t = fraction of adsorption sites occupied by polymer molecules of size t

Now

$$\phi_t = A_t t/N_s \quad (6)$$

$$d\phi_t = (t/N_s)dA_t \quad (7)$$

$$\phi = \sum_t \phi_t \quad (8)$$

$$\partial\phi/\partial\phi_t = 1 \quad (9)$$

$$\frac{\partial \Delta F}{\partial A_t} = \frac{t}{N_s}\frac{\partial \Delta F}{\partial \phi} \quad (10)$$

Therefore

$$\frac{\partial \Delta F^{(a)}}{KT\partial A_t} = t[K_1 - 2K_1\phi - 1 - \ln(1-\phi)] + \ln(A_t t/N_s) + 1 \quad (11)$$

On adsorption, there is a change in the vibrational, rotational and translational motions of the molecule. For the adsorbed molecule, these motions would be based on the unit mer, and so the partition function per mer, j_a, should be independent of molecular weight. For the dissolved molecule bulk translational motion is relatively small, and the partition function per unit mer, j_u, should also be predominantly independent of molecular weight.[9]

The free energy change $F^{(j)}$ due to changes in the vibrational, rotational and translational motions of the molecule on adsorption would therefore be

$$\frac{\Delta F^{(j)}}{kT} = -\sum_t A_t t \ln j_a + \sum_t A_t t \ln j_u \quad (12)$$

$$\frac{\partial \Delta F^{(j)}}{kT\partial A_t} = -t\ln\frac{j_a}{j_u} \quad (13)$$

Equilibrium conditions can now be found by equating the partial free energy of the polymer in solution to that of the adsorbed polymer. Thus, after first making the approximations that in dilute solutions

$$v_t \approx tU_t/N_0 \quad (14)$$

$$1 - v_t \approx 1 \quad (15)$$

$$1 - v_u \approx 1 \quad (16)$$

equating eq. 2 to the sum of eq. 4, 11 and 13 yields

$$\frac{A_t}{U_t} = \frac{N_s}{N_0}\left[\frac{j_a}{j_u}(1-\phi)e^{[H/kT + K_2 - K_1(1-2\phi)]}\right]^t \quad (17)$$

Equation 21 indicates that preferential adsorption of either the high or the low molecular weight species can take place, depending on whether or not the terms in the brackets are greater or less than unity. Preferential adsorption of the higher molecular weights is favored by high heats of adsorption.

II. Three-Dimensional Case.—An adsorbed molecule in this, the general case, would have some segments unadsorbed and some segments on the surface of the adsorbent. Let p be the probability that any segment of an adsorbed molecule is itself adsorbed, or on the surface. This probability p is a function of the molecular weight of the polymer, and according to Simha, *et al.*,[7] it is a small number and inversely proportional to $t^{1/2}$, or the square root of the number of segments.

Equations 4 and 13 now become

$$\frac{\partial \Delta F^{(H)}}{kT\partial A_t} = -ptH/kT \quad (18)$$

$$\frac{\partial \Delta F^{(j)}}{kT\partial A_t} = -pt\ln\frac{j_a}{j_u} \quad (19)$$

It is difficult to formulate the expression for the mixing of the adsorbed segments with the adsorption sites and for the mixing of the unadsorbed segments of the adsorbed molecules with the solvent. Simha, *et al.*, in their first paper[7] assumed that the groups of adjacent adsorbed segments can take any unoccupied position on the surface, thus neglecting restrictions in position caused by the unadsorbed segments connecting the adsorbed ones. This oversimplification would require preferential adsorption of the low molecular weight species,[6] even though Frisch and Simha[10] say that high molecular homogeneous polymers are adsorbed to a greater extent than the low molecular weight species. A crude model easily can be set up and solved, however, and the results are in qualitative agreement with the two-dimensional case.

Let us use a lattice treatment, similar to the ones already used, but with the qualifications that the lattice includes the surface sites and extends into the solvent such a distance that the fraction of occupied sites in the lattice is equal to the fraction of occupied sites on the surface. Adsorbed polymer would then be defined as any polymer segments included in this lattice. Analogously to eq. 1, the free energy change upon adding pure amorphous polymer to this lattice, neglecting the restriction that every polymer molecule in this lattice must have at least one segment on the surface, can be found as

$$\frac{\Delta F^{(a)}}{kT} = N_0'\ln(1-\phi) + \sum_t A_t \ln\phi_t + (N_0' + \sum_t A_t t)K_1'\phi(1-\phi) \quad (20)$$

where

N_0' = the no. of solvent molecules in this lattice
$N_0' + \sum_t A_t t$ = the total number of sites
K_1' = parameter expressing nearest neighbor interactions

Now

$$\phi_t = A_t pt/N_s \quad (21)$$

$$\phi = \sum_t \phi_t = (pt/N_s)\sum_t A_t t \quad (22)$$

(9) The entropy of fusion per unit mer for polymers has only a slight dependence on molecular weight, as is shown in Flory's book,[8] pp. 573–574.

(10) H. L. Frisch and R. Simha, THIS JOURNAL, **58**, 507 (1954).

$$\phi = \frac{\sum_t A_t t}{N_0' + \sum_t A_t t} \quad (23)$$

$$N_0' = \sum_t A_t t \left[\frac{1-\phi}{\phi}\right] = (N_s/p)(1-\phi) \quad (24)$$

Therefore

$$\frac{\Delta F^{(a)}}{kT} = (N_s/p)(1-\phi)\ln(1-\phi) + \sum_t A_t \ln \phi_t + (N_s/p)K_1'\phi(1-\phi) \quad (25)$$

Noting that

$$\frac{\partial \Delta F}{\partial A_t} = \frac{pt}{N_s}\frac{\partial \Delta F}{\partial \phi} \quad (26)$$

then

$$\frac{\partial \Delta F^{(a)}}{kT\partial A_t} = t[K_1' - 2K_1'\phi - 1 - \ln(1-\phi)] + \ln A_t pt/N_s + 1 \quad (27)$$

Equation 27, for this crude three dimensional case, is identical to equation 11, for the two-dimensional case.

Utilizing equations 14, 15 and 16 and equating equation 2 to the sum of equations 18, 19 and 27 yields the desired result.

$$\frac{A_t}{U_t} = \frac{N_s}{N_0 p}[(1-\phi)(j_a/j_u)^p e^{[pH/kT + K_2 - K_1'(1-2\phi)]}]^t \quad (28)$$

Equation 28, the crude general case, is identical to equation 17, the two-dimensional case, except for the addition of several p's. According to Simha, *et al.*,[7] p, the probability that a given segment of an adsorbed molecule lies on the surface of the adsorbent, is inversely proportional to the molecular weight, or

$$p = q/t^{1/2} \quad (29)$$

Equation 28 would then become

$$\frac{A_t}{U_t} = \frac{N_s t^{1/2}}{N_0 q}[(1-\phi)e^{K_2 - K_1'(1-2\phi)}]^t[(j_a/j_u)e^{H/kT}]^t q^{t^{1/2}} \quad (30)$$

As before, preferential adsorption of either the high or low molecular weight species is possible. In both cases, high heats of adsorption favor preferential adsorption of the higher molecular weight species. The conclusions are unchanged even if the probability function p is independent of molecular weight, or if it is inversely proportional to molecular weight.

C. Discussion and Conclusions

These equations, expressing preferential adsorption in terms of the properties of the polymer-adsorbent-solvent system, were derived under the assumptions: (1) the same lattice treatment holds for the polymer, the solvent, and the adsorption sites; (2) the concentration of polymer in the solution phase is low; (3) the solution is at its theta temperature, and K_2 is therefore equal to 0.5[8]; (4) the adsorbed segments are not mobile; (5) for the general (three-dimensional) case, the adsorbed layer may be represented by a lattice of such a thickness that the average polymer density is equal to the density on the surface, and that the polymer distribution is uniform within this lattice.

The good qualitative agreement between the cruder three-dimensional solution and the more accurate two-dimensional picture only indicates internal consistency in these models.

I. Molecular Weight Distribution and Polymer Fractionation.—Equations 17 and 28 or 30 indicate that, under certain conditions, adsorption is so preferential that polymers can be fractionated or molecular weight distribution curves determined directly[6] by simple equilibrium experiments. Thus, when the terms raised to the "t"th power are greater than unity, the high molecular weight species will be very preferentially adsorbed. It is not now yet possible to predict in what systems this will occur, outside of the fact that it is more likely to occur with a good adsorbent. Molecular weight distribution curves of several polyisobutenes and a butyl rubber have been determined[6] by this technique using benzene as the solvent and the furnace black Vulcan R as adsorbent.

II. Homogeneous Polymers–Adsorption Isotherms.—For a homogeneous polymer

$$\phi = A_t pt/N_s \quad (31)$$

where $p = 1$ for the two-dimensional case, and is equal to $q/t^{1/2}$ in the general case.[7] The solution concentration c in grams per 100 ml. is

$$c = \frac{U_t M_p \rho_0 (100)}{N_0 M_0} \quad (32)$$

where

M_p = molecular weight of a polymer segment
M_0 = molecular weight of the solvent
ρ_0 = density of the solvent

Equation 17 for the two-dimensional case now reduces to

$$\phi\left[\frac{e^{K_1(1-2\phi)}}{1-\phi}\right]^t = c\left\{\frac{M_0}{100 M_p \rho_0}[(j_a/j_u)e^{(H/kT+K_2)}]^t\right\} \quad (33)$$

For the general case, equation (28) reduces to

$$\phi\left[\frac{e^{K_1'(1-2\phi)}}{1-\phi}\right]^t = c\left\{\frac{M_0}{100 M_p \rho_0}\left[\frac{j_a}{j_u}e^{(pH/kT+K_2)}\right]^t\right\} \quad (34)$$

Equations 33 and 34 should be compared with other proposed isotherms[11-13] for the adsorption of homogeneous polymers. In the only three-dimensional study, Frisch and Simha[11] used the method of Guggenheim and Miller to avoid the restriction they were forced to neglect in their earlier work (see above). Their new isotherm is identical with the others,[12,13] when the molecule lies completely on the surface, and so will be used for comparison. This isotherm is

$$\phi\frac{[1-2(t-1)\phi/ts]^{pt-1}}{pt(1-\phi)^{pt}} = \frac{c\,M_0}{100 M_p \rho_0}\frac{[j_a e^{H/kT}]^{pt}\rho_s\left[1-\frac{2t-1}{tz}\right]^{t(z-2)/2+1}}{(2\pi mkT/h^2)^{3/2}\overline{V}} \quad (35)$$

where

$$\rho_s = 1/2s(s-1)^{pt-2}(z-1)^{t(1-p)}$$

(11) H. L. Frisch and R. Simha, *J. Chem. Phys.*, **27**, 702 (1957).
(12) E. L. Mackor and J. H. van der Waals, *J. Colloid Sci.*, **7**, 535 (1952).
(13) L. Sarolea, *Bull. acad. roy. Belg. (Classe Sci.)*, **5°** Series 40, 1131 (1954).

s is the surface coördination number, z is the bulk coördination number, and the partition function for the dissolved molecules is assumed to be equal to that of an independent, non-localized system.

It is to be noted that this isotherm differs from the authors', in that (a) on the left-hand side the authors have the factor $(1 - \phi)$ raised to the "t" power, while Frisch and Simha have it raised to the "pt" power. For the two-dimensional case, this difference, of course, disappears; (b) Frisch and Simha have a "pt" in the denominator of the left-hand side, which the authors do not; (c) Frisch and Simha have assumed for the partition function of the dissolved molecule that it undergoes translational motion as a whole while the authors, though not specifying the exact form, believe that the contribution of each mer to the partition function is almost independent of the total chain length.

The other differences, depending on geometrical factors and interaction parameters, are believed relatively negligible.

The fraction of surface covered, ϕ, is proportional to the weight of polymer adsorbed. Equations 33 and 34 indicate that at low adsorption values, when $(1 - \phi)$ is close to unity, the amount adsorbed is proportional to the solution concentration. As the concentration is further increased, the amount adsorbed reaches an asymptotic value. Equilibrium experiments on polyisobutene confirm this.[6] As the molecular weight, or t, increases, the asymptotic adsorption value will be reached faster. This, too, has been confirmed experimentally.[6]

The terms in the large brackets constitute the adsorption constant, and are a function of the system and the temperature. This constant, and thus the adsorption, should decrease with temperature because of the $e^{pH/kT}$ term, although the behavior of several of the terms is difficult to predict. This temperature behavior has been observed.[6] However, other workers[14] have noticed an increase in adsorption with temperature, but they were not working at the theta temperature, and also may not have reached equilibrium conditions.

As long as the ratio of partition functions for the adsorbed to unadsorbed molecules is sufficiently large that $(j_a/j_u)^p e^{pH/kT+K_2}$ is greater than unity, the adsorption constant and the amounts adsorbed should increase with molecular weight. This too has been confirmed experimentally.[6]

III. Rubber Reinforcement and Adhesion.—In the case of rubber reinforcement and adhesion, the system consists only of polymer and adsorbent, with no solvent present. Now the equations derived here apply only to dilute solution, and cannot be expected to hold when no solvent is present. However, if preferential adsorption takes place from solution, it should also take place from the bulk phase. And if preferential adsorption of the high molecular weights takes place, then the less viscous lower molecular weights would remain unadsorbed, and tend to plasticize the rubber-filler mix or the thin-bonded joint. It is hoped that this work will help lead to a more complete understanding of such polymer–solid interfaces.

Acknowledgment.—The authors acknowledge with thanks the comments and suggestions of Prof. Walter Stockmayer and Prof. Robert Ullman.

(14) E. Jenkel and B. Rumbach, *Z. Elektrochem.*, **55**, 612 (1951).

THE ENTROPY OF MELTING OF SOME LINEAR POLYMERS

BY HOWARD W. STARKWEATHER, JR., AND RICHARD H. BOYD

Polychemicals Department, E. I. du Pont de Nemours & Company, Du Pont Experimental Station, Wilmington, Delaware

Received July 23, 1959

The entropy of melting is discussed for three substantially linear polymers—polyethylene, polytetrafluoroethylene and an acetal polymer, polyoxymethylene. This entropy is considered to be made up of several parts: first, the entropy due to the increase in volume on melting; second, the entropy due to the appearance of long-range disorder, ΔS_D, which is present in all liquids; third, the entropy of rotational isomerism, ΔS_R, *i.e.*, that due to the ability of polymer molecules to have many configurations in the melt through rotation about skeletal bonds. The entropy due to volume change is calculated from experimental data for the three polymers discussed. ΔS_R is calculated theoretically from a lattice model that includes the effects of hindered rotation and steric hindrance. The variation in the entropy of melting among the polymers considered is found to be determined by the energy differences between the rotational isomers. Finally, ΔS_D is found by difference to be comparable to the entropy of melting of the simplest low molecular substances.

The entropy of melting of a crystalline polymer can be calculated from calorimetric data or from the dependence of melting point on pressure, diluents, or the mole fraction of a single crystallizable comonomer.[1,2] The total gain in entropy, ΔS_m, is equal to the ratio $\Delta H_m/T_m$, where ΔH_m is the gain in enthalpy at the melting point and T_m is the melting point of the homopolymer in degrees Kelvin. Throughout this discussion, the thermodynamic quantities will be based on a mole of atoms in the primary chain.

The entropy of melting of simple low molecular weight compounds is considered to be due largely to the destruction of long-range order (excluding those compounds which experience the onset of free rotation at melting) and to a lesser extent to a change in the vibrational state of the system. However, this process is not well understood in detail, principally because of the lack of an adequate theory of the liquid state. In polymers, there is an additional contribution due to rotational isomerism.

(1) P. J. Flory, "Principles of Polymer Chemistry," Cornell Univ. Press, Ithaca, N. Y., 1953, Chapters 12 and 13.

(2) L. Mandelkern, *Chem. Revs.*, **56**, 903 (1956).

By this we mean the ability of a single molecule to assume a number of configurations in the melt through rotation about the skeletal bonds. Furthermore, the entropy associated with rotational isomerism may well be sensitive to the structure of the chain because of energy differences between stable rotational positions. This is the thermodynamic "chain stiffness" effect. The contribution of rotational isomerism (without taking into account energy differences between rotational isomers) has been considered by many as the principal contribution to the entropy of melting of polymers.[1-4]

In this paper, we will discuss the entropy of melting of linear polymers by arbitrarily dividing it into separate contributions from each of the foregoing effects. Although this division is not exact and the contribution from long-range disorder is at least as unamenable to theoretical treatment as in simple liquids, such a discussion is of value. We feel that it gives an interpretation of melting behavior which is shown to be physically reasonable. It examines the features of melting which are peculiar to polymers and especially shows how chain structure influences melting behavior through chain stiffness.

The effects of vibrational differences between liquid and crystal should be minimized and theoretical treatment of rotational isomerism facilitated if the melting process is treated as though it took place at constant volume. The change in entropy due to the expansion at melting can be calculated from experimental data and considered as a separate contribution to the entropy of melting containing most of the vibrational effects and presumably some of the long-range disorder effects.

There are sufficient experimental data to discuss the above effects for three substantially linear polymer chains, polyethylene, polytetrafluoroethylene and an acetal polymer, polyoxymethylene. The possible effects of small amounts of branching have been neglected.

Entropy of Melting at Constant Volume.—The increase in entropy due to the increase in volume at the melting point is [1,2]

$$\left(\frac{\partial P}{\partial T}\right)_v \times \Delta V_m \qquad (1)$$

where ΔV_m is the increase in volume per chain atom. According to the Clapeyron equation, the dependence of the melting point on the pressure is given by

$$\frac{dT_m}{dP} = \frac{\Delta V_m}{\Delta S_m} \qquad (2)$$

If ΔS_m, $(\partial P/\partial T)_v$, and either dT_m/dP or ΔV_m are known, it is possible to calculate the entropy of melting at constant volume, $(\Delta S_m)_v$, from the equation

$$(\Delta S_m)_v = \Delta S_m - \left(\frac{\partial P}{\partial T}\right)_v \times \Delta V_m = \Delta S_m \left[1 - \left(\frac{\partial P}{\partial T}\right)_v \times \frac{dT_m}{dP}\right] \qquad (3)$$

The quantities $(\partial P/\partial T)_v$ and dT_m/dP can be calculated from pressure–volume–temperature relationships just above the melting point such as those presented by Lupton.[5] The experimental quantities are given in Table I.

TABLE I

ENTROPY OF MELTING AT CONSTANT VOLUME

	Polyethylene	Polytetrafluoroethylene	Polyoxymethylene
T_m, °C.	137[6]	327[7]	180[8]
ΔH_m, cal./mole	940[6]	685[5]	890[8]
ΔS_m, cal./deg. mole	2.29	1.14	1.96
$(\partial P/\partial T)_v$, atm./deg.	6.98[5]	2.16[9]	8.91[9]
ΔV_m, cc./mole	3.07[5,6]		
dT_m/dP, deg./atm.		0.154[10]	0.044[9]
$\Delta S_m - (\Delta S_m)_v$, cal./deg. mole	0.52	0.38	0.77
$(\Delta S_m)_v$, cal./deg. mole	1.77	0.76	1.19

Since the experimental uncertainty in $(\Delta S_m)_v$ may be about 5%, the value for polyethylene calculated here is in good agreement with the estimate of 1.84 cal./deg. mole by Quinn and Mandelkern.[6] It is interesting to note that the entropy of melting corrected to constant volume is less for polyoxymethylene than for polyethylene and least for polytetrafluoroethylene. The portion of the total entropy of melting which is attributable to the change of volume, $\Delta S_m - (\Delta S_m)_v$, is greatest for polyoxymethylene.

Rotational Isomerism.—In our treatment we will use a lattice model like that used by Flory[11] for semi-flexible polymer chains but modified[12] to take into account the principal next nearest neighbor steric hindrance by a method described by Lifson.[13] The allowed configurations of the chains are restricted to those resulting from the three stable positions of rotation about each bond. Some previous treatments of the lattice theory[1] have considered the number of positions for the placement of a segment to be one less than the lattice coördination number of 8 to 12. However, that procedure merely represents an attempt to overcome the restrictiveness of the lattice treatment for describing a liquid. In our treatment we take this failing of lattice theories into account completely empirically by later adding a constant term to the entropy corresponding to the disruption of the lattice in the melt (see next section). The effect of the principal steric hindrance, the interference occurring when two adjacent bonds are in *gauche* configurations of the opposite sense has been also included.

(3) S. Mizushima, "The Structure of Molecules and Internal Rotation," Academic Press, New York, N. Y., 1954, p. 110.

(4) R. H. Aranow, L. Witten and D. H. Andrews, THIS JOURNAL, **62**, 812 (1958).

(5) J. M. Lupton, 134th Meeting of the American Chemical Society, Chicago, September, 1958.

(6) F. A. Quinn, Jr., and L. Mandelkern, *J. Am. Chem. Soc.*, **80**, 3178 (1958).

(7) W. E. Hanford and R. M. Joyce, *ibid.*, **68**, 2082 (1946).

(8) ΔH_m calculated from the over-all heat of melting of 42.7 cal./g. from the calorimetric measurements of J. Holmes quoted by W. H. Linton and H. H. Goodman, *J. Appl. Polymer Sci.*, **1**, 179 (1959), and the per cent. crystallinity just below the melting point (72% at 170°) reported by C. F. Hammer, T. A. Koch and J. F. Whitney, *ibid.*, **1**, 169 (1959).

(9) J. M. Lupton, private communication.

(10) P. L. McGeer and H. C. Duus, *J. Chem. Phys.*, **20**, 1813 (1952).

(11) P. J. Flory, *Proc. Roy. Soc.* (*London*), **234A**, 60 (1956).

(12) We are grateful to Dr. Flory for showing us how this modification could be made.

(13) S. Lifson, *J. Chem. Phys.*, **30**, 964 (1959).

In the crystalline state in polyethylene or polytetrafluoroethylene, all of the bonds are in the *trans* configuration (T). On melting, a fraction, f, of the bonds assume a *gauche* configuration (G) for which the energy is higher than that of the *trans* configuration by an amount, ϵ. This is actually a free energy, but it will be assumed that the difference in entropy between the *trans* and *gauche* configurations is negligible. Each *gauche* bond has a choice of two configurations, (G or G′) except that when one *gauche* bond follows another, the second one can have only one configuration. That is, the sequences TT, TG, TG′, GT, G′T, GG, G′G′ are allowed but GG′ and G′G are not. The GG′ sequence exists in cyclohexane, because of the strength of the primary bonds. This is the "pentane interference" which has been discussed by Taylor.[14] This modification to prohibit G,G′ sequences does not alter the resulting free energy greatly over the Flory[11] treatment. However, it seems worthwhile to show its effect in a treatment of restricted rotation especially since it may be done easily. The portion of the partition function of the liquid due to rotational isomerism can be written as a combination of the Flory[11] and Lifson[13] theories as

$$Q_L = \frac{1}{n_2!}\prod_{i=1}^{n_2}\left\{\left[\frac{n - xi}{n - 2(x-1)i/Z}\right]^x \left[\sum_{a,b}\cdots\sum_{w,x} g_{ab}{}^1 g_{bc}{}^2 \cdots g_{vw}{}^{x-2} g_{wx}{}^{x-1}\right]\right\} \quad (4)$$

where

n = total no. of bonds, $n_2(x-1)$
x = no. of chain atoms per molecule
n_2 = no. of polymer molecules
Z = coördination number

The Huggins[15] expression for the occupational probability of the lattice sites has been used in the term in the first set of brackets. It is only slightly dependent on the value of Z which we will arbitrarily take equal to 8.

Then $g_{m,n}{}^j$ is the statistical weight for the jth link (in the ith molecule) being in the conformation, n (= G, T or G′) when the preceding link is in the state, m (= G, T or G′) and $g_{mn}{}^j$ is independent of j and is given by

g_{mn} =

n/m	G	T	G′
G	g	g	0
T	1	1	1
G′	0	g	g

where $g = \exp[-\epsilon/kT]$. The second bracket of equation 4 may be reduced[13] to λ^{x-1} where λ is the largest eigenvalue of the matrix $[g_{mn}]$. Therefore

$$\lambda = [(g+1)/2][1 + \sqrt{1 + 4g/(g+1)^2}] \quad (5)$$

The free energy change per bond due to rotational isomerism follows from equation 4

$$\Delta A_R = -RT\{(Z/2 - 1)\ln(1 - 2/Z) + \ln\lambda\} \quad (5a)$$

for $Z = 8$

$$\Delta A_R = RT\{0.86 - \ln\lambda\} \quad (5b)$$

The free energy change due to rotational isomerism in the melt, ΔA_R, can be thought of as made up of two parts: first, the change due to disordering the polymer molecules without regard to the lattice and the attendant possibility that a lattice site is occupied (the term involving λ in eq. 5b). Secondly, that due to the decrease in entropy on packing the molecules on the lattice (the term $0.86RT$) which is independent of g.

Thus

$$\Delta A_R = \Delta A_g + 0.86RT \quad (5c)$$

where

$$\Delta A_g = -RT\ln\lambda \quad (6)$$

The equilibrium fraction of bonds in the *gauche* configuration, f, is found by the following method. The average total number of such bonds times the energy increase per bond ϵ is equal to the total average energy of rotational isomerism or

$$nf\epsilon = E = \frac{\partial(\Delta A_R/T)}{\partial(1/T)} \quad (7)$$

From this it follows that

$$f = \mathrm{d}\ln\lambda/\mathrm{d}\ln g \quad (8)$$

The dependence of f on ϵ/kT is shown in Fig. 1. The relationship from ref. 11 which does not include the effect of "pentane interference" is also shown. ΔS_g is found by differentiating ΔA_g with respect to T

$$\Delta S_g = -\frac{\partial\Delta A_g}{\partial T} = R[\ln\lambda + f\epsilon/kT] \quad (9)$$

When $\epsilon = 0$, $f = 0.5$, and $\Delta S_g = R\ln(1+\sqrt{2})$. If there were no restrictions on the sequences of rotational isomers, ΔS_g would be $R\ln 3$ when $\epsilon = 0$. This means that "pentane interference" reduces ΔS_g by 0.43 cal./deg. mole in agreement with Taylor,[14] who used a different method for the case of $\epsilon = 0$. The effect of "pentane interference" on ΔS_g decreases as ϵ/RT increases.

If the energy of the *gauche* configuration is lower than the *trans* form as in polyoxymethylene,[16] the equations are the same except that ϵ now has a negative value.

The dependence of ΔS_g on ϵ/kT is shown in Fig. 2. The upper curve is the comparable relation from ref. 11 which does not include the effect of "pentane interference." The experimental values shown are discussed in the next section.

Estimates of ϵ, the difference in potential energy between the *gauche* and *trans* forms, vary from 450[17] to 800[14] cal./mole for linear hydrocarbons. Since $T_m = 410°$K., ϵ/kT is between 0.55 and 0.98. From equation 8, f is 0.37 ± 0.04.

In the case of polytetrafluoroethylene, the value of ϵ is much less certain. Flory[17] has shown how ϵ can be calculated from the dependence of the force exerted by a rubber at constant strain on temperature.

$$\left[\frac{\partial\ln(f/T)}{\partial T}\right]_{P,\alpha} = -\frac{\partial\ln\overline{r_0^2}}{\partial T}$$

(14) W. J. Taylor, *J. Chem. Phys.*, **16**, 257 (1948).
(15) M. L. Huggins, *Ann. N. Y. Acad., Sci.*, **43**, 1 (1942).
(16) T. Uchida, Y. Kurita and M. Kubo, *J. Polymer Sci.*, **19**, 365 (1956).
(17) P. J. Flory, C. A. Hoere and A. Ciferri, *ibid.*, **34**, 337 (1959).

where r_0 is the end-to-end distance of the molecule. Using the data of Nishioka and Watanabe[18] on the modulus of polytetrafluoroethylene above the melting point, it was calculated that $[\partial \ln(f/T)/\partial T]_{P,\alpha}$ is 5.25×10^{-3}/°C. For polyethylene,[17] this quantity is 1.1×10^{-3}/°C. This shows that the differences in energy favoring the extended *trans* configuration is much greater for polytetrafluoroethylene. For a *trans–gauche* model

$$\left[\frac{\partial \ln (f/T)}{\partial T}\right]_{P,\alpha} = \frac{\epsilon/kT}{1 + g/2}$$

From this equation, $\epsilon = 4300$ cal./deg. for polytetrafluoroethylene. Since this value for ϵ is similar to the barrier to internal rotation in hexafluoroethane,[19] it seems possible that the rotational potential energy function may have a shoulder rather than a minimum corresponding to each *gauche* form. This type of function has been discussed by Taylor.[14]

Since $T_m = 600$°K., $\epsilon/kT = 3.6$ and $f = 0.05$ if $\epsilon = 4300$ cal./mole, $\Delta S_g = 0.46$ cal./deg. mole. Since this treatment is based on rotational potential function with three minima, it may not be strictly applicable to polytetrafluoroethylene. However, it is clear that the chains in polytetrafluoroethylene have a much greater stiffness, or more precisely a greater persistence of direction, than the chains in polyethylene.

Polyoxymethylene differs from the other two polymers in that the energy of the *trans* form is higher than that of the *gauche* form by 1740 cal./mole.[16] Since T_m is 453°K., ϵ/kT is -1.93. Application of equations 8 and 9 reveals that f is 0.81 and ΔS_g is 1.19 cal./deg. mole of atoms in the chain. Because of the ease of formation of trioxane, the importance of pentane interference in polyoxymethylene might be questioned. However, the stabilization due to primary bond formation in the ring compound makes it difficult to make conclusions from this type of evidence. If the effects of pentane interference are omitted from the treatment, f is 0.93 and ΔS_g is 1.79 cal./deg. mole. Uchida and co-workers[16] concluded that GG′ sequences should be excluded for this polymer. The three chain structures are summarized for comparison with respect to rotational isomerism in Table II.

TABLE II

ROTATIONAL ISOMERISM

	Polyethylene	Polytetrafluoroethylene	Polyoxymethylene
Higher energy rotational isomer	*gauche*	*gauche*	*trans*
Energy difference between rotational isomers, ϵ, cal./mole	450–800	4300	−1740
Melting point, T_m, °C.	137	327	180
ϵ/kT_m	0.55–0.98	3.6	−1.93
Fraction of *gauche* isomers on melting, f	0.33–0.41	0.05	0.81
ΔS_g, cal./deg. mole	1.59–1.70	0.46	1.19
ΔS_D, cal./deg. mole	1.78–1.89	2.01	1.71

(18) A. Nishioka and M. Watanabe, *J. Polymer Sci.*, **24**, 298 (1957).
(19) E. L. Pace and J. G. Aston, *J. Am. Chem. Soc.*, **70**, 566 (1948).

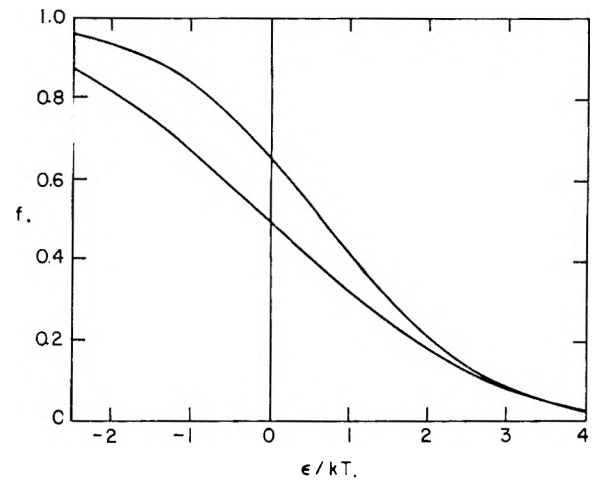

Fig. 1.—Dependence of the fraction of *gauche* isomers on the energy difference between *gauche* and *trans* configurations (upper curve neglecting "pentane interference").

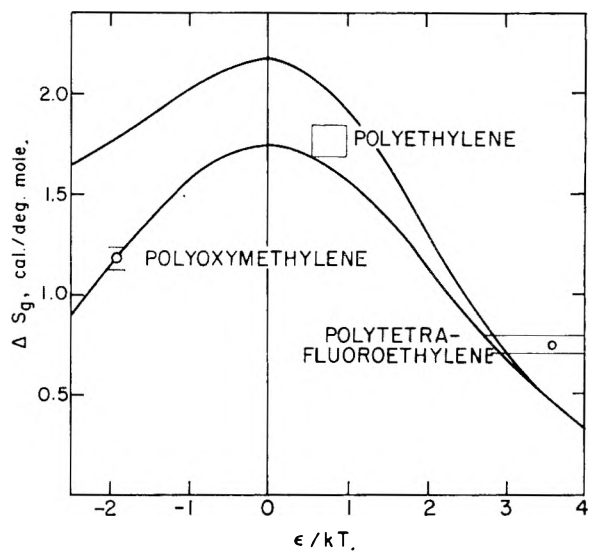

Fig. 2.—Dependence of the entropy of melting on the energy difference between *gauche* and *trans* configurations. (Curve for ΔS_g calculated from equations 8 and 9 upper curve neglecting "pentane interference." Points for experimental values of $(\Delta S_m)_v$, the entropy of melting at constant volume.)

Comparison with Experiment.—The total entropy of melting at constant volume we consider to be made up of the entropy calculated from the lattice model (rotational isomerism) plus an additional contribution common to all liquids arising from the over-restrictiveness of a lattice treatment which we call the long-range disorder contribution.[20] That is

$$(\Delta S_m)_v = \Delta S_R + \Delta S_D = (\Delta S_g - 0.86R) + \Delta S_D \qquad (10)$$

where the rotational isomerism contribution is written as the sum of two terms as indicated in the

(20) It has been proposed by M. V. Volkenshtein [*J. Tech. Physics (U.S.S.R.)*, **26**, 2287 (1956)] that the onset of torsional vibrations at the melting point constitutes the major portion of the melting entropy. However, there seems to be no reason why there should be torsional vibrations in the melt and none in the solid, particularly if the process is carried out at constant volume as discussed here.

preceding section (the gain in entropy due to rotational isomerism without regard to the lattice interferences, ΔS_g, and the decrease due to packing on the lattice). The first term can vary between zero and $R \ln (1 + \sqrt{2})$ depending on "chain stiffness" (ϵ/kT). Due to the lack of an adequate theory of liquids, there is at present no good way of estimating ΔS_D except to say that we would expect it to be similar to the corresponding quantity in low molecular weight liquids and to be insensitive to structure and the energy differences between rotational isomers, that is, of the order of R cal./deg. mole of chain atoms. For instance, in calculations for 12 metals, Oriani[21] found ΔS_D to be between 0.97 and 1.8 cal./deg. mole and 9 of the 12 fell between 1.25 and 1.56. Thus we may expect the last two terms to be largely compensatory and that the first term will be important in determining the melting entropy. Consultation with Fig. 2 shows this to be the case. The experimental values of $(\Delta S_m)_v$ are plotted against the experimental values of ϵ/kT as rectangles indicating the uncertainties discussed in the preceding section (an arbitrary $\pm 5\%$ error is assumed in the experimental values of $(\Delta S_m)_v$). These values fall reasonably close to the curve for ΔS_g indicating that ΔS_g determines the variations in the melting entropy with molecular structure. It is shown in Table II that the values of ΔS_D calculated by difference from equation 10 lie between 1.7 and 2.0 cal./deg. mole for all three polymers.

For polyethylene at the melting point, the temperature is high enough to overcome much of the effect of energy differences between the *trans* and *gauche* states on the melting entropy. This forms the basis for the $R \ln 3$ entropy (ΔS_g for $\epsilon = 0$, without "pentane interference") that has been used by some[3,4] workers for hydrocarbons. However, it seems unlikely that this holds down to the temperatures of the melting points of the lower hydrocarbons which this is supposed to represent.

Polyoxymethylene, the acetal polymer, and especially polytetrafluoroethylene show the effect of reduced melting entropy due to the energy differences between *trans* and *gauche* states. This shows explicitly how the very high melting point of polytetrafluoroethylene is due to the "chain stiffness" effect.

(21) R. A. Oriani, *J. Chem. Phys.*, **19**, 93 (1951).

KINETICS OF $NOUF_6$ HYDROLYSIS IN AIR[1]

BY F. E. MASSOTH,[2] L. R. SWANEY AND W. E. HENSEL, JR.[2]

Goodyear Atomic Corporation, Portsmouth, Ohio

Received August 14, 1959

The kinetics of $NOUF_6$ hydrolysis in air has been determined from 68 to 231°. The results indicate that the hydrolysis reaction follows parabolic kinetics throughout. Variation of the rate constants with temperature showed an Arrhenius dependency when corrected for increasing concentration of hydrated water at lower temperatures. The activation energy for the diffusion process was determined to be 10.9 kcal. per mole of $NOUF_6$.

Reaction between uranium hexafluoride and nitric oxide gas results in the formation of a solid compound having the formula $NOUF_6$.[3] This material undergoes slow hydrolysis in air to form one-half mole of uranyl fluoride and one-half mole of uranium tetrafluoride per mole of $NOUF_6$. The reaction can be represented by the equation

$$NOUF_6 + H_2O \longrightarrow {}^1/_2UO_2F_2 + {}^1/_2UF_4 + NOF + 2HF$$

The uranium products will be hydrated to an extent depending on the temperature.[4,5] All other products are gases[6] and the over-all reaction results in a weight loss. Hence, the kinetics of the reaction can be conveniently studied by following the change in weight with time.

The factors which govern the kinetic laws for gas–solid reactions are: the chemical reaction at the phase boundary, the rates of diffusion of reactants and products, and the rates of nucleation and recrystallization.[7] Usually the diffusion process is slower than the others and is rate-determining. The mathematical form of the kinetic law describing this process is dependent upon the particle geometry. The mathematical treatment of reaction kinetics for cubic particles was discussed previously.[8,9] In the present article, this concept will be extended to disc-like particles.

The mathematical treatment of disc-shaped particles is similar to that used by Farrar and Smith[10] for spherical particles. The following assumptions are made: (1) the $NOUF_6$ consists of roughly disc-shaped particles; (2) the depth of the particle is small compared to its radius; (3) the product film is uniform in thickness; (4) the external dimensions of the particle remain constant throughout the reaction.[11] The fraction converted is obtained from

(1) This work performed under Contract AT-(33-2)-1 with the United States Atomic Energy Commission.

(2) Southwest Research Institute, San Antonio, Texas.

(3) P. R. Ogle, J. R. Geichman and S. S. Trond, "Reactions of Molybdenum, Tungsten, and Uranium Hexafluorides with Nitrogen Compounds. I. Nitrous and Nitric Oxides," (GAT-T-552 Rev. 1), Presented at the American Chemical Society Meeting, Atlantic City, Sept., 1959.

(4) J. J. Katz and E. Rabinowitch, "The Chemistry of Uranium," Part I, Chapter 16, McGraw-Hill Book Co., Inc., New York, N. Y., 1951.

(5) A. V. Grosse, "A New Crystalline Hydrate of Uranium Tetrafluoride, $2UF_4 \cdot 5H_2O$ and its Dehydration to Anhydrous Uranium Tetrafluoride," Columbia University, March, 1941, (A-99).

(6) Nitrosyl fluoride may hydrolyze in air but the products are gaseous. N. V. Sidgwick, "The Chemical Elements and their Compounds." Vol. I, Oxford University Press, New York, N. Y., 1950, p. 701.

(7) S. J. Gregg, "Surface Chemistry of Solids," Chap. 14, Reinhold Publ. Corp., New York, N. Y., 1951.

(8) F. E. Massoth and W. E. Hensel, Jr., THIS JOURNAL, **62**, 479 (1958).

(9) F. E. Massoth and W. E. Hensel, Jr., *ibid.*, **63**, 697 (1959).

(10) R. L. Farrar, Jr., and H. A. Smith, *ibid.*, **59**, 763 (1955).

(11) Assumption (4) would be expected to hold for the reaction under question for the following theoretical reason: there is no gain or loss

experimentally determined quantities by the formula

$$F = \frac{W_0 - W}{W_0\left(\frac{M_p}{M_0} - 1\right)} = \frac{\Delta w}{\Delta w_f} \qquad (1)$$

where W_0 is the initial weight of sample, W is the weight at time t, M_p and M_0 are the molecular weights of the products and of the starting material, respectively, and Δw and Δw_f, are the loss in weight of the sample at time t and at the end of reaction, respectively.

The volume of reactant, v, left at any time is related to the fraction converted and the initial particle volume, v_0, for an average particle by

$$v = (1 - F)v_0 \qquad (2)$$

The volumes of unreacted and initial particles are also given by

$$v = \pi r^2 d \text{ and } v_0 = \pi r_0^2 d_0 \qquad (3)$$

where r and r_0 are the radii of unreacted and initial particles, respectively, and d and d_0 are the depths of unreacted and initial particles, respectively. If the radius is much greater than the depth, a given extent of reaction will have a more significant effect upon the depth than upon the radius since reaction proceeds through the particle to an equal extent in all directions. Hence, the radius can be considered essentially constant throughout the reaction. The error resulting from this assumption diminishes as reaction proceeds since the radius-to-depth ratio continually increases. Combination of equations 2 and 3 and assuming a constant radius gives

$$d = d_0(1 - F) \qquad (4)$$

Finally, the thickness of the product layer, x, is

$$x = {}^1/_2(d_0 - d) = {}^1/_2 d_0 F \qquad (5)$$

The two kinetics laws usually applicable to gas–solid reactions involving powders are the linear and parabolic laws

	Differential form	Integrated form
Linear:	$\frac{dx}{dt} = k$	$x = kt$
Parabolic:	$\frac{dx}{dt} = \frac{k}{x}$	$x^2 = 2kt$

The modified parabolic law is sometimes useful in correlating the initial phase of the reaction since the parabolic law is not expected to apply at low values of x. The modified law is

	Differential form	Integrated form
Modified parabolic:	$\frac{dx}{dt} = \frac{k}{m + x}$	$x^2 + 2mx = 2kt$

where m is a constant which is usually not strongly temperature dependent. These three laws, expressed in terms of F, are

$$\text{Linear: } F = \frac{2k}{d_0} \times t = k_l t \qquad (6)$$

$$\text{Parabolic: } F^2 = \frac{8k}{d_0^2} \times t = kpt \qquad (7)$$

$$\text{Modified parabolic: } F = \frac{2m}{d_0}\left[\left(1 + \frac{2k}{m^2}t\right)^{1/2} - 1\right] = q\left[(1 + k_m t)^{1/2} - 1\right] \qquad (8)$$

Thus, the three cases can be distinguished experimentally by establishing the particular relationship between F and t. The above expressions can be used to correlate data for particles of any geometry provided the depth of the unreacted particle is much less than its other two dimensions.

Experimental

Material and Products.—The $NOUF_6$ material was prepared in this Laboratory.[3] A wet chemical analysis of the compound gave these results: *Anal.* Calcd.: U, 62.3; N, 3.7; F, 29.8. Found: U, 62.4; N, 3.2; F, 29.6.

The X-ray diffraction pattern was characteristic of $NOUF_6$.[12] The compound was stored in a nitrogen-purged dry box (dew point −50°F.) to prevent reaction with moisture in the air. Electron micrographs indicated that the material consisted of flat, circular particles, the size of which was greater than 2 μ. Conclusive determinations of particle shape could not be made because of the extreme reactivity of the material. For mathematical treatment these particles were considered as discs. The surface area as determined by the krypton adsorption was 0.90 m.²/g.

Wet chemical analysis of the reaction products showed equal molar quantities of uranium(IV) and uranium(VI). Since chemical analysis[13] of the products showed no uranium was lost on hydrolysis, the uranium-containing products corresponding to the valence states established by wet chemical analysis were expected to be uranyl fluoride and uranium tetrafluoride. These compounds were expected to be hydrated to a varying degree depending upon the temperature of the reaction. A three-quarters hydrate of uranium tetrafluoride was identified by X-ray diffraction analysis of the solid reaction product of a run at room temperatuce. Wet chemical analysis was used to establish the presence of uranyl fluoride since it could not be identified with the diffraction patterns available.

The hydrolysis of $NOUF_6$ represents an over-all weight loss. The empirical weight loss corresponding to the unhydrated products was not attained at the end of the reaction. Chemical analysis of the solid reaction products revealed the absence of nitrogen; no fluorine was found in excess of that which would be due to uranyl fluoride and uranium tetrafluoride. Hence, any weight in excess of that due to the unhydrated products was regarded as due to water.

Apparatus and Procedure.—A nickel cap $^1/_2$ inch deep, having an inside diameter of 1 inch and walls $^1/_8$ inch thick, was used to hold the sample. A hot plate was used for heating, the temperature being measured with an iron-constantan thermocouple soldered to a separate nickel cap. Weight measurements were made on a direct reading Sartorius analytical balance with a $^1/_8$-inch Teflon pad placed on the balance pan to minimize heating of the pan and loss of heat from the reactor. The nickel caps exerted a buoyancy effect because of convection currents. Weighing at regular intervals made correction unnecessary since a constant buoyancy effect was maintained at any particular temperature and only weight differences were used. Sample weights, averaging approximately one gram, were obtained by weighing by difference a vial which had been filled in the dry box. The final weight loss due to hydrolysis was usually determined after the reaction had proceeded overnight. Relative humidity prevailing during the reactions was fairly constant, ranging from 48 to 53%.

Results

The data at temperatures from 68 to 231° obtained for $NOUF_6$ hydrolysis in air are presented in Table I. The experimental points of F *versus* time for a typical run is shown in Fig. 1. It can be seen easily, by reference to equation 6, that the

of uranium in the reaction. The atomic volume of uranium would be expected to contribute most to the molecular volume of the reactant and products. Therefore, not much change in molar volume would be expected during reaction and hence the particle size would be expected to remain relatively constant.

(12) F. J. Musil, P. R. Ogle and K. E. Beu, "Powder X-Ray Diffraction and Related Data on $NOUF_6$ and $NOMoF_6$," ASTM X-Ray Diffraction Card File. (Submitted 1959).

(13) Total uranium calculated in sample before hydrolysis, 618 mg.; total uranium found after hydrolysis, 618 mg.

Table I

Reaction Data for Hydrolysis of $NOUF_6$ in Air

Temp. 68°		Temp. 85°		Temp. 111°		Temp. 130°		Temp. 141°		Temp. 157°	
t, sec.	F	t, sec.	F	t, sec.	F	t, sec.	F	t, sec.	F	t, sec.	F
600	0.092	600	0.093	600	0.164	600	0.180	300	0.104	600	0.252
1200	.163	1200	.172	900	.212	900	.244	600	.218	925	.352
1800	.227	1800	.245	1200	.261	1200	.314	900	.316	1200	.442
2400	.284	2400	.305	1500	.315	1500	.384	1200	.408	1500	.528
3000	.340	3000	.364	1800	.364	1800	.453	1500	.500	1800	.610
3600	.397	3600	.424	2400	.473	2100	.523	1800	.580	2100	.682
4800	.469	4800	.536	2700	.521	2400	.581	2100	.650	2700	.805
6000	.582	6000	.642	3000	.570	2750	.657	2400	.713	3300	.895
7200	.645	7200	.729	3600	.661	3000	.702	2700	.776	3900	.950
8400	.702	8400	.808	4200	.739	3300	.755	3000	.829	5200	.990
12000	.816	12000	.927	4500	.770	3600	.797	3300	.863	∞	% W_f = 17.9
18000	.915	14400	.954	4800	.800	3900	.831	3600	.897		
∞	% W_f = 14.2	18000	.967	5400	.861	4200	.866	4300	.960		
		∞	% W_f = 15.2	6000	.897	4800	.935	∞	% W_f = 17.4		
				6300	.915	5400	.970				
				7200	.958	∞	% W_f = 17.2				
				7900	.987						
				∞	% W_f = 16.6						

Temp. 157°		Temp. 170°		Temp. 185°		Temp. 200°		Temp. 205°		Temp. 231°	
t, sec.	F	t, sec.	F	t, sec.	F	t, sec.	F	t, sec.	F	t, sec.	F
500	0.204	400	0.212	300	0.161	600	0.324	500	0.275	300	0.180
750	.292	700	.313	600	.289	900	.468	800	.407	600	.333
1000	.375	1000	4.19	900	.417	1200	.587	1100	.544	900	.481
1300	.470	1300	.525	1200	.545	1500	.710	1400	.654	1200	.612
1600	.558	1600	.620	1500	.661	1800	.810	1800	.780	1500	.738
1900	.630	1900	.715	2100	.868	2100	.893	2000	.835	1800	.837
2200	.716	2200	.793	2400	.929	2400	.939	2300	.901	2150	.908
2500	.774	2500	.872	2700	.973	∞	% W_f = 18.2	2900	.973	2400	.940
2800	.828	2800	.922	3000	.990			3200	.1000	2700	.968
3100	.867	3100	.961	∞	% W_f = 18.1			∞	% W_f = 18.2	3000	.973
3400	.900	∞	% W_f = 17.9							3300	.979
3700	.928									∞	% W_f = 18.4
4000	.955										
4300	.973										
4600	.983										
∞	% W_f = 17.9										

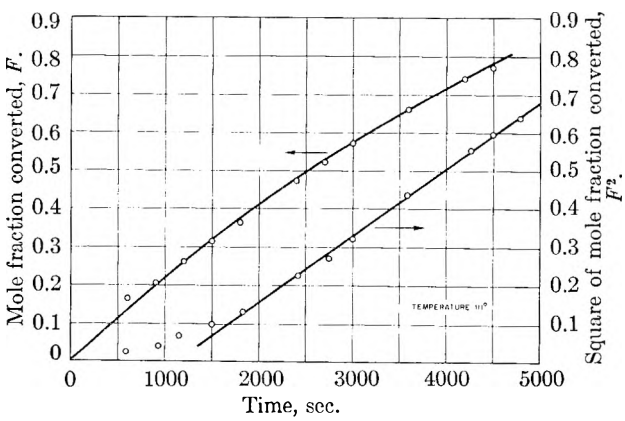

Fig. 1.—Experimental data plotted to determine conformance with parabolic and modified parabolic law.

reaction does not obey the linear law. To determine if parabolic kinetics are followed, the data for this run were plotted as F^2 *vs.* time (Fig. 1). The straight line obtained, after an initial period, indicates conformance to parabolic kinetics. Straight lines were obtained for all the runs. The slope of the straight line is the reaction rate constant, k_p. Variation of the slopes with temperature is shown in Fig. 2, where the logarithm of the slope is plotted against the reciprocal of the absolute temperature. The curvature in this plot will be discussed later.

The deviation in the F^2 plot at low values of time is expected from the parabolic law, and data in this region were correlated through use of the modified version of this law. Application of equation 8 gave good fits, up to 0.6 mole fraction conversion, by trial and error fitting of best values of q and k_m. The agreement between the theoretical curve (solid line) and the experimental points is shown in the F-plot of Fig. 1. The value for q was found to be approximately the same at all temperatures, and a value of 0.8 was used throughout. An Arrhenius plot of log k_m *vs.* $1/T$ (not shown) exhibited a curvature similar to that obtained with the parabolic law.

Discussion

The results indicate that the hydrolysis reaction follows parabolic kinetics throughout. The curvature in the Arrhenius plot may be explained on the basis of the variation of concentration of hydrated water in the product layer with temperature.[10] The experimental rate constant is a function of concentration as well as temperature, whereas the true diffusion rate constant is dependent on temperature alone. The experimental rate constants were adjusted for change of water concentration with temperature on the assumption that the rate constant is directly proportional to the equilibrium water concentration. As shown in Table I, the final per cent. weight loss, % W_f,[14] increased with increasing temperature, indicating that the equilibrium concentration of hydrated water was decreasing with temperature. Comparison of the final weight gain, obtained experimentally, with

(14) Theoretical for unhydrated products is 18.6%.

the calculated weight gain assuming no hydration of products enables one to calculate the amount of water adsorbed at equilibrium at that particular temperature. From this the equilibrium water concentration can be calculated.

All rate constants obtained were corrected to an arbitrary constant value of water concentration which was chosen at the highest temperature employed. The proportionality constant γ is defined as the ratio of this arbitrary value (2.0 mg. H_2O/g. product) to the concentration at the given temperature and is given by the expression, $\gamma = 0.2/(18.6 - \%\ W_f)$. Multiplication of the experimentally obtained rate constants by the appropriate γ value gives a rate constant which is proportional to the diffusion rate of water vapor through the nearly unhydrated product. The variation of the new rate constant with temperature should now follow the normal temperature dependency expected for a diffusion process with constant concentration (Arrhenius equation). The Arrhenius plots for these new constants are presented in Fig. 2, where the expected straight-line relationships are obtained. The least squares slopes of these curves yield approximately the same activation energy, *viz.*, 10.9 ± 0.4 and 10.2 ± 0.3 kcal./mole, as would be expected if the same mechanism prevailed during the entire reaction.

Since a parabolic mechanism was found, it is evident that the product film is protective; the reaction rate decreases as the thickness of the film increases. A protective film is expected only when there is not much change in molar volume during reaction.[8,15] Hence, assumption (4) in the introductory section is experimentally verified. A parabolic mechanism indicates that the rate-controlling step is volume diffusion through the film.[16,17] The controlling step is probably the diffusion of water vapor from the surface to the reaction interface, although the desorption of gaseous reaction products also might be controlling.

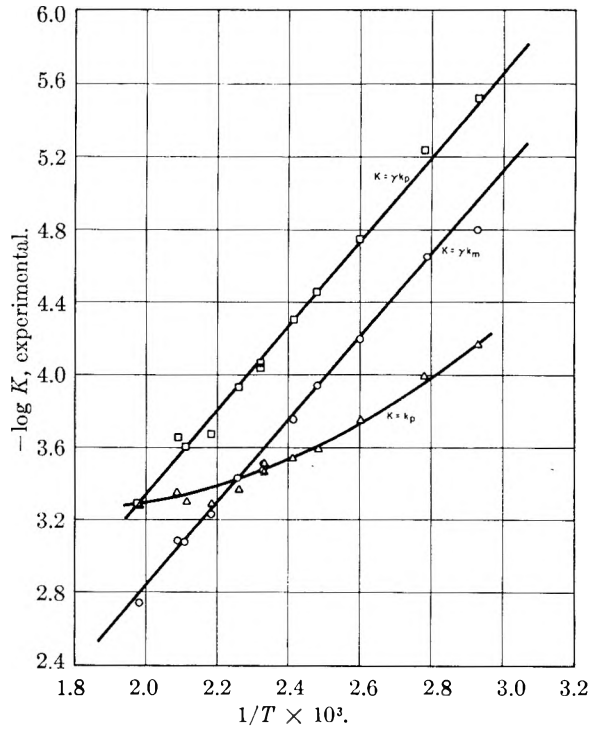

Fig. 2.—Arrhenius plots for parabolic kinetics; T = absolute temperature.

(15) J. M. Dunoyer, *Ann. Chim.*, [12] **6**, 165 (1951).

(16) N. Cabrera and N. F. Mott, *Repts. Prog. Phys.*, **12**, 163 (1949).

(17) E. A. Gulbranson and K. F. Andrew, *J. Electrochem.*, **99**, 402 (1952).

ELECTROCHEMISTRY OF CRYSTAL-POLYMER MEMBRANES. PART I. RESISTANCE MEASUREMENTS

BY R. M. BARRER AND S. D. JAMES

Physical Chemistry Laboratories, Chemistry Department, Imperial College, S. W. 7, England

Received August 27, 1959

Attempts have been made to prepare membranes in which microcrystalline ion-exchanging zeolites are bonded by inert polymeric fillers in such a way that the electrochemical behavior is determined by the crystals and by crystal contacts. Measurements of electrical conductance of the bonded membranes have, however, shown that some crystal-resin pores arise which have an influence upon electrical transport. The effect of these pores upon transport can be limited by soaking the membranes in an electrochemically inert liquid. Electrolyte in crystal-resin pores does not possess the properties of bulk electrolyte, but reduces interfacial polarization at points of contact between crystallites. This polarization becomes more marked if crystal-resin pores are in part filled by electrochemically inert liquid; it is, however, reduced by a rise in temperature.

1. Introduction

Since the pioneering work of Teorell[1] and Meyer and Sievers[2] made possible the quantitative interpretation of membrane potentials, much work has been devoted to the study of transport processes in membranes containing ion-exchange materials. With the notable exception of the work of Marshall, *et al.*,[3] this work has been concerned with organic polyelectrolytes.[4]

The present study, on the other hand, utilizes some of the crystalline zeolites having robust, 3-

(1) T. Teorell, *Proc. Soc. Exptl. Biol. Med.*, **33**, 282 (1935).

(2) K. H. Meyer and J. F. Sievers, *Helv. Chim. Acta*, **19**, 649 (1936).

(3) C. E. Marshall, THIS JOURNAL, **43**, 1155 (1939); C. E. Marshall and W. E. Bergman, *J. Am. Chem. Soc.*, **63**, 1911 (1941); C. E. Marshall and C. A. Krinbill, *ibid.*, **64**, 1814 (1942); C. E. Marshall and A. D. Ayer, *ibid.*, **70**, 1297 (1948); C. E. Marhsall, THIS JOURNAL, **52**, 1284 (1948).

(4) *E.g.*, *Faraday Soc. Disc.*, no. **21** (1956).

dimensional crystal lattices. The aluminosilicate framework of these crystals bears a net negative charge, compensated by cations located in the intracrystalline channels and cavities. The zeolites employed include the most open crystalline structures known. They are ionic solids, permeated by channel systems and intracrystalline cavities which constitute a large proportion of the crystal volume. These channel systems are permeable to simple cations and also to small uncharged molecules such as water.

The known ion-exchange properties of the zeolites[5-7] indicate that, as single crystals, they possess excellent potentialities for use in cation-exchange membranes. They have crystal structures which undergo little or no swelling in contact with electrolyte solution and the dimensions of which are unappreciably affected by ion exchange. Their high exchange capacities (4–6 meq./hydrated g.)[8] and small pore dimensions render the zeolites highly effective in the exclusion of Donnan diffused salt from the crystal structure. Uptake of anions (or in general of neben-ions) from electrolyte solution, which above concentrations of about 0.1 *m* NaCl results in loss in selectivity by the organic gel exchanger membranes, occurs only to a very limited extent in the crystalline zeolites.[9] However single, crystal plates of these materials cannot normally be obtained, and accordingly we have investigated the behavior of crystalline powders, in matrices of inert polymer, in order to see how nearly the ideal behavior of ion-sieve single crystal plates of zeolite can be approached by such heterogeneous membranes. The ion exchangers used[10] in these membranes were NaX (synthetic near-faujasite, $Na_2O \cdot Al_2O_3 \cdot 2.67SiO_2 \cdot 6.7H_2O$) and NaA (a synthetic zeolite of which our sample had the composition $Na_2O \cdot Al_2O_3 \cdot 2SiO_2 \cdot 0.14NaAlO_2 \cdot 4.77H_2O$).

2. Experimental

Membranes were, in general, prepared by the compression moulding (using a book-press) of intimate mixtures of a finely powdered polymer and the zeolitic crystals under examination. Seven membranes were prepared using a hydraulic moulding pressure of 12 tons/sq.in. Thermoplastic resins used were: polythene, polystyrene, and polymethyl methacrylate; the only thermosetting resin employed was a stage B phenol resin. The finished membranes were about 2.7 cm. in diameter and 1 mm. thick. Some of these membranes were treated with an electrochemically inert liquid (silicone fluid or dinonyl phthalate) subsequent to their fabrication by moulding. The liquid was introduced into the membranes under vacuum after an outgassing period of 0.5–1 hour at 10^{-3} mm. A few membranes were prepared by the polymerization of methyl methacrylate in compressed plugs of zeolitic crystals. Methyl methacrylate, containing ~0.1% benzoyl peroxide, was admitted to the compressed plug under vacuum, and subsequently polymerized at 50°. Membrane thickness was reduced to the required value (usually about 1 mm. or less) by machining on a lathe.

The electrical resistance of membranes was measured using an a.c. Wheatstone bridge, usually at 1000 c./sec. The membranes were clamped, in NaCl solution, between rubber gaskets and the ground-glass flanges of "Industrial Glass Piping," $^5/_8$" joints. Electrical contact with the salt solution was made through stout discs of platinized platinum welded to tungsten rods sealed through the glass wall of the half-cell. The resistance cell was placed under a thick, thermally insulating layer of cotton wool in a brass tank which was clamped in a water-bath thermostated to within ±0.1°.

3. Electrical Resistance and Apparent Activation Energies for Cationic Migration

The electrical resistance of newly moulded membranes was substantially decreased by continued exposure to salt solution; the resistance at 25° of an unequilibrated membrane was lowered by as much as 60% after the resistance had been studied as a function of temperature up to 75°. Hence, before measurements were made, the membranes were equilibrated in ambient 0.1 *N* NaCl solution at 80° for 3–4 days. After this treatment, plots of resistance *vs.* temperature normally became reproducible.

The measured resistances in 0.1 *N* NaCl solution at 25° of equilibrated membranes containing NaX, varied with the crystal content from about 200Λ for membranes containing 50% (by volume) of crystals to 14000Λ for a 20% membrane. This corresponds to a variation in specific resistance from 4×10^3 to 2.8×10^5Λ/cm.

The apparent activation energy E, obtained from the slopes of plots of log[Resistance] against the reciprocal of the absolute temperature, shows considerable variation. For twelve NaX membranes varying in % NaX and in the nature of the inert resin, the mean value of E in the interval 25–75° varies from 4.6_1 kcal./mole for a 45% NaX and polythene membrane to 6.7_0 kcal./mole for a 50% NaX and polystyrene membrane (Table I). In the Arrhenius plots for the membranes there is a distinct and smooth curvature through the temperature range (Fig. 1); in all cases, the E value measured by the slope of the curve at the lower temperature is considerably greater than that at the higher temperature. Usually the value of E in the interval 25–35° is higher by about 2 in 6 kcal./mole than E in the interval 65–75°.

The above results suggest that membrane resistance is largely determined by the imbibing of ambient salt solution. It is highly unlikely that the activation energy for cationic migration within crystals of NaX changes, in a 40° interval, by the proportion cited above for NaX membranes. The curvature of Arrhenius plots must, therefore, reflect the presence of imbibed salt solution in the membranes. There is a strong resemblance between the curvature of these plots and that of similar plots made for 0.1 *N* NaCl solution. The wide variation in E values among the twelve NaX membranes studied can be attributed to a variation in the state of agglomeration of zeolitic crystals in the resin matrix, and in particular to a variation in the extent to which crystal–resin pores permit permeating salt solution to bypass the crystals electrically.

This conclusion is supported by measurements made on the water absorption of the membranes. They were shown to absorb quantities of water up

(5) R. M. Barrer, W. Buser and W. F. Grutter, *Helv. Chim. Acta*, **39**, 518 (1956).

(6) R. M. Barrer and L. M. Meier, *Trans. Faraday Soc.*, **54**, 1074 (1958); **55**, 130 (1959).

(7) R. M. Barrer and D. C. Sammon, *J. Chem. Soc.*, 2838 (1955); 675 (1956).

(8) R. M. Barrer, *Proc. Chem. Soc.*, 99 (1958).

(9) R. M. Barrer and W. M. Meier, *J. Chem. Soc.*, 299 (1958).

(10) These materials were kindly provided by Linde Air Products Co. They are samples, respectively, of Linde Molecular Sieves 13X and 4Λ.

TABLE I

VALUES OF E IN KCAL./AVOGADRO NO. OF UNIT PROCESSES FOR ZEOLITE–POLYMER MEMBRANES IN 0.1 N NaCl

Membrane designation	Vol. compn.	How prepared	E (25–75°)
	(a) NaX–Polymer membranes		
MPX2	45% NaX; polythene	Book press	4.67
MPX1	50% NaX; polythene	Book press	6.23
MMX1	50% NaX; "perspex"	Book press	5.26
MMX3	50% NaX; "perspex"	Hydraulic press	6.58
MBX2	50% NaX; B phenol resin	Hydraulic press	5.46
MSX4	20% NaX; polystryene	Hydraulic press	4.75
MSX3	35% NaX; polystyrene	Hydraulic press	5.31
MSX8	50% NaX; polystyrene	Hydraulic press	5.35
MSX2	50% NaX; polystyrene	Book press	5.41
MSX7	35% NaX; polystyrene	Book press	5.66
MSX5	50% NaX; polystyrene	Hydraulic press	6.23
MSX1	50% NaX; polystyrene	Book press	6.70
	(b) NaA–Polymer membranes		
MPA2	50% NaA; polythene	Book press	4.30
MSA3	50% NaA; polystyrene	Hydraulic press	6.14
MSA2	50% NaA; polystyrene	Book press	6.27

to 30% of the volume of the zeolite crystals in the membrane. The absorption of similar volumes of salt solution will obviously tend to shunt electrically the relatively higher intrinsic resistances of the crystal particles, and to decrease the observed membrane resistance. It seems reasonable to infer that the absorbing pores in the membrane are present, not in the bulk resin, but between crystal particles and the resin, where incomplete wetting of crystal surfaces by resin had occurred, either during moulding or because polymer surfaces are lifted from the crystals during conditioning in the electrolyte. E values obtained with membranes containing NaA crystals (Table I) showed similar variations between membranes, and Arrhenius plots exhibited the same curvature as was noted for NaX-polystyrene membranes.

Resistance measurements also were made on two NaX-polystyrene membranes in 0.01 N NaCl solution. The resistance increased by ~50%, but values of E did not alter significantly, as shown in Table II.

TABLE II

VALUES OF E IN KCAL./AVOGADRO NO. OF UNIT PROCESSES FOR ZEOLITE–POLYMER MEMBRANES IN 0.1 N AND 0.01 N NaCl

Membrane design.	Mean values of E (25–75°) in 0.1 N NaCl	in 0.01 N NaCl
MSX2	5.41	5.15
MSX3	5.31	4.65

4. Quartz–Polymer Membranes

The activation energies obtained for conductance processes in membranes containing NaA and NaX were all larger than those for aqueous NaCl solutions. In order to see how far they were characteristic of intra-crystalline conduction and how far they were associated with conduction by the electrolyte in crystal–resin pores, a membrane was prepared comprising 50% by volume of quartz

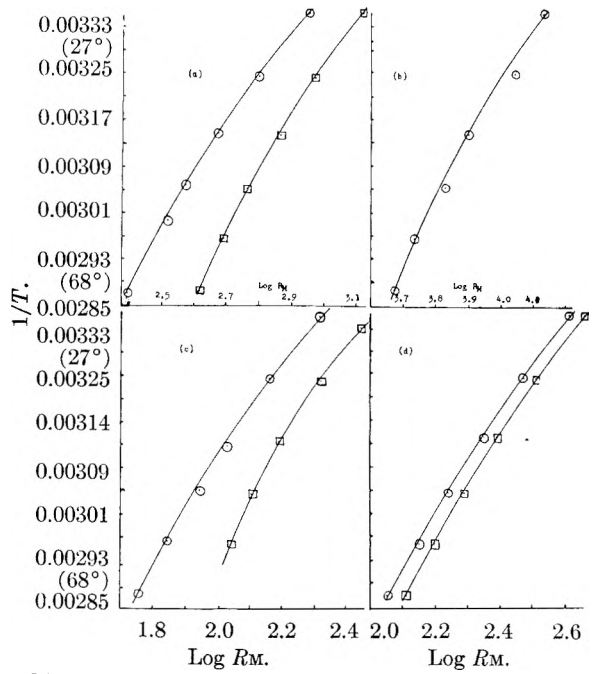

Fig. 1.—Arrhenius plots for NaX/resin membranes in NaCl solution: (a) MSX3 (NaX/polystyrene) in 0.1 N (○) and 0.01 N (□); (b) MSX4 (NaX/polystyrene) in 0.1 N; (c) MSX2 (NaX/polystyrene) in 0.1 N (○) and 0.01 N (□); (d) MBX2 (NaX/phenol resin) (○) + MSX8 (NaX/polystyrene) (□) in 0.1 N.

particles admixed with polystyrene. Moulding conditions and sizes of crystallites were comparable with those for NaX–polystyrene membranes. During conditioning in 0.1 N NaCl solution the resistance dropped to 16 kΛ in 5 days, reaching a constant value of 5 kΛ after 5 more days in 0.1 N NaCl at 80°. The finite resistance can only be due to electrolyte in crystal–resin pores permitting solution conductance across the thickness of the membrane. Apparent energies of activation from the Arrhenius plot were 4.7 kcal./Avogadro No. of unit conduction processes in the temperature interval 25–35° and 4.0 kcal. in the interval 65–75°. Corresponding values of E in 0.1 N NaCl were 3.4 and 2.5 kcal./Avogadro No. of unit conduction processes.

Moreover, the e.m.f. of an NaCl concentration cell, with calomel reference electrodes, and in which solutions of strength 0.205 and 0.062 m were separated by the quartz membrane, was 47.2 mv. This gives a mean Hittorf transport number, T^+, of Na^+ in the membrane of 0.84, whereas T^+ at these concentrations is 0.38 in free NaCl solution. Thus, in the pores of the quartz membrane there is considerable immobilization of the Cl^- ion as compared with bulk solution.

These differences between the properties of salt solution in bulk and in the quartz crystal–resin pores are likely to be even greater for the zeolitic membranes where cation-exchange sites must be present to some extent on external crystal surfaces.

5. Attempts to Minimize Crystal–Resin Pores

From the foregoing experiments it is evident that no heterogeneous membrane is likely to fullfil the ideal of the single crystal plate of ion-sieve zeolite.

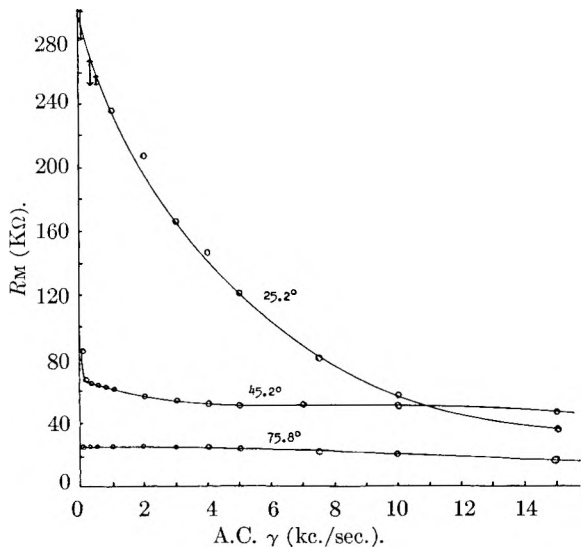

Fig. 2.—Frequency dependence of resistance of membrane MSX4 (NaX/polystyrene) in 0.1 *N* NaCl solution. Membrane contains imbibed dinonyl phthalate.

The best heterogeneous crystal-polymer membrane will be a compromise between a state in which each zeolite crystallite is fully wetted by inert resin and one in which only a small degree of wetting has occurred. In the first state, however, the conductance would be virtually zero. In the second state the perfect selectivity of the crystals might be obscured by conduction by imbibed salt solution. Considerable attention was, however, given in the following ways to preparing membranes embodying the most desirable compromise.

(a) **Adjustment of Composition of NaX Membranes.**—Variation in the proportion of zeolite to polymer below 50% of NaX tended to give lower apparent activation energies, and did not improve their electrochemical behavior.

(b) **Use of Different Polymers.**—The variation in values of E for polymethyl methacrylate–NaX membranes was comparable with this variation for polythene– and polystyrene–NaX membranes. It was considered that particle size in the resin was important. The smallest particles were those of the thermosetting stage B phenol resin, which were still about five times larger than were the NaX crystals (2–3 μ). The phenol resin also possessed greater fluidity at the moulding temperature than did the thermoplastic resins, so that better wetting of the crystals with the phenol resin should occur during moulding. However, this membrane was not significantly better than those formed using thermoplastics.

(c) **Moulding Pressure.**—Membranes made using the hydraulic press were formed at a considerably higher pressure than those made in the book press, and would thus be expected to have fewer crystal-resin pores. However, the values of E obtained from the resistance *vs.* reciprocal temperature measurements on six hydraulically prepared membranes were no more consistent or temperature independent than those measured for membranes prepared using the book press.

(d) **Polymerization of Methyl Methacrylate.**—Membranes were made by polymerizing methyl methacrylate *in situ* around NaX crystals centrifuged in the monomer. This was done to ensure as complete wetting of crystals as possible, and so to minimize crystal-resin pores. The conductance of such membranes was not examined in detail, but the membrane potentials (Part II) showed that solution paths and pores developed in the polymer-crystal matrix, after an initial period during which the resistance was exceptionally high.

(e) **Imbibition of Inert Liquids.**—The most successful method of minimizing crystal-resin pores and of producing selective membranes (Part II) was to impregnate them in inert liquids (silicone oil or dinonyl phthalate). The inert liquids filled many of the pores from which, especially in the case of silicone impregnation, they were only very slowly displaced by aqueous electrolytes. This treatment, however, resulted in frequency dependent resistances, such as those shown in Fig. 2 for an NaX-polystyrene membrane which had imbibed dinonyl phthalate and was then conditioned in 0.1 *N* NaCl solutions.

6. Discussion

The frequency dependence found after imbibition of inert liquids may be explained in terms of interfacial polarization at crystal-crystal contacts. These contacts are limited and restrict the flow of charge across them, so that excess positive charge accumulates on one side, and drains from the other. This behavior is most marked when inert liquid fills crystal-resin pores. The more rapidly the applied voltage alternates, however, the less the polarization, and consequently the more nearly independent of frequency the resistance becomes, as seen from Fig. 2. On the other hand, in absence of the inert liquid, electrolyte eventually fills the pores, according to the evidence presented in this paper. The electrolyte acts as a depolarizer by conducting current readily from crystal to crystal, so that the resistance then tends to be independent of a.c. frequency.

Three kinds of conducting path can be envisaged in the crystal-polymer matrix: solution paths; paths directly through crystals; and paths to the conductivity of which both crystals and solution contribute. In the frequency-dependent range of resistance this system can be considered in terms of impedance, allowing for capacity effects due to interfacial polarization and for resistance. Except to note that frequency-dependence becomes less important as temperature rises (Fig. 2) we will not analyze this range further, but will consider instead the frequency-independent resistance.

In the frequency-independent range of conductivity we may write the total contributions of each of the three kinds of conducting path as K_s, K_c and K_{cs}. For the over-all conductivity K_m of the membrane, we then have

$$K_m = K_s + K_c + K_{cs} \qquad (1)$$

and also for paths involving both crystals and solution

$$\frac{1}{K_{cs}} = \frac{1}{K_{c_1}} + \frac{1}{K_{s_1}} \qquad (2)$$

where K_{c_1} and K_{s_1} are contributions to conductivity

due to crystals and to solution, respectively. Thus finally

$$K_m = K_s + K_c + \frac{K_{c_1}K_{s_1}}{K_{c_1} + K_{s_1}} \quad (3)$$

Two limiting cases arise: $K_{s_1} >> K_{c_1}$ and $K_{c_1} >> K_{s_1}$, which, from (3), give, respectively

$$K_m = K_s + K_c + K_{c_1} \quad (4)$$

and

$$K_m = K_s + K_{s_1} + K_c \quad (5)$$

If we now assume that Arrhenius equations may be applied to K_m, K_c, K_{c_1} and K_{s_1} at any particular temperature, we have

$$K_m = K_m^0 \exp(-E_m/RT);\ K_c = K_c^0 \exp(-E_c/RT);$$
$$K_{c_1} = K_{c_1}^0 \exp(-E_c/RT);\ K_{s_1} = K_{s_1}^0 \exp(-E_s/RT) \quad (6)$$

K_m^0, E_m, $K_{s_1}^0$ and E_s can be temperature-dependent,[11] but studies of the electrical conductivity[12,13] of ionic crystals indicate that this should not be true of K_c^0, $K_{c_1}^0$ and E_c. By differentiation and substitution we derive from eq. 4 and 5

$$K_m E_m = K_s E_s + (K_c + K_{c_1})E_c \quad (7)$$

or

$$K_m E_m = (K_s + K_{s_1})E_s + K_c E_c \quad (8)$$

and from eq. 7 and 4, and 8 and 5, we may eliminate K_s or $K_s + K_{s_1}$, respectively, to obtain

$$\frac{K_m}{(K_c + K_{c_1})} = \frac{(E_c - E_s)}{(E_m - E_s)};\ \text{or}\ \frac{K_m}{K_c} = \frac{E_c - E_s}{E_m - E_s} \quad (9)$$

These relations have the same form and we cannot differentiate between $(K_c + K_{c_1})$ and K_c, so that they are effectively identical. If K_m is $> (K_c + K_{c_1})$, or K_c, in the relevant expression, then $E_c > E_m$. Since K_m represents the whole membrane conductivity and K_c a part only, these inequalities should be satisfied. However, as an example we consider further one of the expressions (9).

The values of E_s may as a first approximation be taken as those or E_m for the quartz-polystyrene membrane, where crystal conductivity need not be considered (4.7 kcal. at 30° and 4.0 kcal. at 70°). In the expression $K_c = K_c^0 \exp(-E_c/RT)$ we may, as noted above, take K_c^0 and E_c to be independent of temperature. Then using the relevant results for K_m and E_m for the NaX-polystyrene membrane MSX3 at 30 and at 70°[15] we may eliminate K_c and obtain

$$E_c(0.0837) + 0.0673 = \log\left(\frac{E_c - 4.7}{E_c - 4.0}\right)$$

where E_c is in kcal. Thence $E_c \sim 3.4$ kcal., a value which is almost certainly considerably too small, since as noted we would expect $E_c > E_m$. However, the method of analysis, even if oversimplified, may have some general application to heterogeneous membranes. It would be of interest to develop it further if a more reliable means of obtaining E_s can be devised.

(11) E_s refers to the conductivity of the electrolyte not in bulk solution, but in the thin electrolyte films constituting the solution paths. It is likely therefore to be modified relative to E for bulk electrolyte.

(12) J. F. Laurent and J. Bénard, *J. Phys. Chem. Solids*, **3**, 7 (1957); **3**, 218 (1957).

(13) R. M. Barrer, "Diffusion in and through Solids," C.U.P., 1951, Chapter 6.

(14) In a chain of crystals in physical contact, and in absence of a conducting liquid forming menisci around the points of contact, current flow lines would converge through the contacts, and space charge effects might modify E_c, as compared with this energy for parallel flow lines in a single crystal. However, the liquid provides alternate flow paths and so convergence of flow lines is probably not important. Thus it is expected that E_c should be similar for K_c and K_{c_1}. Equality is assumed in eq. 6.

(15) For this membrane at T = 30°, K_m^{30} = 0.00134 mho, E_m^{30} = 6780 cal./Avogadro no. of unit conduction processes, while at T = 70°, K_m^{70} = 0.003751 mho and E_m^{70} = 4640 cal.

ELECTROCHEMISTRY OF CRYSTAL–POLYMER MEMBRANES. PART II. MEMBRANE POTENTIALS

BY R. M. BARRER AND S. D. JAMES

Physical Chemistry Laboratories, Chemistry Department, Imperial College, London, S. W. 7, England

Received August 27, 1959

The selectivity of membranes consisting of crystalline zeolite powders in inert polymer matrices has been investigated by e.m.f. measurements of membrane cells in homoionic and heteroionic electrolyte solutions. The zeolites used were Linde Sieve A, near-faujasite (Linde Sieve X), chabazite, analcite, and in addition an aluminosilicate gel exchanger. Selectivity was imperfect when moulded membranes were used, or large pieces of crystal sealed into plastic. Polymerization of methyl methacrylate around partly dried gel zeolite or crystal powder produced selective membranes, and also some excellent selective membranes were obtained when moulded membranes containing Linde Sieve A or X were impregnated with silicone oil.

Introduction

A single crystal plate of a zeolite crystal if free of cracks should act as a membrane permeable to suitable cations and impermeable to anions. Moreover such a plate would show ion-sieve activity toward cations of different size, so that to sufficiently large cations it could be electrochemically inert. However, as pointed out earlier (Part I),[1] such single crystal membranes are fragile and difficult to prepare and preserve. Heterogeneous membranes composed of a sufficient concentration of zeolite crystallites bonded by inert polymers fall short of the above ideal, as a study of their resistance has shown,[1] but considerable interest attaches to their electromotive behavior

(1) R. M. Barrer and S. D. James, THIS JOURNAL, **64**, 417 (1960).

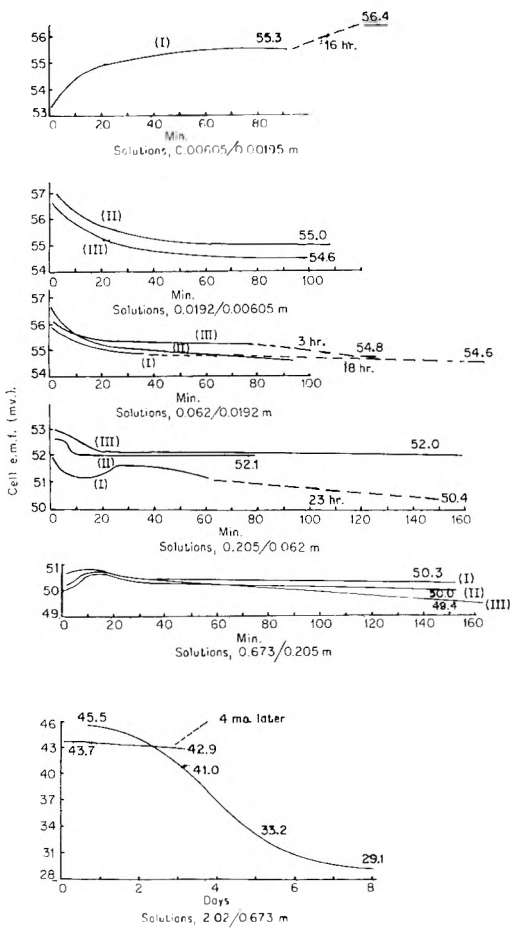

Fig. 1.—Time dependence of membrane cell e.m.f. in NaCl solutions (MSX5: NaX/polystyrene). Ag/AgCl electrodes; Nernst e.m.f. = 56.4 mv. I, II, etc., indicate the introduction of fresh solutions into the cell.

and selectivity as compared with organic gel[2–6] or clay[7] membranes. Accordingly a study has been made of membrane potentials of a series of heterogeneous membranes in which the dispersed phases were Linde Sieve A, Linde Sieve X (synthetic near-faujasite), chabazite, analcite and a synthetic aluminosilicate gel zeolite.

Experimental

The preparation of typical membranes has been described in Part I.[1] The selectivity of membranes to cation transport was examined by observing the e.m.f. of concentration cells

reference electrode reversible to Cl^-	NaCl m_1	membrane containing Na-zeolite	NaCl m_2	reference electrode reversible to Cl^-

The reference electrodes were initially silver/silver chloride, but calomel electrodes were later employed, having proved freer of bias potentials under the operative conditions. The e.m.f. of the membrane cells was determined potentiometrically. Amplification of the out-of-balance current made possible an accuracy of ±0.1 m.v. even with membranes of low conductivity.

With some membranes the initial electrical resistance was very high resulting in instability of the measured e.m.f.'s due to electrical interferences. This was obviated by surrounding the whole of the electrical circuits including the membrane cell, by earthed screens. Accurate measurements could then be made much earlier than would otherwise have been possible. After prolonged conditioning in salt solution the membrane resistance usually became low enough for the screens to be dispensed with.

The membranes were supported between salt solutions as for the resistance measurements,[1] and provision was made for a rapid stream of nitrogen bubbles to be directed against the faces of the membrane in order to agitate layers of solution adjacent to the membrane. The humidity of this nitrogen stream was suitably adjusted by passage through the appropriate thermostated electrolyte solution, before it entered the cell, so that no concentration changes occurred in the cell as a result of the stirring. The membrane cells were thermostated in an air-bath at 25° (±0.3°). The seven NaCl solutions (~2–0.002 *m*) used in characterizing membrane selectivity in homoionic cells are identical with those employed by Spiegler, *et al.*[8] The ratio of mean electrolyte activity between consecutive pairs of these solutions is constant at 3.00 (±0.02). Thus, six pairs of solutions were available for direct comparison of membrane selectivity over the range ~2–0.002 *m*, the maximum cell e.m.f. (corresponding to complete selectivity) being 56.4 mv. (±0.3) in each case.

Measurements also were made of the e.m.f. of cells in which the membrane separated two solutions each containing two cations, such as sodium and cesium or sodium and tetraethylammonium chlorides. Activity coefficients (γ) of tetraethylammonium chloride were evaluated by the method of Randall[9] from osmotic coefficient data given by Lange.[10] Activity coefficients in binary mixtures of electrolytes were calculated by means of Glueckauf's equation.[11]

Time Dependence of the Cell E.M.F.'s.—The general procedure in e.m.f. measurement was as follows. After a period for equilibration (usually overnight) during which the membrane cell was set up in the thermostat, the NaCl solutions were discarded and fresh solutions, always at the cell temperature, were introduced. The cell e.m.f. was then measured till a steady value was recorded. The solutions were refreshed again until a reproducible value of the stable e.m.f. was observed. The variations of the e.m.f.'s with time are shown in a typical instance in Fig. 1 (membrane MSX5, Part I,[1] silver chloride electrodes). In the different runs, using one particular concentration ratio, the e.m.f. rarely followed the same initial curve, but the quasi-stable e.m.f. usually occurred at about the same value. In a period of hours or days following the subsiding of initial effects a gradual decrease in e.m.f. was generally observed, which was often detectable only as a very long term effect (Fig. 1), and was more marked in the stronger sodium chloride solutions. This probably is not due to osmotic transfer of water through the membranes, since a direct experiment failed to detect measurable transfer in a period of some days. In this experiment movement was studied of liquid levels in fine capillaries attached to sealed cell compartments completely filled by different electrolyte solutions and separated by a moulded membrane. Very long time-scale drifts may therefore be a result of slow widening, and increase in number of, the direct solution paths, with consequent gradual diminution in selectivity. This behavior could follow breaking of polymer–crystal contacts by the electrolyte solution. Any drifts observed on this time scale depended upon the character and history of the membrane, and were for some membranes almost imperceptible.

Selectivity of Moulded Membranes.—The e.m.f. of a membrane cell (of the kind already indicated) is given by[12]

(2) *E.g.*, *Faraday Soc. Dis.* No. 21 (1956).
(3) K. Sollner, *Svensk. Kemi. Tidskrift*, **6–7**, 267 (1958).
(4) S. Dray and K. Sollner, *Biochim. Phys. Acta*, **21**, 126 (1956).
(5) F. Helferich and H. D. Ocker, *Z. physik. Chem., Neue Folge*, **10**, 213 (1957).
(6) M. Nagasawa, *J. Chem. Soc. Japan (Pure Chem. Section)*, **70**, 160 (1949).
(7) C. E. Marshall, THIS JOURNAL, **43**, 1155 (1939); **52**, 1284 (1948); C. E. Marshall and W. E. Bergmann, *J. Am. Chem. Soc.*, **63**, 1911 (1941); C. E. Marshall and C. A. Krinbill, *ibid.*, **64**, 1814 (1942); C. E. Marshall and A. D. Ayer, *ibid.*, **70**, 1297 (1948).
(8) K. S. Spiegler, R. L. Yoest and M. R. T. Wyllie, *Faraday Soc. Disc.*, **21**, 174 (1956).
(9) M. Randall, *J. Am. Chem. Soc.*, **48**, 2512 (1926).
(10) J. Lange, *Z. physik. Chem.*, **168**, 147 (1934).
(11) E. Glueckauf, *Nature*, **163**, 414 (1949).

$$e = \frac{2T^+RT}{F} \ln a_1^{\pm}/a_2^{\pm} + t_w \frac{RT}{F} \ln a_1^w/a_2^w \quad (1)$$

where $a^{\pm}$ is the mean activity of the sodium chloride; a_w is the activity of water; T^+ is the Hittorf transport number of Na^+ in the membrane; and t_w denotes the number of moles of water transferred in the direction of positive current per faraday of electricity passed through the cell. These transport numbers are mean values between molalities m_1 and m_2 in the two cell compartments. If, as some of the results to be described suggest, the second term of the right-hand side of eq. 1 is negligible, then

$$e = \frac{2T^+RT}{F} \ln a_1^{\pm}/a_2^{\pm} \quad (2)$$

A membrane which is wholly impermeable to anions then gives the maximum e.m.f., e_{max}, for which $T^+ = 1$, and the selectivity can be evaluated from eq. 2, since $e/e_{max} = T^+$. With the reference solutions of NaCl used, e_{max} should, as noted earlier, be 56.4 ± 0.3 mv. If conduction paths contained electrolyte with the same properties as the bulk sodium chloride, T^+ would be 0.38, and so this non-selective membrane would lead to a minimum cell e.m.f. of 21.4 mv.

In Fig. 2 the cell e.m.f.'s are recorded as a function of log $1/a_2^{\pm}$, where $a_1^{\pm}/a_2^{\pm} = 3$, $a_2^{\pm}$ being the mean activity in the more dilute cell compartment. The membranes to which these curves refer are some of the moulded membranes described in Part I[1] and the concentrations covered by the seven sodium chloride solutions are in the range ~2.0 to ~0.002 *m*. The membranes, however formed (Part 1),[1] are all very imperfectly selective at high sodium chloride concentrations. At high dilution membranes MSX2 and MSX5 approach the ideal selectivity, but all the other membranes still show varying degrees of non-ideality. The figure provides clear evidence of solution paths which dominate the electromotive behavior of the crystal–resin membranes.

There is a partial correlation between this electromotive behavior and the Arrhenius energy of activation E for membrane conductivity.[1] It would be expected that the nearer E approached to that for bulk NaCl solutions the more dominant must be solution paths in the crystal–resin membrane and the smaller must be the role played by the crystals themselves. The extent of the correlation is shown in Table I; membranes with poor selectivity have the smallest values of E, although neither E nor T^+ ever falls as low as in aqueous sodium chloride. A feature of Fig. 2 is that at the highest dilutions certain membranes, instead of showing a continuously increasing selectivity, give a maximum e.m.f. and then the e.m.f. begins to diverge again, as dilution increases, from the ideal where $T^+ = 1.0$. Apart from possible electrode asymmetries, it is difficult to explain this behavior.

Attempts to Prepare Membranes of Greater Selectivity.—(a) Several attempts were made to prepare membranes in which a relatively large zeolite crystal was sealed by means of a resin into a hole in a thick sheet of polymer, so that the zeolite crystal presented two faces directly to the two solutions. This was done with a sodium chabazite crystal using "Araldite" as sealing compound and an "Araldite" membrane 1.5 mm. thick. However, after conditioning with NaCl solutions of 2.0 and 0.7 *m* the quasi-stable e.m.f. was only 34 m.v., indicating that solution paths existed around the crystal or through cracks in it. A similar experiment in which an Na-chabazite crystal was sealed in a rubber membrane with "Araldite" gave a quasi-stable e.m.f. of 44.3 m.v. in the same pair of NaCl solutions, still well below the value for ideal selectivity.

(b) The initial electrical resistance of cells with membranes in which methyl methacrylate had been polymerized *in situ* around the crystalline powder was always very high initially, a fact which suggested that even after conditioning a small number of solution paths might be present. However, deterioration proved to be relatively rapid once it commenced, for the e.m.f. of membrane

(12) G. Scatchard, *J. Am. Chem. Soc.*, **75**, 2883 (1953).

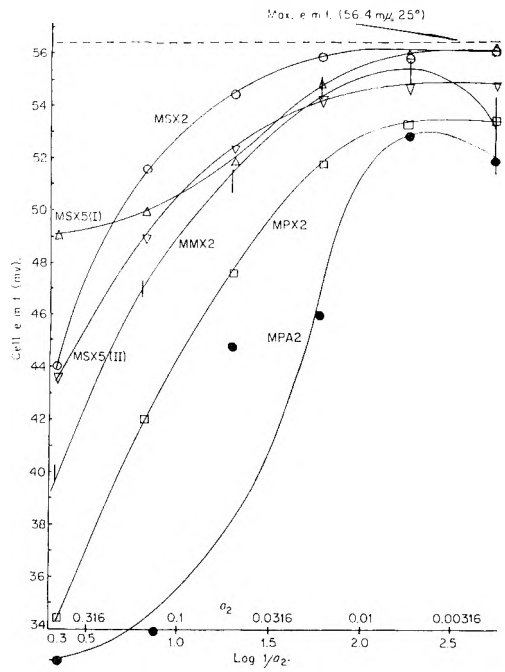

Fig. 2.—E cell–log $1/a_2$ curves where $a_1/a_2 = 3$ (constant) and the a_2 value at each point is that of the more dilute solution: ○, MSX2 (NaX/polystyrene); △, MSX5(I) (NaX/polystyrene); ▽, MSX5(II) measurements 4 months later; |, MMX2 (NaX/"Perspex"); □, MPX2 (NaX/polythene); ●, MPA2 (NaX/polythene).

TABLE I

CORRELATION BETWEEN SELECTIVITY AND ARRHENIUS ACTIVATION ENERGY FOR MEMBRANE CONDUCTIVITY

Membrane	$T^+ = \frac{e}{e_{max}}$ for $\frac{a_1^{\pm}}{a_2^{\pm}} = 3$, and with $a_2^{\pm} = 0.5$	0.1	0.01	E^1 (kcal./Avog. No. of unit conduction processes) between 25 and 75°, obtained using 0.1 *N* NaCl soln.
MPA2	0.58	0.63	0.91	4.3_0
MPX2	.60	.79	.94	4.67
MMX2	.69	.85	.97	..
MSX5(ii)	.75	.89	.95	6.2_3
MSX2	.75	.94	$.99_5$	5.4_1
MSX5(i)	.87	.90	.98	6.2_3

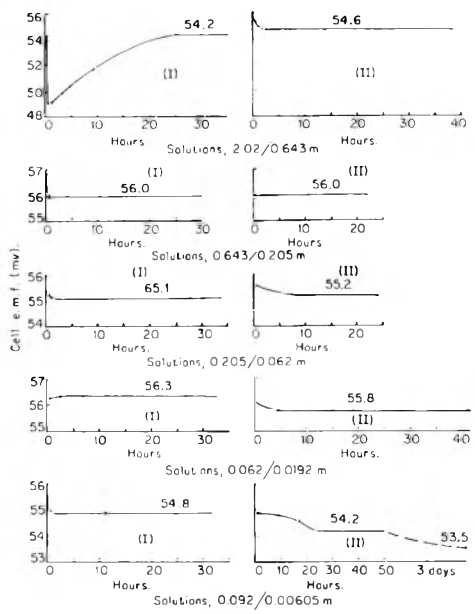

Fig. 3.—E.m.f.'s given by membrane MMAI (NaA/polymerized methacrylate); NaCl solutions (calomel electrodes): (I), (II), etc., indicate the introduction of fresh solutions into the cell; Nernst e.m.f. = 56.4 mv.

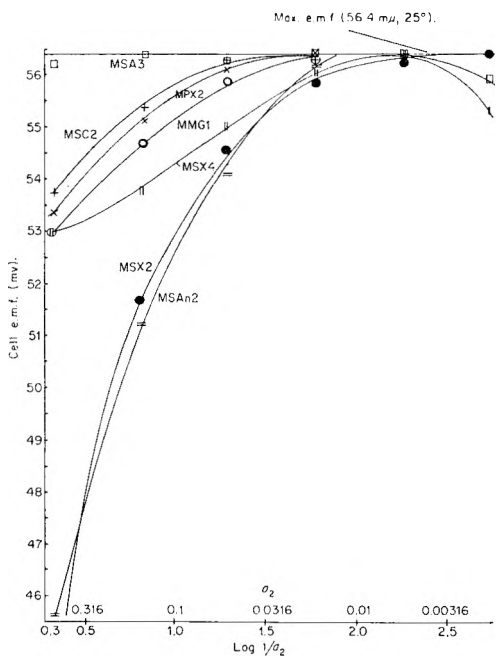

Fig. 4.—Cell e.m.f.–log $1/a_2$; where $a_1/a_2 = 3$ (constant) and the a_2 value at each point is that of the more dilute solution: □, MSA3 (NaA/polystyrene/silicone fluid); +, MSC2 (Na chabazite/polystyrene/silicone fluid); ×, MPX2 (NaX/polystyrene/silicone fluid); ‖, MSX4 (NaX/polystyrene/dinonyl phthalate); =, MSAn2 (Na analcite/polystyrene/silicone fluid); O, MMG1 (Na gel zeolite/polymerized methacrylate); ●, MSX2 (NaX/polystyrene, unfilled membrane).

MMX6 (containing the synthetic near-faujasite crystals, NaX) fell during use to 21.5 mv., corresponding to virtually the same value of T^+ as in aqueous sodium chloride. Similar unsatisfactory results were obtained with a membrane, MMAn1, in which the crystalline component was analcite.

On the other hand using a commercial gel aluminosilicate exchanger and, subsequently, crystals of NaA (Linde Sieve A) in methyl methacrylate polymerized *in situ* around the gel or crystals a more satisfactory behavior was observed. In the first membrane ideal selectivity was achieved at some concentration between 0.2 and 0.06 *m* NaCl solutions, and even between 2.0 and 0.7 *m* solutions an e.m.f. of 53 mv. was recorded. The second membrane (containing NaA) gave equally good results, the e.m.f. *vs.* time curves being recorded in Fig. 3. In both cases, even after prolonged conditioning in the sodium chloride solutions the resistance was relatively high. After very long periods however there was evidence of deterioration in membrane performance.

The better selectivities achieved in these two membranes are probably related to a common factor in their preparation, which was absent in the preparation of MMX6 and MMAn1. Both gel and NaA zeolite were outgassed before immersion in the methyl methacrylate monomer, and polymerization no doubt occurred of monomer which had penetrated into small pores in the gel or into intracrystalline channels in the porous crystal. This tended to anchor polymer chains to the exchanger, so that solution paths were now less readily formed by lifting the polymer away from the exchanger during conditioning in sodium chloride solution.

(c) In a further series of experiments fine crystals of NaA zeolite were compressed in molten paraffin wax. This membrane gave a reproducible e.m.f. only 1 mv. below the ideal value of 56.4 mv. between solutions of 2.0 and 0.7 *m* NaCl. However, introduction of more dilute solutions (0.7 and 0.2 *m*) appeared to initiate deterioration, and in this and subsequent experiments the e.m.f. began to fall. Permanence of the contact between inert filler and crystal surface in presence of the NaCl solutions is evidently still a problem.

Selectivity of Moulded Membranes Containing Inert Liquids.—Evidence obtained by electrical resistance measurements[1] suggests that membranes containing inert liquids could give the best selectivity. Accordingly the electromotive behavior of a number of these membranes was examined, the results being presented in Fig. 4. A comparison of Fig. 4 with Fig. 2 shows that the imbibition of inert fluids leads to an all-round improvement in membrane performance. For comparison, curves are shown of e.m.f. *vs.* log $^1/a_2^{\pm}$ for the membrane MSX2, the best unfilled moulded membrane of Fig. 2, and also for MMG1, the membrane referred to in the previous section and which was prepared from methyl methacrylate and gel aluminosilicate zeolite. Even the least selective of the membranes which have imbibed inert fluid (MSAn2) is equal in performance to membrane MSX2, and several of the membranes are better in performance than MMG1.

The electrical conductivity of analcite would be expected to be much less than that of chabazite, Linde Sieve A (NaA) or near-faujasites such as Linde Sieve X (NaX), because analcite is a relatively non-porous zeolite. Accordingly, crystal

conductivity in membrane MSAn2 would be least important, and most likely to be dominated by conduction in any solution paths through the crystal-resin membrane. The less satisfactory performance of this membrane can therefore be understood. As a pore-filling liquid, dinonyl phthalate did not behave as well as silicone oil, the aqueous solutions apparently being more quickly able to create solution paths. The less satisfactory behavior of membrane MSX4 than that of the silicone-filled membranes MPX2, MSC2 and MSA3 was attributed to this cause.

The membrane MSA3 was ideally selective for sodium chloride concentrations at least up to 2 *m*. Even after measurements lasting seven weeks had been made using this membrane in various aqueous solutions the e.m.f. in 2.02 and 0.673 *m* sodium chloride solutions had fallen by only 3 mv. from the ideal value of 56.4 mv. Thus the silicone fluid is only very slowly displaced and the creation of solution paths correspondingly delayed. A comparison of the silicone-filled membranes is given in Table II, which indicates limits of complete selectivity and deviations from the ideal e.m.f. of 56.4 mv. with solutions of 2 and 0.7 *m* in the cell compartments. In all, three membranes containing NaA and three containing NaX were examined, and it was observed that those containing the A-zeolite were more selective at high sodium chloride concentrations than those containing the X-zeolite. This difference may reflect only differences in mode of preparation. However, it is known that in 2 *m* NaCl solution the X-zeolite can imbibe a small amount of sodium chloride[13] (about 3% of the total intracrystalline mobile ions is then Cl^-), and this may set an upper limit to the cell e.m.f. in 2.02/0.673 *m* solutions. Thus, if Na^+ and Cl^- were equally mobile in the crystal, giving $T^+ = 0.97$ (*i.e.*, ignoring water transport and assuming only intracrystalline transport of ions), the cell e.m.f. would be 1.7 mv. below the maximum value of 56.4 mv.

Heteroionic Cells.—The selectivity of suitably prepared crystal-resin membranes as between Na^+ and Cl^- ions has been demonstrated to be nearly complete under appropriate conditions. It was then of interest to consider how far ion-sieve effects exist between two cations of different radii. Accordingly, the cell e.m.f.'s were measured where membranes separated solutions containing mixtures of cations with a common anion.

(a) Na^+, Cs^+ Mixtures.—A series of e.m.f. measurements then was made with NaCl + CsCl mixed solutions separated by the membrane MSAn2 of the previous section. Cs^+ at room temperature is virtually unable to diffuse in analcite crystals,[14] so that analcite could be electrochemically inert to this ion. The membrane itself would be electrochemically inert to Cs^+ only if no solution paths existed. In the previous section it was established that MSAn2 was ideally selective to Na^+, and so impermeable to Cl^-, at concentrations of NaCl of 0.06 *m* or less. Accordingly all mixed electrolyte concentrations were kept below this value. The mixed solutions A_1, A_2 and A_3 used had the compositions given in Table III. Then Fig. 5 shows the observed e.m.f.'s as a function of time for several combinations of the mixed electrolytes and of 0.00605*m* NaCl in the cell compartments.

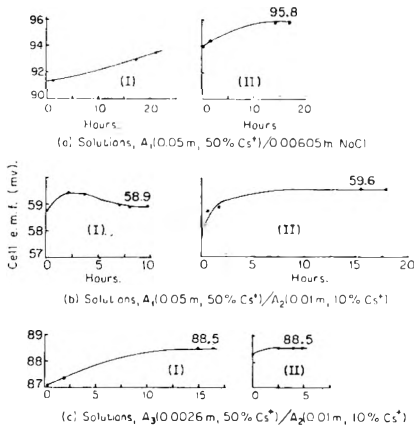

Fig. 5.—E.m.f. behavior in aqueous NaCl/CsCl mixtures of membrane MSAn2 (Na analcite/polystyrene/silicone fluid); calomel electrodes: (I), (II) indicate the introduction of fresh solutions into the cell.

If the membranes were impermeable to Cs^+ (as well as Cl^-) the e.m.f.'s would be governed only by $a^{\pm}$ for the NaCl in the two compartments. Then the calculated e.m.f.'s for the three combinations of Fig. 5, taken in order from top to bottom, would be 86.9, 51.2 and 95.2 mv. The observed values were 95.8, 59.6 and 88.5 mv., respectively, so that Cs^+ must contribute to transport within the membrane. Since Cs^+ would not, as noted above, contribute to intracrystalline conductivity the above result is further convincing evidence of solution paths in the membrane MSAn2. Estimates of transport numbers of Na^+ and Cs^+ in the membrane may be made using the equation given by Wyllie[15] for the membrane potential e_M

$$e_M = \frac{RT}{F} \ln \left\{ \frac{\sum_i (a_i v_i)_1}{\sum_i (a_i v_i)_2} \right\}$$

where the a_i's are the single ion activities of the ith cation in cell compartments, 1 and 2, and v_i's are the corresponding intra-membrane ionic mobilities. For the CsCl and NaCl mixtures this expression gives

$$e_M = \frac{RT}{F} \ln \frac{(Na^+)_1 + (Cs^+)_1 \frac{v_{Cs^+}}{v_{Na^+}}}{(Na^+)_2 + (Cs^+)_2 \frac{v_{Cs^+}}{v_{Na^+}}}$$

where (Na^+), (Cs^+) denote activities of Na^+ and Cs^+, respectively. Thus, if we subtract $(RT/F)\ln[(Cl^-)_1/(Cl^-)_2]$ from the observed cell e.m.f. we may evaluate e_M and then interpret it according to Wyllie's equation. Activity coefficients for Na^+ and Cs^+ single ions were taken as equal to mean activity coefficients for the NaCl and CsCl, respectively, in the mixed electrolyte, and for Cl^- were taken as the mean activity coefficients of

(13) R. M. Barrer and W. M. Meier, *J. Chem. Soc.*, 299 (1958).
(14) *E.g.*, R. M. Barrer, *Trans. Brit. Cer. Soc.*, **56**, 155 (1957).
(15) M. R. J. Wyllie, THIS JOURNAL, **58**, 67 (1954).

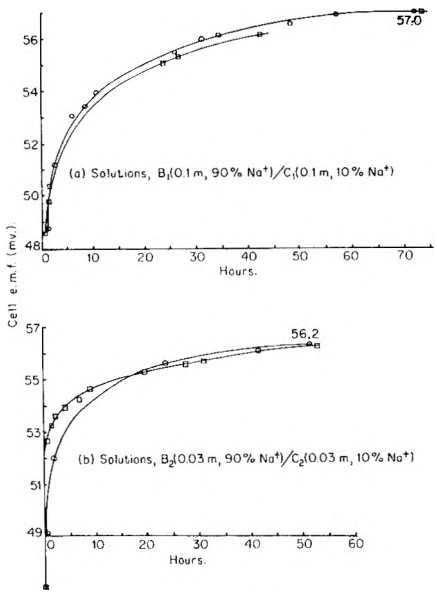

Fig. 6.—E.m.f. behavior in aqueous NaCl/Et_4NCl mixtures of membrane MSA4(NaA/polystyrene/silicone fluid). Readings O represent measurements made after the final refreshing of cell solutions; calomel electrodes: (a) direction of cell e.m.f. S. T. solution C_1 is positive; (b) direction of cell e.m.f. S. T. solution C_2 is positive.

sodium chloride solutions of the same molality as the Cl^-. Recalling that $T_{Cs^+} + T_{Na^+} = 1$, and taking $v_{Cs^+}/v_{Na^+} = T_{Cs^+}/T_{Na^+}$, the mean cesium ion transport numbers in the membrane are

Cell 1 (Soln. A_1 and 0.00605 *m* NaCl) $T_{Cs^+} = 0.294$
Cell 2 (Soln. A_1 and A_2) $T_{Cs^+} = 0.309$
Cell 3 (Soln. A_3 and A_2) $T_{Cs^+} = 0.256$

These figures are physically reasonable, and demonstrate the active role played by solution paths in the membrane.

(b) Na^+, $(C_2H_5)_4N^+$ Mixtures.—It has been established that $(C_2H_5)_4N^+$ ions are too large to penetrate the lattice of the A zeolite.[16] Thus Linde Sieve A should be electrochemically inert toward this ion, as would the crystal–resin membrane if no solution paths existed. Two stock solutions B_1 and C_1 were prepared having the compositions given in Table IV. When a membrane of NaA plus resin separates these two solutions the Na^+ and $(C_2H_5)_4N^+$ gradients are in opposite directions across the membrane and so the e.m.f. of the cell should be very sensitive to the extent to which electrical transport is divided between these two cations. If T_{Na^+} is 1, the solution C_1, more dilute with respect to Na^+ than B_1, should be about 60 mv. more positive than B_1, while if $T_{(C_2H_5)_4N^+}$ is 1, the converse is the case. To measure the variation of $T_{(C_2H_5)_4N^+}$ with total concentration, solutions B_1 and C_1 were diluted to give other pairs of solutions B_2, C_2 (Table IV).

The membrane MSA4 (NaA, polystyrene, silicone oil) was used to separate the solutions, the total molalities chosen being less than those at which the membrane was ideally selective to Na^+ so that the membrane was impermeable to Cl^-. Any effects of water transport were ignored. The solutions paired are those given in Table IV. In Fig. 6 the e.m.f.'s are shown as functions of time for several pairings of these solutions. The e.m.f.'s slowly approach reproducible limiting values. Calculations of mean transport numbers of the tetraethylammonium ions in the membrane gave, according to the procedure already outlined, the values

Cell 1 (Soln. B_1 and C_1) $T_{(C_2H_5)_4N^+} = 0.017$
Cell 2 (Soln. B_2 and C_2) $T_{(C_2H_5)_4N^+} = 0.020$

That these transport numbers are much lower than are values for Cs^+ in membrane MSAn2 is in accordance with the behavior in homoionic solutions, from which it was established that solution paths were less important in MSA4 than in MSAn2. Thus the former membrane shows in dilute solutions complete selectivity for Na^+ as compared with Cl^- and a nearly complete selectivity for Na^+ against $N^+(C_2H_5)_4$. The study of heteroionic cells gives clear guidance as to the relative importance of solution and intracrystalline conduction paths in crystal–resin membranes.

(16) R. M. Barrer and W. M. Meier, *Trans. Faraday Soc.*, **54**, 1074 (1958).

TABLE II

ELECTROMOTIVE BEHAVIOR OF FILLED MOULDED MEMBRANES

Membrane	Zeolite	Inert matrix	Upper limit of complete selectivity (molality of NaCl)	% Dev. from 56.4 mv. with NaCl at 2 and 0.7 *m* in cell
MSA3	NaA	Polystyrene–silicone oil	At least 2	0
MSC2	Chabazite	Polystyrene–silicone oil	0.2	4.8
MPX2	NaX	Polythene–silicone oil	0.06–0.2	5.5
MSAn2	Analcite	Polystyrene–silicone oil	0.06	19.3

TABLE III

COMPOSITIONS OF SOLUTIONS OF CsCl + NaCl

Solution	Molality, *m* Na^+	Cs^+	Cl^-
A_1	0.0262	0.0263	0.0525
A_2	.0119	.00133	.0132
A_3	.00131	.00131	.00262

TABLE IV

COMPOSITIONS OF SOLUTIONS NaCl + $(C_2H_5)_4NCl$ USED

Solution	Molality, *m* Na^+	$(C_2H_5)_4N^+$	Cl^-
B_1	0.0864	0.00943	0.0958
C_1	.00838	.0862	.0946
B_2	.0302	.00330	.0335
C_2	.00291	.0299	.0328

Discussion

The selectivity of the membranes studied in this work may be compared with that obtained for a variety of other membranes examined in homoionic membrane cells. Some results are summarized in Table V. It can be seen that the best crystal–resin membranes of this work (Table II and Fig. 2) compare well with any others. The life of the crystal–resin membranes is so far not

(17) M. Nagasawa and I. Kagawe, *Faraday Soc. Disc.*, **21**, 55 (1956).
(18) H. P. Gregor and K. Sollner, THIS JOURNAL, **54**, 330 (1950).
(19) C. E. Marshall and W. E. Bergmann, in ref. 7.
(20) C. E. Marshall and C. A. Krinbill, in ref. 7.
(21) H. P. Gregor, THIS JOURNAL, **61**, 141 (1957).
(22) K. Sollner, *ibid.*, **61**, 156 (1957).
(23) M. R. J. Wyllie, *ibid.*, **54**, 204 (1950).

TABLE V

RANGE OVER WHICH CELL E.M.F.'S OBEY IDEAL EQUATION $e = \frac{2RT^+}{F} \ln a_1^{\pm}/a_2^{\pm}$ ($T^+ = 1$)

Membrane	Soln.	Range of ideality	Ref.
Homogeneous cation exchanger Nepton CR51	NaCl	Non-ideal over whole range; 1.1 mv. too low at 0.001 N	17
Homogeneous anion exchanger of protamine collodion	KCl	Non-ideal over whole range; 1.1 mv. too low at 0.001 N	18
Homogeneous cation exchangers: single crystals of chabazite and apophyllite	NaCl	<0.1 N	19
Heterogeneous cation exchanger: films of clay platelets. Best results with beidellite	NaCl	< .1 N < .3 N	19 20
Heterogeneous cation exchanger: sulfonated polystyrene in PVC inert matrix	KCl	< .02 N	21
Homogeneous anion exchanger: inert collodion matrix with adsorbed[a] R^+Br^-	KCl	< .2 N	22
Heterogeneous cation exchangers in inert matrices: 25% Na-amberlite 1R 100 plus polymethyl methacrylate	NaCl	<3 N	23
25% Na-amberlite 1R 100 plus polystyrene		<2 N	
Bentonite plus polymethyl methacrylate		<2 N	

[a] R^+ denotes poly-2-vinylmethylpyridinium cation.

indefinite, and when about 1 mm. thick they give settled e.m.f.'s rather slowly. Nevertheless they may be made thinner and if bonding of the inert matrix to the crystals could be made permanent their effective life might be extended indefinitely. A limit to the performance of the membranes may then be set only by the high electrical resistances which could arise.

Where "ideal" e.m.f.'s as given by eq. 2 with $T^+ = 1$ are obtained with membrane cells, the neglect of t_w, a term which arises if there is electro-osmotic migration of water, would appear justified. Data on such transfer of water through ion-exchange resin membranes[24,25] would indicate that a low t_w would be associated with cation migration in the dense, high-exchange capacity zeolite crystals. There can be little free water in these crystals available for electro-osmotic transfer as water not bound to cations is in the field of the negatively charged aluminosilicate giant anion. Channels in these anions are indeed too narrow for normal double layer considerations to apply.[26] In solution paths involving crystal–resin pores, however, electro-osmotic transport may still play a part additional to loss of selectivity where the e.m.f. is observed to fall below the ideal value.

(24) R. T. Stewart and W. F. Graydon, THIS JOURNAL, **59**, 86 (1955).

(25) J. W. Lorimer, *Faraday Soc. Disc.*, **21**, 141 (1956).

(26) *E.g.*, R. M. Barrer, Vol. X of the Colston Papers, "The Structure and Properties of Porous Materials," Butterworths, 1958, p. 6.

MEASUREMENT OF THE SURFACE POTENTIALS OF METALS DUE TO ADSORPTION OF ORGANIC COMPOUNDS FROM SOLUTION

BY MELVIN H. GOTTLIEB[1]

Central Research Laboratories, Interchemical Corporation, New York, N. Y.

Received August 27, 1959

The surface potential as a function of the quantity adsorbed per unit area was studied in several systems. Adsorbates studied were stearic acid, octadecyl alcohol, octadecyl acetate and polyvinyl acetate; surfaces were platinum, stainless steel and chrome plate; solvents were benzene, chloroform and carbon tetrachloride. Similar surface potential—surface coverage data were obtained on all surfaces and with all solvents. For octadecyl acetate a linear relationship was found up to saturation adsorption of the ester, where a surface potential of about 500 mv. was found. The polyvinyl acetate data were initially linear, but abruptly levelled off, at about 500 mv., far below the saturation coverage of the polymer. Reproducible data could not be obtained with the acid and alcohol.

Introduction

The surface potential, *i.e.*, the change in the contact potential due to material adsorbed on a surface, is to a first approximation proportional to the number and the normal component of the dipole moments of the adsorbed molecules.[2] It is therefore in principle an attractive method for the determination of the detailed structure of the adsorbed layers. Such data have proven valuable in the study of adsorbed gases on metal surfaces[3a] and of spread monolayers of complex molecules on water.[3b] Surface potential measurements have not been applied to the study of adsorption on metals from solution,[4] undoubtedly largely because of the extreme ease with which clean metal surfaces

(1) Bell Telephone Laboratories, 463 West Street, New York, New York.

(2) I. Langmuir, *J. Am. Chem. Soc.*, **54**, 2798 (1932).

(3) (a) For example, J. C. P. Mignolet, *Bull. soc. chim. Belg.*, **64**, 126 (1955); (b) for examples see W. D. Harkins, "Physical Chemistry of Surface Films," Reinhold Publishing Co., New York, N. Y., 1952.

(4) F. M. Fowkes has recently studied the closely related problem of potentials of monolayers adsorbed at the metal–oil interface. The author wishes to express his appreciation for a preprint of this work. THIS JOURNAL, **64**, in press (1960).

are contaminated and the difficulties involved in utilizing, in a study of adsorption from solution, the high vacuum techniques which are necessary to keep the surfaces clean. Because surface potential data can now be accompanied by data on the quantity adsorbed at the surface by using radioisotopically labelled adsorbates, and because of a particular interest in the adsorption of polymers on metals, which can only take place from solution, an effort has been made to devise a practicable method of obtaining surface potential data.

Attempts to obtain the contact potentials of various metal plates whose surfaces had been freed of organic contamination were unsuccessful, since the potentials fluctuated markedly while the plates were exposed to the atmosphere for the potential measurement. It was therefore decided not to attempt measurements on surfaces free of organic material, but instead to work with surfaces which, after being initially freed of organic contamination, had been immersed in solvent (and the solvent subsequently allowed to evaporate). Relatively constant potentials were obtained, the residual adsorbed solvent apparently stabilizing the surface against adsorption from the atmosphere.

Since the contribution of the preadsorbed solvent to the potential is not known, the significance of the absolute values of the surface potential defined in this manner is not known. The shape of the surface potential–surface coverage curves for a given adsorbate–adsorbent system, as well as comparison of data for various adsorbates from the same solvent on a given metal, may, however, give valuable information.

The technique consists essentially of measuring the contact potential of a metal after immersion in a pure solvent and evaporation of the solvent, and again after immersion in a solution, followed by rinsing and evaporation of the solvent. The validity depends on there being no further change in the measured potential of the clean surface on further immersion in solvent after the preliminary solvent immersion. If this condition can be shown to have been met, any change in potential on immersion in a solution after a preliminary solvent immersion can be ascribed to the solute which is adsorbed from solution.

To be of value, this method for determining the surface potential must be capable of giving information on the surface potential as a function of the quantity adsorbed. The technique as developed permits the measurement of the surface potential for a given piece of metal at only one surface coverage; the data for a number of individual pieces must fall on a smooth curve. This problem is essentially one of obtaining metal surfaces which are macroscopically homogeneous from the point of view of the effect of adsorbed molecules on the surface potential.

The metals which were studied were those which it was believed might give most reproducible surfaces after a gentle flaming to remove organic surface contamination: platinum, chrome plate and stainless steel. No attempt has as yet been made to obtain data for adsorption on metal surfaces which are of most significant interest, *i.e.*, single crystal faces, ultra-smooth surfaces and surfaces whose oxide layers had been reduced.

The adsorbates which were studied on these surfaces were stearic acid, octadecyl alcohol, octadecyl acetate and a high polymer, polyvinyl acetate.

The solvents which were tried were: benzene, chloroform, carbon tetrachloride, toluene, acetone and ethylene dichloride.

Experimental

The procedure adopted for the measurement of the surface potential consists of (1) cleaning the metal surface by appropriate means, (2) immersing the sample in pure solvent for a standard period of time, usually one minute, (3) removing the sample from the solvent, draining the solvent, and allowing the plate to dry, (4) measuring the contact potential of the "solvated" surface, (5) immersing the plate in solution for up to two minutes, (6) removing the plate from solution, rinsing in solvent and drying as in (3), and (7) measuring the contact potential of the surface with the adsorbed solute. The difference between the contact potential measurements is the surface potential.

The adsorption of solute, in moles/cm.^{2}, is then calculated from measurements of radioactivity on the plate and the area of the plate.

Contact Potential Measurement.—Contact potentials were measured using the vibrating electrode apparatus as described by Zisman.[5]

As used in our laboratory, the apparatus was housed in a heavy metal stage. One metal plate, which was used as a permanent reference surface, was attached through a Lucite rod to the voice coil from a telephone speaker which was thus used as an oscillator. The plate which was to be measured was placed parallel to the reference plate on a removable metal platform. The reference plate and coil attachment were arranged so that their height could be varied easily, permitting the distance between the plates to be readily adjusted.

Measurements generally were made at 60 cycles per second, the voice coil driven by the 110 volt line stepped down to about 2 volts. The distance between the plates was approximately 0.5 mm. The current detecting system consisted of a two stage amplifier and an oscilloscope. A *p*H meter was used to measure the potential which was applied to the plates through a battery and slidewire.

The apparatus was sensitive to ± 2 mv.

According to the theory of the operation of the vibrating electrode system as outlined by Zisman,[5] the measured potential should be independent of the frequency of vibration of the plates. Contact potentials were found to be independent of frequency between 60 cycles per second and 1000 cycles per second. Similarly, the current generated by the vibrating electrodes should be proportional to the potential between the plates. A linear relationship between current and applied potential was found over a 200 mv. region on either side of the balance point of the instrument.

The reference plate used was a square of platinum, about one centimeter on a side, which had been well aged in air. The potential difference between this plate and a second platinum plate did not vary by more than 10 mv. over a period of a month. Since it is only necessary for the work function of the reference electrode to be constant between the measurements on the clean surface and the surface containing the adsorbed material, a period of several minutes, the platinum electrode was considered to be entirely suitable as a reference electrode.

The potential of the plate after withdrawal from the solvent remained constant for at least one minute. Thereafter, there was generally a decrease in potential of about 50 to 100 mv. over the following ten minutes. The initial potential reading was taken as the contact potential. The drifts with time were essentially the same regardless of whether the plate had been exposed previously to pure solvent or to solution; therefore the surface potential, which is the difference between two measurements, would remain unaffected by the time chosen for the measurement, provided it were kept constant.

(5) W. Zisman, *Rev. Sci. Instr.*, **7**, 367 (1932).

The drift in potential with time was most marked on humid days. Little drift was observed when the relative humidity was 50% or less. Currently, measurements are made in a room in which the relative humidity is kept below 50%.

Radioactive Materials.—Radioactive stearic acid was obtained from Tracerlab, Incorporated, Waltham, Mass., labeled with C-14 in the carboxyl position, at specific activity of 1 millicurie per millimole. It was added to a twenty-fold excess of recrystallized, highest purity non-radioactive stearic acid.

Radioactive octadecyl alcohol was obtained from New England Nuclear Company, Boston, Mass., labeled with C-14 in the 1 position, at a specific activity of 2 mc./mmole. It was added to a forty-fold excess of recrystallized, highest purity, non-radioactive octadecyl alcohol.

Radioactive octadecyl acetate was prepared from the radioactive octadecyl alcohol by reaction with acetic anhydride. One hundred and fifty mg. of the alcohol was dissolved in 1 ml. of pyridine and the solution chilled. One tenth ml. of acetic anhydride was added and the solution allowed to stand overnight at room temperature. The solution was then partitioned between 10 ml. of benzene and 15 ml. of 1 *N* HCl in H_2O. The benzene layer was washed with distilled water several times and dried with $MgSO_4$. No -OH was detected using a micro $LiAlH_4$ technique sensitive to 0.3% OH. The melting point of the sample was 32.0°, that of a recrystallized highest purity sample 31.8°, and of a mixture of the two 31.8°.

Radioactive polyvinyl acetate was obtained from Tracerlab, Incorporated. This material had been polymerized by irradiation of vinyl acetate labeled with C-14 at the 2-vinyl position and had a specific activity of 1.1 mc./g. It was used as received. The intrinsic viscosity in benzene at 30.0° was determined to be 0.95 dl./g. using a capillary viscometer; the slope of the reduced viscosity–concentration curve was 0.28. The molecular weight estimated from this data is 140,000.[6]

Metal Surfaces.—All metal samples were first extracted with benzene in a Soxhlet apparatus for 24 hours and stored under benzene. They were flamed in a non-luminous bunsen flame for about five seconds and immediately immersed in the solvent for the initial potential measurement. The surfaces were completely wettable by distilled water after flaming.

The chrome plate was commercial ferrotype plate from Apollo Metal Works, Chicago, Illinois. This is 1.2×10^{-5} cm. of chromium on steel, with intermediary layers of nickel and copper.

The stainless steel was 18/8 type 304. Samples were prepared both without further treatment and with two acid treatments as described by O'Connor and Uhlig[7]: 25% HCl and 25% H_2SO_4 at 35°, and 15% HNO_3 and 15% HF at 90°. These authors obtained surface roughness factors from BET measurements of 3.4 and 1.4, respectively, on the untreated and the two acid treated surfaces.

Platinum was used without further treatment.

Solvents.—All solvents were C.P. and were further purified by passing through silica gel and alumina columns.

Adsorption Procedure.—The metal plates were immersed in the various solutions for up to two minutes after the preliminary immersion in pure solvent and then were rinsed in three portions of solvent to prevent "carry out" of solution. Preliminary studies had shown no decrease in activity on the plates on rinsing in solvent after immersion in solutions which were dilute enough so that the effects of "carry out" would be negligible. It was thus concluded that no desorption took place during the rinse period.

Various degrees of surface coverage were obtained by varying the immersion time and also by varying solution concentration. Polyvinyl acetate solutions were from 10^{-3} to 10^{-2}%; solutions of the other materials from 0.1 to 1.0%.

The quantity of each adsorbate which could be adsorbed on each surface was determined by exposing the plates to solutions of a range of concentrations for various periods. The plates were flamed and immersed in solvent for one minute prior to immersion in the solution.

Autoradiographs made of the chrome plate surfaces after adsorption of each of the materials to various extents indicated that the adsorption on the surface was uniform to within the resolution of the Ansco Super Hypan film used, 80 lines/mm.

Determination of Quantity Adsorbed.—The quantity adsorbed on the metal plate was determined by counting using a thin window gas flow counter and a conventional scaling unit. The counting rate was converted to moles/cm.^{2} by comparing that of the plate with that of an aliquot of the solution of the same specific activity and of known concentration, evaporated to dryness on a plate of the same metal. The concentration of the known solution was sufficiently low so that no correction for sample thickness was necessary. No correction for backscattering was necessary since the unknown samples were on the same substrate. A straight line passing through the origin was always obtained on plotting counting rate against quantity of material on the plate.

Results

The contact potentials which were obtained after a preliminary immersion in solvent and again after a second immersion are given in Table I. Since in all cases there was some change in potential, an arbitrary limit of 20 mv. was set as an acceptable change in the potential. Chrome plate, platinum and untreated stainless steel may then be immersed in solution for up to two minutes, the acid treated steels for up to one minute.

Other solvents also were tested, using chrome plate, with unsatisfactorily high potential changes after a half minute or one minute preliminary immersion and a one minute second immersion: acetone, 50 mv.; ethylene dichloride, 150 mv. and xylene, 70 mv.

The surface potential at a given quantity adsorbed per unit area was not significantly dependent on the specific radioactivity of the ma-

TABLE I

Solvent	Preliminary immersion time, min.	E_0, mv.	Final immersion time, min.	E_t, mv.	ΔE, mv.
		Chrome plate			
Benzene	1	+350	1/4	+340	−10
	1	+430	1/2	+410	−20
	1	+440	1	+430	−10
	1	+480	2	+460	−20
	1	+425	3	+380	−45
	2	+500	1	+480	−20
	2	+580	2	+520	−60
	1/2	+490	2	+480	−10
	1/2	+380	3	+330	−50
CCl_4	1	+280	1/2	+270	−10
	1	+490	1	+480	−10
	1	+300	2	+275	−25
$CHCl_3$	1	+440	2	+420	−20
		Platinum			
Benzene	1	+385	1	+380	− 5
	1	+240	2	+230	−10
		Stainless steel (no acid treatment)			
Benzene	1	+400	1	+380	−20
	1	+370	2	+370	0
		Acid treatment #1			
Benzene	1	+240	1	+220	−20
	1	+200	2	+170	−30
		Acid treatment #2			
Benzene	1	+120	1	+100	−20
	1	+150	2	+110	−40

(6) V. Varadaiak, *J. Polymer Sci.*, **19**, 477 (1956).

(7) T. L. O'Connor and H. H. Uhlig, THIS JOURNAL, **61**, 402 (1957).

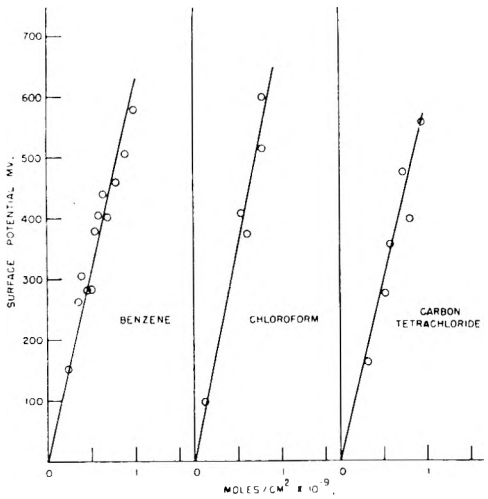

Fig. 1.—Surface potential as a function of surface coverage for octadecyl acetate adsorbed on chrome plate from various solvents.

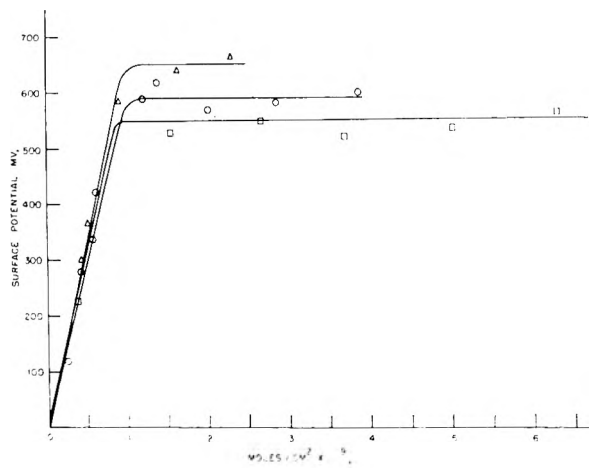

Fig. 2.—Surface potential as a function of surface coverage for polyvinyl acetate adsorbed on chrome plate from various solvents; benzene, ○; chloroform, △; carbon tetrachloride, □.

terial adsorbed, on the concentration of the solution used for adsorption, or on the immersion time in the solution.

Stearic Acid and Octadecyl Alcohol.—A wide scatter was obtained in the data for stearic acid and octadecyl alcohol on all surfaces studied. Essentially the same scatter and the same magnitude of potentials were found on platinum and on chrome plate.

The potentials for the alcohol appear to be significantly higher than those for the acid, maximum potentials of 250 and 150 mv., respectively, being obtained. The scatter did not permit the determination of the shape of the surface potential–surface coverage curve. Lower potentials were found on the stainless steel surfaces, with no significant differences between the alcohol and the acid.

Octadecyl Acetate and Polyvinyl Acetate.—Contrasted to the results obtained with the acid and alcohol, little scatter was observed with octadecyl acetate and with polyvinyl acetate. The curves for the surface potential as a function of surface coverage on chrome plate on adsorption from various solvents are shown in Figs. 1 and 2. (*Moles* in the case of polyvinyl acetate refers to monomer units, not polymer molecules.)

The curves for octadecyl acetate adsorbed from benzene on platinum, stainless steel and chrome are given in Fig. 3, the corresponding curves for polyvinyl acetate adsorbed from benzene in Fig. 4.

Adsorption Data.—In every case, excepting the adsorption of polyvinyl acetate from carbon tetrachloride, a limiting coverage was obtained which was not further increased by either increasing the solution concentration or increasing the immersion time in the solution. The maximum quantities which could be adsorbed on the various surfaces are given in Table II.

TABLE II

Metal	Adsorbate	Solvent	Max. adsorption obtainable, moles/cm.² × 10^{-9}
Chrome plate	Stearic acid	Benzene	3.8
	Stearic acid	Chloroform	4.0
	Stearic acid	Carbon tetrachloride	3.6
	Octadecyl alcohol	Benzene	4.2
	Octadecyl alcohol	Chloroform	4.2
	Octadecyl alcohol	Carbon tetrachloride	3.8
	Octadecyl acetate	Benzene	1.0
	Octadecyl acetate	Chloroform	0.88
	Octadecyl acetate	Carbon tetrachloride	0.92
	Polyvinyl acetate	Benzene	3.0
	Polyvinyl acetate	Chloroform	4.2
	Polyvinyl acetate	Carbon tetrachloride	>11
Platinum	Stearic acid	Benzene	4.4
	Octadecyl alcohol	Benzene	3.6
	Octadecyl acetate	Benzene	1.2
	Polyvinyl acetate	Benzene	4.3
Stainless steel	Octadecyl acetate	Benzene	1.0
	Polyvinyl acetate	Benzene	3.0
Stainless steel Treatment #1	Octadecyl acetate	Benzene	1.2
	Polyvinyl acetate	Benzene	4.1
Stainless steel Treatment #2	Octadecyl acetate	Benzene	1.3
	Polyvinyl acetate	Benzene	3.5

Discussion

The role played by the solvent in determining the surface potential is not as yet known and will have to be elucidated before the significance of these surface potential measurements is fully understood. It will be necessary to know the amount of solvent which remains on the clean surface after the latter has apparently dried, how much is irreversibly adsorbed, and how much is subsequently replaced by the adsorbate. This information will make it possible to determine the relative contributions to the surface potential of the removal of solvent molecules and the addition of adsorbate molecules to the surface, and to define precisely

the state of the surface before and after adsorption of the adsorbate in question. Radioactively labelled solvents of high specific activity would be necessary for this purpose. It is very significant that self-consistent surface potential data were obtained, as indicated by Figs. 1–4, although the absolute values of the contact potentials of nominally identical systems varied widely (Table I).

It is very possible that the surface potential data which are obtained are not characteristic of the structure of the adsorbed layers as adsorbed from the solution but refer to structures which result from rearrangements which take place on removal from the solution. Similar considerations apply to results obtained from other techniques used to study such adsorbed layers, *e.g.*, contact angles and electron diffraction measurements.

It is believed that most of the scatter in the data of Figs. 1–4 is due to non-uniformity of the metal surfaces and uncontrollable variations in the conditions under which the surfaces were flamed. It is not clear why reproducible data for the surface potential were not obtained with stearic acid and octadecyl alcohol, while reproducible data were obtained with the esters. The saturation adsorptions of stearic acid and octadecyl alcohol from benzene as indicated by Table II, were in all cases three to four times greater than those obtained for octadecyl acetate, indicating possible multimolecular adsorption of the former materials. It is possible that the sorption of the alcohol and acid are particularly sensitive to traces of water because of the –OH groups of these materials. (A referee has suggested that the scatter with these materials might be due to slow orientation processes.)

Langmuir has used the relationship

$$V = 2\pi\sigma\mu \qquad (1)$$

where V is the surface potential, σ the number of adsorbed dipoles per square centimeter and μ the dipole moment of the adsorbed material. This equation was derived for adsorption on a metal surface, assuming that each adsorbed dipole induced a "mirror image" dipole within the metal. The surfaces used in the present study were undoubtedly covered with the oxide of the metal, so that the concept of an induced electric image charge may not be applicable. Under these conditions, Mignolet[8] suggests the substitution of 4 for 2 in equation 1.

The data of Figs. 1 and 3 indicate at least qualitative agreement with equation 1 for octadecyl acetate, that is, a linear proportionality between surface potential and surface coverage. This would indicate that there is no major difference between the orientation of an octadecyl acetate molecule which is adsorbed at high surface coverage and one adsorbed at low coverage.

From equation 1 it is possible to calculate the dipole moment of the adsorbed octadecyl acetate. At a coverage of 1×10^{-9} mole/cm.^{2}, the surface potential is about 0.50 volt. Thus, in equation 1, $V = 0.500/300$ volts e.s.u., and $\sigma = 1 \times 10^{-9} \times 6.06 \times 10^{23}$ molecules/cm.^{2}. This leads to a value of 0.44×10^{-18} debye for the dipole moment; if the factor 4 were used in equation 1, μ would be

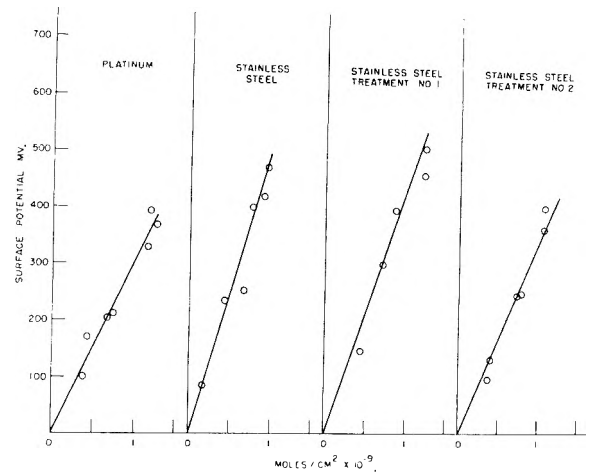

Fig. 3.—Surface potential as a function of surface coverage for octadecyl acetate adsorbed from benzene on various surfaces.

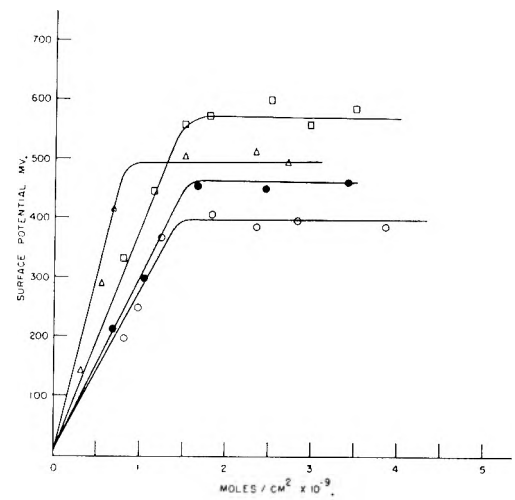

Fig. 4.—Surface potentials as a function of surface coverage for polyvinyl acetate adsorbed from benzene onto various surfaces: platinum, O; stainless steel, Δ: stainless steel treatment 1, □. Stainless steel treatment 2, ●.

0.22×10^{-18} debye. Both of these values are smaller than the actual dipole moment of a ester, for ethyl acetate, 1.8×10^{-18} debye.

Since only the component of the dipole moment perpendicular to the plane of the surface contributes to the measured potential, it might be expected that the roughness of the surface is responsible for the low moments obtained. It is believed that this factor is small however, since a roughness factor of either 4 or 8 would be required, and approximately the same surface potential and adsorption values were obtained on all surfaces. If the low values values are attributed solely to a non-perpendicular orientation of the dipoles, the angle between the dipole and the surface is calculated to be either 7 or 14°. This is considered to be improbably small.

The surface potentials which have been obtained on the metal surfaces are of the same magnitude, but lower than those found for insoluble monolayers of these materials on water. The surface potentials of condensed monolayers on water are: stearic acid (on dilute HCl) 400 mv.,[9]

(8) J. C. P. Mignolet, *Bull. soc. chim. Belg.*, **64**, 122 (1955).

(9) W. D. Harkins and E. K. Fischer, *J. Chem. Phys.*, **1**, 852 (1933).

octadecyl alcohol, 400 mv.[10] and octadecyl acetate 800 mv.[11]

These quantities also lead to low values for the calculated dipole moments. Harkins and Fischer[9] mention some reasons for the non-applicability of equation 1 to the calculation of the dipole moment from surface potential data; Schulman and Rideal[12] ascribe the discrepancies to the assumption of a dielectric constant of unity in equation 1. The fact that highest potentials were obtained with the ester leads to the conclusion that both carbon–oxygen dipoles of this group contribute to the potential, *i.e.*, both oxygen atoms are in the plane of the surface with the intermediate carbon atom out of this plane.

Crisp,[13] Hotta[14] and Schick[15] have determined the force–area and surface potential–area curves for polyvinyl acetate on water. If the surface potential data of these authors are plotted, as in this paper, as a function of surface coverage expressed as moles/cm.^{2} rather than Å.^{2}/molecule as used in film balance work, a curve is obtained which is similar to those obtained for the metal surfaces. There is an initial linear increase of potential with coverage and a leveling of the potential at 500 mv. at about 1×10^{-9} mole/cm.^{2}. The transition between the proportionality region and the plateau is somewhat more gradual on water than on the metal surfaces. This transition was interpreted in terms of the lifting of acetate groups from the surface at the higher film pressures.

The structure of adsorbed polymer molecules on solid surfaces has been discussed recently by several authors.[16–18] Conclusions in this regard may be made from a comparison of the surface potential–surface coverage data for the polyvinyl acetate with that for the octadecyl acetate. The experimental facts stand out: (1) the linear portion of the surface potential–surface coverage curve for the polymer essentially follows the straight line obtained with octadecyl acetate, and (2) the plateau of the polyvinyl acetate curve begins at the surface coverage which corresponds to the maximum quantity of octadecyl acetate which can be adsorbed. This implies that at surface coverages below the plateau region, all of the acetate groups from the polymer are oriented in contact with the metal surface, and that the arrangement of the acetate groups of the polymer at the surface is similar to that obtained with the independent ester groups of the octadecyl acetate.

The region in which the potential is independent of surface coverage is believed to correspond to the adsorption of polymer molecules with only a small fraction of the segments in contact with the surface, the remainder extended into solution in a coiled configuration of low net dipole moment. An alternate explanation of the plateau in the surface potential–surface coverage plot is that the plateau region corresponds to the adsorption of randomly coiled polymer molecules on top of the first layer of oriented polymer.

These structures are very different from that deduced by the Simha, Frisch and Eirich theoretical treatment of adsorption of macromolecules. These authors concluded that at all surface coverages only a few units of the chain are attached to the surface, with the remainder of the molecule extended, in a coil, into the solution. It is probable that this would hold for systems for which the interaction energy between surface and adsorbate was less than that in the system studied.

Many workers in this field have observed that[18,19] the maximum quantity of polymer which could be adsorbed from a given solvent is greatest for the poorer solvents for the polymer, that is, those in which the polymer has the lowest intrinsic viscosity. This was interpreted to indicate that the polymer was adsorbed in a configuration which depended on its configuration in solution. The theory which is postulated on the basis of the surface potential results states that the surface is first covered by a number of polymer groups which is independent of the solvent, with almost all of the polar groups oriented and in contact with the surface; subsequent polymer adsorption is determined by the configuration of the polymer molecule in the solution. The data of Fig. 2 and Table II indicate that although the maximum quantity of polyvinyl acetate which can be adsorbed from each solvent is different, the coverage at which the surface potential becomes independent of coverage is approximately the same.

Acknowledgments.—The author wishes to acknowledge the contribution of Mr. C. A. Kumins in many discussions of the work, and of Mr. G. Xenakis in constructing the contact potential apparatus. I also wish to express my appreciation to the Directors of Interchemical Corporation for permission to publish this work.

(10) N. K. Adam, J. F. Danielli and J. B. Harding, *Proc. Roy. Soc. (London)*, **A147**, 491 (1934).

(11) A. E. Alexander and J. H. Schulman, *ibid.*, **A161**, 115 (1937).

(12) J. H. Schulman and E. Rideal, *ibid.*, **A130**, 260 (1931).

(13) D. J. Crisp, *J. Coll. Sci.*, **1**, 49 (1949).

(14) H. Hotta, *ibid.*, **9**, 504 (1954).

(15) M. J. Schick, *J. Polymer Sci.*, XXV, 465 (1957).

(16) R. Simha, H. L. Frisch and F. R. Eirich, THIS JOURNAL, **57**, 584 (1953).

(17) H. L. Frisch and R. Simha, *ibid.*, **58**, 507 (1954).

(18) J. Koral, R. Ullman and F. Eirich, *ibid.*, **62**, 541 (1958).

(19) R. Stromberg, A. Quasius, S. Toner and M. Parker, *J. Research Natl. Bur. Standards*, **62**, 71 (1959).

POTENTIAL ENERGY BARRIER FOR ROTATION AND THE CONDENSATION COEFFICIENTS OF H_2 AND D_2 ON ALUMINA BY GAS CHROMATOGRAPHY

BY EARL M. MORTENSEN[1] AND HENRY EYRING

Department of Chemistry, University of Utah, Salt Lake City, Utah

Received September 10, 1959

From the retention times of ortho- and parahydrogen and deuterium on a chromatographic column the potential energy barrier hindering rotation and condensation coefficients were determined. The height of the barrier was found to be 460 cal./mole and the condensation coefficients, α, were calculated to be $\alpha_{p-H_2} = 1.0$, $\alpha_{O-H_2} = 0.53$, $\alpha_{p-D_2} = 0.55$, and $\alpha_{O-D_2} = 0.97$ on an alumina surface at 77.4°K.

In studying the evaporation and condensation from solids and liquids much attention has been given to determining the condensation coefficient[2] which is the ratio of the number of molecules that strike the surface and stick to the total number which strike. From the retention times on a chromatographic column we are able to calculate condensation coefficients of H_2 and D_2 on alumina.

Recently Moore and Ward[3] have shown that ortho- and parahydrogen could be separated by means of chromatography at 77.4°K. using an alumina column. Similarly they also showed that ortho and paradeuterium could be separated. By taking measurements off their graph the retention times t' for the ortho- and parahydrogen and deuterium to pass through the column are

$t'_{O-H_2} = 317$ sec. $\quad t'_{O-D_2} = 418$ sec.

$t'_{p-H_2} = 259$ sec. $\quad t'_{p-D_2} = 454$ sec.

From the dimensions of their column and the flow rate of the helium carrier gas, the average length of time t_{He} for the helium to pass through the column is approximately three seconds. This is the same average time that the ortho- and parahydrogen and deuterium spend in the vapor phase. The time, t, which the hydrogen and deuterium spend on the surface is, therefore

$t_{O-H_2} = 314$ sec. $\quad t_{O-D_2} = 415$ sec.

$t_{p-H_2} = 256$ sec. $\quad t_{p-D_2} = 451$ sec.

If we assume that the experiments were carried out on the linear portion of the isotherm, which is likely considering the small amounts of hydrogen or deuterium used, and if we assume that there is equilibrium between the vapor and the adsorbed molecules on the surface, then the ratio of the concentrations of ortho and para species on the surface to the concentration in the vapor phase is just proportional to t/t_{He}. Hence

$$\frac{[\text{O-X}_2(\text{s})]}{[\text{O-X}_2(\text{g})]} = \frac{at_{O-X_2}}{t_{He}}, \quad \frac{[\text{P-X}_2(\text{s})]}{[\text{P-X}_2(\text{g})]} = \frac{at_{P-X_2}}{t_{He}} \qquad (1)$$

where a is the constant of proportionality and X represents either H or D. In addition we may write

$$\frac{[\text{O-X}_2(\text{s})]}{[\text{O-X}_2(\text{g})]} = K_O'(X_2)\frac{f^r_{O,s}(X_2)}{f^r_{O,g}(X_2)}, \quad \frac{[\text{P-X}_2(\text{s})]}{[\text{P-X}_2(\text{g})]} = K_P'(X_2)\frac{f^r_{P,s}(X_2)}{f^r_{P,g}(X_2)} \qquad (2)$$

where $f^r_{O,s}(X_2)$, $f^r_{O,g}(X_2)$ and $f^r_{P,s}(X_2)$, $f^r_{P,g}(X_2)$ are the rotational partition functions for the surface and vapor, and $K_O'(X_2)$ and $K_P'(X_2)$ that part of the equilibrium constant containing the translational and vibrational degrees of freedom for the ortho and para species, respectively. In equation 2 we are not completely justified in separating the rotational motion from that of translation because we know that the molar volume[4] for liquid parahydrogen is greater than for the ortho species indicating that the rotational motion of orthohydrogen in the liquid is more restricted which results in greater orientation and, hence, a tighter packing due to van der Waal forces. We might expect a similar situation to exist for the adsorbed hydrogen or deuterium and the alumina surface. Now if the rotational and translational degrees of freedom were seperable, then we would expect that $K_O'(X_2)$ would equal $K_P'(X_2)$. Instead a better approximation would be to put

$$\frac{K_O'(H_2)}{K_P'(H_2)} \times \frac{K_O'(D_2)}{K_P'(D_2)} = 1 \qquad (3)$$

In equation 3 the configuration integral for $K_O'(H_2)$ which includes both the contributions of the potential energy associated with translation and that due to the coupling of the rotational and translational motions should equal the configuration integral of $K_P'(D_2)$. Likewise the configuration integrals of $K_P'(H_2)$ and $K_O'(D_2)$ should be equal. Upon combining equation 1 and 2 using equation 3 we obtain

$$\frac{f^r_{O,s}(H_2)f^r_{P,g}(H_2)f^r_{P,g}(D_2)f^r_{O,s}(D_2)}{f^r_{O,g}(H_2)f^r_{P,s}(H_2)f^r_{P,s}(D_2)f^r_{O,g}(D_2)} = \frac{t_{O-H_2}t_{O-D_2}}{t_{P-H_2}t_{P-D_2}} \qquad (4)$$

On the alumina surface we shall assume that there is some preferential direction of orientation and that the potential energy V may be approximated by an equation of the form

$$V = \tfrac{1}{2}V_0(1 - \cos 2\beta) \qquad (5)$$

Wilson[5] solved the wave equation for the linear rotator using equation 5 for the potential energy. Stern[6] calculated the energy levels of the hindered rotation for a few of the lowest levels in terms of the two parameters μ and λ defined by[7]

$$\lambda^2 = \frac{8\pi^2 I V_0}{h^2}, \quad \mu = \frac{8\pi^2 I}{h^2} W - \lambda^2$$

(1) Supported by the Standard Oil Company of California through a predoctoral research fellowship.

(2) O. Knacke and I. N. Stanski, "Progress in Metal Physics," Vol. 6, Pergamon Press Ltd., London, 1956, pp. 181–235; E. M. Mortensen and Henry Eyring, THIS JOURNAL, **64**, in press (1960).

(3) W. R. Moore and H. R. Ward, *J. Am. Chem. Soc.*, **80**, 2909 (1958).

(4) R. B. Scott and F. G. Brickwedde, *J. Chem. Phys.*, **5**, 736 (1937).

(5) A. H. Wilson, *Proc. Roy. Soc.* (*London*), **A118**, 628 (1928).

(6) T. E. Stern, *ibid.*, **A130**, 551 (1931).

(7) We are using a definition of V_0 which is twice as large as Stern's.

where I is the moment of inertia and W is the energy of the state. In order for the left-hand side of equation 4 to agree with the ratio of experimental t's on the right-hand side it was necessary to take

$$V_0 = 460 \text{ cal./mole}$$

The rotational energy levels $W_{J,M}$ then were determined using Stern's paper where the subscript J is the total angular momentum quantum number of the state when the hindering potential vanishes and M is the quantum number which specifies the component of angular momentum along the Z-axis. A few of the lowest rotational energy levels for both hydrogen and deuterium are found to be

hydrogen		deuterium	
$W_{0,0}$	= 260 cal./mole	$W_{0,0}$	= 260 cal./mole
$W_{1,0}$	= 480	$W_{1,0}$	= 340
$W_{1,1}$	= 670	$W_{1,1}$	= 520
$W_{2,0}$	= 1230	$W_{2,0}$	= 760
$W_{2,1}$	= 1260	$W_{2,1}$	= 750
$W_{2,2}$	= 1350	$W_{2,2}$	= 910

where $W_{J,M} = W_{J,-M}$.

Now, if we assume that there is no activation energy needed for condensation, the condensation coefficient α is the ratio of the internal partition function for the surface molecules to the internal partition function for the molecules in the vapor phase.[2] Since the vibrational partition function for the molecules on the surface and in the vapor is expected to be the same, the ratio of the internal partition functions just becomes the ratio of rotational partition functions.

Since the energies of the rotational partition functions for the surface are referred to a state having no rotation rather than to the zero point energy, the above rotational partition functions must be suitably corrected. The zero point energy for the para state of hydrogen is just $W_{0,0}$, and for the ortho state $W_{1,0} - E_1$ where E_1 is the rotational energy for a molecule in the vapor phase with $J = 1$. The condensation coefficients for hydrogen then are given by

$$\alpha_{P-H_2} = \frac{e^{-(W_{0,0}-W_{0,0})/RT} + e^{-(W_{2,0}-W_{0,0})/RT} + 2e^{-(W_{2,1}-W_{0,0})/RT} + 2e^{-(W_{2,2}-W_{0,0})/RT} + \ldots}{f^r{}_{P,g}(H_2)}$$

$$\alpha_{O-H_2} = \frac{e^{-[W_{1,0}-(W_{1,0}-E_1)]/RT} + 2e^{-[W_{1,1}-(W_{1,0}-E_1)]/RT} + \ldots}{f^r{}_{O,g}(H_2)}$$

so that

$$\alpha_{P-H_2} = 1.0$$
$$\alpha_{O-H_2} = 0.53$$

Similarly we find

$$\alpha_{P-D_2} = 0.55$$
$$\alpha_{O-D_2} = 0.97$$

We note that the condensation coefficients of both parahydrogen and orthodeuterium are at or near their maximum value. This is not surprising since neither species is rotating (except a few in excited states) in the vapor phase, and so all of these molecules which evaporate from the surface have essentially the gas phase distribution of rotational states giving rise to the maximum rate of evaporation. The molecules of orthohydrogen and paradeuterium do not have the same distribution of rotational states on the surface as in the vapor phase, and so upon evaporation these molecules do not go over into the same distribution as found in the vapor phase. As a result these molecules do not evaporate at the maximum rate. The reason that the condensation coefficient of orthodeuterium is not unity is because there are an appreciable number of molecules in excited rotational states and these behave in a similar manner to the molecules in the rotational states of orthohydrogen and paradeuterium. In parahydrogen the number of molecules in excited rotational states is negligible.

Acknowledgment.—The authors wish to express their appreciation to Dr. George Stewart for discussions on certain phases of this work and to Professor Paul Harteck for helpful suggestions.

THE PREPARATION AND IDENTIFICATION OF SOME INTERMETALLIC COMPOUNDS OF POLONIUM[1]

BY W. G. WITTEMAN, A. L. GIORGI AND D. T. VIER

Contribution from the University of California, Los Alamos Scientific Laboratory, Los Alamos, New Mexico

Received September 11, 1959

A micro technique for the preparation of intermetallic polonium compounds is described. Several compounds were prepared by this technique, and their composition and crystal structure were investigated by X-ray powder diffraction. The diffraction results obtained are summarized in Table II. Similar investigations indicated that (1) nickel and polonium apparently form compounds with a composition and a crystal structure which vary continuously between NiPo and $NiPo_2$ and between NiAs and $Cd(OH)_2$ structures, respectively; (2) gold and polonium form solid solutions over a wide range of composition; (3) tantalum, tungsten, molybdenum and carbon do not react with polonium; and (4) copper and silver formed compounds with polonium, but good X-ray data were not obtained.

Introduction

Little is known concerning high temperature reactions of polonium metal with other metals. The early literature on this phase of polonium chemistry contains only fragmentary information of doubtful significance. More recently, in an investigation of the action of molten polonium on gold, platinum, nickel and tantalum surfaces, compound or alloy formation with the first three metals was evident, but no reaction with tan-

(1) Work performed under the auspices of the Atomic Energy Commission.

talum was observed.[2] In addition, the preparation and identification of zinc polonide (ZnPo), lead polonide (PbPo), sodium polonide (Na_2Po), platinum polonide ($PtPo_2$), and nickel polonide (NiPo) have been reported by L. G. Fauble, R. E. Brockelhurst, L. F. Vassamillet, A. W. Martin, J. M. Goode, D. L. Timma and L. K. Lantz.[3]

Since such information is useful for an understanding of the chemistry and metallurgy of polonium, an investigation of the high temperature reactions of polonium with other metals appeared desirable. This paper summarizes all results that have been obtained in this investigation. A few of these results have been reported previously.[4]

Severe limitations are imposed on experimental procedures that can be considered for an investigation of high temperature reactions involving polonium metal. The known volatility[5,6] and oxide forming properties[7,8] of polonium metal require the reaction to be carried out in a closed system and either in an inert atmosphere or *in vacuo*. The small quantities of polonium available, as well as the high specific α-activity of polonium (32 curies of polonium weigh 7 mg. and produce 1 watt of heat), exclude macro techniques. Finally, the radioactive decay of polonium to form lead at the rate of 0.5% per day[9-11] requires both a purification of the polonium immediately before use and a short period of investigation with a particular sample.

Because of these limitations, a method for studying these reactions was developed which takes advantage of the high vapor pressure of polonium metal. The method offers a general micro technique for studying the reactions of any element which has a sufficiently high vapor pressure.

Experimental

The intermetallic compounds of polonium were prepared by two separate techniques: (1) a differential furnace technique for compounds of relatively low vapor pressure, and (2) a selective distillation technique for compounds of higher vapor pressure. In both techniques, the reaction chamber consisted of an evacuated and sealed quartz capillary of sufficient length to allow the section of the capillary containing the product to be flame-sealed and separated for subsequent X-ray diffraction analysis and calorimetric assay.[9,11]

In the first method, the metal to be investigated was placed in one end of the capillary, and a relatively large excess of freshly purified polonium metal was distilled into the other. The distillation technique is illustrated in Fig. 1. Up to 18 hours at 400° were required for the distillation. The capillary then was sealed, separated, and positioned within a differential furnace that maintained the metal end of the capillary at a higher temperature than the polonium end. Thus, the metal was exposed to polonium vapor at a pressure corresponding to the vapor pressure of polonium at the temperature of the colder end of the furnace and was free of excess polonium. The rate of reaction was conveniently followed by counting the γ-rays originating at the metal end of the capillary. For this purpose, a stilbene-type scintillation γ-counter was used with a lead slit system ($^3/_4$ inch wide, 6 inch long hole) which permitted the crystal to "see" only the base metal end of the capillary. Completion of the reaction was assumed when the γ-count reached a constant maximum value.

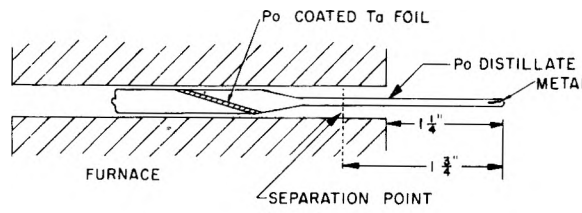

Fig. 1.

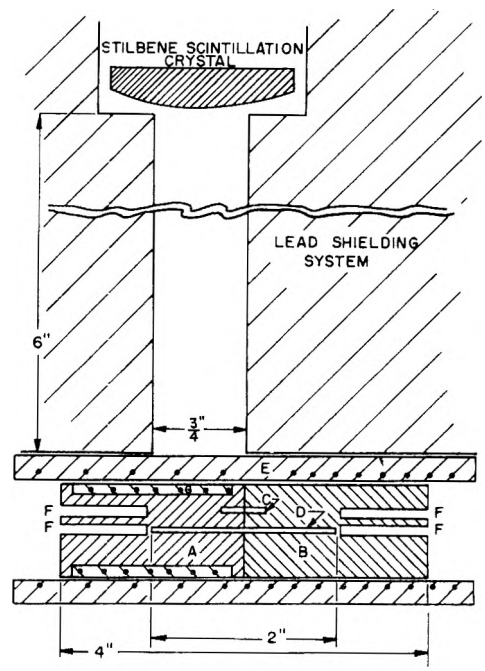

Fig. 2.

The experimental arrangement is illustrated in Fig. 2. The furnace was constructed from stainless-steel rod and was made up of two sections, (A) and (B). A capillary well (D) extended into both sections and was aligned in assembly by three studs (C). Two thermocouple wells (F) were included in each section. The temperature of the polonium section (B) was controlled by a tube furnace (E). The metal section (A) contained an insulated heater winding (G) which kept this section at a fixed higher temperature. Temperatures were maintained within $\pm 10°$.

In the second method, the capillary was first prepared as described above. The capillary then was placed in a horizontal tube furnace. The reaction, at increasingly higher temperatures, was followed conveniently by periodically removing the capillary for visual inspection. Completion or partial completion of the reaction was assumed when the base metal deposit fluoresced in a darkened room. Upon partial completion of the reaction, the position of the capillary was changed to expose a section outside the furnace so that selective distillations of the excess metals and the reaction product could be achieved.

Although attempts were made to determine the formula of the compounds by using weighed quantities of metal and by determining the polonium content of the compound by calorimetry, these attempts were not fruitful. Accordingly, formulas are assigned on the basis of X-ray data alone, and

(2) W. G. Witteman, G. N. Spillert and D. T. Vier, Los Alamos Scientific Laboratory Report LA-1546, 1953 (classified).

(3) H. V. Moyer, editor, "Polonium," TID-5221, Office of Technical Services, Department of Commerce, Washington 25, D. C., 1956.

(4) W. G. Witteman, A. L. Giorgi and D. T. Vier, Los Alamos Scientific Laboratory Reports LA-1562, 1953, and LA-1890, 1955.

(5) L. S. Brooks, *J. Am. Chem. Soc.*, **77**, 3211 (1955).

(6) A. L. Giorgi, recent investigation in this Laboratory, to be reported in a separate article.

(7) G. H. Moulton, J. D. Farr and D. T. Vier, Los Alamos Scientific Laboratory Report LA-1523, 1953.

(8) K. W. Bagnall, "Chemistry of the Rare Radioelements," Academic Press, Inc., New York, and Butterworths Scientific Publications, London, 1957.

(9) W. H. Beamer and W. E. Easton, *J. Chem. Phys.*, **17**, 1298 (1949).

(10) D. C. Ginnings, A. F. Ball and D. T. Vier, *J. Research Natl. Bur. Standards*, **50**, 75 (1953).

(11) J. F. Eichelberger, K. C. Jordon, S. R. Orr and J. R. Parks, *Phys. Rev.*, **96**, 719 (1954).

TABLE I

POLONIDE PREPARATION

Metal	Source of metal	Metal temp., °C.	Po temp., °C.	Po pressure, mm.	Reaction time, hr.	Remarks
Be	Brush Be	600	575	7	7	
Mg	Brawn	450	425	0.3	5	
Ca	Merck	550	525	3	7	
Sr	MacKay	500	500	1	24	Po was distilled off at 400°
Ba	King Labs.	525	525	3	5	Po was distilled off at 400°
Zn	N.B.S.	550	535	3	5	ZnPo condensed in center of capillary
Cd	Baker	550	550	4	16	Metals were distilled off at 475°. CdPo distilled at 525°
Hg	Quick Silver Prod.	200	200	17	4	Hg was distilled off at 200°. HgPo distilled at 400°
Pb	Gen. Chem.	350	350	0.02	3	Metals were distilled off at 665°. PbPo distilled at 700°

such questions as the solubility of the metal or polonium in the polonide are left unanswered. However, analogy with the sulfides, tellurides and selenides, including comparison of calculated covalent radii, would indicate that the compounds are near stoichiometric.

The polonium was obtained as a metallic deposit on platinum gauze. It contained varying amounts of lead and, possibly, bismuth. The polonium purification procedure consisted of the following steps.

(a) The polonium was distilled from the platinum gauze onto a glass surface where it was deposited as a polonium mirror.

(b) The polonium mirror was dissolved in 15 ml. of 7.8 N HNO_3, and diluted to 78 ml. volume and the polonium electroplated on a tantalum foil[12] (0.010 inch thick).

(c) The polonium metal was distilled from the tantalum foil into the quartz reaction chamber to give 99+% pure Po.

All exposures were taken on Eastman Type-A X-ray film in a North American Philips 114.59 mm. diameter powder camera. Copper radiation from a General Electric CA-6 X-ray diffraction tube was used in a General Electric XRD-1 unit. The films were measured without magnification with a pointer attached to a slide. A vernier scale permitted measurements of any one sharp line to within a possible error of ±0.1 mm.

A nickel foil (0.001 cm. thick) was used over the camera pinhole assembly to filter out the K-β radiation from the copper. Since the high α-activity of polonium caused the quartz capillary to fluoresce strongly, it was necessary to cover the film in the camera with a sheet of black photographic paper (0.001 cm. thick). This procedure proved to be completely effective in eliminating any fogging from the fluorescence and had no effect on the normal exposure time of 18 to 20 hours used in all runs. The samples were contained in quartz capillary tubes of approximately 0.5 mm. diameter and 0.15 mm. wall thickness.

The relative intensities of the powder lines were calculated from the expression

$$I_{calc} \sim \frac{1 + \cos^2 2\theta}{\sin^2 \theta \cos \theta} pF^2$$

with no corrections for the absorption and temperature factors being made. It was impossible to determine accurately the temperature of the diffraction samples at exposure time since the decay of polonium caused a small temperature rise in the sample which varied with the size and configuration of the sample.

Preparation of Samples and X-Ray Diffraction Results

Group II Polonides and Lead Polonide.—The experimental conditions used in the preparation of these polonides are shown in Table I. All polonides were prepared from high purity, commercially available metals. Except for liquid mercury, the metals were used in the form of 150-mesh powder or filings.

With the exception of MgPo and HgPo, each compound had the same crystal structure as the corresponding sulfide, selenide and telluride, as evidenced by the agreement between calculated and observed X-ray line intensities. Accordingly, the polonide was assigned the same formula as the corresponding sulfide, selenide and telluride of the metal. Examination of calculated covalent radii (and R-X distances) supported this assignment.

In the case of MgPo, the unit cell was smaller than that of MgTe as reported by Zachariasen.[13] Since the radius of the polonium atom is larger than that of the tellurium atom, the unit cell would be expected to be larger if the two compounds were isomorphous. It would appear, therefore, that the magnesium polonide cell is not the same type (ZnO) as that of MgTe. A similar situation existed in the case of mercury polonide, which indicated that this compound did not have the same type of structure (ZnS) as that reported for HgTe.[14] The assignment of the structure type and formula in these two cases is discussed below.

The results of the X-ray diffraction analysis are shown in Table II. Also included are a description of the physical appearance of the polonide and the total amount of polonium in the X-ray sample. The latter is the maximum size of the sample since it was not always possible to completely eliminate polonium from the extremity of the X-ray capillary.

Nickel Polonide.—Nickel wire (0.0015 inch diameter, Grade A, W. B. Driver Co.) was used in the preparation of nickel polonide samples by the differential furnace method. Several reactions were carried out in which known weights of wire were heated between 300 and 600°, in polonium vapor. A crystalline metal product resulted in each case. From the amount of polonium contained in each sample, the experimental mole ratios of polonium to nickel were calculated. Mole ratios consistent with the X-ray lattice parameters and heating temperature were not obtained, but in most cases the ratio Po/Ni was between 1 and 2. The calculated experimental mole ratios assumed that none of the nickel was lost by volatilization of the polonide. This assumption was not valid since the nickel polonide was quite volatile and tended to distil toward the cold end of the capillary, particularly at temperatures above 500°. At these temperatures crystal plates of the polonide were formed whose surfaces exhibited a high metallic luster.

The X-ray diffraction patterns indicated a hexagonal, close-packed structure for the nickel polonide with lattice constants $a_0 \cong 3.95$ Å. and $c_0 = 5.68$ Å.

Tungsten, Molybdenum, Tantalum and Carbon Polonides.—Similar experiments were performed using tungsten, molybdenum, tantalum and carbon bathed in polonium vapor at temperatures up to 700°, but no reaction occurred.

Gold, Copper and Silver Polonides.—Gold was found to dissolve polonium vapor at temperatures above 650°, the solubility depending both on the temperature of the gold and the relative temperature of the gold and polonium ends of the capillary. However, no compound was observed.

Copper and silver both formed compounds (see ref. 3, also), but good X-ray data were not obtained. Copper polonide was both unstable and volatile at about 400°.

Volatility of Polonides.—In the preparation of these polonides, the volatility of the polonide often dictated its method of preparation. Also, the volatility of polonides is of general interest in high temperature use of polonium deposits. Accordingly, order-of-magnitude estimates of vola-

(12) M. G. Bowman and N. H. Krikorian, Los Alamos Scientific Report LA-1402, 1953 (classified).

(13) W. H. Zachariasen, *Z. physik. Chem.*, **124**, 277 (1926).

(14) R. W. G. Wyckoff, "Crystal Structures," Vol. I, Interscience Publishers, Inc., New York, N. Y., 1951.

TABLE II

POWDER DIFFRACTION RESULTS

Formula of polonide	Description	Wt. of Po, mg.	Symmetry	Type	Unit cell dimensions, Å.	X-Ray density, g./cc.
BePo	Black powder	202	f.c.c.	ZnS	5.838 ± 0.006	7.3
MgPo	Black	86	h.c.p.	NiAs	4.345 ± .010	
					7.077 ± .020	6.7
CaPo	Grey, non-metallic	294	f.c.c.	NaCl	6.514 ± .006	6.0
SrPo	Grey, metallic	63	f.c.c.	NaCl	6.796 ± .003	6.3
BaPo	Grey, metallic	47	f.c.c.	NaCl	7.119 ± .003	6.3
ZnPo	Metallic crystalline	20	f.c.c.	ZnS	6.309 ± .004	7.2
CdPo	Grey, metallic, crystalline	16	f.c.c.	ZnS	6.665 ± .004	7.2
HgPo	Metallic	12	f.c.c.	NaCl	6.250 ± .003	11.1
PbPo	Metallic, crystalline	12	f.c.c.	NaCl	6.590 ± .003	9.6

tility as obtained from this investigation are given in Table III.

TABLE III

TEMPERATURE AT WHICH THE SUBLIMATION (OR VAPOR) PRESSURE OF POLONIDE IS ESTIMATED TO BE 0.1 MM.

	Volatile				Non-volatile		
Polonide	Hg	(Po), Cu	Zn, Cd, Ni	Pb	Mg	Be, Ca	Sr, Ba
Temp., °C.	300	400	500	700	>500	>600	>650

The high volatility of HgPo and its ease of formation at 200° (or below) are of special interest. For instance, this indicates that precautionary measures must be taken when polonium is handled in a vacuum system to avoid contamination of the polonium by HgPo.

X-Ray Powder Diffraction Data.—Comparisons of the calculated and observed intensities for the polonides are shown in Tables IV through XII.

TABLE IV

BERYLLIUM POLONIDE

Indices *hkl*	$\sin^2\theta$ Obsd.	$\sin^2\theta$ Calcd.[a]	Relative intensities Obsd.[b]	Calcd. (ZnS)
111	0.0524	0.0522	VS	1.00
200	.0699	.0696	MS	0.49
220	.1395	.1393	MS	.42
311	.1912	.1915	MS	.49
222	.2097	.2089	W	.13
400	.2781	.2785	F	.07
331	.3303	.3307	MW	.19
420	.3480	.3482	MW	.17
422	.4171	.4178	W	.14
511–333	.4700	.4700	W	.16
440	....	.5571	Nil	.05
531	.6107	.6093	MW	.18
442–600	.6260	.6267	W	.11
620	....	.6963	Nil	.09
533	....	.7485	Nil	.09
622	.7676	.7659	VW	.10
444	....	.8356	Nil	.04
711–551	.8889	.8878	W	.30

[a] $\sin^2\theta$ values calculated for a_0 = 5.838 A. [b] VS = very strong, S = strong, MS = moderately strong, M = moderate, MW = moderately weak, W = weak, F = faint, VF = very faint, B = broad.

TABLE V

MAGNESIUM POLONIDE

Indices *hkl*	$\sin^2\theta$ Obsd.	$\sin^2\theta$ Calcd.[a]	Relative intensities Obsd.	Calcd. (NiAs)	Calcd. (ZnO)
100	0.0418	0.0419	MS	0.12	0.35
002	.0474	.0474	MS	0.20	0.31
101	.0539	.0538	VS	1.00	1.00
102	.0897	.0893	MW, B	0.27	0.21
110	0.1255	0.1257	S	0.27	0.32
103	.1481	.1486	M, B	.25	.35
112	.1733	.1731	S	.20	.32
201	.1797	.1795	M	.19	.19
004	.1894	.1896	W	.05	.04
202	.2161	.2150	W	.07	.06
203	.2743	.2743	MW	.09	.13
210	.2934	.2933	VW	.04	.04
211	.3051	.3052	M	.15	.16
114	.3151	.3153	M	.12	.09
105	.3405	.3382	W, B	.06	.09
212		.3407		.06	.06
300	.3765	.3771	MW	.04	.05
213	.3995	.4000	MW	.10	.14
302	.4244	.4245	MW, B	.05	.05
006		.4266		.01	.01
205	.4643	.4639	F	.05	.05
106		.4685		.02	.02
220	.5044	.5028	F	.03	.04
222	.5531	.5502	W, B	.04	.05
116		.5523		.04	.04
311		.5566		.07	.09
304	.5679	.5667	W	.05	.04
215	.5903	.5896	W, B	.06	.09
312		.5921		.03	.03
206		.5942		.01	.01
313	.6520	.6511	VW	.06	.09
224	.6954	.6924	VW	.05	.04

[a] $\sin^2\theta$ values calculated for a_0 = 4.345 Å., and c_0 = 7.077 Å.

Discussion

Magnesium Polonide.—The X-ray diffraction pattern for the magnesium polonide sample conformed to the hexagonal system. The cell dimensions give an axial ratio of 1.629 which favors a ZnO structure type. However, the unit cell of MgPo is smaller than the unit cell of MgTe. Since the radius of the polonium atom is larger than that of the tellurium atom, the unit cell would be expected to be larger if the two compounds were isomorphous. It would appear, therefore, that the magnesium polonide cell is not of the ZnO type. A NiAs arrangement is suggested as this would more conveniently accommodate the atoms.

For purposes of comparison, relative line intensities were computed for a magnesium polonide structure of the ZnO type (MgTe type) and of a NiAs type. In the calculations for the NiAs arrangement, the polonium parameter was varied

TABLE VI

CALCIUM POLONIDE

Indices *hkl*	$\sin^2\theta$ Obsd.	$\sin^2\theta$ Calcd.[a]	Relative intensities Obsd.	Relative intensities Calcd. (NaCl)
111	0.0425	0.0419	S	0.81
200	.0563	.0559	VS	1.00
220	.1129	.1118	S	0.77
311	.1546	.1538	MS	.44
222	.1684	.1678	M	.28
400	.2248	.2237	MW	.13
331	.2660	.2656	M	.19
420	.2805	.2796	MS	.37
422	.3361	.3355	MS	.26
511–333	.3774	.3775	M	.14
440	.4474	.4474	VW	.09
531	.4895	.4893	M	.15
442–600	.5035	.5033	M	.18
620	.5592	.5592	W	.13
533	.6014	.6012	VW	.06
622	.6150	.6151	W	.13

[a] $\sin^2\theta$ values calculated for $a_0 = 6.514$ Å.

TABLE VII

STRONTIUM POLONIDE

Indices *hkl*	$\sin^2\theta$ Obsd.	$\sin^2\theta$ Calcd.[a]	Relative intensities Obsd.	Relative intensities Calcd. (NaCl)
111	0.0385	0.0385	M	0.30
200	.0509	.0514	VS	1.00
220	.1030	.1028	S	0.78
311	.1413	.1413	W	.17
222	.1543	.1541	M	.29
400	.2060	.2055	W	.14
331	.2448	.2441	F	.08
420	.2574	.2569	M	.37
422	.3085	.3083	M	.27
511–333	.3474	.3468	F	.06
440	.4117	.4111	F	.09
531	.4480	.4496	F	.06
600–442	.4630	.4624	M	.18
620	.5143	.5138	W	.13
533	....	.5524	Nil	.02
622	.5660	.5652	M	.12
444	.6187	.6166	F	.04
711–551	....	.6551	Nil	.05
640	.6677	.6680	W	.11
642	.7184	.7194	M	.24
731–553	.7595	.7579	F	.08
800	....	.8221	Nil	.04
733	....	.8607	Nil	.03
820–644	.8727	.8735	M	.35
660–822	.9261	.9249	M	.34

[a] $\sin^2\theta$ values calculated for $a_0 = 6.796$ Å.

TABLE VIII

BARIUM POLONIDE

Indices *hkl*	$\sin^2\theta$ Obsd.	$\sin^2\theta$ Calcd.[a]	Relative intensities Obsd.	Relative intensities Calcd. (NaCl)
200	0.0472	0.0468	VS	1.00
220	.0941	.0937	VS	0.80
222	.1414	.1405	M	.30
400	.1884	.1873	W	.14
420	.2351	.2341	S	.39
422	.2816	.2810	M	.29
440	.3750	.3746	W	.09
600–442	.4222	.4214	M	.19
620	.4688	.4683	MW	.13
622	0.5158	0.5151	W	0.12
444	.5621	.5621	F	.04
640	.6091	.6087	W	.10
642	.6557	.6556	S	.21
800	....	.7492	Nil	.03
820–644	.7951	.7960	S	.24
822–660	.8418	.8429	S	.21
662	.8885	.8897	M	.17
840	.9344	.9365	MW	.11

[a] $\sin^2\theta$ values calculated for $a_0 = 7.119$ Å.

TABLE IX

ZINC POLONIDE

Indices *hkl*	$\sin^2\theta$ Obsd.	$\sin^2\theta$ Calcd.[a]	Relative intensities Obsd.	Relative intensities Calcd. (ZnS)
111	0.0449	0.0447	VS	1.00
200	.0597	.0596	M	0.21
220	.1195	.1192	VS	.64
311	.1638	.1640	S	.50
222	.1793	.1789	W	.06
400	.2393	.2385	W	.11
331	.2840	.2832	M	.21
420	.2990	.2981	W	.09
422	.3588	.3577	M	.21
511–333	.4038	.4024	M	.15
440	.4778	.4770	VF	.07
531	.5214	.5217	M	.17
600–422	.5268	.5366	F	.05
620	.5963	.5962	W	.12
533	.6404	.6409	F	.07
622	.6550	.6558	VF	.03
444	.7150	.7155	VF	.04
711–551	.7606	.7602	W	.16
640	....	.7751	Nil	.04
642	.8339	.8347	M	.30
731–553	.8802	.8784	M	.34

[a] $\sin^2\theta$ values calculated for $a_0 = 6.309$ Å.

TABLE X

CADMIUM POLONIDE

Indices *hkl*	$\sin^2\theta$ Obsd.	$\sin^2\theta$ Calcd.[a]	Relative intensities Obsd.	Relative intensities Calcd. (ZnS)
111	0.0404	0.0401	VS	1.00
200	....	.0534	Nil	0.08
220	.1077	.1068	S	.75
311	.1477	.1469	MS	.52
222	....	.1603	Nil	.03
400	.2146	.2137	W	.13
331	.2545	.2538	M	.22
420	....	.2671	Nil	.04
422	.3208	.3205	MS	.26
511–333	.3610	.3606	M	.16
440	.4292	.4274	F	.08
531	.4674	.4674	W	.16
600–442	....	.4808	Nil	.02
620	.5336	.5342	W	.13
533	.5735	.5743	VF	.07
622	....	.5876	Nil	.01
444	....	.6411	Nil	.04
711–551	....	.6811	W	.13
640	....	.6945	Nil	.01
642	.7490	.7479	M	.26
731–553	.7872	.7880	M	.23

[a] $\sin^2\theta$ values calculated for $a_0 = 6.665$ Å.

from 0.22 to 0.28. The most satisfactory agreement between calculated and observed line intensities was obtained for a polonium parameter of 0.250. The latter are the values listed in Table V.

TABLE XI

MERCURY POLONIDE

Indices hkl	$\sin^2\theta$ Obsd.	$\sin^2\theta$ Calcd.[a]	Relative intensities Obsd.	Relative intensities Calcd. (NaCl)
200	0.0612	0.0608	VS	1.00
220	.1217	.1215	S	0.77
222	.1825	.1823	M	.28
400	.2431	.2430	MW	.13
420	.3041	.3038	MS	.36
422	.3650	.3645	M	.27
440	.4871	.4860	F	.09
600–442	.5474	.5468	M	.20
620	.6076	.6075	W	.15
622	.6680	.6683	W	.15
444	....	.7290	Nil	.05
640	.7888	.7898	W	.17
642	.8496α_1	.8505α_1	M	.41
	.8537α_2	.8548α_2		

[a] $\sin^2\theta$ value calculated for $a_0 = 6.250$ Å.

TABLE XII

LEAD POLONIDE

Indices hkl	$\sin^2\theta$ Obsd.	$\sin^2\theta$ Calcd.[a]	Relative intensities Obsd.	Relative intensities Calcd. (NaCl)
200	0.0548	0.0546	VS	1.00
220	.1093	.1093	VS	0.79
222	.1637	.1639	MS	.29
400	.2194	.2185	M	.14
420	.2738	.2731	S	.38
422	.3285	.3278	MS	.27
440	.4385	.4370	W	.09
600–442	.4925	.4917	M	.19
620	.5473	.5463	M	.14
622	.6008	.6009	M	.13
444	....	.6555	VF	.04
640	.7102	.7102	MW	.14
642	.7649	.7648	M	.29
800	.8731	.8741	F	.05
820–644	.9278α_1	.9287α_1	MS	.53
	.9327α_2	.9333α_2		
822–660	.9822	.9833	MS	.82

[a] $\sin^2\theta$ values calculated for $a_0 = 6.590$ Å.

Except for the reflections from the 102 and 103 planes, the observed line intensities are in good agreement with the values calculated for the NiAs structure. Of special interest are the sharp reflections from the 211 and 114 planes. Here one would expect approximately equal intensities from the NiAs-type structure and a difference of almost a factor of 2 between the intensities of the two lines from a ZnO-type structure. A NiAs-type structure is suggested since the two lines are actually of about equal intensity. Although the lines from the 102 and 103 planes are less intense than expected for a NiAs-type structure, one may still accept this structure for magnesium polonide since the lines are rather broad and diffuse and, hence, may be expected to appear less intense. Further, consideration of either the ionic or atomic radii of magnesium and polonium atoms, together with the interatomic distances calculated for the two structures, renders the ZnO structure inherently unlikely and suggests that magnesium polonide has a NiAs-type of structure. On this basis, the formula of magnesium polonide is presumed to be MgPo.

Mercury Polonide.—Consideration of the relative scattering factors of the two atoms, and the observation that only those reflections were found on the pattern where h, k and l were even, suggested that the cell was of the NaCl type. Close agreement between the observed and calculated intensities based on a NaCl f.c.c. cell indicates that mercury polonide is of the NaCl type and has the formula HgPo.

Nickel Polonide.—The first sample of nickel polonide was in the form of rather large crystals and yielded an X-ray pattern comprised of a large number of spots rather than the usual diffraction lines. The X-ray sample was heated above the melting point of the polonide (~625°) and then cooled rapidly in an attempt to decrease crystal size. This treatment not only decreased the size of the crystals (as evidenced by lines in the diffraction pattern), but also induced changes:

(a) Polonium lines were found in the pattern, indicating a lower Po/Ni ratio in the compound than existing before heating.

(b) The lattice constants increased from $a_0 \cong 3.95$ and $c_0 \cong 5.68$ to $a_0 \cong 3.96$ and $c_0 \cong 5.70$ Å.

(c) The order of the relative intensity of diffraction lines had changed, suggesting a change in the structure of the unit cell.

As a result of this experience, several additional samples of nickel polonide were prepared under various experimental conditions. Variations in the lattice constants for the hexagonal cell were observed between the limits $a_0 = 3.95$ and $c_0 = 5.68$ to $a_0 = 3.98$ and $c_0 = 5.71$ Å. Correlation of mole ratios with lattice constants was not achieved. However, the variations in the lattice constants suggest the formation of nickel-polonium compounds of varying composition. These observations indicate that the Ni–Po system may be very similar to the Ni–Te system. Klemm and Fratini[15] have established that nickel and tellurium form compounds of continuously varying composition between NiTe and $NiTe_2$ and that the lattice constants for the hexagonal cell increase with a decrease in the Te/Ni mole ratio. A change in structure of the unit cell (NiAs type for NiTe and Cd-$(OH)_2$ type for the $NiTe_2$) also was observed.

Summary

1. Nine compounds of polonium—BePo, MgPo, CaPo, SrPo, BaPo, ZnPo, CdPo, HgPo, PbPo—have been prepared on a microgram scale and identified by analysis of their X-ray diffraction data.

2. With the exception of MgPo and HgPo, all compounds that have been identified appear to be isomorphous with the corresponding compounds of sulfur, selenium and tellurium.

3. The lattice dimensions, crystal systems, $\sin^2\theta$ values, and relative line intensities of the polonium compounds are given.

4. Reactions of polonium with nickel, copper, silver, gold, carbon, molybdenum, tantalum and tungsten are described.

Acknowledgment.—The authors are deeply grateful to W. H. Zachariasen for his assistance

(15) W. Klemm and N. Fratini, *Z. anorg. allgem. Chem.*, **251**, 222 (1943).

in determining the crystal structure of magnesium polonide, and to N. H. Krikorian, R. Krohn, L. H. Treiman and R. B. Bevan for the purification and calorimetry of the polonium.

HEATS OF MIXING OF NON-ELECTROLYTE SOLUTIONS. I. ETHANOL + BENZENE AND METHANOL + BENZENE[1,2]

BY A. G. WILLIAMSON AND R. L. SCOTT

Department of Chemistry, University of California, Los Angeles, California

Received September 21, 1959

A calorimeter suitable for measuring heats of mixing of fluorocarbon + hydrocarbon mixtures is described. The calorimeter is similar to that of Adcock and McGlashan but uses a thermistor as the temperature sensitive element. In the course of testing the calorimeter a discrepancy between our measurements and the published data for the system ethanol + benzene at 45° was observed; our new results have since been confirmed by new measurements by the original workers. The new data on ethanol + benzene at 45° and methanol + benzene at 25 and 45° correlate well with the available data for other alcohol + benzene systems.

Introduction

In recent years there has been a considerable interest in the thermodynamic properties of mixing of fluorocarbon + hydrocarbon mixtures. Vapor-liquid equilibrium measurements have been made and the excess Gibbs free energies of mixing have been derived for several such systems. However even very good excess Gibbs free energy data may not lead to values of the excess entropy and heat of mixing of useful accuracy. It has been our aim therefore to construct a calorimeter suitable for measuring the heats of mixing directly. Since the fluorocarbons are not readily available in high purity and since the fluorocarbon + hydrocarbon mixtures have large volumes of mixing our criteria in selecting a calorimeter for this work have been that it should require only a small quantity of material for each measurement and that it should be one in which volume changes on mixing are not restricted so as to produce pressure changes during the mixing process. In addition to these requirements the vapor space in the calorimeter should be as small as possible to prevent errors arising from evaporation or condensation in the calorimeter. Of the calorimeter designs published during the last few years[3-5] that of Adcock and McGlashan[3] seems the most suitable for our purposes. The apparatus described by these workers uses only 1–2 ml. of each component per measurement, has virtually no vapor space and imposes no restrictions on volume changes. We have therefore used a modified version of their design. In the course of the trial measurements a large discrepancy was observed between our measurements and those of Brown and Fock[5] and this paper is concerned with the resolution of the discrepancy. Measurements on fluorocarbon + hydrocarbon mixtures will be published in a later paper.

(1) This work is supported by the U. S. Atomic Energy Commission under Project 13 of Contract AT(11-1)-34 with the University of California.

(2) Presented at the 135th National Meeting of the American Chemical Society, Boston, Mass., April 9, 1959.

(3) D. S. Adcock and M. L. McGlashan, *Proc. Roy. Soc. (London)*, **A226**, 266 (1954).

(4) G. M. Cheesman and A. B. M. Whitaker, *ibid.*, **A212**, 406 (1952).

(5) I. Brown and W. Fock, *Aust. J. Chem.*, **8**, 361 (1955).

Apparatus.—The calorimeter is essentially one-half of the twin instrument described by Adcock and McGlashan[3] with the thermopile replaced by a thermistor. The thermistor (a "Veco" type 31A2, $R_{25} \leq 1000\Omega$) is made one arm of a Wheatstone bridge which is brought to balance at the beginning of each experiment. Temperature changes in the calorimeter during the measurement are recorded in terms of the "off balance" current in the detector arm of the bridge. In about half of the experiments recorded here the detection was by means of a galvanometer (Leeds and Northrup type 2385-G). Galvanometer readings were taken every 30 seconds during the course of the experiment and were used to construct a temperature *vs.* time curve for the experiment. In the remainder of the experiments the detector arm of the bridge was connected to the input circuit of a Liston–Becker model 14 breaker amplifier. The output of the amplifier was then used to drive a 10 mv. span Varian strip chart recorder. In both cases the current through the thermistor was kept to about 25 μamp. The sensitivity of the galvanometer detector was about 15 mm. deflection per joule. With the amplifier-recorder arrangement and the amplification adjusted so that the noise level did not exceed $\pm 1/2$ division a sensitivity of about 30–40 chart divisions per joule was obtained. Obviously with either system of detection a higher sensitivity could be obtained with higher thermistor currents. However this was considered undesirable because of the possibility of thermal inhomogeneity in the calorimeter arising from heat dissipation by the thermistor.

Heat is supplied to the calorimeter from a 50Ω resistance heater wound non-inductively on the outer bell of the calorimeter. The resistance of this heater was measured accurately after it had been mounted. The current in the heater was ascertained by measuring the potential drop across an accurately calibrated 10Ω resistance placed in series with the heater. The current flow was timed with a Standard Electric Time Company clock which could be read to 0.01 sec. The mercury pool switches operating the heater and the clock were coupled (see ref. 3) so that they could be switched on and off simultaneously. Test of the switching equipment showed that the error in timing was not more than ± 0.04 sec. The method of operating the calorimeter was that described by Adcock and McGlashan[3] (*i.e.*, for endothermic processes the heat of mixing was estimated to within about 5% and compensating heat was supplied to the calorimeter simulaneously with the mixing process). In this way temperature changes in the calorimeter were reduced to a minimum. Following each experiment a calibration was made by supplying a known amount of heat to the calorimeter and noting the galvanometer or recorder deflection. Since the calibration is required only to correct for the difference between the heat of mixing and the electrical heating in the first part of the experiment it need not be known to better than ±3–4%.

Measurements were made with the calorimeter immersed in a water filled thermostat in which temperature fluctuations did not exceed $\pm 0.002°$.

Trial Measurements.—The system ethanol + benzene at 45° was chosen initially as a test system because the heat effect in the calorimeter was about the same as that expected

for the fluorocarbon + hydrocarbon systems. When the discrepancies with the published data were observed two other systems, carbon tetrachloride + chloroform[3,4,6] at 25° and benzene + *n*-heptane[7] at 20° were investigated. These measurements on the first system in the region $x_{CCl_4} = 0.47$ yielded values which were 0.7 to 1.0 cal. mole^{-1} (1–2%) higher than the previous work. Conversely three measurements on the second system gave values which were 4–5 cal. mole^{-1} (2%) lower than the previous work. We concluded therefore that our calorimeter was reliable to within one or two per cent. and that the previous measurements on benzene + methanol must have been in error and should be repeated.

Materials.—A sample of purified benzene was available which had been shown by freezing curve analysis[8] to be 99.9 mole % pure. Chloroform, carbon tetrachloride and *n*-heptane were purified using the methods described by the authors with whose work our own was to be compared.

Absolute ethanol was freed from benzene by fractional distillation and further dried by treatment with aluminum amalgam.[9] A few measurements in the range $x_{C_2H_5OH}$ = 0.5–0.6 were made with samples of ethanol which had been purified and dried by methods other than that referred to above. Baker "Analyzed" methanol 99.9% pure was used from a freshly opened bottle.

The alcohols gave single peaks in a gas chromatographic analysis using a 2.5 m. column with Perkin-Elmer type "F" packing.

Results

The heats of mixing for ethanol + benzene at 45° and for methanol + benzene at 25 and 45° are shown in Tables II, III and IV. The results have been fitted with expressions of the type

$$\Delta H = x(1 - x)\{A_0 + A_1(1 - 2x) + A_2(1 - 2x)^2 + \ldots\} \quad (1)$$

where x is the mole fraction of the alcohol. The values of the constants were obtained by the method of least squares on the Western Data Processing Center IBM 709 computer using a program devised by Mr. D. Myers of this department. The number of constants used is the smallest number for which the deviations between the experimental results and those given by the equation are of about the same magnitude as the estimated maximum experimental error in a single measurement. The values of the constants in eq. 1 together with their standard deviations are shown in Table IV and the values of ΔH calculated using these constants are shown in Tables I, II, and III.

TABLE I

HEATS OF MIXING OF ETHANOL + BENZENE AT 45°

Mole fraction of ethanol	ΔH/cal. mole^{-1} Exp.	Calcd.
0.168	239	237
.264	269	271
.346	273	273
.398	266	267
.482	249	249
.548	232	230
.549	229	230
.551	232	229
.571	224	223
.572	227	222
.588	213	216
.629	196	201
.758	136	138
.877	70	67

TABLE II

HEATS OF MIXING OF METHANOL + BENZENE AT 25°

Mole fraction of methanol	ΔH/cal. mole^{-1} Exp.	Calcd.
0.175	156	153
.221	163	165
.326	168	170
.359	165	168
.510	147	143
.633	115	114
.796	68	72
.901	35	31

TABLE III

HEATS OF MIXING OF METHANOL + BENZENE AT 45°

Mole fraction of methanol	ΔH/cal. mole^{-1} Exp.	Calcd.
0.179	206	205
.207	214	215
.298	224	227
.345	225	225
.419	217	216
.530	193	193
.703	138	139
.803	95	95
.899	48	47

The standard deviations of ΔH given in Table IV were calculated using the relation

$$\sigma_{\Delta H} = [\Sigma d_i^2/(m - n)]^{1/2} \quad (2)$$

where the d_i's are the individual deviations, m is the number of experimental points, and n is the number of parameters (here 4) in eq. 1.

Discussion

The difference between our results on benzene + ethanol (Table II) and those of Brown and Fock[5] range from 11 to 17%, far exceeding the claimed precision of either set of measurements. The consistency of our results in the region $x_{C_2H_5OH}$ = 0.5–0.6 where several different samples were used suggested that the differences are not a result of differences in purity of materials. We communicated our results to Dr. Brown in Melbourne and just recently learned from him[10] that new measurements at C.S.I.R.O., Melbourne (April, 1959) on the system ethanol + benzene are in substantial agreement with our results. The disagreement between their earlier work and ours is therefore completely resolved.

Brown and Fock[11] have plotted the maximum heats of mixing for several alcohol + benzene systems as a function of chain length. Our new values for ΔH_{max} (computed from eq. 1 and shown in Table V) define some revised smooth curves, but we leave a detailed comparison to the Australian group when they have completed all their new measurements. It is worth noting that the measurements of Brown and Fock[11] with 1-propanol and 1-butanol were made using a technique less

(6) K. W. Moreom, Thesis, University of Reading, 1957.

(7) A. R. Mathieson and J. C. J. Thynne, *J. Chem. Soc.*, 3708 3713 (1956).

(8) R. Satterfield, this department, unpublished.

(9) J. A. Barker, I. Brown and F. Smith, *Disc. Faraday Soc.*, **15**, 142 (1953).

(10) I. Brown, private communication.

(11) I. Brown and W. Fock, *Austral J. Chem.*, **10**, 417 (1957).

TABLE IV

CONSTANTS FOR EQUATION 1

System	t, °C.	A_0	σA_0	A_1	σA_1	A_2	σA_2	A_3	σA_3	$\sigma \Delta H$
Ethanol + benzene	45	978	4	554	24	473	31	478	74	3
Methanol + benzene	25	580	10	407	39	351	47	247	111	4
Methanol + benzene	45	799	4	448	17	466	19	434	47	2

susceptible to error through heat exchange than that used in the original ethanol + benzene studies.[6]

The heat of mixing of methanol + benzene at 20° has been measured by Scatchard, Ticknor, Goates and McCartney[12] who fitted their data to eq. 1 with four parameters, $A_0 = 600$, $A_1 = 250$, $A_3 = 550$, $A_4 = 800$. Since they omitted A_2 and we omitted A_4 exact comparison of their parameters with ours is impossible. However, Table V shows that their value of ΔH_{max} at 20° fits well with ours at 25 and 45°.

TABLE V

MAXIMUM HEATS OF MIXING IN ALCOHOL + BENZENE SYSTEMS

Alcohol	t, °C.	ΔH_{max}, cal. mole^{-1}	at x_2	Ref.
Methanol	20	159	0.30	12
	25	179	.30	This work
	45	237	.30	This work
Ethanol	45	287	.31	This work
1-Propanol	45	320	.3	11
1-Butanol	45	340	$.3_5$	11

Acknowledgments.—We wish to thank Dr. I. Brown of C.S.I.R.O., Melbourne for helpful discussion and for sending us his unpublished results. Our thanks are also due to Mr. D. B. Myers of this department for the computer program used in the least squares treatment of the results.

(12) G. Scatchard, L. B. Ticknor, J. R. Goates and E. R. McCartney, *J. Am. Chem. Soc.*, **74**, 3721 (1952).

A NEW METHOD FOR THE DETERMINATION OF ACTIVITY COEFFICIENTS OF COMPONENTS IN BINARY LIQUID MIXTURES[1]

BY SHERRIL D. CHRISTIAN, EDWARD NEPARKO AND HAROLD E. AFFSPRUNG

The University of Oklahoma, Norman, Oklahoma

Received October 5, 1959

A new, extremely rapid method is described for the determination of activity coefficients of components in binary liquid mixtures, based on measurement of total pressure and equilibrium vapor density alone. Partial pressures and activities are calculated directly from the measured pressure and density values and solution mole fractions are computed from the constant temperature, constant pressure form of the Gibbs–Duhem equation, which may be written $-\mathrm{d} \ln a_2/(\mathrm{d} \ln a_1 - \mathrm{d} \ln a_2) = x_1$, where a_2 and a_1 are the activities of components 1 and 2, respectively, and x_1 is the mole fraction of component 1 in the liquid phase. Methods are given for curve-fitting experimental activities to obtain the best analytical expressions for activity coefficients as functions of x_1. The apparatus consists of a fused silica gas density balance suspended directly above the thermostated solution container and connected to a closed-end manometer. For each concentration, total pressure is measured, vapor density is determined from the position of a pointer on the balance and vapor temperature is measured. Concentrations are changed between readings by distilling in one of the pure components through a ground-glass valve. No liquid samples or vapor samples are collected and the apparatus is closed from the atmosphere during an entire run, covering half the concentration range. Results of measurements made on several binary organic systems are reported.

Introduction

Most previous vapor pressure methods for determining activity coefficients of components in volatile binary liquid mixtures have made use of the relations

$$y_1 p = p_1; \ (1 - y_1)p = p_2 \qquad (1)$$

and

$$p_1/(x_1 p_1^0) = \gamma_1; \ p_2/(1 - x_1)p_2^0 = \gamma_2 \qquad (2)$$

where x_1 and y_1 are mole fractions of component 1 in the liquid and vapor phase, respectively; p_1 and p_2 are partial pressures of components 1 and 2 above the equilibrium mixture; p_1^0 and p_2^0 are the vapor pressures of pure 1 and pure 2; p is the total vapor pressure and γ_1 and γ_2 are the activity coefficients of components 1 and 2.[2] A common procedure is to determine p, x_1 and y_1 experimentally and calculate γ_1 and γ_2 directly from equations 1 and 2.

In recent years a number of techniques have been developed for determining activity coefficients from measurements of p and x_1 alone.[3,4] The application to these data of an independent relation, the Gibbs–Duhem equation, permits the calculation of p_1 and p_2 and, hence, γ_1 and γ_2. Thus, one may write (again assuming ideality of the vapor phase and ignoring the effect of variation in total pressure on activities)

$$p_1 + p_2 = p; \ x_1 \mathrm{d} \ln p_1 + x_2 \mathrm{d} \ln p_2 = 0$$

and these two equations involve only the two unknown pressures, p_1 and p_2. The mathematical analysis is somewhat complicated in most procedures of this type, and experimentally it usually is necessary to remove liquid phase samples after

(1) Presented before the Division of Physical Chemistry, 136th National Meeting of the American Chemical Society, Atlantic City, N. J., Sept., 1959.

(2) Equations 1 and 2 assume ideality of the vapor phase.

(3) G. Scatchard, *Ann. Rev. Phys. Chem.*, **3**, 259 (1952).

(4) J. A. Barker, *Aust. J. Chem.*, **6**, 207 (1953).

each pressure determination for subsequent analysis.

The method described here involves the determination of total vapor pressure and vapor composition alone, followed by the application of the constant temperature, constant pressure form of the Gibbs–Duhem equation for the calculation of solution concentrations and, consequently, activity coefficients. The assumption is made throughout that the vapor phase is ideal and that the variation in total pressure does not affect the activity or chemical potential. In the apparatus used here, vapor composition is determined by means of a fused silica vapor density balance supported directly above the liquid mixture. The procedure is extremely rapid, since the determination of vapor composition is accomplished without the necessity of condensing vapor samples. No liquid samples are collected and the composition of the liquid mixture can be changed at will by distilling into the system one of the pure components through a ground glass valve. The apparatus is enclosed from the atmosphere during an entire run, covering half the mole fraction range.

The method has been applied to several binary organic systems and activity results are reported. A detailed comparison of the results obtained here for the system C_6H_6–CCl_4 and the results calculated from the work of Scatchard, Wood and Mochel[5] is given.

Experimental

A. Apparatus.—The apparatus, shown in Fig. 1, consists of a gas density balance (A) supported on two fine horizontal silica fibers attached to a silica support (B). The entire balance is mounted on a Pyrex glass platform which may be removed from the Pyrex glass balance case for adjustment and repair. A large bore glass tube (about 80 mm. in diameter) connects the balance case to the solution vessel (E). It is necessary to use a tube of this size to ensure rapid equilibration between the liquid and vapor phases. The vapor phase temperature is not regulated, but it is measured to ± 0.1°, and this temperature is used in subsequent partial pressure calculations. The height of the pointer (C) is observed through the window (D) with a precision cathetometer. The solution (E) is stirred by a stirrer bar (F), which is controlled by a magnetic stirrer placed below the thermostated bath (G) and the solution vessel. (The bath in the present experiment was maintained at 20.00 ± 0.02°.) The system may be opened to vacuum or the atmosphere through tube (H). The pressure of the system is measured to ± 0.05 mm. by means of a closed end manometer. One of the pure components is added to the solution vessel (E) through one of the openings of a Y-tube connecting at (J). The other arm of the Y-tube connects to a sample tube containing a second component, which can be added in incremental amounts by means of a magnetically-operated ground glass valve. The water level in the thermostated bath is kept above the solution vessel (E) but below the balance in order to prevent vapor condensation on the buoyancy bulb.

B. Procedure.—The apparatus is calibrated in the following manner. The system is evacuated to its lowest pressure and both the pressure and pointer position are recorded. The gas temperature in the vicinity of the buoyancy bulb is also measured. Then, a small amount of vapor of known molecular weight is bled into the system and the pressure, pointer position and gas temperature are recorded. This is repeated in intervals up to a total pressure of about 100 mm. A plot of scale deflection *vs.* pressure yields a straight line passing through the origin, and from the slope of this line the force constant of the balance is calculated.

A binary mixture is investigated by introducing component 1 into the sample tube and degassing by a number of freezing-thawing cycles. The ground glass valve is closed and component 1 is frozen with liquid air. The system is swept out with dry air several times to eliminate vapors of component 1. Component 2 is introduced into the vessel (E) through one arm of the Y-tube, which can be blown open or closed by heating with a torch. The system is thoroughly degassed and the pressure and pointer deflection for pure component 2 are recorded. An increment of component 1 is added by removing the liquid air and heating gently with a torch until the liquid boils vigorously, the magnetic valve being held open by a permanent magnet supported outside the tube. Component 1 is frozen again, the system is evacuated briefly and the pointer position, gas temperature and pressure readings are recorded. Increments of component 1 are added in this manner until an entire run, covering half the concentration range, is completed. The other half of the concentration range is covered in an analogous manner.

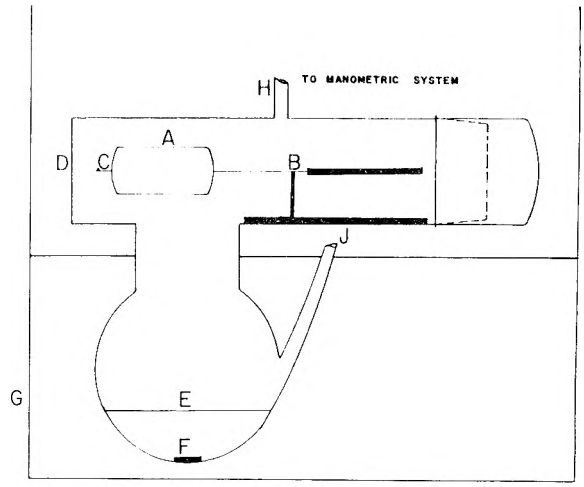

Fig. 1.—Activity apparatus.

It should be noted that once the pure components are degassed and the system is evacuated, no air is admitted during the rest of the run. Attainment of equilibrium vapor composition is so rapid that no drift of pointer position occurs if the entire apparatus is allowed to stand. Not only pressure equilibrium, but diffusion equilibrium as well appear to be reached within three or four minutes after addition of a component to the solution.

C. Materials.—All liquids were Reagent Grade organic compounds, purified by distillation through a 30-plate Oldershaw column at reflux ratios in excess of 10 to 1. Only middle fractions varying less than 0.1° in boiling point were collected.

Treatment of Data

A. Calculation of Activities.—The vapor density d of the equilibrium vapors is determined directly from the position of the pointer on the silica balance. In the case of systems of components which obey the ideal gas law, the activity of each component may be calculated from the expressions

$$dRT = \bar{M}p = p_1M_1 + (p - p_1)M_2 \qquad (3)$$

and

$$a_1 = p_1/p_1^0;\ a_2 = (p - p_1)/p_2^0 \qquad (4)$$

where $\bar{M}$ is the average molecular weight of the vapors, M_1 and M_2 are the molecular weights of pure components 1 and 2, and a_1 and a_2 are the activities of components 1 and 2.

In the case of systems in which one component dimerizes (*e.g.*, the system CCl_4–CH_3COOH) expressions corresponding to (3) and (4) may be written in terms of the dimerization constant K_D and the partial pressure of the monomer of the as-

(5) G. Scatchard, S. E. Wood and J. M. Mochel, *J. Am. Chem. Soc.*, **62**, 712 (1940).

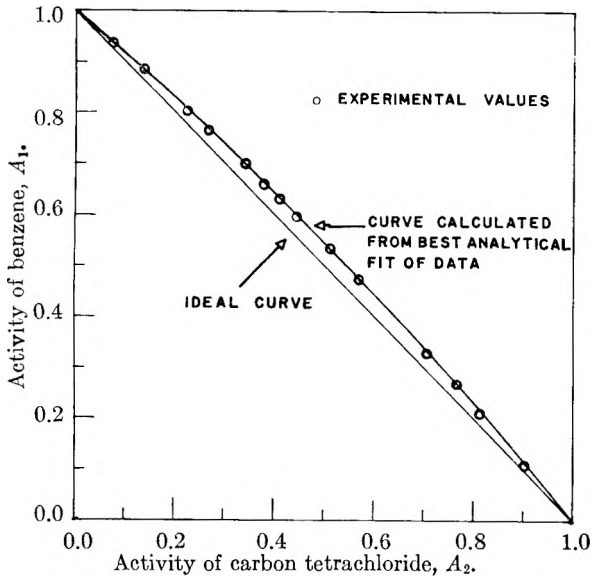

Fig. 2.—Activities of the system benzene–carbon tetrachloride.

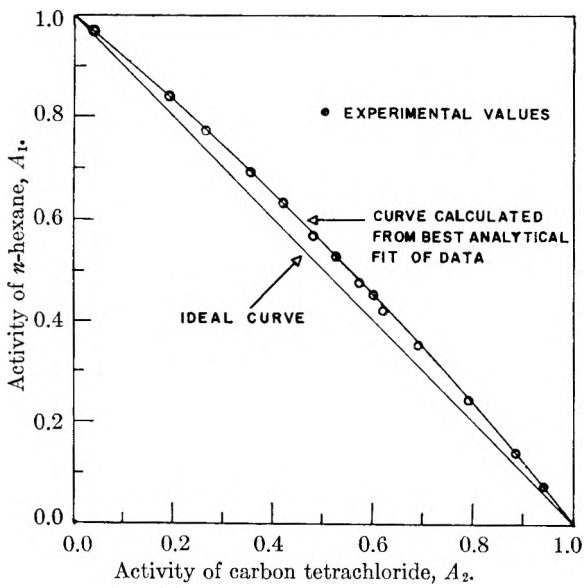

Fig. 3.—Activities of the system *n*-hexane–carbon tetrachloride.

sociating compound, p_1. Thus

$$dRT = \bar{M}p = p_1M_1 + 2K_Dp_1^2M_1 + (p - p_1 - K_Dp_1^2)M_2 \quad (5)$$

and

$$a_1 = p_1/p_1^0;\ a_2 = (p - p_1 - K_Dp_1^2)/p_2^0 \quad (6)$$

where the assumption is made that monomers and dimers, once formed, obey the ideal gas law. Similar expressions may be developed for systems in which both components associate in the vapor phase.

B. Calculation of Liquid Composition.—The constant temperature, constant pressure form of the Gibbs–Duhem equation may be rearranged to give

$$-\mathrm{d}\ln a_2/(\mathrm{d}\ln a_1 - \mathrm{d}\ln a_2) = x_1 \quad (7)$$

The determination of $\ln a_2$ and $\ln a_1$ as functions of any arbitrary variable, x_1^*, would allow the calculation of x_1 according to the equation

$$\frac{-(\mathrm{d}\ln a_2/\mathrm{d}x_1^*)}{(\mathrm{d}\ln a_1/\mathrm{d}x_1^*) - (\mathrm{d}\ln a_2/\mathrm{d}x_1^*)} = x_1 \quad (8)$$

It can be shown that for systems deviating but slightly from ideality

$$x_1 = \frac{(1 - a_2)}{(1 - a_2) + (1 - a_1)} \quad (9)^6$$

For this reason, the function $x_1^* = (1 - a_2)/(2 - a_1 - a_2)$ was chosen for use in equation 8 as the independent variable. Defining

$$\gamma_1^* = a_1/x_1^* \text{ and } \gamma_2^* = a_2/(1 - x_1^*) \quad (10)$$

one can determine analytical expressions of the type

$$\ln \gamma_1^* = (1 - x_1^*)^2 \sum_{i=0} A_i x_1^{*i}$$

and

$$\ln \gamma_2^* = x_1^{*2} \sum_{i=0} B_i x_1^{*i} \quad (11)$$

directly from experimental values of a_1 and a_2.[7]

Actually, only one of the expressions in (11) need be used, since it is obvious that once either γ_1^* or γ_2^* is fit as a function of x_1^*, the other γ^* is determined by equations 10.

Equations 10 can be differentiated to give

$$\mathrm{d}\ln a_1/\mathrm{d}x_1^* = \mathrm{d}\ln \gamma_1^*/\mathrm{d}x_1^* + 1/x_1^*$$

and

$$\mathrm{d}\ln a_2/\mathrm{d}x_1^* = \mathrm{d}\ln \gamma_2^*/\mathrm{d}x_1^* - 1/(1 - x_1^*) \quad (12)$$

From equations 11 and 10, expressions for $\mathrm{d}\ln \gamma_1^*/\mathrm{d}x_1^*$ and $\mathrm{d}\ln \gamma_2^*/\mathrm{d}x_1^*$ can be calculated and substituted into equations 12. Hence, application of equation 8 will yield x_1 as a function of x_1^* and the activity coefficients γ_1 and γ_2 may be calculated.

Results

A. System C_6H_6–CCl_4.—For the system benzene (1)–carbon tetrachloride (2) at 20°, the following analytical expressions have been obtained

$$\ln \gamma_1^* = 0.14(1 - x_1^*)^2 \text{ and } x_1 = x_1^* \quad (13)$$

Table I lists the experimental activities, a_1 and a_2; x_1; calculated activity coefficients, γ_1^{calcd} and γ_2^{calcd}; and calculated activities, a_1^{calcd} and a_2^{calcd}, from equation 13. Also given for reference are activity values calculated from a smoothed extrapolation of the data of Scatchard, *et al.*,[5] which were taken at temperatures ranging from 30 to 70°. Figure 2 shows experimental values of a_1 and a_2 and the solid line representing the calculated a_1 *vs.* a_2 curve, as well as the ideal curve.

(6) Note that for an ideal solution, $x_1 = a_1$ and $x_2 = a_2$, making relation (9) an identity. Systems deviating not greatly from ideality normally follow the relations $\ln \gamma_1 = A(1 - x_1)^2$ and $\ln \gamma_2 = Ax_1^2$, from which $\gamma_1 \approx 1 + A(1 - x_1)^2$, $a_1 \approx x_1 + Ax_1(1 - x_1)^2$ and $a_2 \approx (1 - x_1) + Ax_1^2(1 - x_1)$. Substitution of these values for a_1 and a_2 into equation 9 verifies that

$$x_1 \approx \frac{(1 - a_2)}{(1 - a_2) + (1 - a_1)}$$

(7) The form of equations 11 is suggested by the relations commonly used to express activity coefficients as a function of solution mole fraction. Although x_1^* and γ_1^* are not the actual mole fraction and activity coefficient, they ordinarily will not differ considerably from these variables, and the expressions in (11) are thus convenient for curve-fitting data. For a discussion of these power series expansions of $\ln \gamma$, see J. H. Hildebrand and R. L. Scott, "The Solubility of Non-Electrolytes," Reinhold Publ. Corp., New York, N. Y., 1950, Chapter III.

B. System *n*-Hexane–Carbon Tetrachloride.—For the system *n*-hexane (1)–carbon tetrachloride (2) at 20°, these expressions have been obtained

$$\ln \gamma_1^* = 0.18(1 - x_1^*)^2 \text{ and } x_1 = x_1^* \qquad (14)$$

Figure 3 shows experimental results for this system.

C. System Benzene–*n*-Hexane.—For the system benzene (1)–*n*-hexane (2) at 20°, analytical expressions have been obtained

$$\ln \gamma_1^* = 0.35(1 - x_1^*)^2 \text{ and } x_1 = x_1^* \qquad (15)$$

Figure 4 shows experimental results for this system.

D. System Ethyl Acetate–Carbon Tetrachloride.—For the system ethyl acetate (1)–carbon tetrachloride (2) at 20°, the analytical expressions (16) have been obtained

$$\ln \gamma_1^* = 0.40(1 - x_1^*)^2 \text{ and } x_1 = x_1^* \qquad (16)$$

Figure 5 shows experimental results for this system.

TABLE I

SYSTEM C_6H_6–CCl_4

DEPENDENCE OF ACTIVITIES AND ACTIVITY COEFFICIENTS ON LIQUID MOLE FRACTION AT 20°

a_1	a_2	x_1[1]	γ_1^{calcd}	γ_2^{calcd}	a_1^{calcd}	a_2^{calcd}	a_1(S)	a_2(S)
1.000	0 000	1.000	1.000		1.000	0.000	1.000	0.000
0.937	.069	0.937	1.000	1.131	0.937	.071	0.937	.071
.878	.133	.877	1.002	1.114	.879	.137	.879	.136
.797	.214	.795	1.006	1.092	.800	223	.799	.224
.759	.266	.753	1.008	1.083	.760	267	.759	.267
.688	.333	.681	1.014	1.067	.690	.340	.691	.339
.648	.379	.638	1.019	1.059	650	.383	.649	.383
.629	.402	.615	1.022	1.054	.628	.406	.628	.404
.592	.444	.577	1.025	1.048	.594	.443	.591	.443
.519	.520	.499	1.036	1.035	.517	.518	.517	.518
.517	.523	.497	1.037	1.035	.515	.521	.514	.520
.469	.570	.447	1.045	1.028	.467	.568	.466	.568
.319	.699	.307	1.068	1.013	.328	.702	.328	.702
.260	.756	.248	1.083	1.009	.262	.759	.262	.758
.204	.812	.191	1.094	1.005	.209	.813	.208	.813
.107	.902	.099	1.123	1.001	.111	.902	.109	.903
.000	1.000	.000		1.000	.000	1.000	.000	1.000

Discussion

The method presented here for the determination of activity coefficients has a number of important advantages. First, it is extremely rapid, making it possible to determine activities and activity coefficients of both components in a binary mixture, over the entire concentration range, in a period of less than a day. Second, the problem of reaching equilibrium is not nearly so difficult as in methods depending on the condensation and analysis of vapors bled from the equilibrium mixture. (The apparatus used here, which had an 80 mm. Pyrex tube connecting the vapor density balance and the liquid solution, seemed to allow almost instantaneous attainment of equilibrium—no drift of the balance pointer was ever observed during runs.) Further, compounds which react with water vapor or air can be kept under their own vapor pressure throughout an entire run. Another advantage is that the system may be used in the determination of vapor densities and, hence, association constants, of compounds which associate in the vapor phase. Thus, corrections may be made for the formation of associated species, which is one of the factors leading to deviation of the vapors from ideality.

The precision of the method appears to be a function of the sensitivitity of the vapor density balance. Although it is possible to construct a silica balance capable of detecting a change in vapor density of less than 10^{-7} g. cm.$^{-3}$, such a balance would be thrown completely off scale during a run involving binary systems whose components have high vapor pressures and widely different molecular weights. The balance used here was capable of determining average molecular weights in the range of 50 to 200, at a total pressure between 50 and 150 mm., to within ±0.5%.

The one system for which it was possible to make detailed comparison of results obtained here with previously reported values was the system C_6H_6–CCl_4. From Table I it can be seen that the activity values calculated from the present data, by the curve-fitting technique described, and those calculated from the data of Scatchard, Wood and Mochel[5] agree in general to within 0.001. The

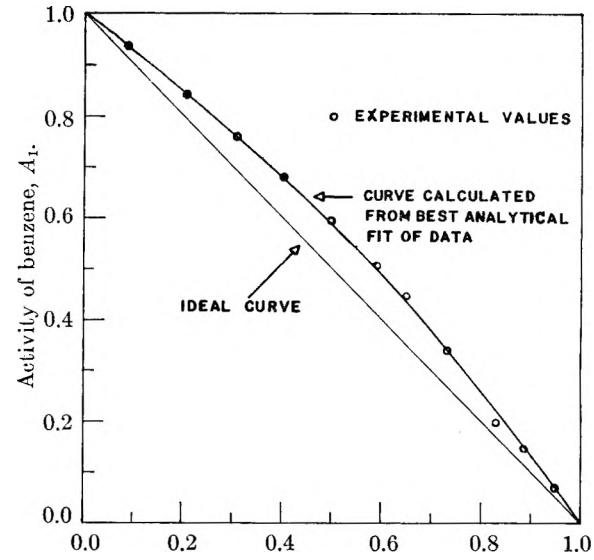

Fig. 4.—Activities of the system benzene-*n*-hexane.

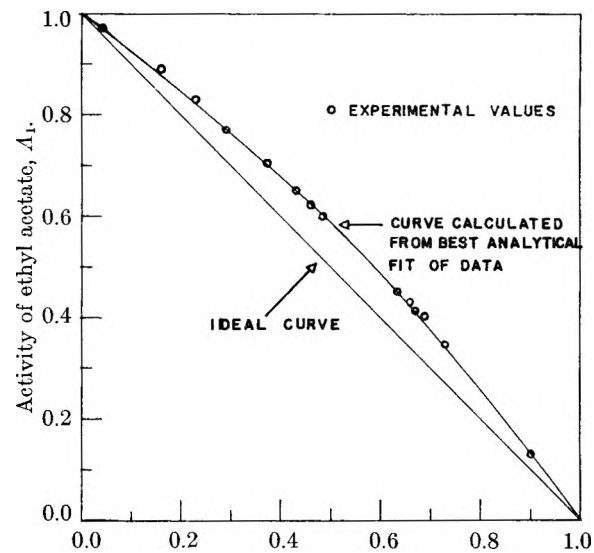

Fig. 5.—Activities of the system ethyl acetate–carbon tetrachloride.

directly measured values of activity appear to be in general in agreement with those of Scatchard, *et al.*, to within 0.004. While the activity values obtained by this method are by no means as precise as those of Scatchard and co-workers, the agreement between those data and the data reported here is satisfactory.

Acknowledgment.—The authors are indebted to the National Science Foundation for support of the work described in this paper.

KINETICS OF THE FISCHER–TROPSCH SYNTHESIS ON IRON CATALYSTS. PRESSURE DEPENDENCE AND SELECTIVITY OF NITRIDED CATALYSTS

BY F. S. KARN,[1] J. F. SHULTZ[1] AND R. B. ANDERSON[1]

Central Experiment Station, Bureau of Mines, Pittsburgh, Penna.

Received October 7, 1959

The variations of rate and selectivity of the Fischer–Tropsch synthesis on nitrided fused iron catalysts as a function of operating conditions have been studied. With $1H_2 + 1CO$ feed, the integral rate compared at constant conversion of $H_2 + CO$ was found to vary with the operating pressure to about the first power. However, at any given operating pressure the differential reaction rate decreased more rapidly than the partial pressure of synthesis gas as the conversion was increased indicating that the rate is inhibited by reaction products. The relative usage of hydrogen to carbon monoxide decreased with increasing conversion, passed a minimum and then increased. Apparently water is the principal primary product and carbon dioxide is produced by subsequent water-gas-shift reaction. Methane formation decreased initially with increasing conversion but subsequently increased. The olefin content of C_2 and C_3 hydrocarbons decreased with conversion. When the hydrogen content of the feed was increased, the relative usage of hydrogen to carbon monoxide, the production of methane increased, and the olefin content of C_2 and C_3 hydrocarbons decreased. This work is a part of Federal Bureau of Mines investigations of processes for converting coal to liquid fuels.

A recent paper[2] from the Bureau of Mines, U. S. Department of the Interior, described the variations of rate of the Fischer–Tropsch synthesis with feed gas composition, flow and temperature (225–255°) on reduced and nitrided fused-iron catalysts. The present paper considers rate as a function of operating pressure on nitrided iron catalysts and the selectivity of the process.

Frye, Pickering and Eckstrom[3] studied the synthesis of iron at 300–330°. For many catalysts the interpretation of kinetic data was difficult, as variation of operating variables produced an instantaneous change in rate followed by a time-dependent change that was attributed to a change of composition of the active surface. In the present and previous investigations,[2] the variation of operating variables produced no significant time-dependent changes in rate; the observed rate was constant after the period of time—1 to 3 hours—required to purge the system. Our results indicate that the time-dependent changes in rate are not important in studies at temperatures below 260 or 270°.

Experimental

Apparatus and experimental procedures were described previously.[2] Studies on pressure dependence were made with 6- to 8-mesh nitrided iron catalyst D-3001 with $1H_2 + 1CO$ gas at 240°. At each pressure the conversions of $H_2 + CO$ and exit gas composition were determined as a function of space velocity.[4] Tests were made in the order: 21.4, 14.6, 11.2 and 7.8 atm. To maintain the period of operation relatively short, fewer experimental determinations were made than in the previous work to avoid progressive changes in catalytic activity; nevertheless, the activity increased slightly in the course of the experiments.

Results

1. Pressure Dependence of Rate.—Plots of exit gas composition and conversion of $H_2 + CO$, x, against reciprocal space velocity were similar to those reported previously[2] for $1H_2+1CO$ gas on nitrided iron catalyst at 240°. Plots of the first-order empirical equation, $-\ln(1 - x) = kS^{-1}$, where S is the space velocity and k is a rate constant which is equal to the differential reaction rate at zero conversion, r_0, were linear over a wide range of conversions as shown in Fig. 1. If the rate equation can be separated into the form $r = g(x)\ h(P)$, where P is the system pressure, then $(xS)_x = k'h(P)$, where $(xS)_x$ are values of xS determined at constant values of x as pressure is varied, and k' is a constant.[5] Double logarithmic plots of $(xS)_x$ against P are presented in Fig. 2 for values of x of 0, 0.2, 0.4 and 0.6. The limiting values of xS as $x \rightarrow 0$ is obtained from the slopes of the curves of Fig. 1. The plots for constant conversions can be approximated by a straight line. Slopes of the lines, as determined by least-squares methods, were 0.95, 0.92, 0.97, 0.94 for values of x of 0, 0.2, 0.41 and 0.6, respectively, and averaged 0.94. Thus $h(P) \cong P^{0.94}$.

Figure 3 presents double logarithmic plots of the differential reaction rate ($r = \mathrm{d}x/\mathrm{d}S^{-1}$) determined by graphical differentiation for the pressure-dependence series as a function of the sum of the partial pressures of H_2+CO for conversions varying from 0 to 0.81. In the course of tests at each pressure the rate varies approximately as $(p_{H_2} + p_{CO})^{1.7}$ as the partial pressure is decreased by

(1) U. S. Department of the Interior, Bureau of Mines, Region V, Pittsburgh, Pa.

(2) F. S. Karn, B. Seligman, J. F. Shultz and R. B. Anderson, THIS JOURNAL, **62**, 1039 (1958).

(3) C. G. Frye, H. L. Pickering and H. C. Eckstrom, *ibid.*, **62**, 1508 (1958).

(4) Space velocity is defined as volumes (S.T.P.) per bulk volume of catalyst per hour.

(5) $k' = x/\int_0^x \{1/g(x)\}\,dx$, a function only of x.

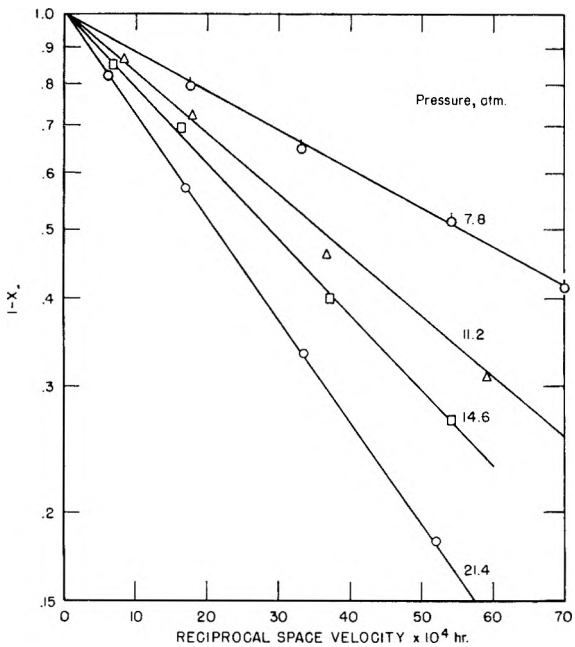

Fig. 1.—Plots of first-order empirical equation for nitrided catalyst D-3001 at 240° with $1H_2 + 1CO$ gas.

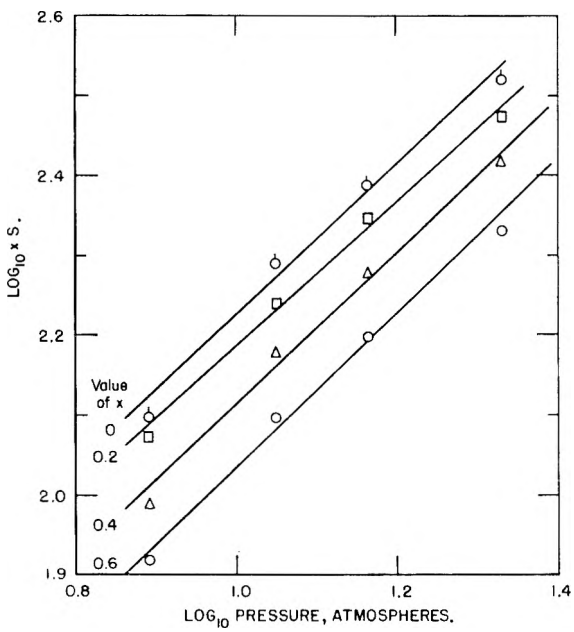

Fig. 2.—Double logarithmic plots of $(xS)_x$ against operating pressure for tests with $1H_2 + 1CO$ at 240°.

conversion. The apparent contradiction between this expression and the linear dependence of rate on operating pressure when compared at constant conversion as well as the empirical first-order equation results from two factors.

(a) The reaction is inhibited by reaction products. (b) The partial pressure of synthesis gas, $p_{H_2} + p_{CO}$, decreases less rapidly than $(1 - x)$ as conversion x is increased, according to the approximate equation which ignores the production of gaseous hydrocarbons

$$p_{H_2} + p_{CO} = (p_{H_2} + p_{CO})_0 (1 - x)/(1 - 0.67x)$$

where the subscript 0 denotes partial pressure at $x = 0$.

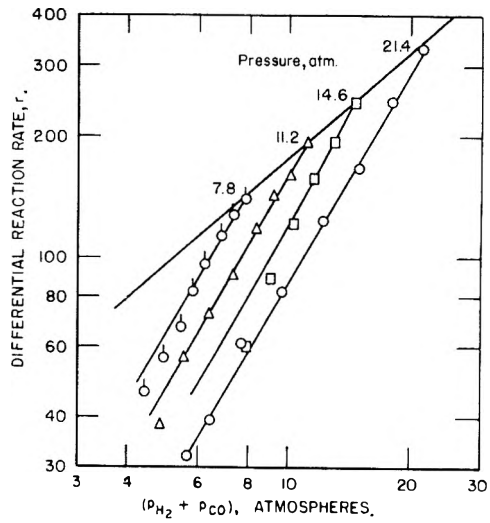

Fig. 3.—Double logarithmic plots of differential reaction rate r as a function of partial pressure of $H_2 + CO$ for tests with $1H_2 + 1CO$ at 240°.

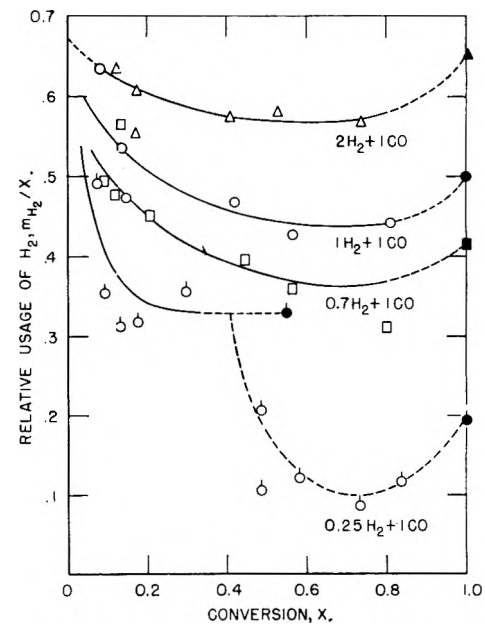

Fig. 4.—Relative usage of hydrogen as a function of conversion for nitrided catalyst D-3001 at 21.4 atm. and 225°.

2. Selectivity.—Selectivity data are reported for experiments with nitrided iron catalysts at 225 and 240° and 21.4 atm. with feed gases varying from $2H_2 + 1CO$ to $0.25H_2 + 1CO$; rate data for these experiments were reported previously.[2] As data at 225 and 240° showed the same trends and usually only minor quantitative differences, only experimental points for tests at 225° are shown in several of the figures.

Figure 4 presents plots of the relative usage of hydrogen, moles of H_2 consumed per mole of H_2+CO consumed, as a function of fraction of H_2+CO reacted, x. These plots are of the form m_{H_2}/x as a function of x, where m_{H_2} is given as moles H_2 consumed per mole of H_2+CO feed. In these plots if $x = 1$, the relative usage of hydrogen must equal the feed ratio; these points are designated by solid symbols. For $0.25H_2+1CO$

gas a point is also shown for the maximum conversion possible with a usage ratio H_2/CO of 0.5.

The general trend of the differential selectivity, dm_{H_2}/dx, can be constructed readily from the integral curves of Fig. 4 using the relationship $dm_{H_2}/dx = m_{H_2}/x$ at $x = 0$ and $d(m_{H_2}/x)/dx = 0$.

The relative usage of hydrogen, m_{H_2}/x, decreases with decreasing hydrogen content of the feed. With increasing conversion m_{H_2}/x decreases, passes through a minimum (not clearly defined in a few of the present data), and then increases. Extrapolation to solid points at $x = 1$ seems reasonable. With $0.25H_2+1CO$ feed the relative usage of hydrogen is less than 0.33, the lower limit for the production of aliphatic hydrocarbons, for conversions greater than about 0.4 for tests at 225° and 0.5 for tests at 240°. Reactions producing carbon, in addition to synthesis, can explain these results.

Similar plots of CO_2 production, moles CO_2 produced per mole of H_2+CO consumed, m_{CO_2}/x, as a function of conversion x increased with increasing values of x, passed through a maximum in the range 0.5 to 0.6, and then decreased. The production of CO_2 increased with increasing content of carbon monoxide in the feed gas; for example: the values of m_{CO_2}/x of the maxima were 0.20 for $2H_2+1CO$, 0.237 for $1H_2+1CO$, 0.28 for $0.7H_2+1CO$, and 0.325 for $0.25H_2+1CO$. The maxima occur at about the same conversion as the minima in the curves of Fig. 4. For all feed compositions except $0.25H_2+1CO$ these maxima may also be expected, because the total consumption of the gas according to equation 1 of the previous paper[2] demands lower final values than the maximum. With $0.25H_2+1CO$ gas at conversions greater than 0.40 at 225° and 0.5 at 240°, the process is probably complicated by carbon-forming reactions of the type (a) $2CO \rightarrow C + CO_2$ and (b) $3Fe + 4CO \rightarrow Fe_3O_4 + 4C$. Apparently both reactions occur with reaction (b) increasing in magnitude with increasing conversion; for example, two anomalous values of $m_{CO_2}/x = 0.35$ are observed at about $x = 0.6$ followed by values decreasing to as low as 0.16 at $x = 0.89$.

Methane production (moles CH_4 produced per mole of H_2+CO consumed, m_{CH_4}/x) in Fig. 5 is shown to increase with increasing hydrogen content of the feed. All of the curves decrease, pass through a minimum, and then increase as the conversion is increased. Points for $1H_2+1CO$ and $0.7H_2+1CO$ feeds overlap and are represented by a single curve. The initial decrease in methane production cannot be explained by variations of the ratio of H_2/CO as the gas is converted because this ratio increases with conversion for $2H_2+1CO$, $1H_2+1CO$ and $0.7H_2+1CO$ feed gases. Methane formation varies inversely with the concentrations of water vapor and carbon dioxide in this initial portion. However, the increasing ratio of H_2/CO with conversion may eventually produce the minimum and the increasing portion of the curves.

With $0.25H_2+1CO$ feed the minimum and subsequent increase is difficult to explain. Above conversions of 0.65 at 240° and 0.49 at 225° the moles of both H_2 and CH_4 per mole of feed increased. This range includes conversions at which anomalous results were found for the relative usage of hydrogen and production of CO_2. Reactions involving dehydrogenation and cracking of molecules adsorbed in pores of the catalyst could provide an explanation of these observations.

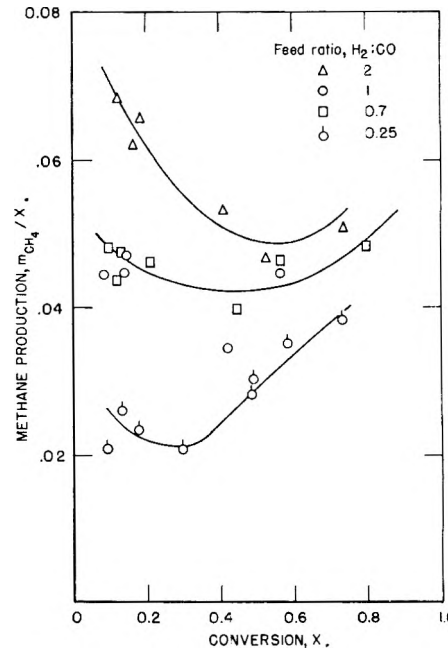

Fig. 5.—Methane production as a function of conversion for nitrided catalyst D-3001 at 21.4 atm. and 225°.

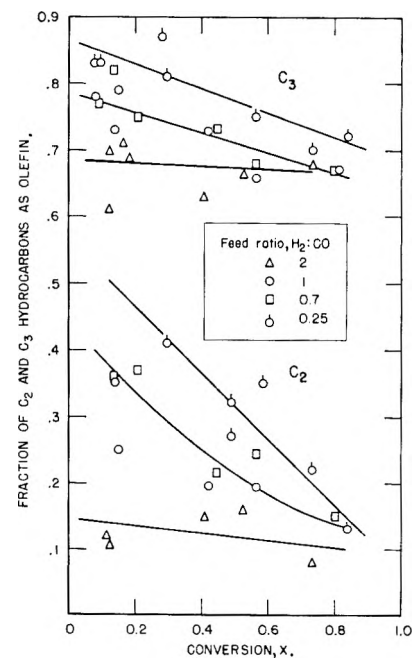

Fig. 6.—Olefins in C_3 and C_2 fractions as a function of conversion for nitrided catalyst D-3001 at 225° and 21.4 atm.

The variation of unsaturation in the C_2 and C_3 fractions as a function of feed composition and conversion is presented in Fig. 6. As the concentrations of these hydrocarbons in the exit gas were less than 2.5% for even the highest conversions, the data proved erratic when calculated in the same way as methane formation; however, reasonable trends were obtained by plotting the fraction of

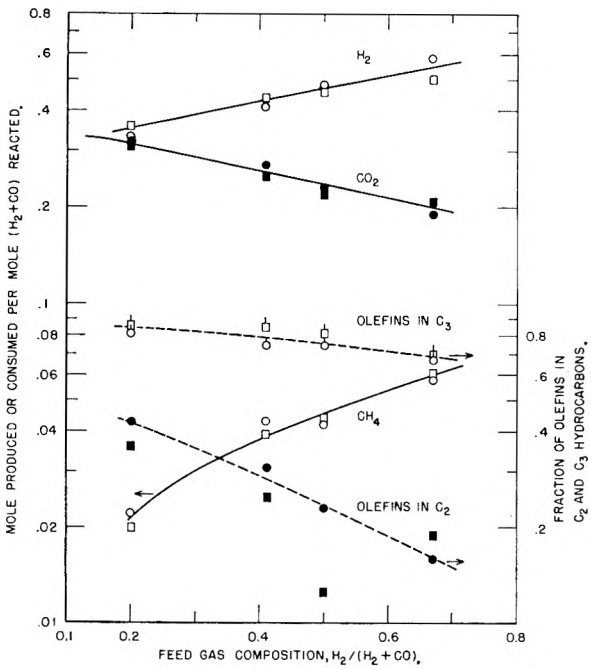

Fig. 7.—Selectivity as a function of feed gas composition, at 21.4 atm. and conversion of 30%. Circles represent 225° and squares 240°.

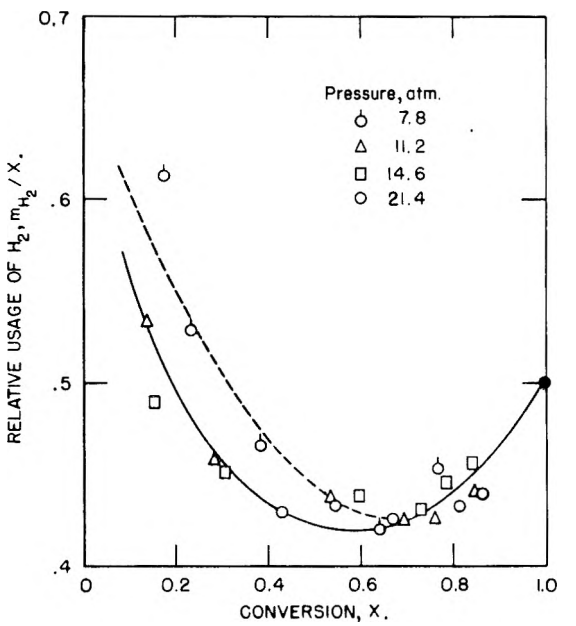

Fig. 8.—Relative usage of hydrogen as a function of conversion and operating pressure: $1H_2 + 1CO$ gas at 240°.

olefins in the C_2 and C_3 fractions. Unsaturation decreases with increasing hydrogen content of the feed and with increasing conversion. At conversions greater than 0.15 to 0.2 the ratio H_2/CO of the exit gas increased with increasing conversion for all of the feed gases except $0.25H_2+1CO$. Plots of unsaturation against the ratio $H_2/(H_2+CO)$ of the exit gas showed a fair over-all relationship of decreasing unsaturation with increasing hydrogen content. However, this plot consisted principally of four clusters of points corresponding to the four feed gases, and poor correlation existed within points for a given feed gas. Thus, the plots in Fig. 6 are considered the best representation of these data.

Figure 7 compares selectivity data for 225 and 240° at a conversion of 30% with the feed composition.

Pressure had only a small influence on selectivity, as indicated by the tests of nitrided iron catalyst D-3001 with $1H_2+1CO$ gas at 240° and 7.8 to 21.4 atm.; the rate data for these tests were described earlier in this paper. As shown in Fig. 8, the relative usage of hydrogen was essentially the same, except for the somewhat higher values at 7.8 atm. for conversions below 0.5. Methane production decreased with increasing pressure; for example, the values of m_{CH_4}/x at a conversion of 0.4 were 0.053, 0.047, 0.043 and 0.043 at 7.8, 11.2, 14.6 and 21.4 atm., respectively. Unsaturation and CO_2 production were essentially the same at all pressures.

Discussion

Previous studies have disclosed that the synthesis on reduced iron catalysts is approximately proportional to the operating pressure.[6] This relationship holds for nitrided iron catalysts in the present paper, and the results may be expressed in the form $r = g(x)p^{0.94}$. Comparison of the differential reaction rate with the partial pressure of H_2+CO showed that the rate decreased more rapidly with increasing conversion than the partial pressures of H_2+CO. Thus, the rate process is inhibited by products of the reaction, possibly carbon dioxide but more likely water vapor. As the activity of iron catalysts is not significantly impaired by submersing the catalyst in synthesis oils, the inhibition of rate observed in the present experiments can hardly be attributed to hydrocarbon.

Uchida and co-workers[7] investigated the kinetics of the Fischer–Tropsch synthesis on iron catalysts with $1H_2+1CO$ gas at 24 atm., tested several rate equations, and obtained reasonable agreement for three of these equations. However, the equations considered satisfactory by Uchida and most other rate equations of Hougen and Watson type[8] cannot account for the first-order dependence of rate on operating pressure and at the same time provide the proper decrease in rate with increasing concentration of products. A semi-fundamental equation in terms of partial pressures will be presented in a subsequent paper.

Previous workers[6a,9,10] have postulated that the primary synthesis reaction produces water, $m_{H_2}/x = 0.67$, and that carbon dioxide is produced by a subsequent water-gas-shift reaction. The present data can be explained by this hypothesis. As relative H_2 consumption and CO_2 production are essentially independent of temperature and pres-

(6) (a) R. B. Anderson, B. Seligman, J. F. Shultz, R. Kelly and M. A. Elliott, *Ind. Eng. Chem.*, **44**, 391 (1952); (b) C. C. Hall, D. Gall and S. L. Smith, *J. Inst. Petrol.*, **38**, 845 (1952).

(7) H. Uchida, M. Kuraishi, H. Ichinokawa and K. Ogawa, *Bull. Chem. Soc. Japan*, **29**, 181 (1956).

(8) O. A. Hougen, and K. M. Watson, *Ind. Eng. Chem.*, **35**, 529 (1943).

(9) H. Koelbel, P. Ackermann, E. Ruschenburg, R. Langheim and F. Engelhardt, *Chem. Ing. Tech.*, **23**, 153 (1951).

(10) H. Tramm, *Brennstoff-Chem.*, **33**, 21 (1952).

sure and are functions only of conversion and feed composition, as shown by the present and previous data, the subsequent water-gas-shift must vary in approximately the same manner as the rate of synthesis when pressure and temperature are changed. The rate equation of Kul'kova and Temkin[11] for the water-gas-shift on iron

$$r_{wg} = k_1[p_{CO}(p_{H_2O}/p_{H_2})^{1/2} - (1/K)\ p_{CO_2}(p_{H_2}/p_{H_2O})^{1/2}] \quad (1)$$

where r_{wg} is the differential reaction rate, k_1 is a rate constant with an activation energy of 16.5 kcal./mole, K is the equilibrium constant, has the same pressure dependence as the synthesis and nearly the same temperature dependence. Activation energies for synthesis vary from 19 to 23 kcal./mole.

The differential product of CO_2 may be related to r_{wg} as

$$dm_{CO_2}/dx = [dm_{CO_2}/d(1/S)]/[dx/d(1/S)] = r_{wg}/r_{syn} \quad (2)$$

where S is the space velocity of feed gas and r_{syn} is the rate of synthesis. Calculations based on equation 2 show at least a qualitative agreement between CO_2 production and equation 1; however, the present experimental data are not sufficiently precise to provide a positive test. Thus, the Temkin equation provides at least a first approximation to the kinetics of CO_2 production in the Fischer–Tropsch synthesis on iron.

The production of CO_2 could also result entirely or in part from reactions coupled with the primary synthesis mechanism, such as the reaction of water vapor with an intermediate of the synthesis. Water-gas-shift equilibrium is usually not attained during synthesis on iron, and tests with $C^{14}O_2$ added to $1H_2+1CO$ feed indicate that the reverse shift and the direct synthesis from CO_2 proceed very slowly.[12] One cannot distinguish here between mechanisms involving irreversible reactions and slow reverse reactions. For example, for typical concentrations of reactants and products from iron catalysts the forward reaction according to eq. 1 is about 50 times faster than the reverse shift.

Methane is a primary product of the synthesis. Its production increases with H_2/CO ratio of the feed; however, at low conversions CH_4 production, m_{CH_4}/x, decreases with increasing conversion, although the ratio H_2/CO of the gas remaining increases. Inhibition of CH_4 production may possibly be attributed to water vapor. At higher conversions, the effect of the increasing inhibitor concentration is outweighed by the increasing H_2/CO ratio of the gas remaining, and CH_4 production passes through a minimum and increases.

Olefins are also primary products of the synthesis, and olefin production decreases with increasing ratio H_2/CO of the feed gas.[13] Olefin production decreases with increasing conversion and with increasing ratio H_2/CO of the exit gas, which also usually increases with increasing conversion; however, the H_2/CO ratio is not the only factor determining unsaturation. A complete explanation of olefin production probably involves the hydrogenation of olefins in subsequent parts of the catalyst bed.

Some of the results with $0.25H_2+1CO$ feed were unexpected. For conversions above 0.4 at 225° and 0.6 at 240°, reactions consuming principally carbon monoxide occurred: first of the type $2CO \rightarrow C + CO_2$ and at higher conversions $4CO + 3Fe \rightarrow Fe_3O_4 + 4C$. Above conversions of about 0.4, methane production increased, and at somewhat higher conversions, the moles of H_2 per mole of feed as well as partial pressure of H_2 at the outlet of the bed increased. These results apparently can be explained only by cracking and dehydrogenation of adsorbed carbonaceous material in the catalyst pores.

The present results with iron catalysts may be compared with similar data from this laboratory on cobalt catalysts at atmospheric pressure and 190–205° with feed gases of composition $3.5H_2+1CO$, and $1H_2+1CO$.[14] For cobalt catalysts, the relative usage of hydrogen was about 0.70 and was essentially independent of temperature, feed gas and conversion. The production of CO_2 on cobalt was about 10% of that on iron, but apparently most of the CO_2 was also produced by a subsequent water-gas-shift reaction. Carbon dioxide formation increased with increasing carbon monoxide content of feed, conversion and temperature. Methane production increased with H_2/CO ratio of feed and with temperature. Unsaturation of the C_4 fraction decreased with increasing H_2/CO ratio of the feed, but appeared to be largely controlled by the H_2/CO ratio of the gas remaining. Thus, for the hydrogen-rich gases, the ratio H_2/CO of gas remaining increased, and unsaturation decreased with increasing conversion. For $1H_2+1CO$ feed, the

TABLE I

COMPARISON OF RESULTS OF IRON AND COBALT CATALYSTS

(Conversion = 0.3)

	Iron catalysts[a]			Cobalt catalysts[b]		
Feed gas	$2H_2+1CO$	$1H_2+1CO$	$0.25H_2+1CO$	$3.5H_2+1CO$	$2H_2+1CO$	$1H_2+1CO$
Relative H_2 usage, m_{H_2}/x	0.54	0.47	0.34	0.70	0.70	0.67
CO_2 production, m_{CO_2}/x	.200	.225	.31	.003	.019	.033
Methane production, m_{CH_4}/x	.059	.046	.021	.059	.041	.025
Unsaturation[c]	.69	.77	.84	.45	.66	.71

[a] Reduced and nitrided Fe_3O_4–MgO–K_2O catalyst at 21.4 atm. and 225–240°. [b] Reduced Co–ThO_2–kieselguhr catalyst at atmospheric pressure and about 195°. [c] Unsaturation is given as the fraction of olefins in C_3 fraction for iron catalysts and in C_4 fraction for cobalt.

(11) N. V. Kul'kova and M. I. Temkin, *Zhur. Fiz. Khim.*, **23**, 695 (1949).

(12) W. K. Hall, R. J. Kokes and P. H. Emmett, *J. Am. Chem. Soc.*, **79**, 2983 (1957).

(13) Kummer, Podgurski, Spencer and Emmett (*ibid.*, **73**, 564 (1951)) found that olefin production of alkali-free iron catalysts at atmospheric pressure was low in the absence of water or of the alcohol added to the feed. These results may or may not be typical of synthesis on alkalized iron at elevated pressures. If these results are applicable to the present system, the curves in Fig. 6 would be expected to decrease sharply as the conversion and hence the concentration of water vapor approach zero.

(14) R. B. Anderson, A. Krieg, R. A. Friedel and L. S. Mason, *Ind. Eng. Chem.*, **41**, 2189 (1949). These results have been replotted in the same form as in the present paper by R. B. Anderson in "Catalysis," Vol. IV, edited by P. H. Emmett, Reinhold Publ. Corp., New York, N. Y., 1956, pp. 274–280.

ratio H_2/CO decreased, and the unsaturation increased with increasing conversion. Selectivity data for iron and cobalt catalysts are compared at a conversion of 0.3 in Table I.

THE CHEMISORPTION OF GASES ON CHROMIA SURFACES AT LOW TEMPERATURES[1]

By D. S. MacIver and H. H. Tobin

Gulf Research & Development Company, Pittsburgh 30, Pennsylvania

Received October 10, 1959

The chemisorptions of carbon monoxide, oxygen, nitrogen and hydrogen at −195° and of carbon dioxide at −78° on a reduced chromia surface have been measured and the effect of these chemisorptions on the rate of the hydrogen–deuterium exchange reaction determined. It was found that the hydrogen and carbon monoxide adsorptions took place on essentially all the available surface sites; the nitrogen, oxygen and carbon dioxide adsorptions covered approximately 20, 60 and 80% of the surface, respectively. Carbon monoxide effectively poisoned the surface with regard to both the exchange reaction and the subsequent chemisorption of other gases; oxygen and carbon dioxide were less poisonous. Chemisorbed nitrogen was found to have no effect on the exchange rate. These results are discussed in terms of a specific model for the surface of α-chromia and it is suggested that the ability of this surface to react with a variety of gases at low temperatures is related to the d-electron configuration of the chromium ions.

Introduction

During recent years some emphasis has been placed on the role of the d-electron configuration of the metal ion in determining certain surface properties of the transition metal oxides. For example, Dowden, Mackenzie and Trapnell[2,3] have reported that the hydrogen–deuterium exchange activities of these oxides seem to be related more to the d-electron configuration of their metal ions than to their bulk semi-conductivity properties, the condition for high activity being a moderate, but not excessive, number of unpaired d-electrons. The general importance of d-electrons in the chemisorption of gases by oxides has been further discussed by Dowden,[4] who concludes that the degree of occupancy of the d-levels with electrons will be a determining factor in the rate of formation and the stability of the adsorbent–adsorbate complexes. It has been suggested[2−4] that such considerations may provide a common basis for understanding the behavior, insofar as chemisorption is concerned, of both metal and oxide surfaces.

In order to evaluate these and other ideas, it seems particularly desirable to have more information on the reactivity of the transition metal oxides with gases at fairly low temperatures where extensive alteration of the adsorbent by oxidation or reduction may be avoided and where the nature of the bonds between the adsorbate and the surface may, in some cases, be analogous to those involved in various coördination compounds. As a starting point for a study along these lines, chromia appeared to be a logical choice since it has been observed that a reduced chromia surface is capable of reacting with a number of gases even at liquid air temperatures.[5] As far as adsorption data on this oxide are concerned, there are several relevant papers in the literature,[5−9] the most pertinent for present purposes being that of Beebe and Dowden[5] who measured the heats of adsorption of several gases on a reduced chromia surface from −195 to 0°. Unfortunately, these workers did not report surface areas and hence it is somewhat difficult to estimate the exact coverages involved. The measurements of Dowden and Garner[7] were made at room temperature where the adsorption processes may differ somewhat from those observed by Beebe and Dowden; once again little information is available on the extent to which the various adsorbates covered the surface. Finally, while the study of Weller and Voltz[9] has clarified many details of the surface chemistry of chromia, the principal emphasis in their work was on the adsorption of hydrogen and oxygen. It appeared, therefore, that while earlier work indicated chromia surfaces to be quite reactive at low temperatures, some question remained as to the extent to which various gases would be chemisorbed and to the influence of the chemisorption upon surface properties.

In view of the foregoing discussion, a re-examination of certain features of low temperature adsorption and catalytic processes on chromia was undertaken with special emphasis being directed toward modifications in the surface properties by chemisorption of various gases. It was hoped that such a study, in addition to augmenting our understanding of chromia surfaces, would also provide information for comparison with similar studies on other transition metal oxides.

Experimental

Materials.—Hydrogen and prepurified nitrogen were obtained from the Air Reduction Company; oxygen, carbon

(1) Presented at the Symposium on Theoretical Aspects of Heterogeneous Catalysis, Division of Colloid Chemistry, 134th National Meeting of the American Chemical Society, Sept. 13–18, 1959, Atlantic City, N. J.

(2) D. A. Dowden, N. Mackenzie and B. M. W. Trapnell, *Advances in Catalysis*, **9**, 65 (1957).

(3) D. A. Dowden, N. Mackenzie and B. M. W. Trapnell, *Proc. Roy. Soc. (London)*, **237A**, 245 (1956).

(4) D. A. Dowden, "Chemisorption," ed. by W. E. Garner, Academic Press, New York, N. Y., 1957, Chapter 1.1.

(5) R. A. Beebe and D. A. Dowden, *J. Am. Chem. Soc.*, **60**, 2912 (1938).

(6) J. Howard and H. S. Taylor, *ibid.*, **56**, 2259 (1934).

(7) D. A. Dowden and W. E. Garner, *J. Chem. Soc.*, 893 (1939).

(8) P. H. Emmett and M. Cines, *J. Am. Chem. Soc.*, **68**, 2535 (1946).

(9) S. W. Weller and S. E. Voltz, *ibid.*, **76**, 4695 (1954).

dioxide and helium from the Matheson Company; deuterium from the Stuart Oxygen Company; and argon from the Linde Company. The hydrogen was purified by passing it through a "Deoxo" unit, over magnesium perchlorate, and through an activated charcoal trap at −195°. The nitrogen and argon were passed over reduced copper at 450°, then through magnesium perchlorate and a −78° cold trap while the oxygen was simply flowed through the −78° trap. The deuterium and helium were treated by passage over activated charcoal at −195°. Carbon monoxide was prepared by the sulfuric acid decomposition of formic acid at 120°; the gas was passed over "Ascarite" and magnesium perchlorate, through a −78° trap, and finally distilled at −195°. The carbon dioxide was frozen and evacuated several times at −195° and then expanded into a storage bulb in such a fashion that only the middle portion was retained for use. Mass spectrometric analysis of all gases indicated purities of at least 99.9%.

The chromia used in the work reported here was prepared by the method of Turkevich, Fehrer and Taylor.[10] One hundred g. of $Cr(NO_3)_3 \cdot 9H_2O$ and 33 g. of ammonium acetate, both reagent grade, were dissolved in 625 g. of water. The solution was heated to boiling for a few minutes, cooled to room temperature, and then transferred to a polyethylene tray. A saturated solution of ammonia was prepared by passing ammonia through water in a polyethylene beaker; 90 cc. of this solution was diluted with 250 cc. of water and added slowly, with rapid stirring, to the salt mixture. The whole was warmed on a water-bath until a strong gel was formed. This was partially dried at 50° for 60 hours, washed, and then dried at 60° to a hard solid which was broken up and heated at 200° for 60 hours. The solid was then ground and sieved to yield 50–140 mesh particles which were heated in a stream of hydrogen to 500° at a rate of two degrees per minute. At 400° a brief exothermic process took place which caused the temperature of the bed to rise momentarily about 50°; a second heating in hydrogen under the same conditions showed no such rise. The X-ray diffraction pattern of the finished product was that of α-Cr_2O_3; other phases were either absent or present in amounts too small to be detected. Emission analyses indicated the possibility of Ni, Fe, Si, Cu, Mn, Ca, Mg, Na and Al being present to the extent of less than 0.001% each.

Apparatus.—The absorption data were obtained using a standard, volumetric gas adsorption system[11] with pressures being read to ±0.1 mm. on a mercury manometer. The sample tube was provided with both an inlet and an outlet line so that gases could be either flowed over the catalyst or circulated in a closed cycle through the adsorbent bed *via* an all-glass gas circulating pump. When necessary, the adsorbent was protected with cold traps from contamination by mercury of stopcock grease vapor. Elevated temperatures were obtained with a small ceramic furnace regulated by a Foxboro Potentiometer Controller; temperatures from 0 to −120° were maintained using a pentane cryostat[12] or a Dry Ice–acetone bath. The temperature of the liquid nitrogen refrigerant was measured with a nitrogen vapor pressure thermometer; other temperatures were determined *via* calibrated thermocouples inserted into the thermowell of the sample tube.

Procedure.—In general, the results reported here were obtained on the reduced form of the chromia; in these cases the standard pretreatment consisted of first flowing oxygen over the catalysts for three hours at 500°, atmospheric pressure, and a gaseous hourly space velocity of 5000, evacuating briefly, then flowing hydrogen for six hours under the same conditions, and finally evacuating for 16 hours at 500°. In all cases the hydrogen and oxygen were purified as described above. This pretreatment was, of course, repeated following each series of adsorption measurements so as to provide a clean surface for the next series. Varying the time of oxidation, reduction or evacuation by a factor of two either way had no noticeable effect upon the results. As will be discussed presently, it was often desirable to stabilize chromia surfaces by repeated oxidation–reduction cycles; these were exactly the same as the standard pretreatment except that the 16-hour evacuation step was omitted between cycles.

The adsorption measurements were carried out in the usual fashion. Prior to any such measurements the adsorbent was cooled to the desired temperature in several millimeters of helium and held for 30 minutes; the helium was then removed and the adsorbent contacted with the gas of interest. In all cases adsorption points were taken only after the pressure had remained constant for at least 15 minutes; in some instances points were checked by equilibration for periods as long as 16 hours. It was often necessary to measure adsorption isotherms at −195° before and after evacuation at −78°. In such cases the adsorbent was first evacuated for 15 minutes at −195° following the first isotherm, then allowed to warm to −78° and held for one hour or longer, the evacuation continuing all this time; the sample was then cooled in helium and the second isotherm measured. The same technique was employed in work between −78 and 25°. In computing relative adsorbate pressures, liquid vapor pressure data for argon,[13] nitrogen,[14] oxygen,[15] carbon monoxide[16] and carbon dioxide[17] were obtained from the literature. The adsorbate cross-sectional areas employed were those determined by Pickering and Eckstrom[18] with the exception of oxygen. For this adsorbate a value of 15.5 Å.^{2} was used; this was determined by comparison of the BET V_m values obtained in this Laboratory for argon and oxygen at −195° on a sample of γ-Al_2O_3.

The hydrogen-deuterium exchange activities of the chromia surfaces were measured using the same sample tube in which the adsorptions were carried out. The stabilized catalyst (0.5 g.), after pretreatment, was cooled in helium to the reaction temperature. The helium was then removed and an equimolar mixture of hydrogen and deuterium circulated at 300 mm. in a closed system over the catalyst *via* the all-glass circulation pump. Small samples were withdrawn from time to time and analyzed in a mass spectrometer. The results were computed in terms of the usual first-order rate constant

$$k = -\frac{1}{S\tau} \ln (1 - x_\tau/x_\infty)$$

where τ is the time in minutes, S the surface area in m.^{2} and x_τ and x_∞ the mole fraction of HD in the gas phase at time τ and at equilibrium, respectively. In cases where no reaction took place over a 20-hour period, the rate constant was assumed to be essentially zero.

Results

As indicated by Weller and Voltz,[9] freshly prepared chromia often is characterized by a rather unstable surface which must be subjected to repeated oxidation and reduction at elevated temperatures in order to obtain a constant and reproducible area. Accordingly, the sample of chromia employed in the majority of the work reported here was stabilized by alternate oxidation and reduction at 500°; the BET area as determined by argon adsorption decreased from 50 m.^{2}/g. after a single cycle to 22 m.^{2}/g. after 12 cycles. The area then remained constant (within 10%) despite some 50 additional treatments. This particular surface will be referred to as "stabilized" in future discussion. The area of the surface was always checked after each high temperature treat-

(10) J. Turkevich, H. Fehrer and H. S. Taylor, *J. Am. Chem. Soc.*, **63**, 1129 (1941).

(11) W. E. Barr and V. J. Anhorn, "Scientific and Industrial Glass Blowing and Laboratory Techniques," Instruments Publishing Co., Pittsburgh, Pa., 1949, Chapter 12.

(12) W. K. Hall and P. H. Emmett, This Journal, **63**, 1102 (1959).

(13) A. M. Clark, F. Din, J. Robb, A. Michels, T. Wassenaar and T. Zweitering, *Physica*, **17**, 876 (1951).

(14) A. S. Friedman and D. White, *J. Am. Chem. Soc.*, **72**, 3931 (1950).

(15) H. J. Hoge, *J. Research Natl. Bur. Standards*, **44**, 321 (1950).

(16) J. O. Clayton and W. F. Giauque, *J. Am. Chem. Soc.*, **54**, 2610 (1932).

(17) C. H. Meyers and M. S. Van Dusen, *J. Research Natl. Bur. Standards*, **10**, 381 (1933).

(18) H. L. Pickering and H. C. Eckstrom, *J. Am. Chem. Soc.*, **74**, 4775 (1952).

ment in order that any data might be put on a unit area basis.

Having obtained an adsorbent of reproducible area, adsorption isotherms of carbon monoxide, oxygen and nitrogen at −195° and carbon dioxide at −78° were measured on the reduced surface before and after evacuation for one hour at −78 or 25° in the case of carbon dioxide. The results shown in Figs. 1 and 2[19] clearly indicate the formation, in each case, of a strongly adsorbed phase which was not removed from the surface during the evacuation. Argon isotherms run before and after the chemisorption of the various gases indicated that there were no changes in BET surface areas due to the presence of chemisorbates. BET plots of the second isotherms of carbon monoxide, oxygen, nitrogen and carbon dioxide gave V_m values of 5.4, 4.9, 4.5 and 3.0 cc. (STP)/g., respectively. On the basis of the V_m values obtained with argon, monolayer volumes of 5.3, 5.0, 4.8 and 3.2 cc. (STP)/g. were calculated for these four gases. In view of the uncertainty involved in estimating adsorbate cross-sectional areas, the agreement seems sufficient to suggest that, in each case, the second isotherm represents primarily physical adsorption taking place on a layer of chemisorbed gas remaining from the first isotherm. For carbon monoxide and oxygen, the chemisorbed films were quite stable in that extension of the evacuation period to several hours caused no displacement of the second isotherms. The nitrogen and carbon dioxide layers, however, seemed less firmly bound to the surface since a 16-hour evacuation at −78 and 25°, respectively, removed 45% of the strong nitrogen adsorption and 30% of the strong carbon dioxide adsorption. In view of these results, it seemed reasonable to take the difference between the successive isotherms for carbon monoxide, oxygen, nitrogen and carbon dioxide as representing the amount of chemisorbed gas. A similar definition has been successfully employed in the case of such materials as iron synthetic ammonia catalysts.[20]

Chemisorptions of carbon monoxide and oxygen also were measured on an unstabilized surface in order to determine whether the extent of surface coverage depended on the degree of sintering of the chromia. The values obtained using an area of 45 to 48 m.²/g. were identical, on a unit area basis, with those found on the stabilized surface. The facts that both carbon monoxide and oxygen form stable chemisorbed films and that the amounts so adsorbed seem directly proportional to the surface area suggest the use of one or the other of these gases as a means of measuring the fraction of the total surface of a supported chromia catalyst which can be attributed to chromia.[21]

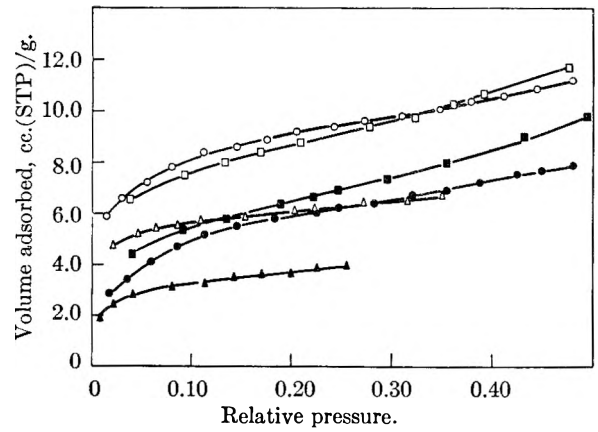

Fig. 1.—Adsorption of gases on a reduced chromia surface. Open and solid symbols represent adsorptions before and after evacuation for one hour at −78° in the cases of carbon monoxide and oxygen and at 25° in the case of carbon dioxide: (○, ●) carbon monoxide at −195°; (□, ■) oxygen at −195°; (△, ▲) carbon dioxide at −78°.

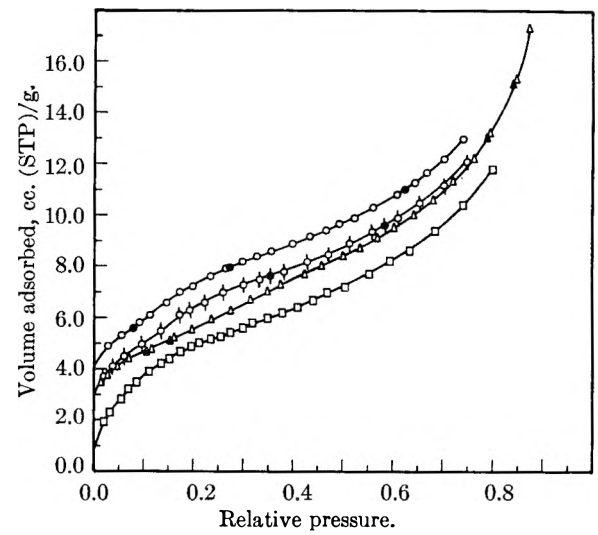

Fig. 2.—Adsorption of nitrogen on chromia surfaces at −195°. Open and solid symbols represent adsorption and desorption points, respectively: (○, ◊) clean surface before and after evacuation at −78°; (△, □) oxygen surface and carbon monoxide surface, respectively, before and after evacuation at −78°.

Having determined the extent to which individual gases reacted with the surface, it was of interest to investigate the influence of these chemisorbed films upon subsequent adsorption of other gases. This was accomplished by evacuating the catalyst at −78° (25° in the case of carbon dioxide) for one hour following completion of the second isotherm of a particular gas and then measuring two isotherms for the second gas in the usual fashion. The isotherms so obtained are illustrated in Fig. 2 for the case of nitrogen.[22] Results for a number of adsorbate combinations are summarized in Table I. It should be understood that the surface designated in this table as "clean" refers to the surface obtained upon reduction and evacuation

(19) The rather unusual shape of the upper two isotherms in Fig. 2 was always observed when either nitrogen or argon was adsorbed on a clean, reduced chromia surface. As will be discussed at greater length in a forthcoming publication, it is believed that this feature may be due to the presence of a somewhat homogeneous surface resulting from the stabilizing pretreatment of the chromia.

(20) S. Brunauer and P. H. Emmett, *J. Am. Chem. Soc.*, **62**, 1732 (1940).

(21) A similar suggestion has been made by Weller and Voltz[9] who attempted to relate the "excess oxygen content" of a number of chromia catalysts, oxidized at 500°, to their surface areas. A scatter of some 30% observed in the results indicated that the method was capable of giving only approximate chromia areas. It seems possible that this excess oxygen was not confined to the surface. In the present case, however, the chemisorbed oxygen is probably restricted to the surface and hence may be directly related to the area of supported chromia.

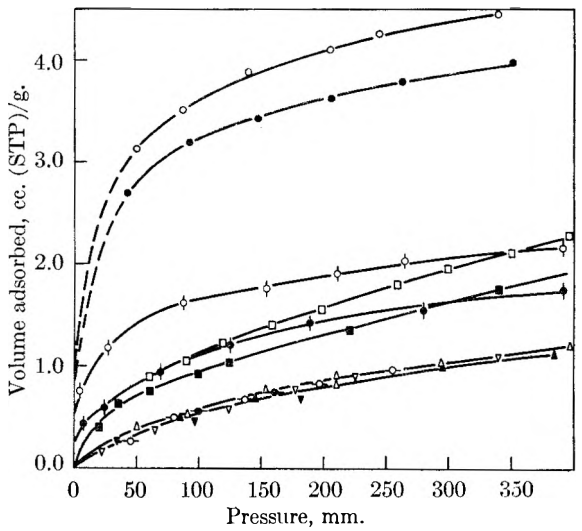

Fig. 3.—Adsorption of hydrogen on chromia surfaces at −195°. Open and solid symbols represent adsorptions before and after evacuation for one hour at −78°, respectively: (○, ●) clean surface; (□, ■) oxygen surface; (◇, ◆) carbon dioxide surface; (△, ▲) carbon monoxide surface; (⊖, ⊖) oxygen + carbon monoxide surface; (▽, ▼) carbon dioxide + oxygen surface.

at 500°. Mass spectrometric analyses of the gas phases present during measurement of the second series of isotherms indicated that, in no case, did any appreciable amount of the original adsorbate desorb during the course of the isotherm determination. Further, the fact that the second isotherm of the second series coincided with that expected for purely physical adsorption suggests that no desorption of either the first or second chemisorbate took place during the intervening evacuation between the two isotherms of the second series.

Table I

Chemisorption of Gases on Chromia Surfaces

Surface	Volume chemisorbed, cc. (STP)/m.² O_2[a]	CO[a]	CO_2[b]	N_2[a]	H_2[c]
Clean	0.10	0.14	0.12	0.04	0.15
0.10 cc. (STP) O_2/m.²	...	.03	...	0	.04
.14 cc. (STP) CO/m.²	0	...	...	0	~0
.12 cc. (STP) CO_2/m.²	0.06	.04	...	0	0.07

[a] At −195°. [b] At −78°. [c] At −195° and 300 mm.

The distinction between physical and chemical adsorption of hydrogen was not as obvious as in the case of the adsorbates discussed above. An examination of the results shown in Fig. 3 for the clean, reduced surface suggested the occurrence of at least three types of hydrogen adsorption; namely, physical adsorption, a weak chemisorption, and a strong chemisorption not removed at −78°. The existence of a weak chemisorption seems necessitated by the known hydrogen exchange activity of chromia surfaces; certainly it is not reasonable to expect that hydrogen so firmly held to the surface that it cannot be removed during extended periods of evacuation plays a very large role in the exchange reaction. Rather, it would appear that hydrogen active in the exchange reaction was desorbed during the evacuation along with any physically adsorbed hydrogen. In an attempt to gain more information as to the extent of the total adsorption, a study was made of the hydrogen–deuterium exchange activities of the chromia surface with various other gases chemisorbed on it; at the same time hydrogen adsorption isotherms were measured on the surfaces at −195°. Specific rate constants for the exchange reaction are given in Table II while the isotherms are shown in Fig. 3. In general, the first-order plots of exchange rates were linear and reproducible (within 10%). In some cases, however, the rate was so rapid that only a single gas sample could be withdrawn before equilibrium obtained. Thus the rates on the clean surface at −112° and on the oxygen covered surface at −78° were calculated from duplicate runs in which a single sample of gas was taken after a reaction time of five minutes. At −78° the clean surface was too active to permit any reliable estimate of the rate constant.

Table II

Hydrogen–Deuterium Exchange Activities of Chromia Surfaces

Surface	$k(-195°)$, m.$^{-2}$ min.$^{-1}$	$k(-112°)$, m.$^{-2}$ min.$^{-1}$	$k(-78°)$, m.$^{-2}$ min.$^{-1}$
Clean	4.9×10^{-5}	3.0×10^{-2}	Fast
0.14 cc. (STP) CO/m.²	0	0	6.8×10^{-6}
0.10 cc. (STP) O_2/m.²	0	7.8×10^{-3}	3.6×10^{-4}
0.12 cc. (STP) CO_2/m.²	0	1.5×10^{-4}	6.0×10^{-5}
0.10 cc. (STP) O_2 + 0.03 cc. (STP) CO/m.²	0	1.2×10^{-4}	6.0×10^{-4}
0.12 cc. (STP) CO_2 + 0.06 cc. (STP) O_2/m.²	0	5.0×10^{-6}	5.9×10^{-5}
0.12 cc. (STP) CO_2 + 0.04 cc. (STP) CO/m.²	0	0	3.5×10^{-5}
0.04 cc. (STP) N_2/m.²	5.1×10^{-5}	...	...

It was found that, in general, the presence of a chemisorbate reduced both the exchange activity of the catalyst and the extent to which it would adsorb hydrogen at −195°. When the surface was inactive, or nearly so, the hydrogen adsorption was quite small and could be more or less completely removed from the surface at −78°; when the surface was active the increased adsorption was to some extent irreversible at −78°. It would seem reasonable to conclude, therefore, that the adsorptions on the inactive surfaces were primarily physical in nature and that the difference between the isotherms on these and on the more active surfaces could be attributed to a corresponding amount of chemisorbed hydrogen. Thus the amount of hydrogen chemisorbing at −195° on a particular surface was taken as the difference between the

(22) The depression of the nitrogen isotherm on the carbon monoxide covered surface was due to the presence of the chemisorbed film. Similar behavior has been noted by other workers for a cobalt catalyst.[23] In the present case, a BET plot of the nitrogen isotherm on the carbon monoxide surface gave the same V_m value as did the isotherm on the oxygen covered surface. These points will be discussed at greater length in a forthcoming publication.

(23) M. V. C. Sastri, T. S. Viswanathan and T. S. Nagarjunan, This Journal, 63, 518 (1959).

isotherms on that surface and on the inert, carbon monoxide covered surface at 300 mm. This particular pressure was chosen because it was at this pressure that the exchange activities were measured and because, except in the case of the oxygen covered surface, the isotherms were essentially parallel in this region. As can be seen from Fig. 3, the isotherm on the oxygen covered surface is somewhat atypical in that the slope appears greater at higher pressures than is the case for the other isotherms. This may be due to a change in the electronic character of the hydrogen adsorption sites upon chemisorption of oxygen. The amounts of hydrogen chemisorption defined in the above manner are summarized in Table I. It is not intended that this definition should be taken as implying that all the hydrogen chemisorbed on the active surfaces was equally significant in the exchange reaction, although the major portion of the chemisorbate presumably was dissociated.

In general, the data reported in Table I are believed to represent reasonable estimates of the extent to which the various adsorbates react with a chromia surface under the conditions employed. Obviously, the definition of chemisorption used in many cases is somewhat arbitrary since it depends upon the extent to which physically adsorbed gas may be separated from any chemical adsorption by evacuation of the adsorbent under certain arbitrarily chosen conditions (*i.e.*, time and temperature). However, as mentioned above, the amount of adsorption taking place after the evacuation period generally could be accounted for in terms of physical adsorption. Further justification for the definition used seems to be provided by the magnitude of the chemisorption heats reported by other workers. Thus Beebe and Dowden[5] found that on a reduced chromia surface, carbon monoxide and oxygen were chemisorbed with heats of about 12 and 24 kcal./mole, respectively, while the heat of carbon monoxide chemisorption on an oxygen covered surface was about 10–12 kcal./mole. Dowden and Garner[7] found that carbon dioxide was chemisorbed on reduced chromia at room temperature with a heat of 20–30 kcal./mole; presumably this heat would still be appreciable at −78°. Thus, for the adsorbates discussed, the heats of chemisorption seem sufficient to allow fairly unambiguous separation of the physical adsorption by evacuation for, say, an hour at −78° in the case of oxygen and carbon monoxide or at 25° in the case of carbon dioxide.[24] With nitrogen more care has to be exercised since the heat of chemical adsorption, as reported by Beebe and Dowden,[5] is only 8 kcal./mole or about twice that for physical adsorption. Nevertheless, once again a reasonable estimate of the extent of chemisorption appears possible. Presumably no nitrogen was chemically adsorbed on the oxygen covered surface since the isotherm obtained gave the expected BET parameters and since the adsorbed gas was easily removed at −78°. The fact, then, that the second nitrogen isotherm on the clean surface gave the same BET monolayer volume as the isotherm on the oxygen covered surface certainly suggests that only physical adsorption was involved in this second isotherm. Hydrogen as indicated above presents more of a problem; the values given in Table I for this gas seem reasonably well justified. Several hydrogen adsorption isotherms on reduced and oxidized chromia surfaces reported by Weller and Voltz[9] appear to agree in magnitude with those of Fig. 3.

(24) Actually, the possibility of small amounts of chemisorption taking place during the second isotherms still remains and the values reported in Table I must be considered as indicating the minimum chemisorption occurring. An illustration of this point is provided by the case of oxygen adsorption on the carbon monoxide covered surface. Here no evidence of any oxygen chemisorption was found at −195° although Beebe and Dowden[5] reported a small amount of oxygen adsorption at −183° having a heat of 13 kcal./mole.

Discussion

The surface of an oxide may, as a first approximation, be regarded as consisting of two types of adsorption centers, the metal ions and the oxide ions, although the detailed nature of adsorbate interactions with these centers remains generally obscure. Adsorption involving oxide ions is often irreversible in that desorption is generally in the form of a different chemical species. Thus carbon monoxide may be desorbed from reducible oxides as carbon dioxide.[25] With the cations, on the other hand, adsorption usually is reversible and probably involves, in the case of transition metal ions, some form of covalent bonding with the d-electron shell of the cation. When both types of chemisorption are possible, the reversible adsorption seems to be favored at low temperature, the adsorption often becoming irreversible as the temperature is increased.[25]

In the present case, because of the low temperature employed and the reversible nature of the adsorption,[5] it is believed that the carbon monoxide and hydrogen chemisorptions, as given in Table I, take place primarily on chromium ions at the surface of the adsorbent. In order to discuss these adsorptions in terms of surface coverage, it is useful, therefore, to postulate some reasonable model for the surface recognizing, of course, that the assignment of any specific structure to the surface of an oxide such as chromia must be made with considerable reservations as to the degree of correspondence with reality. In the case of α-Cr_2O_3, Davis[26] recently has presented arguments suggesting that at the surface, the chromium ions are situated in a hexagonal array similar to that prevailing in the (001) plane of the bulk oxide. This simple picture presumably would have to be modified in light of the work of Weller and Voltz[9] who showed that chromia, reduced and evacuated at 500°, contains appreciable amounts of strongly bound hydrogen, some of the chromic ions apparently being reduced to chromous ions. To what extent these latter may be associated with the surface and thus perturb the arrangement postulated by Davis is not clear. In any case, the picture advanced by Davis remains useful in that it allows some estimate to be made of the number

(25) B. M. W. Trapnell, "Chemisorption," Butterworths Scientific Publications, London, 1955, p. 191.

(26) R. J. Davis, "Chemisorption," ed. by W. E. Garner, Academic Press, New York, N. Y., 1957, Chapter 4.5.

of chromium ions which may be assigned to the surface. Assuming, therefore, that the cation layer in the undistorted (001) plane of α-chromia may be associated with the surface, the number of surface chromium ions is estimated to be about 9.8×10^{18}/m.^{2}. The hydrogen adsorption on this surface, as given in Table I, is presumably dissociative and amounts to 8.0×10^{18} atoms/m.^{2}, enough to cover at least 80% of the available surface sites assuming that the adsorbed complexes involve chromium ions. In fact, the agreement between the number of cations possible at the surface and the number of adsorbed hydrogen radicals is probably within the uncertainty involved in estimating the former. Comparing the carbon monoxide adsorption to the hydrogen adsorption, the data in Table I indicate that the 3.8×10^{18} carbon monoxide molecules/m.^{2} adsorbed on the clean surface prevented the subsequent adsorption of approximately the same number of hydrogen molecules. In other words, assuming that the hydrogen adsorption is dissociative, the carbon monoxide chemisorption apparently involves most of the 8×10^{18} hydrogen adsorption sites/m.^{2}. A surface complex consistent with this situation would be one in which each carbon monoxide molecule was effectively bonded to two surface chromium ions. An obvious alternative explanation would involve the molecular adsorption of hydrogen and single site adsorption of carbon monoxide. To date, however, there seems to be little evidence for such adsorption in the case of hydrogen and the former model seems more reasonable. Thus it is believed that both carbon monoxide and hydrogen are chemisorbed over most, if not all, of the available chromia surface with both adsorptions occurring principally on the same sites; the latter are assumed to be surface chromium ions.

The chemisorption of oxygen on reduced chromia probably involves the formation of O^- or $O^=$ ions by electron transfer from the adsorbent and may, therefore, be regarded in terms of a partial oxidation of the surface. Although the data at hand are not sufficient to justify anything more than a speculative discussion, it is interesting to consider a possible model for this oxygen adsorption process. As mentioned earlier, Weller and Voltz[9] found that chromia, reduced and evacuated at 500°, was nonstoichiometric with respect to the +3 state of chromium, some chromium ions apparently being reduced to chromous ions. Taking the data given for the particular chromia sample they studied and converting to a unit area basis, the amount of oxygen necessary to restore stoichiometry appears to be about 0.09 cc. (STP)/m.^{2}. Similarly, assuming that there are about 9.8×10^{18} Cr^{+2} ions/m.^{2} at the surface, the amount of oxygen required to oxidize these to Cr^{+3} ions is again 0.09 cc.(STP)/m.^{2} assuming $O^=$ ions are formed. This figure is in close agreement with the observed oxygen chemisorption of 0.10 cc. (STP)/m.^{2}. Thus the oxygen chemisorption can be rationalized in the following terms. Reduction and evacuation of the chromia results in the reduction of the surface chromium ions to chromous ions. Upon chemisorption of oxygen, these are converted to chromic ions with the concurrent formation of $O^=$ ions. In such a model, the differences in adsorptive properties between the clean and the oxygen covered surfaces could be attributed to a corresponding difference in the electronic nature of the two surfaces. Obviously, the model suggested is not a unique one and other possible formulations may be equally consistent with the experimental data.

An alternative mechanism for the oxygen adsorption process involves the formation of O^- ions. The concurrent surface oxidation could again conceivably involve chromous ions, resulting from the reduction treatment, going to chromic ions. If one O^- ion was assigned to each surface chromium ion, the observed oxygen chemisorption would cover about 60% of the available surface. It would be interesting in this respect to have information concerning conductivity changes upon the chemisorption of oxygen at low temperatures; in the absence of such data, discussion of the nature of the absorbed species must remain speculative.

This last statement is also applicable to the carbon dioxide chemisorptions although it seems probable that, in this case, a surface carbonate is formed.[7] If, for sake of argument, the adsorbed complex is assigned the cross-sectional area of a physically adsorbed molecule, the carbon dioxide adsorption reported in Table I is sufficient to cover about 80% of the total surface. The amount of carbon monoxide required to cover the remaining surface is estimated to be about 0.03 cc. (STP)/m.^{2}; this agrees with the observed adsorption in Table I. In this connection, it is informative to compare the hydrogen–deuterium exchange activities of the oxygen covered and the carbon dioxide covered surfaces. The former is the more active at −112° by a factor of about 50, although it chemisorbs only half as much hydrogen as the latter at −195°. For this behavior two explanations may be suggested. Either the carbon dioxide adsorption blocks the more active sites or the oxygen covered surface has an activity in its own right. The latter possibility seems quite rational. If the chemisorption of oxygen involves the oxidation of, say, chromous ions ($3d^4$) to chromic ions ($3d^3$), this would result in a surface of lower intrinsic exchange activity as compared to the clean surface, if the resulting electronic configuration were less favorable for hydrogen activation. The work of Dowden, Mackenzie and Trapnell[2,3] would seem to imply that any such changes in the electronic configurations of transition metal ions should have a direct effect upon the specific rate constants for hydrogen exchange.

One of the most remarkable features of chromia, and one which apparently makes it almost unique among oxides, is its ability to chemisorb nitrogen at low temperatures. That such chemisorption takes place seems fairly well established. Thus, as mentioned earlier, Beebe and Dowden[5] report a heat of adsorption of 8 kcal./mole which, while not large, is significantly in excess of that expected from purely van der Waal interactions. In the present work the difficulty with which the adsorbed gas was removed from the surface at −78° seems to be very good evidence for chemisorption.

Finally, the fact that the adsorption was poisoned by the presence of adsorbates such as oxygen or carbon dioxide suggests a specificity in the nitrogen interaction with certain sites that is not generally considered to be characteristic of physical adsorption. Thus it seems evident that the adsorption is chemical in nature and that, at −195°, it is sufficient in magnitude to cover about 20% of the surface. It will be observed from the data in Table II that the chemisorbed nitrogen had no effect on the exchange activity. Apparently, either the nitrogen was associated with sites not involved in the exchange or the hydrogen displaced the nitrogen from the surface. Some evidence for the latter possibility is provided by the fact that the resulting hydrogen–deuterium mixture was found to contain traces of nitrogen.

Conclusions

This work has confirmed and extended earlier observations concerning the reactivity of reduced chromia surfaces at low temperatures. Both carbon monoxide and hydrogen are chemisorbed in sufficient quantities at −195° to cover essentially the entire surface, the carbon monoxide poisoning the surface both for the hydrogen–deuterium exchange reaction and for the subsequent chemisorption of other gases. The data suggest that the carbon monoxide adsorption may involve a dual site mechanism. The adsorptions of oxygen at −195° and carbon dioxide at −78° are not as extensive, the former covering about 60% and the latter 80% of the total surface. The oxygen chemisorption is considered to be a surface oxidation with the resulting change in hydrogen exchange activity being a consequence of a change in the d-electron configuration of the surface chromium ions. Additional evidence has been obtained for the chemisorption of nitrogen on a reduced chromia surface, this adsorption corresponding to a surface coverage of some 20%. Following other workers, it is suggested that the ability of this surface to chemisorb a variety of gases at these temperatures is due to the availability, at the surface, of a suitable number of unpaired d-electrons.

Acknowledgments.—The authors take this opportunity to thank Dr. George F. Crable for making the mass spectrometric analysis. Thanks are also due to Drs. C. W. Montgomery and Frank Morgan for their interest and encouragement and to Gulf Research & Development Company for permission to publish.

MASS SPECTROMETRIC STUDY OF HIGH TEMPERATURE REACTIONS OF $H_2O(g)$ AND $HCl(g)$ WITH Na_2O AND Li_2O[1a,b]

BY RICHARD C. SCHOONMAKER[2] AND RICHARD F. PORTER

Department of Chemistry, Cornell University, Ithaca, New York

Received October 15, 1959

The gaseous products formed by reactions of $H_2O(g)$ and $HCl(g)$ with condensed Li_2O and Na_2O phases at high temperatures have been identified mass spectrometrically. At low water pressures the major species produced by reaction of $H_2O(g)$ with $Li_2O(s)$ is $LiOH(g)$. In Na_2O–$H_2O(g)$ experiments, monomers and dimers of NaOH are formed. A small concentration of NaOH trimer in the vapor is also indicated. An estimate of the relative heats of dimerization of LiOH and NaOH was obtained from the results of experiments with the Na_2O–Li_2O–$H_2O(g)$ system. In the systems Na_2O–$NaCl$–$H_2O(g)$ and Na_2O–$HCl(g)$ the mixed anion dimer, $Na_2(OH)Cl(g)$, is formed in addition to $Na_2(OH)_2(g)$ and $Na_2Cl_2(g)$. Because of ambiguities due to the ion fragmentation patterns of $Na_2(OH)_2$, Na_2Cl_2 and $Na_2(OH)Cl$ the existence of the latter species is necessarily inferred from the dependence of ion current intensities on flow rate of the reactant gas. Similar behavior was noted for the system Na_2O–NaF–$H_2O(g)$. Some previously proposed processes of ion formation by electron impact of sodium hydroxide vapors have been confirmed. Comparison of ion fragmentation patterns obtained in studies with pure LiCl and with the Li_2O–$HCl(g)$ system indicates that Li^+ ions are formed from both $LiCl(g)$ and $Li_2Cl_2(g)$ molecules at high electron energies.

Introduction

Several mass spectrometric studies of the vaporization of alkali metal hydroxides[3] and halides[4,5] have been reported recently. Identification of the vaporizing species from condensed lithium hydroxide by mass spectrometric means is made difficult because of the high decomposition pressure of water. In the present work, studies were undertaken to provide information concerning the stabilities of gaseous species in the Li–OH system, to investigate the existence of gaseous dimers containing mixed anions ($M_2(OH)X(g)$, where X is a halide) and to provide additional information related to several mechanisms of ion formation which had been proposed previously.

Experimental

The experimental method involves the use of a mass spectrometer to identify the vapor species effusing from the orifice of a Knudsen cell containing a condensed phase over which various reactant gases may be leaked from a source external to the instrument. Thermochemical data may be obtained from a study of the ions produced and the dependence of ion current intensities on temperatures and leak rate.

Effusing neutral gaseous molecules, formed by interaction

(1) (a) This research was supported by the U. S. Air Force through the Air Force Office of Scientific Research of the Air Research and Development Command under contract No. AF 18(603)-1. (b) Part of a thesis presented by R.C.S. to the faculty of Cornell University in partial fulfillment of the requirements for the degree of Doctor of Philosophy.

(2) General Electric Predoctoral Fellow (1958–1959).

(3) (a) R. F. Porter and R. C. Schoonmaker, *J. Chem. Phys.*, **28**, 454 (1958); (b) R. C. Schoonmaker and R. F. Porter, *ibid.*, **31**, 830 (1959).

(4) (a) J. Berkowitz and W. A. Chupka, *ibid.*, **29**, 653 (1958); (b) R. F. Porter and R. C. Schoonmaker, *ibid.*, **29**, 1070 (1958); (c) Milne, Klein and Cubicciotti, *ibid.*, **28**, 718 (1958).

(5) R. C. Schoonmaker and R. F. Porter, *ibid.*, **30**, 283 (1959).

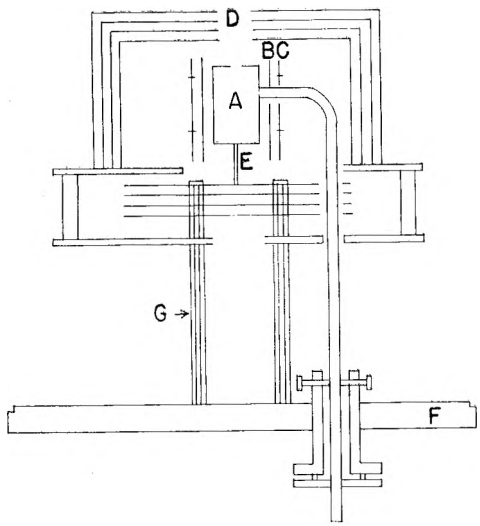

Fig. 1.—Schematic diagram of high temperature furnace assembly with leak system: A, crucible; B, electron bombardment shield; C, filaments; D, radiation shield; E, thermocouple; F, furnace pot flange; G, quartz spacers.

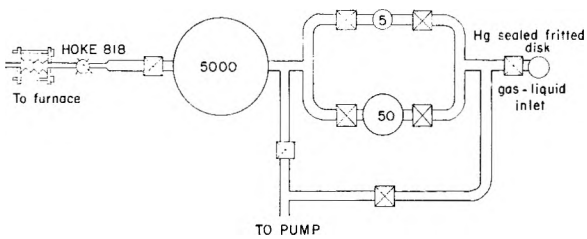

Fig. 2.—Schematic diagram of external leak system.

of leak gas with the condensed phase in the Knudsen cell, pass through a shutter plate and into the ion source of a 12-inch radius of curvature, direction focusing mass spectrometer where ions are formed by bombardment with electrons of selected energy in the range 5–150 volts. The ion beam thus produced is electrostatically collimated and accelerated before being mass analyzed in a variable magnetic field. The detection system consists of an electron multiplier and associated amplification and recording circuitry. The purpose of the shutter plate is to provide a means for distinguishing ions formed by electron impact on condensable effusing species from those formed from background gas at the same mass.

Details of the mass spectrometer, furnace assembly, and experimental procedure have been described previously.[6] The furnace assembly used in this investigation differs from the conventional system in that a platinum side arm tube is palladium-welded into the platinum effusion cell to provide a method of introducing gases at low, controlled pressure into the cell from an external source. The leak allows one to shift the prevailing equilibria in the cell and to study the interaction of the foreign gas with a condensed phase. The internal elements of the leak system furnace assembly are depicted in Fig. 1 and the external control system is shown in Fig. 2. Temperatures are measured with a Pt–Pt, 10% Rh thermocouple. The ratio of orifice cross sectional area, which includes the area of the leak, to sample evaporating surface area is less than 0.02. Utilization of the Hoke No. 818 vacuum needle valve makes it possible to maintain a vacuum tight seal and at the same time provides positive control of the flow rate into the effusion cell. If the gas inlet and effusion hole areas and the total pressure within the Knudsen cell are sufficiently small, effusion conditions should be maintained and introduction of the leak gas should not interfere with the attainment of equilibrium in the oven.

It has been found that in higher temperature runs radiation from the furnace region may cause instability in instrument sensitivity due to overheating of the ion source. During these experiments a heavy copper cylinder, closed at the top except for a hole to pass effusing vapors, was mounted between the furnace and shutter plate and connected through heavy gauge copper rod and tubing to an external metal Dewar flask. Conduction of heat from the cylinder to the liquid nitrogen or ice-water filled reservoir was sufficient to maintain the ion source at a temperature where adverse effects were not encountered.

Runs were made with the system: $Na_2O(s)$, $Li_2O(s)$, Na_2O–NaF(c) and Na_2O–NaCl(c), with water vapor as leak gas; and $Na_2O(s)$ and $Li_2O(s)$ with HCl as leak gas. Further experiments were conducted with pure NaCl and LiCl. Samples of Li_2O and Na_2O were obtained by thermal decomposition of the hydroxide and peroxide, respectively.

Results

$Na_2O(s)$–$H_2O(g)$.—Studies with $Na_2O(s)$ and $H_2O(g)$ were conducted in the temperature range 534–866°. Ion species which were detected were Na^+, $NaOH^+$, Na_2O^+, Na_2OH^+ and in one run $Na_3(OH)_2^+$. With the exception of $Na_3(OH)_2^+$, these ions have been observed in similar experiments[3] with vapors from liquid NaOH. On the basis of these previous observations, the formation of these ions by electron impact in the ion source was attributed to primary ionization processes (*i.e.*, by either simple ionization or fragmentation). The occurrence of second-order reactions as, for example, $NaOH(g) + NaOH^+ \rightarrow Na_2OH^+ + OH$ has been ruled out as a major process since second-order dependence of Na_2OH^+ on $NaOH^+$ as a function of cell temperature (or NaOH vapor pressure) was not observed. The design of the ion source[3] greatly reduces the likelihood of collisions between NaOH molecules and ions formed from these molecules. As evidenced from the ion intensities observed in these experiments with $Na_2O(s)$–$H_2O(g)$ the flux of molecules entering the ion source is comparable to those referred to in reference 1 and thus there is no reason to suspect that Na_2OH^+ observed in the present work is formed by a different mechanism. At a cell temperature of about 800° the variation of ion intensities of Na_2OH^+ with $NaOH^+$ was observed by changing the leak rate of H_2O. For a system involving gaseous equilibrium between monomer and dimer at constant temperature the dimer pressure should change as the square of the monomer pressure (under the conditions of these experiments we have an additional degree of freedom since the condensed phase is not pure NaOH). Over a limited range in leak rate, corresponding to a change of a factor of approximately 5 in $I_{Na_2OH^+}$, Na_2OH^+ was found to have very nearly a second order dependence on $NaOH^+$ as could be anticipated if these species are formed exclusively from the dimer and monomer, respectively.

In general, ion intensities followed the $H_2O(g)$ leak rate; but, at lower temperatures, where condensed phase saturation is more nearly attainable, ion intensities originating from the monomer (Na^+, $NaOH^+$) persisted, though diminishing with time, after the leak was terminated. This observation suggests that under certain conditions the condensed phase is not well defined during the period of gas leakage. In the case cited here, for example, the condensed phase would consist of a mixture of Na_2O and NaOH in which the mole fraction ratios would be undetermined but markedly dependent on temperature and $H_2O(g)$ leak rate. Ion in-

(6) See Ph.D. Thesis of R. C. Schoonmaker, Cornell University.

tensity ratios $Na_2OH^+/NaOH^+$ were generally less than unity, but at high flow rates of H_2O, corresponding closer to condensed phase saturation, the intensities of Na_2OH^+ and $NaOH^+$ were nearly equal. In one run at 811° $Na_3(OH)_2^+$ was also observed. The intensities for 100 volt electrons were in the approximate ratios $NaOH^+$: Na_2OH^+:$Na_3(OH)^+_2$ = 1:2:0.07. The absolute intensity of $Na_3(OH)_2^+$ was not sufficiently large to allow unambiguous determination of its origin. However, it arises, presumably, from dissociative ionization of $Na_3(OH)_3(g)$.

Confirmation of the previous assertion[2] that Na_2O^+ arises from dissociative ionization of $Na_2(OH)_2(g)$ has been obtained by noting that Na_2O^+ does not appear in the mass spectrum until water vapor is introduced into the system at a partial pressure sufficient to cause formation of $Na_2(OH)_2(g)$ as evidenced by the appearance of $Na_2(OH)^+$. Whenever Na_2OH^+ was detected, the ratio $I_{Na_2OH^+}/I_{Na_2O^+}$ was approximately 10 and independent of experimental conditions. The invariance of the ratio I_{Na^+}/I_{NaOH^+} over a wide range of experimental conditions provides sufficient evidence to corroborate the original assumption that the Na^+ detected in earlier experiments[2] with NaOH(c) contained in a silver crucible was formed primarily by fragmentation of NaOH(g).

$Li_2O(s)$–$H_2O(g)$.—Only Li^+ and $LiOH^+$ ion species were observed in the temperature range 780–900° with $Li_2O(s)$ as condensed phase and H_2O as leak gas. The intensities of these ion species were dependent on the leak rate and disappeared altogether whenever the H_2O leak was turned off. The ion intensity ratio I_{Li^+}/I_{LiOH^+} was approximately 0.1 and independent of experimental conditions. By consideration of the earlier data for the other alkali hydroxides[3b] it is assumed that Li^+ and $LiOH^+$ are formed by the respective mechanisms of dissociative and simple ionization of the gaseous LiOH molecule. Clearly, condensed LiOH has an appreciable decomposition pressure in this temperature range since the water partial pressure due to the leak was never high enough to form any appreciable concentration of LiOH(c) (the $LiOH^+$ ion intensity dropped abruptly to zero upon termination of the leak). In these studies the upper limit to the leak gas pressure which is attainable in the effusion cell is determined by the pump out capacity of the vacuum equipment in the system. If the evacuation rate is exceeded, the effusing gas builds up a background pressure in the mass spectrometer with consequent scattering effects. The upper limit in the operational pressure of H_2O in the effusion cell is estimated to be about 10^{-2} mm. The dissociation pressure of LiOH(s) in the temperature range investigated is apparently high enough that it is impossible with the present equipment to increase the water vapor partial pressure to a value where $Li_2(OH)_2(g)$ can be detected.

$Li_2O(s)$–$Na_2O(s)$–$H_2O(g)$.—A mixture of $Li_2O(s)$–$Na_2O(s)$ with $H_2O(g)$ has been investigated in order to obtain information on the relative stabilities of $Li_2(OH)_2(g)$ and $Na_2(OH)_2(g)$. The major ion species detected were Na^+, $NaOH^+$, Na_2OH^+, $LiOH^+$ and the mixed ion $NaLiOH^+$. A mass spectrum record of the ion species is shown in Table I. Under the conditions of these experiments $I_{Na_2OH^+} < I_{NaOH^+}$. This situation probably results from the decrease in thermodynamic activity due to mixing and from the low water pressures employed. From the ion current data obtained in these studies, it is possible to estimate the difference in heats of dimerization of NaOH(g) and LiOH(g). The mixed equilibrium constant, $K_{eq} = (I_{NaLiOH^+})^2/(I_{Li_2OH^+})(I_{Na_2OH^+})$ for the reaction $Na_2(OH)_2(g) + Li_2(OH)_2(g) = 2NaLi(OH)_2(g)$ is estimated to lie between 4 and 8 from considerations involving the entropy change for the reaction and values for the corresponding reaction with lithium and sodium fluoride dimers.[5] This assumption places the calculated intensity of Li_2OH^+ between 0.8 and 1.4 units relative to the data in Table I. This small intensity would not be distinguishable above background at mass 31. A relative equilibrium constant calculation[5] using total ionization cross sections, gives a value between 4 and 6 kcal./mole of dimer for the difference in enthalpies of dimerization for LiOH(g) and NaOH(g). This magnitude for $\Delta H^0_{LiOH} - \Delta H^0_{NaOH}$ (dimerization) has been predicted on the basis of the analogy between the alkali fluorides and hydroxides.[3b]

TABLE I

MASS SPECTRUM OF ION SPECIES FORMED WITH Li_2O–$Na_2O(c)$ IN THE PRESENCE OF $H_2O(g)$

T, °K.	I_{Na^+}	I_{NaOH^+}[a]	$I_{Na_2OH^+}$	I_{NaLiOH^+}	I_{LiOH^+}
1082	63	100	85	21.6	5.8

[a] Ionizing electron energy = 100 volts, total intensities relative to $NaOH^+$ = 100.

TABLE II

DEPENDENCE OF ION CURRENT INTENSITIES ON FLOW OF HCl(g) OVER $Na_2O(s)$ AT T = 973°K.

Relative change in leak rate of HCl(g)	I_{NaOH^+}[a]	$\frac{I_{NaOH^+}}{I_{Na_2OH^+}}$	$I_{Na_2Cl^+}$	I_{NaCl^+}
Leak on	100	2.1	27	90
Decrease	95	3.0	14	50
Increase	82	1.2	68	110
Leak off	Small	..	0.0	0.0
Leak on	45	2.5	Small	25
Increase	48	1.3	23	57

[a] Ionizing electron energy = 100 volts.

$Na_2O(s)$–$HCl(g)$, Na_2O–$NaCl(c)$–$H_2O(g)$ and the Existence of $Na_2(OH)Cl(g)$ Molecules.—In the temperature range around 700°, the ion species observed when HCl(g) was passed over $Na_2O(s)$ were Na^+, $NaCl^+$, $NaOH^+$, Na_2Cl^+ and Na_2OH^+. The $NaCl^+$ and $NaOH^+$ were usually of about equal intensities while HCl^+ was virtually undetected indicating that the uptake of gas is nearly complete. In most cases the ions formed from polymeric species were lower in intensity than those formed from the monomers. This behavior, which is the result of the activity effect, is to be expected in these experiments and is in contrast to the observations of the vapors of pure NaCl and NaOH in which ions representing dimers are the major species. The interpretation of the mass spectrum

is complicated in the present studies as a result of the fragmentation pattern of the dimers. The presence of dimers containing mixed anions, $Na_2(OH)Cl$, should lead to the formation of Na_2Cl^+ and Na_2OH^+ ions on electron impact, but these same species arise from fragmentation of $Na_2Cl_2(g)$ and $Na_2(OH)_2(g)$, respectively. Under no conditions have $Na_2(OH)Cl^+$ ions been detected. For systems with mixed cations and a common anion (*e.g.*, NaOH-KOH) the fragmentation pattern is simplified because only one unique ion (*e.g.*, $NaKOH^+$) is formed from the mixed dimer. The formation of $Na_2(OH)Cl(g)$ in the vapor phase may be inferred from the present studies with $Na_2O(s)$–$HCl(g)$ and Na_2O–$NaCl(c)$–$H_2O(g)$. At a fixed cell temperature HCl(g) was passed into an effusion cell containing $Na_2O(s)$ and a mass spectral scan was made. When the flow gas was turned off ion intensities did not vanish immediately. This observation indicates that residual hydroxide and chloride were present in the condensed phase. The variation of ion intensities with HCl(g) leak rate is given in Table II. The ratio $I_{Na_2OH^+}/I_{NaOH^+}$ was found to increase considerably with increasing HCl(g) leak rate while the intensity of $NaOH^+$ was altered only slightly. This effect would not be consistent with an increase in $Na_2(OH)_2(g)$ concentration resulting from thermodynamic activity changes, but may be accounted for by postulating the existence of $Na_2(OH)Cl(g)$ which can dissociate to Na_2OH^+ on electron impact. Further illustration of this effect is observed in the data obtained with Na_2O–$NaCl(c)$–$H_2O(g)$, shown in Table III, in which the ratio $I_{Na_2Cl^+}/I_{NaCl^+}$ is increased considerably with increasing $H_2O(g)$ leak rate while I_{NaCl^+} is essentially unaffected. Although these data show that $Na_2(OH)Cl(g)$ fragments to both Na_2OH^+ and Na_2Cl^+ there is no *a priori* justification for the assumption that the molecule will fragment equally in both directions. It is difficult to establish the exact percentage fragmentation in each direction. In many circumstances the amount of one pure dimer in the system may be small while the other pure dimer may be large. If, for example, the $NaOH^+$ and Na_2OH^+ intensities were large when the $NaCl^+$ intensity was small, the Na_2Cl^+ must originate almost entirely from the $Na_2(OH)Cl(g)$ molecule.

TABLE III

DEPENDENCE OF ION CURRENT INTENSITIES ON FLOW OF $H_2O(g)$ OVER Na_2O–NaCl(c) AT T = 1038°K.

Relative change in leak rate of $H_2O(g)$	$I_{NaCl^+}{}^a$	$\frac{I_{NaCl^+}}{I_{Na_2Cl^+}}$	I_{NaOH^+}	$I_{Na_2OH^+}$
Leak on	100	3.2	Small	37
Increase	81	0.9	112	280
Decrease	75	3.0	87	50
Increase	56	1.5	150	160

[a] Ionizing electron energy = 100 volts.

Na_2O–NaF(c)–$H_2O(g)$.—Results analogous to those discussed for Na_2O–$NaCl(c)$–$H_2O(g)$ were obtained for Na_2O–$NaF(c)$–$H_2O(g)$ and are shown in Table IV. Reasoning similar to that previously developed leads to the conclusion that $Na_2(OH)F(g)$ exists in the vapor phase. The marked decrease

TABLE IV

DEPENDENCE OF ION CURRENT INTENSITIES ON FLOW OF $H_2O(g)$ OVER Na_2O–NaF(c) AT T = 1066°K.

Relative change in leak rate of $H_2O(g)$	$I_{Na^+}{}^a$	$\frac{I_{Na^+}}{I_{Na_2F^+}}$	I_{NaOH^+}	$I_{Na_2OH^+}$
Leak off	100	4.7	0.0	0.0
Increase	31	2.6	38	28

[a] Ionizing electron energy = 100 volts. I_{Na^+} is corrected intensity due only to fragmentation of NaF(g).

in the Na^+ intensity (representing NaF(g)) when the leak was turned on may be due either to an activity or scattering effect. In either case the basic argument remains unchanged.

$Li_2O(s)$–HCl(g) and LiCl(c).—Ions of Li^+, $LiOH^+$, $LiCl^+$ and Li_2Cl^+ were the major species observed when HCl(g) was passed over $Li_2O(s)$ in the temperature range 744–822°. In all runs $LiOH^+$ was much smaller than $LiCl^+$. The uptake of HCl(g) was apparently complete since no HCl^+ was detected. Examination of the data in Table V pertaining to pure LiCl and $Li_2O(s)$–HCl(g) provides an interesting result. The I_{Li^+}/I_{LiCl^+} ratio in the table is noticeably dependent on experimental conditions. This effect is in marked contrast with LiF where I_{Li^+}/I_{LiF^+} was found to be relatively insensitive to experimental conditions. In the leak studies the activity of LiCl(c) was reduced to a point where the dimer, $Li_2Cl_2(g)$, was very small relative to the monomer. Since Li^+ originating from LiOH(g) or $Li_2O(s)$ decomposition is negligible under the conditions employed here, virtually all of the Li^+ in the leak study, represented by the data in Table V, may be attributed to dissociative ionization of LiCl(g). In the case of pure LiCl(c), however, a similar assumption is apparently invalid, since as the dimer/monomer ratio in the vapor increases there is a consequent increase in the I_{Li^+}/I_{LiCl^+} ratio. A comparison of ion intensities for pure LiCl runs and leak system studies shows that the contribution of Li^+ from fragmentation of $Li_2Cl_2(g)$ is at least 0.12 times the Li_2Cl^+ intensity. Thus, in studies with pure LiCl(c) in the temperature range where the $Li_2Cl_2(g)$ concentration in the vapor is large the absolute amount of Li^+ attributable to fragmentation of the dimer may be comparable to or larger than that arising from fragmentation of the monomer. This effect is likely to be more pronounced for LiCl, LiBr and LiI than for many of the other alkali halides, since there are relatively larger concentrations of dimers in the lithium halide vapors. From appearance potential curves Friedman[7] found evidence for the formation of Li^+ from $Li_2I_2(g)$. Similar behavior was observed with NaCl in the present studies although the situation is somewhat more complicated for that system as a result of fragmentation of NaOH(g) to form Na^+ in runs with H_2O and HCl as flow gases with $Na_2O(s)$ and Na_2O–NaCl(c) in the condensed phase. However, after the necessary correction for dissociative ionization of NaOH(g) has been made, a comparison of data from leak system studies and runs with pure NaCl shows that there is some con-

(7) L. Friedman, *J. Chem. Phys.*, **23**, 477 (1955).

tribution to Na^+ from fragmentation of the NaCl dimer.

TABLE V

VARIATION OF ION INTENSITY RATIOS FOR LiCl VAPORS WITH EXPERIMENTAL CONDITIONS

System	T, °K.	I_{Li^+}/I_{LiCl^+}[a]	$I_{Li_2Cl^+}/I_{LiCl^+}$[a]
Pure LiCl	868	0.72	3.9
$Li_2O(s)$–HCl(g)	1083	0.25	0.06

[a] Ionizing electron energy = 70 volts; total intensities corrected for isotopic abundances.

Discussion

The small values of the ratio $I_{M_2OH^+}/I_{MOH^+}$ observed with $Li_2O(s)$–$H_2O(g)$ in contrast to that found for the $Na_2O(s)$–$H_2O(g)$ system are qualitatively consistent with predictions based on a relatively high decomposition pressure for LiOH(s). In the $Li_2O(s)$–$H_2O(g)$ system the degree of water saturation is apparently well below the decomposition pressure of H_2O from LiOH while for $Na_2O(s)$–$H_2O(g)$ the degree of saturation is much higher for the same water pressure. It should be emphasized that the estimated higher stability of the $Li_2(OH)_2(g)$ dimer (*i.e.*, $|\Delta H_{LiOH}| > |\Delta H_{NaOH}|$:2-MOH = $M_2(OH)_2$) is not inconsistent with these observations since under the conditions of these experiments the amount of $Li_2(OH)_2(g)$ in the vapor phase should be small due to the thermodynamic conditions. The decomposition pressure of H_2O from condensed LiOH is estimated to reach an atmosphere between 700 and 800°.[8] Thus the low pressures employed here are several orders of magnitude below saturation values. At high pressures of H_2O near an atmosphere the LiOH dimer should become a more important gaseous species than the monomer since the dimer has a stronger dependence on water pressure. Since, in the reaction of $H_2O(g)$ with $Li_2O(s)$, the monomer should have a more positive heat of formation per mole than the dimer, the dimer will increase less rapidly with increase in temperature for a fixed water pressure. At lower temperatures, the ratio of dimer to monomer should, therefore, increase at constant water pressure although the partial pressures of both species will decrease. The formation of LiOH(g) as the major species at low water pressures confirms the assumption of van Arkel, *et al.*,[9] who studied the transport of hydroxide by utilizing H_2O as carrier gas with $Li_2O(s)$ in transpiration measurements in the temperature range around 1000°. Flow experiments with higher water pressures may provide information about the LiOH dimer.

Comparison of mass spectra obtained for pure salts with these observed with salt mixtures or in systems where the partial pressures of the vaporizing species are diminished below the saturation value by other means (*i.e.*, double oven) provides information on the mode and degree of dissociative ionization for heavier polymers in the vapor. As described here the condensed phase activity may be diminished and varied by forming the gaseous species by the reaction of a solid with a controlled flow of gas. The utilization of these techniques may become more important in systems where several polymeric species exist (*e.g.*, sulfur,[10] selenium,[11] etc.). The identification of the species in the vapor phase and the determination of the extent of ion fragmentation may be aided by the study of compounds or solutions in which the activity of the component of interest is decreased to a varying degree thus altering the ratios of the various species in the equilibrium vapors.

In principle it is possible to measure directly the activity, relative to the pure component, of a constituent of a mixed condensed phase if polymeric species are present in the equilibrium vapors. The method involves comparison of ion intensity ratios obtained with pure and mixed condensed phases at the same temperature. For example, if monomers and dimers were present in the equilibrium vapors, the ratio $[(I_d/I_m)_{mixed}/I_d/I_m)_{pure}]$ at constant temperature would be equal to the activity of the component in the mixture relative to an activity of unity for the pure material. It should be noted that the ratio is insensitive to instrumental factors, and ionization cross section and electron multiplier ion detection efficiency terms cancel exactly. If higher polymers were present an analogous expression may be developed to utilize the ion intensities corresponding to these species. However, the diminution in the partial pressure of polymeric species depends upon the activity raised to a power which is equal to the degree of polymerization. Thus, instrument sensitivity may be a limiting factor in the application of this method to systems where the polymeric constituents of the vapor contain several monomeric units.

(8) See for example, N. W. Gregory and R. H. Mohr, *J. Am. Chem. Soc.*, **77**, 2142 (1955).

(9) van Arkel, Spitsbergen and Heyding, *Can. J. Chem.*, **33**, 446 (1955).

(10) Goldfinger, Ackerman and Jeunehomme, Technical Report AF 61(052)-19, University of Brussels, 1959.

(11) P. Goldfinger and M. Jeunehomme, Institute of Petroleum, Hydrocarbon Research Group and ASTM Committee E14 Joint Conference on Mass Spectrometry, London, 1959, Pergamon Press (to be published).

CHEMICAL THERMODYNAMIC EQUILIBRIA AND FREE VALENCE INDICES AS APPLIED TO A LOW-TEMPERATURE BITUMINOUS COAL PYROLYZATE

BY CLARENCE KARR, JR.

Low-Temperature Tar Laboratory, Branch of Bituminous Coal, Bureau of Mines, Morgantown, West Virginia

Received October 19, 1959

The distributions of a large number of isomers in a low-temperature bituminous coal pyrolyzate, or tar, have been compared with the thermodynamic chemical equilibrium distributions, and also with the "kinetic" distributions, as obtained from the free valence indices, or numbers, assuming a free radical mechanism for isomerization. It was concluded that the isomeric composition of the tar produced at 500° by fluidized carbonization may be significantly determined by coal structure in addition to thermodynamic and kinetic distributions.

Introduction

The pyrolyzate obtained by low-temperature (500°) carbonization of coal may be examined either from the standpoint of chemical thermodynamic equilibria or chemical kinetics. In the former case, if thermodynamic equilibrium has been achieved under the conditions of carbonization, the proportions of various isomers will be the same as those predicted by theory. In the latter case, if thermodynamic equilibrium is far from being obtained, due to insufficient time (residence time at 500°), then the most abundant isomers would be those predicted from the relative rates of formation. Isomeric distributions outside of the range presented by the combined thermodynamic and kinetic systems might indicate dependence on coal structure.

Until recently a detailed isomeric analysis for several classes of compounds in a low-temperature coal pyrolyzate (tar) has been lacking. However, the U. S. Bureau of Mines' Low-Temperature Tar Laboratory has now made available information on 21 phenols,[1,2] 51 tar bases (pyridines, anilines, and quinolines),[3] and 52 aromatic hydrocarbons,[4] or a total of 124 compounds in a single low-temperature bituminous coal tar.

Not a great deal of precise information is available on the proportions of isomers at equilibrium at various temperatures, as determined by studies in chemical thermodynamics. The equilibrium concentrations of C_8 and C_9 alkylbenzenes at 500° may be obtained from figures published by Taylor, Wagman, Williams, Pitzer and Rossini.[5] Other data required for the present comparison were obtained from experiments by others in isomerization, alkylation, and other reactions in which the investigators concluded that equilibrium distribution of isomers had been approached. An example of this would be the work by Pigman, Del Bel and Neuworth[6] on the silica–alumina catalyzed isomerization of xylenols at 344°. Catalysts may be utilized to speed up the approach to equilibrium at a given temperature without distorting the proportions of isomers, as shown experimentally by Rossini, Mair and Streiff.[7]

Whereas the reaction mechanisms need not be known in a consideration of the thermodynamic equilibria, a knowledge of them is required in an examination of products obtained under non-equilibrium conditions. The compounds involved in the present comparisons probably should be considered as having been formed in a free radical process. These isomeric compounds would all be in the gas phase at 500°, and at these conditions of phase and temperature it is generally assumed that a free radical mechanism predominates. It is generally accepted that a rate-determining factor in free radical substitution on an aromatic nucleus is the free valence index, F_r, at each carbon atom, r. Isomeric compounds that are structurally related to the reactant isomers of largest values of F_r will be formed at the fastest rates and thus will predominate in the non-equilibrium mixture. Thus, among given disubstituted benzenes, like dialkyl benzenes, those with 1,2-substitution are formed the most rapidly because the 2-position of a benzene ring has the largest F_r value.[8] Conversely, among these same dialkyl benzenes those with 1,3-substitution are more stable[5] at 500°.

Approximation of Kinetic Distributions

1. Development of Equation.—Kooyman and Farenhorst[8] have experimentally established that

$$F_{max} = a \log K_r' + b \qquad (1)$$

for a series of aromatic hydrocarbons, where F_{max} is the highest free valence number calculated for each molecule by the molecular orbital method, and K_r' is the reactivity for the CCl_3 radical reaction. The differences between the free valence numbers within each molecule are so considerable that reactivity can be expected to be due mainly to the most reactive positions, that is, F_{max} is in effect F for the most reactive position, which is the *ortho* position for a monosubstituted benzene ring. K_r' is evaluated by determining the relative reactivity of the aromatic hydrocarbon, that is, by comparing the rate constant for the hydrocarbon to the rate constant for some standard in a com-

(1) C. Karr, Jr., P. M. Brown, P. A. Estep and G. L. Humphrey, *Anal. Chem.*, **30**, 1413 (1958).

(2) C. Karr, Jr., P. M. Brown, P. A. Estep and G. L. Humphrey, *Fuel*, **37**, 227 (1958).

(3) C. Karr, Jr., and T.-C. L. Chang, *J. Inst. Fuel*, **31**, 522 (1958).

(4) T.-C. L. Chang and C. Karr, Jr., *Anal. Chim. Acta*, **21**, 474 (1959).

(5) W. J. Taylor, D. D. Wagman, M. G. Williams, K. S. Pitzer and F. D. Rossini, *J. Research Natl. Bur. Standards*, **37**, 95 (1946).

(6) I. Pigman, E. Del Bel and M. B. Neuworth, *J. Am. Chem. Soc.*, **76**, 6169 (1954).

(7) F. D. Rossini, B. J. Mair and A. J. Streiff, "Hydrocarbons from Petroleum," Reinhold Publ. Corp., New York, N. Y., 1953, pp. 463, 464.

(8) E. C. Kooyman and E. Farenhorst, *Trans. Faraday Soc.*, **49**, 58 (1953).

petitive reaction with the CCl_3 radical. The values of K_r' are independent of the numerical value for the rate constant of the standard, so that the relative reactivity of each hydrocarbon is directly proportional to the rate constant for that hydrocarbon. Levy and Szwarc[9] observed a linear relationship between the relative rates of addition of methyl radicals and the relative rates of addition of CCl_3 radicals found by Kooyman and Farenhorst. This means that the slope, a, is the same for these two radicals. In addition, it can be assumed that alkylbenzenes would be very similar to benzene, phenylpyridines to biphenyls, methylquinolines to naphthalenes, and so on, in these free radical reactions, so that these compounds would fall fairly close to Kooyman and Farenhorst's plot, and the same value of a would apply to them.

Since $K_r' = k_A/c$, where k_A can be the rate constant for isomer A in the free radical reaction and c is a constant, and since F_{max} is in effect F for the most reactive position, eq. 1 may be rewritten as $F_A = a \log (K_A/c) + b$, F_A being the free valence number for isomer A, or

$$k_A/c = 10^{(F_A - b)/a} \quad (2)$$

From this

$$k_A/k_B = (10^{F_A/a})/10^{F_B/a}) \quad (3)$$

The ratios of isomers will be independent of the concentrations of the reacting species, as shown by Ingold and Shaw[10] for competitive substitution reactions. This means that at any given time in the initial period of reaction the mole % of any of the isomers is directly proportional to its rate constant.

With the inclusion of a term, p, for the number of equivalent positions, the relationship (4) is obtained

$$\text{mole \% A/mole \% B} = p_A k_A/p_B k_B = (p_A\ 10^{F_A/a})/(p_B\ 10^{F_B/a}) \quad (4)$$

This equation has the same form as those which can be derived readily from equations presented by Glasstone, Laidler and Eyring[11] for determining the relative amounts of *ortho*-, *meta*-, and *para*-substitution in ionic reactions. Comparison of these equations with eq. 4 shows that the term a is directly proportional to the absolute temperature, which is, of course, required by the general theory of absolute reaction rates. Kooyman and Farenhorst have experimentally determined the value of a at 91° to be about 0.022; at 500° a should be 0.047.

The approximate isomeric distributions can be obtained from the free valence numbers or indices by means of eq. 4. These could be called the "kinetic" distributions, in contrast to the thermodynamic equilibrium distributions. The values for these two types of isomeric distributions are listed in Table I for 38 alkylated compounds and their amounts found in a single low-temperature bituminous coal tar produced at 500° by fluidized carbonization.

(9) M. Levy and M. Szwarc, *J. Am. Chem. Soc.*, **77**, 1949 (1955).
(10) C. K. Ingold and F. R. Shaw, *J. Chem. Soc.*, 2918 (1927).
(11) S. Glasstone, K. J. Laidler and H. Eyring, "The Theory of Rate Processes," McGraw-Hill Book Co., Inc., New York, N. Y., 1941, pp. 458–464.

TABLE I
ISOMERIC DISTRIBUTIONS IN TAR, COMPARED WITH THERMODYNAMIC EQUILIBRIUM AND KINETIC DISTRIBUTIONS

Alkylated compounds	Isomeric distribution in tar, mole %	Thermodynamic equilibrium distribution, mole %	Free valence, F_r of position alkylated	Kinetic distribution, mole %
1-Methyl-2-ethylbenzene	27	19	Toluene:[b]	91
			ortho, 0.122	
1-Methyl-3-ethylbenzene	37	50 [a]	*meta*, .077	4
1-Methyl-4-ethylbenzene	36	31	*para*, .095	5
1,2,3-Trimethylbenzene	44	16		37
1,3,5-Trimethylbenzene	17	22 [a]		1
1,2,4-Trimethylbenzene	39	62		62
1-Methyl-2-isopropylbenzene	13	5		91
1-Methyl-3-isopropylbenzene	40	60 [c]		4
1-Methyl-4-isopropylbenzene	47	35		5
1,2,4,5-Tetramethylbenzene	38	17		13
1,2,3,5-Tetramethylbenzene	62	83 [d]		87
			Pyridine:[f]	
2-Phenylpyridine	46	53	*ortho*, 0.091	51
3-Phenylpyridine	0	32 [e]	*meta*, .079	29
4-Phenylpyridine	54	15	*para*, .086	20
2-Methylquinoline	32		Quinoline:[g]	23
			2-position, 0.344	
3-Methylquinoline	0		3-position, .290	1.5
4-Methylquinoline	44		4-position, .356	43
5-Methylquinoline	0		5-position, .338	17
6-Methylquinoline	6		6-position, .290	1.5
7-Methylquinoline	14		7-position, .296	2
8-Methylquinoline	4		8-position, .331	12
2,5-Dimethylaniline	14		Aniline:[h]	50
			ortho, 0.425	
2,6-Dimethylaniline	38		*meta*, .397	40
3,5-Dimethylaniline	48		*para*, .415	10
N-Benzyl-2-methylaniline	40		N-Methylaniline:[h]	62
			ortho, 0.431	
N-Benzyl-3-methylaniline	0		*meta*, .399	13
N-Benzyl-4-methylaniline	60		*para*, .426	25
			Phenol:[k]	49
o-Cresol	31	18 21	*ortho*, 0.410	
m-Cresol	41	60 [i] 61	*meta*, .399	28
p-Cresol	28	22 18	*para*, .408	23
2,3-Xylenol	5	9 10		16
2,4-Xylenol	36	30 26		30
2,5-Xylenol	15	24 22 [j]		16
2,6-Xylenol	6	11 2		10
3,4-Xylenol	15	12 17		22
3,5-Xylenol	23	14 23		6
o-Ethylphenol	38	43 [j]		63
m-Ethylphenol	62	57		37

[a] At 500°: ref. 5. [b] Estimated from data of ref. 13. [c] At 370°: J. E. Mahan, U. S. Patent 2,564,488 (Aug. 14, 1951). [d] At 75° with $AlCl_3$: D. V. Nightingale and F. Wadsworth, *J. Am. Chem. Soc.*, **63**, 3514 (1941). [e] At 105°: D. H. Hey, C. J. M. Stirling and G. H. Williams, *J. Chem. Soc.*, 3963 (1955). [f] D. W. Davies, *Trans. Faraday Soc.*, **51**, 449 (1955). [g] C. Sándorfy and P. Yvan, *Compt. rend.*, **229**, 715 (1949). [h] S. S. Perez, M. A. Herráez and F. J. Igea, *Anales real soc. españ. fís. y quím.*, **50B**, 243 (1954). [i] At 164° with $AlCl_3$: H. P. Meissner and F. E. French, *J. Am. Chem. Soc.*, **74**, 1000 (1952). [j] At 380°: P. H. Given, *J. Appl. Chem.*, **7**, 182 (1957). [k] F. J. I. López-Vázquez, *Anales real soc. españ. fís. y quím.*, **51B**, 203 (1955). [l] At 344°: ref. 6.

2. Sample Calculation.—Assuming that the three trimethylbenzenes were isomerized by a free

radical mechanism involving a stepwise shift of methyl groups,[6] the products would be formed by the attack of a methyl radical on the xylene isomers. 1,2,3-Trimethylbenzene would be produced by the attack of the methyl radical on the 2(*ortho*)-position of 1,3-dimethylbenzene, and on the 3-(1/2 *ortho*, 1/2 *meta*)- and 6(1/2 *ortho*, 1/2 *meta*)-positions of 1,2-dimethylbenzene. The respective values of $p\ 10^{F/a}$ would be $1 \times 10^{0.122/0.047}$ and $2 \times 1/2\ (10^{0.122/0.047} + 10^{0.077/0.047})$, with a total of 1909. 1,3,5-Trimethylbenzene would be produced by the attack of the methyl radical on the 5(*meta*)-position of 1,3-dimethylbenzene, so that $p\ 10^{F/a}$ would be $1 \times 10^{0.077/0.047}$ or 44. 1,2,4-Trimethylbenzene would be produced by the attack of the methyl radical on the 4(1/2 *meta*, 1/2 *para*)- and 5(1/2 *meta*, 1/2 *para*)-positions of 1,2-dimethylbenzene, on the 4-(1/2 *ortho*, 1/2 *para*)- and 6-(1/2 *ortho*, 1/2 *para*)-positions of 1,3-dimethylbenzene, and on the 2,3,5- and 6-positions (each 1/2 *ortho*, 1/2 *meta*) of 1,4-dimethylbenzene. The respective values of $p10^{F/a}$ would be $2 \times 1/2\ (10^{0.077/0.047} + 10^{0.095/0.047})$, $2 \times 1/2\ (10^{0.122/0.047} + 10^{0.095/0.047})$, and $4 \times 1/2\ (10^{0.122/0.047} + 10^{0.077/0.047})$, with a total of 3138. The grand total for the three trimethylbenzenes would be 5091, the percentage contributions being 37, 1, and 62 for the 1,2,3-, 1,3,5- and 1,2,4-isomers, respectively.

Discussion

Both the molecular orbital theory and experiments on radical attack indicate that the effect of various substituent groups is independent of their polarity.[12] Therefore, the F_r numbers for the *ortho*, *meta* and *para* positions may differ only a little in going from biphenyl to toluene, ethylbenzene, isopropylbenzene, styrene, and so forth, For example, the free valence numbers[13] for the *ortho*, *meta* and *para* positions for biphenyl are 0.118, 0.077 and 0.094, and for styrene are 0.125, 0.076 and 0.096. On this assumption, average values of 0.122, 0.077 and 0.095 were assigned to toluene and the other alkylbenzenes. This would at least be in agreement with the well-established fact[14] that the *ortho* position of toluene is by far the most reactive toward free radical attack whereas the *meta* position is almost the same as that for any of the six equivalent positions of benzene, the F_r of which is 0.081.

The accuracy of the quantitative determinations of the tar components was generally quite adequate for the comparisons made in Table I. These quantities were determined by infrared analysis, or gas–liquid chromatography, or both. The infrared values had maximum deviations of about ±5% from the true values for distillate fractions containing only about three components, and deviated up to about ±10% for fractions containing about six or more components, that is, a value of 20% for a component in such a fraction was actually 20 ± 2%.[3] The gas–liquid chromatography values were demonstrated to have deviated not more than ±3% from the true values when the peaks were essentially completely resolved, and up to about ±5% for typical overlapping peaks.[4] The reliability of the thermodynamic values is perhaps best indicated by the fair agreement between Given's values at 380° and Pigman, Del Bel and Neuworth's values at 344° for the xylenols, and the good agreement between Given's values at 380° and Meissner and French's values at 164° for the cresols. The values of F_r are probably fairly reliable since in several cases these were calculated by two different methods with fairly good agreement. The kinetic distribution values, however, should be considered as approximations although a twofold change in the value of a, for example, would have, in general, little effect on the distribution values.

Examination of Table I shows no over-all agreement of isomeric distributions in the tar with either thermodynamic equilibrium distributions or kinetic distributions, although some isolated instances of fair agreement can be picked out, as for example the thermodynamic distributions of the xylenols or the kinetic distributions of the methylquinolines. This cannot be explained solely on the basis of inaccuracies, in view of the previously discussed accuracy of these values. Of particular significance is the large proportion of tar values that fall completely outside of the range presented by the combined thermodynamic and kinetic systems. In the case of the methylethylbenzenes and the methylisopropylbenzenes the *meta* isomers should predominate in a thermodynamic distribution and the *ortho* isomers in a kinetic distribution. However, the *para* isomers are present in relatively large proportions. Also, the *para* isomers are predominant in the case of the phenylpyridines and the N-benzyltoluidines. Thus in four different sets of *ortho–meta–para* isomers there are relatively large proportions of *para* isomers that cannot be explained from the standpoint of either thermodynamic or kinetic distributions.

A plausible explanation is that the isomers found in the tar reflect in some manner the coal structure. That is, if a significant proportion of the compounds found in the tar are the original compounds produced by thermal decomposition of the coal, then the distribution of isomers could be considerably different from that demanded by either the thermodynamic or kinetic system. This explanation is to be outlined in more detail in a future paper describing the consistently high proportions of para isomers found in four different low-temperature subbituminous coal tars.

(12) H. H. Greenwood, *Nature*, **176**, 1024 (1955).

(13) F. H. Burkett, C. A. Coulson and H. C. Longuet-Higgins, *Trans. Faraday Soc.*, **47**, 553 (1951).

(14) D. H. Hey, B. H. Pengilly and G. H. Williams, *J. Chem. Soc.*, **6**, (1955).

ELECTROMOTIVE FORCE MEASUREMENTS OF THE ETHANOL–HYDROCHLORIC ACID–WATER SYSTEM[1]

BY CARLYLE L. LEBAS AND M. C. DAY

Contribution from the Coates Chemical Laboratories, Louisiana State University, Baton Rouge, Louisiana

Received October 26, 1959

An investigation of the effects of water and HCl variations on the cell Pt, H_2(1 atm.)/HCl(m), ethanol, water(m)/AgCl, Ag have been carried out, where the water concentration was varied from zero to 11.670 weight % and that of the HCl varied over a range of 0.002195 to 0.0791 molal. The most significant change in e.m.f. occurred when small amounts of water were added to the pure ethanol–HCl solvent system. The relationship of this change in e.m.f. with the addition of water at a constant HCl molality was found to be a straight line when E_{obs} was plotted against (H_2O concentration)$^{1/2}$ up to a water weight % of 6.450. Estimates of the E^0 values of the silver–silver chloride electrode within this range were made.

Introduction

Several determinations of standard state electrode potentials have been made in anhydrous ethanol with the major emphasis on the silver–silver chloride electrode. Using the cell without liquid junction

Pt, H_2(1 atm.)/HCl(m), ethanol, water (m)/AgCl, Ag

molal E^0 values have been obtained[2,3] which vary from -0.0442 v. to -0.0884 v. In spite of the fact that no less than six independent determinations have been reported at 25°, no two E^0 values are found to be in agreement. There can be no question that the discrepancies, to some extent, are due to the method of handling the experimental data. However, actual variations in the observed experimental data can most reasonably be attributed to the presence of trace quantities of water in the ethanol of some workers. This opinion was expressed by Scatchard[2] in an attempt to justify a discrepancy in the data of Danner[4] as compared to that of Harned and Fleysher.[5] Studies by Woolcock and Hartley[3] further substantiated this idea, and they were able to show that an ethanol–HCl solution of 0.01 molar HCl concentration containing 0.08% water raised the e.m.f. of the cell by eight millivolts. A yet further substantiation of these effects is seen in the work of Taniguchi and Janz[6] where it is shown that the data of previous workers is consistently higher at all HCl concentrations.

In spite of the several indications of the significant effects of water on the cell potential in anhydrous ethanol, no systematic study has previously been carried out on the effects of these trace quantities of water as a function of the HCl concentration.

Experimental

Chemicals.—The anhydrous ethanol was prepared using a modification of the Bjerrum method.[7] In order to remove trace quantities of benzene, 2% water by volume was added to U.S.I. absolute alcohol, U.S.P. grade, and the mixture was fractionally distilled. When the benzene had been removed as the benzene–water–ethanol azeotrope, magnesium alcoholate prepared from dry ethanol and magnesium was added in the ratio of one gram of magnesium alcoholate to six and a half ml. of benzene-free ethanol. This solution was refluxed until free of water and was then immediately fractionally distilled. The middle fraction was taken as the pure anhydrous ethanol. Both distillations were monitored by means of the Beckman Model DK spectrophotometer. Using this method of detection, the maximum weight per cent. of benzene present should be less than 0.0008 and that of water should be less than 0.02.

The ethanol–HCl solutions were prepared by adding sulfuric acid to a reaction flask filled with analytical grade NaCl. The resultant HCl was passed through a bubbler of concentrated H_2SO_4 and then into the anhydrous ethanol. To reduce the possibility of chemical reaction between the ethanol and the HCl, all solutions were prepared immediately before use. The HCl concentrations were determined by titration with an aqueous NaOH standard solution.

All ethanol and ethanol solutions were kept in a nitrogen dry box with P_2O_5 as a desiccant.

Electrodes.—The silver–silver chloride electrodes were prepared by the thermal-electrolytic method as described by Taniguchi and Janz.[8] All of the prepared electrodes were checked against a hydrogen electrode in a water–HCl solution of known HCl activity. Two electrodes were selected on the basis of their stability and agreement with reported e.m.f. values in the water–HCl system. This agreement was found to be within 0.1 mv. The selected electrodes then were washed and stored in anhydrous ethanol. After several days, when it was assumed that the electrodes had reached equilibrium with the ethanol, the stability and reversibility of the electrodes were verified in anhydrous ethanol–HCl solutions.

The hydrogen electrode was a commercially available one of the Hildebrand type. It was customary to replatinize the electrode before each series of runs. All electrodes were stored in anhydrous ethanol.

Procedure.—The cell was constructed so as to permit the use of two silver–silver chloride electrodes and one hydrogen electrode. For all measurements, the cell was placed in a water-bath thermostated at 25.25 ± 0.005°. A single series of runs required from 12 to 15 hours. This depended on the length of time necessary for the cell to reach equilibrium after the addition of water and on the number of water additions during the series. For a given run, anhydrous ethanol of a particular HCl molality was placed in the cell and water was added in predetermined increments. Potentiometric measurements then were made for each new water concentration. In order to add the initial extremely small increments of water, very dilute solutions of water in ethanol were used. All concentrations should be accurate to within 0.2%. Before introduction into the cell, the electrodes were soaked approximately one hour in an ethanol solution of the same HCl molality as that used for the given run. The hydrogen gas was prepurified grade and was passed through a hydrogen catalytic purifier, a silica gel column, and then into a bubbling tower filled with a solution of identical composition as that present in the cell before it was allowed to enter the cell. The criterion for equilibrium was stable reading for a period of one hour.

Results and Discussion

Electromotive force measurements were taken for various HCl molalities with water concentra-

(1) Taken in part from the masters thesis submitted by C. L. LeBas to the Louisiana State University, 1959.

(2) G. Scatchard, *J. Am. Chem. Soc.*, **47**, 2098 (1925).

(3) J. W. Woolcock and H. H. Hartley, *Phil. Mag.*, [7] **5**, 1133 (1928).

(4) P. S. Danner, *J. Am. Chem. Soc.*, **44**, 2832 (1922).

(5) H. S. Harned and M. H. Fleysher, *ibid.*, **47**, 82 (1925).

(6) H. Taniguchi and G. J. Janz, THIS JOURNAL, **61**, 688 (1957).

(7) H. Lund and J. Bjerrum, *Ber.*, **64B**, 210 (1931).

(8) H. Taniguchi and G. J. Janz, *J. Electrochem. Soc.*, **104**, 123 (1957).

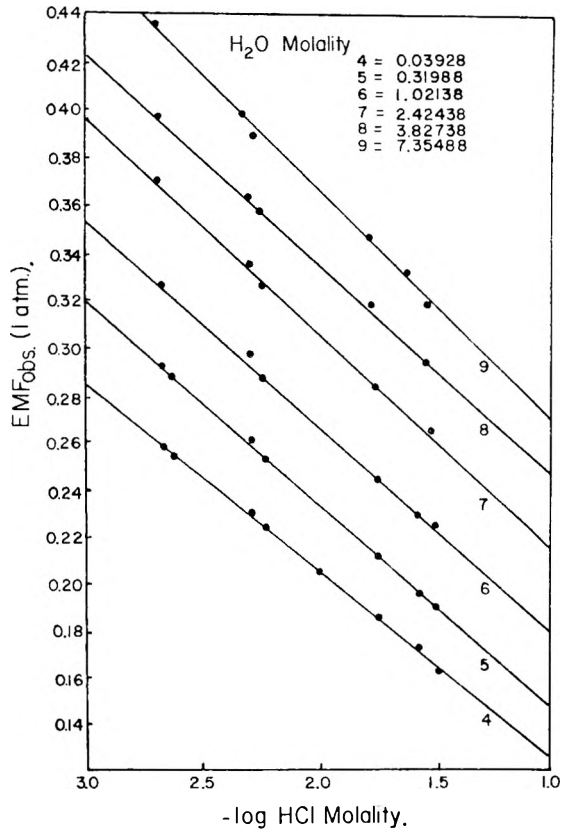

Fig. 1.—The corrected e.m.f. reading plotted as a function of $-\log m_{HCl}$ at various concentrations of H_2O in EtOH.

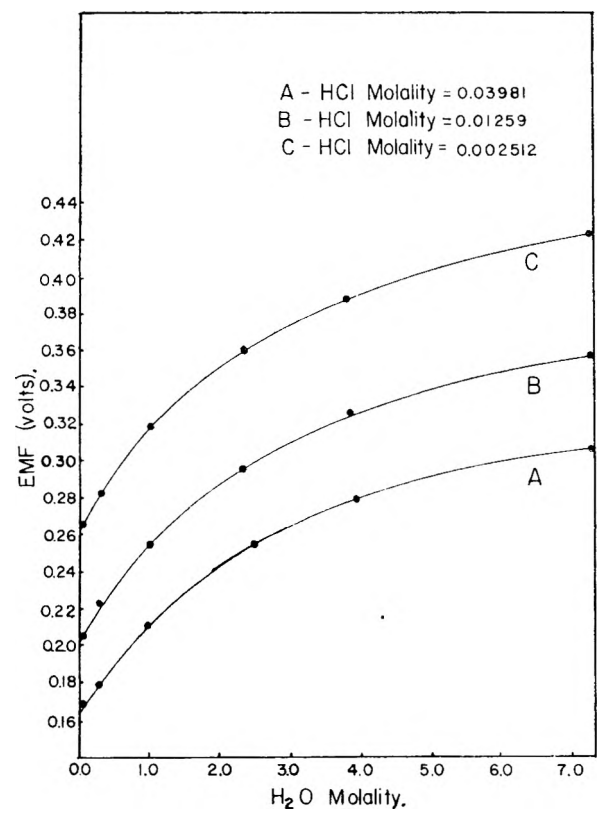

Fig. 2.—The corrected e.m.f. reading plotted as a function of m_{H_2O} for three selected concentrations of HCl in EtOH.

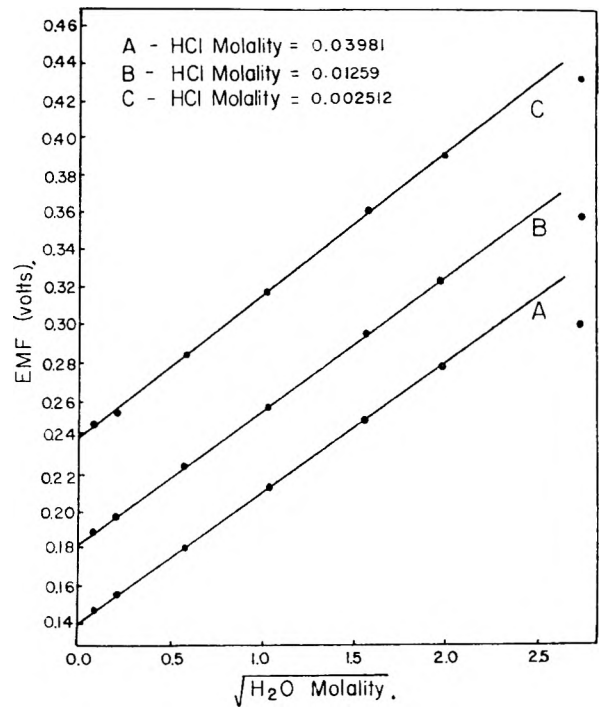

Fig. 3.—A plot showing the linear dependence of observed e.m.f. on m_{H_2O} for small concentrations of H_2O.

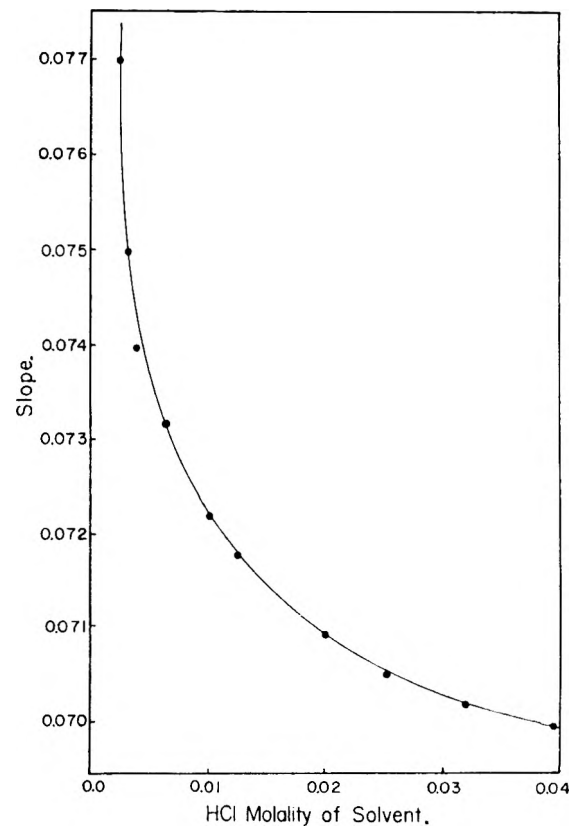

Fig. 4.—The relation of the slope S of eq. 1 to the HCl molality.

tions varying from zero to about 7.4 molal. A portion of the results are presented in Table I, and are summarized in Fig. 1, where the observed e.m.f. is plotted against $-\log$ HCl molality for six different water concentrations. The curve for

anhydrous ethanol and two very dilute solutions were determined, but they fell too close together to be placed on the graph.

A more illustrative representation of the effect of water on the e.m.f. might be seen in Fig. 2. Here, the e.m.f. is plotted against the molality of the water at three selected HCl concentrations. The effect is seen to be considerably more significant at lower water concentrations and becomes less critical as the water concentration is increased. Using these same three HCl concentrations, a plot of the e.m.f. *vs.* $(H_2O$ molality$)^{1/2}$ is seen in Fig. 3. All of the curves were found to be approximately straight lines up to a water molality in the neighborhood of 3.8. Due to this linear character, it should be possible to determine empirically the e.m.f. of the electrode system as a function of water concentration or the converse, the water concentration as a function of the e.m.f. in this very dilute region. We can represent the family of curves by the empirical relationship

$$E^{\beta} = S\sqrt{m_{H_2O}} + E^{\gamma}$$

where E^{β} is the e.m.f. reading at a given HCl molality, S is the slope of the curve for that HCl molality, and E^{γ} is the e.m.f. value of the anhydrous ethanol–HCl solution for that HCl molality. Assuming the curves are linear and using a least squares treatment, slopes for the various HCl molalities can be obtained. These are plotted in Fig. 4.

Table I

Corrected E.m.f. Data at Constant Water Molality

Group 1, m_{H_2O} = 0		Group 4, m_{H_2O} = 0.03928		Group 5, m_{H_2O} = 0.31988	
E.m.f. (v.)	m_{HCl}	E.m.f. (v.)	m_{HCl}	E.m.f. (v.)	m_{HCl}
0.2477	0.002195	0.2590	0.002194	0.2918	0.002185
.2438	.002324	.2545	.002322	.2859	.002313
.2203	.005140	.2313	.005127	.2627	.005106
.2110	.005730	.2239	.005727	.2503	.005704
.1938	.009346	.2055	.009341	.2125	.01775
.1900	.01107	.1845	.01782	.1963	.02608
.1720	.01783	.1729	.02619	.1916	.03105
.1596	.02620	.1618	.03117		
.1538	.03119				
.1255	.06530				
.1171	.07910				

Group 6, m_{H_2O} = 1.0214		Group 8, m_{H_2O} = 3.8274		Group 9, m_{H_2O} = 7.3349	
0.3279	0.002164	0.3972	0.002082	0.4372	0.001988
.2969	.005057	.3621	.004866	.3952	.004647
.2849	.005648	.3539	.005435	.3864	.005190
.2414	.01758	.3176	.01691	.3472	.01615
.2282	.02583	.2906	.02958	.3320	.02373
.2265	.03074			.3171	.02819

As a result of the work, it also has been possible to make reasonable estimates of the standard molal electrode potentials of the Ag–AgCl electrode as a function of trace quantities of water. These estimated values for various water concentrations were obtained by plotting $E_{obs} - 4.6RT/F \log m_{HCl}$ *vs.* $(m_{HCl})^{1/2}$ and extrapolating to infinite dilution. A plot of these estimated E^0 values *vs.* ethanol weight per cent. in the ethanol water mixture is given in Fig. 5, and included in the graph are E^0 values of the silver–silver chloride electrode in the same type system as reported by Sieckmann and Grunwald.[9] As expected, the plot indicates again the extreme manner in which small quantities of water affect the ethanol–HCl e.m.f. data.

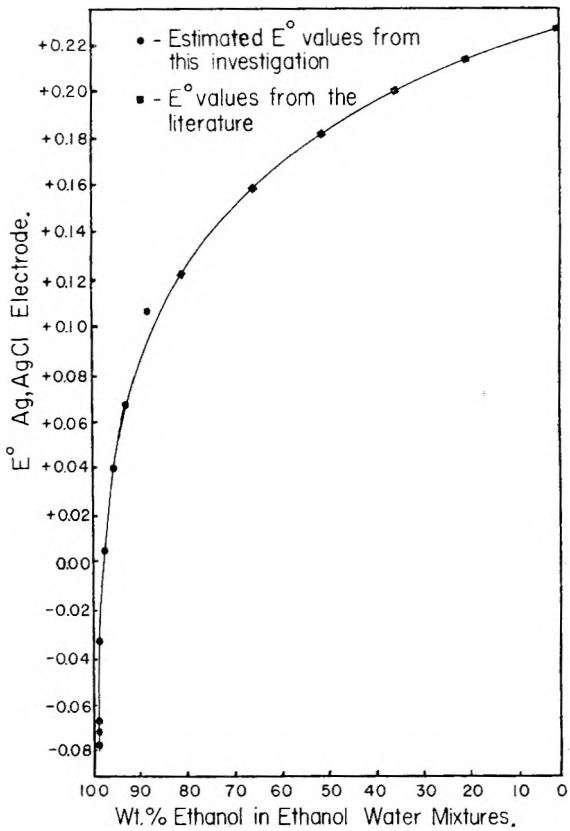

Fig. 5.—Estimated E^0 values for the Ag–AgCl electrode as a function of H_2O concentrations.

Although linear relations and smooth curves are obtained, it is not likely that the dependence of e.m.f. on H_2O concentration is of a simple nature. Qualitatively, the results can be explained by the proton transfer model as presented by Gurney.[10] However, this is certainly an incomplete picture. Previous work in this Laboratory[11] has shown that the dielectric constant of the HCl–H_2O–ethanol system is extremely dependent on trace quantities of H_2O and exhibits a minimum similar to that seen in the conductance curves of this system.[12] Due to the rather low value of the dielectric constant, it would be expected that these extreme variations in the dielectric constant should also contribute to the variations in the observed e.m.f. as a function of the water concentration.

(9) E. F. Sieckmann and E. J. Grunwald, *J. Am. Chem. Soc.*, **76**, 3855 (1954).

(10) R. W. Gurney, "Ionic Processes in Solutions," McGraw-Hill Book Co., New York, N. Y., 1953.

(11) R. W. Clark, "Dielectric Constants of HCl-Ethanol Solutions," M.S. Thesis, L.S.U., 1959.

(12) H. Goldschmidt, *Z. physik. Chem.*, **89**, 129 (1914).

THE DRAPER-BENSON EFFECT IN PHOTOCHLORINATION REACTIONS[1]

BY P. GOLDFINGER, G. HUYBRECHTS, A. M. MAHIEU-VAN DER AUWERA AND D. VAN DER AUWERA

Service de Chimie Physique I, Université Libre de Bruxelles, Brussels, Belgium

Received October 26, 1959

The importance of temperature gradients (Draper effect) in gas phase photochlorination reactions is demonstrated. It is shown that this effect can lead not only to numerical errors in rate constants and activation energies but also to misinterpretations of mechanisms. A method for correcting data for this effect is given.

The expansion upon illumination of gaseous mixtures in which photochlorination reactions proceed has been observed by Draper more than a century ago.[2] The thermal nature of this effect has been established.[3] It is frequently mentioned[4] but its effect on rate measurements for so-called "steady-state" reactions seems to have been disregarded. Benson[5] has discussed it in some detail and has shown that under normal experimental conditions, maximum temperature increases, ΔT_m, of several degrees centigrade may be expected

$$\Delta T_m = \frac{v\Delta H r_0^2}{6\kappa} \qquad (1)$$

where v is the rate in mole cm.$^{-3}$ sec.$^{-1}$ at the temperature of the thermostat, ΔH the reaction heat in cal. per mole, r_0 the radius of the reaction cell considered as spherical in cm. and κ the thermal conductivity in cal. cm.$^{-1}$ deg.$^{-1}$ sec.$^{-1}$. Wilson[6] has worked out more elaborate formulas for different shapes of cells, taking into account also the variation of the rate v due to the temperature increase; for an infinite cylindrical cell he finds

$$\Delta T_m = (v\Delta H a_0^2/4\kappa)(1 + 3\Delta H v E a_0^2/16\,\kappa\, RT_0^2) \qquad (2)$$

where a_0 is the radius of the cell in cm., E the activation energy of the reaction in cal. mole^{-1} and R the gas constant in cal. mole^{-1} deg.$^{-1}$, the other symbols having the same meaning as above. If one assumes a parabolic temperature gradient and neglects the second-order term, the average temperature increase for an infinite cylindrical cell[7] is

$$\Delta T_{mav} = v\Delta H a_0^2/8\,\kappa \qquad (3)$$

In this case the rate v_0 which is observed will be related to the rate v_T at the thermostat temperature by

$$\log(v_0/v_T) = (E/2.303R)\Delta T'/T'^2 = v_0(E/2.303R)\Delta H a_0^2/8\kappa T'^2 = v_0\alpha \qquad (4)$$

E being the activation energy and R the gas constant. From equation 3 it follows that the right-hand side of equation 4 should be $v_T\alpha$; we prefer, however, $v_0\alpha$ since v_0 is obtained directly from experiment and contains the correction term of equation 2. Equation 4 shows that any change in a parameter which causes an increase in rate thus leads to a further rate increase due to the temperature effect.

In the case of the gas phase photochemical chlorine addition to trichloroethylene very accurate measurements of apparent reaction orders gave 0.52 ± 0.01 with respect to absorbed light intensity (I_a) and 1.05 ± 0.02 (95% confidence limit) with respect to chlorine pressure (for instance Table I). Extensive tests have shown that the small but marked difference compared to the expected value 0.50 and 1.00 is not due to wall reactions or impurity effects.

It seems reasonable to explain this difference between measured and expected values of reaction order by means of eq. 4. If one assumes that $v_T = I_a^{1/2}p(Cl_2)k$, the plot (Fig. 1) of log $v_0/I_a^{1/2}p(Cl_2)$ *vs.* v_0 permits one to determine the accurate value of the rate constant as the intercept with the ordinate axis, *i.e.*, the value corresponding to conditions in which the ratio of heat production $v_0\Delta H$, to heat dissipation κ/a_0^2, is small compared to the factor E/RT^2.

The activation energy E = 4870 cal. per mole[4,8] and heat of reaction[9] $\Delta H = 3 \times 10^4$ cal. per mole have been measured previously. The thermal conductivity of C_2HCl_3 does not seem to be known; the value $\kappa = 2.29 \times 10^{-5}$ cal. cm.$^{-1}$ deg.$^{-1}$ sec.$^{-1}$ at 363.2°K. has been calculated according to the methods of Reid and Sherwood[10] and compares well with the data for similar compounds.[11] The methods of the same authors have been used to calculate the thermal conductivities of the mixtures which vary according to the composition from 2.0 to 2.2 $\times 10^{-5}$ using $\kappa = 2.4 \times 10^{-5}$ for Cl_2 (at 363 2°K.) calculated from the value at 273.2°K.[10]

Table I gives a typical experiment. It is clear that there is no influence of the C_2HCl_3 pressure on the reaction rate in agreement with Dainton and collaborators.[4] The rate increases more rapidly than with $I_a^{1/2}$ or $p(Cl_2)$ as mentioned above. Fig. 1 gives the plot according to equation 4, whose slope 6.7 $\times 10^6$ cm.^{3} sec. mole^{-1} with the above values and average $\kappa = 2.1 \times 10^{-5}$ yields a radius of a_0 = 2.15 ± 0.25 cm. for a cylindrical cell of infinite length.

(1) Paper presented at the 136th A.C.S. National Meeting, Atlantic City, September 13–18, 1959. This research has been sponsored in part by the Office, Chief of Research and Development, U. S. Department of Army, through its European Office under contract number DA-91-591-EUC-994 OI-1118-59.

(2) J. Draper, *Phil. Mag.*, **25**, 1 (1844); **25**, 476 (1945).

(3) F. Weigert and Kellerman, *Z. physik. Chem.*, **107**, 1 (1924); Vanpée and S. Benson, private communication.

(4) *E.g.*, F. S. Dainton, D. A. Lomax and M. Weston, *Trans. Faraday Soc.*, **53**, 460 (1957).

(5) S. Benson, *J. Chem. Phys.*, **22**, 46 (1954).

(6) D. J. Wilson, THIS JOURNAL, **62**, 653 (1958).

(7) For an infinite slab of thickness $2l_0$, $\Delta T_{mav} = 2v\Delta H l_0^2/3\kappa$ (3a); it appears thus that for our cell a_0 = 1.8 cm. and l_0 = 6 cm. the heat dissipation at the ends (3a) is negligible compared to that on the sides (3).

(8) G. Chiltz, S. Dusoleil, A. M. Mahieu, P. Goldfinger, G. Huybrechts, G. Martens and D. Van der Auwera, *Bull. soc. chim. Belg.*, **68**, 5 (1959).

(9) L. Smith, *Acta Chim. Scand.*, **7**, 65 (1953).

(10) R. C. Reid and T. K. Sherwood, "The Properties of Gases and Liquids," McGraw-Hill Book Co., New York, N. Y., 1958.

(11) R. G. Vines and L. A. Bennett, *J. Chem. Phys.*, **22**, 360 (1954).

TABLE I

PHOTOCHLORINATION OF TRICHLOROETHYLENE AT 363.2°K.

The incident light intensity, mainly $\lambda = 4358$ Å.,[8] in experiments set H was 4.062×10^{-10} einstein per cm.[2] and sec. and was reduced to 1/4 by a rapidly rotating sector in set S. The pressures are given in mm. measured by a compensated Bourdon gage. The initial rates v_0 are given in mm. per minute and were always obtained from three agreeing calculations: (1) graphical extrapolation; (2) extrapolation by van't Hoffs logarithmic method; (3) using the integrated rate equation $-d(Cl_2)/dt = kp(Cl_2)^{3/2}$. The chlorine concentration is obtained from the pressure measurements and simultaneous absorption measurements. $v_0/I_a^{1/2}p(Cl_2)$ is expressed in liters$^{1/2}$ einstein$^{-1/2}$ sec.$^{-1/2}$. For calculating I_a due corrections have been made for reflections at interfaces.[8]

Exp. no.		$p(C_2HCl_3)$	$p(Cl_2)$	v_0	$y = \log \frac{v_0/I_a^{1/2}}{p(Cl_2)}$
S	2.5	149.7	49.0	0.93	0.993
S	2.8	49.7	50.6	0.98	0.995
S	2.6	75.5	71.5	1.64	1.000
S	2.10	151.8	75.2	1.73	0.990
S	2.2	37.0	75.3	1.78	1.002
S	2.4	75.8	73.7	1.78	1.015
H	2.15	77.2	49.2	1.89	0.998
H	2.18	151.0	49.8	2.00	1.011
H	2.13	50.3	51.8	2.06	1.007
H	2.7	37.3	76.3	3.67	1.008
H	2.16	38.2	76.3	3.69	1.010
H	2.14	75.4	76.5	3.80	1.023
H	2.6	151.5	76.1	3.87	1.033
H	2.5	75.8	76.8	3.90	1.030
S	2.7	148.7	149.7	4.94	1.022
S	2.1	76.8	151.8	4.99	1.020
S	2.3	37.5	152.3	5.04	1.022
H	2.10	38.3	151.5	10.48	1.043
H	2.8	151.1	151.1	10.48	1.044
H	2.9	76.0	152.1	10.62	1.046

In fact the cell used has 1.8 cm. radius and 12 cm. length. The agreement is very gratifying.

An initial pressure increase of the order of 1% corresponding to the calculated $\Delta T_{max} \approx 3$ to 4° has been observed. We did not make however direct temperature measurements because insertion of thermocouples could perturb the system.

It would be nice to investigate the Draper effect in a system with negative temperature coefficient as is the case for the photochlorination of C_2Cl_4 at higher temperatures. Equation 4 shows however that the effect decreases rapidly with increasing temperature. The data at 520°K. which show no such effect may be considered as a confirmation of our interpretation of the data at lower temperatures.

Disregarding the Draper effect would introduce small errors in rate constants and also in activation energies even for reactions having such low activation energies as the photochlorinations ($E \approx 5$ kcal.). Moreover, errors concerning the mechanism could result. Thus it has been shown[12] that the photochlorination of tetrachloroethylene follows the mechanism

$$Cl_2 \longrightarrow 2Cl \quad (1)$$
$$C_2Cl_4 + Cl \longrightarrow C_2Cl_5 \quad (2)$$
$$C_2Cl_5 + Cl_2 \longrightarrow C_2Cl_6 + Cl \quad (3)$$
$$C_2Cl_5 \longrightarrow C_2Cl_4 + Cl \quad (4)$$

(12) D. Van der Auwera, Thesis, Brussels, 1959; to be published.

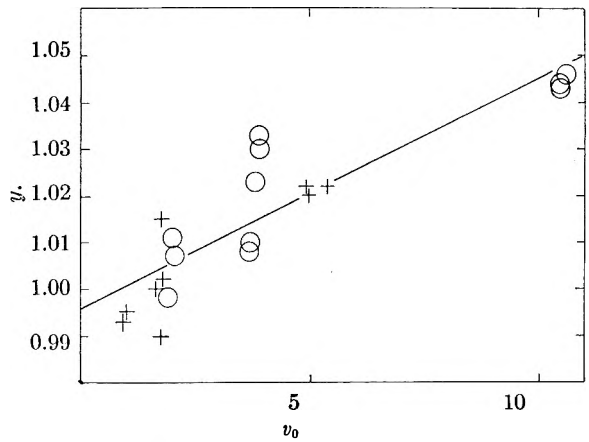

Fig. 1.—$y = \log v_0/I_a^{1/2}p(Cl_2)$ in liters$^{1/2}$ einstein$^{-1/2}$ sec.$^{-1/2}$ vs. v_0 for the photochlorination of trichloroethylene at 363.2°K.; rates (v_0) in mm. per minute. The absorbed light intensity (I_a) in einstein liter^{-1} sec.$^{-1}$ is corrected for multiple reflections[8]; +, 1/4 of intensity of ○. Least squares yield $y = (0.0049_3 \pm 0.0009_1)v_0 + 0.995_8 \pm 0.0057$; or $\alpha = 6.7 \times 10^6$ cm.^{3} mole^{-1} sec.

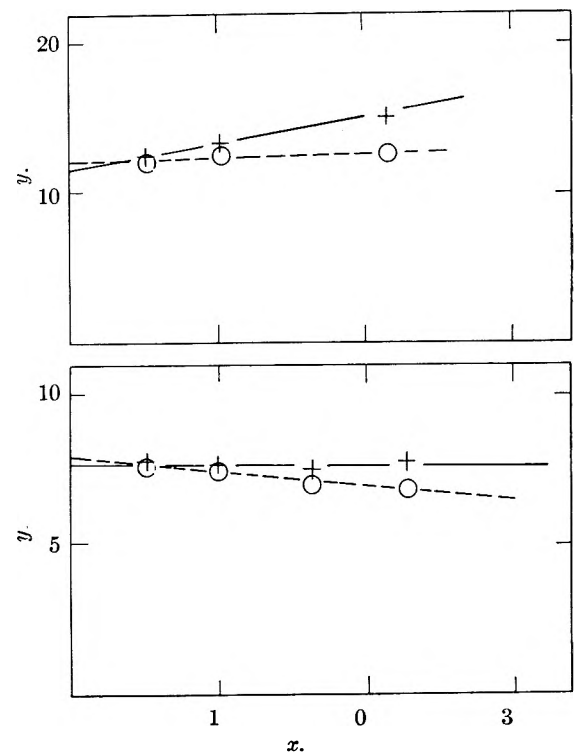

Fig. 2.—$y = I_a p^2(Cl_2)/v^2$ in 10^{-3} einstein sec. per liter vs. $x = p(Cl_2)/p(C_2Cl_4)$; (top) $T = 393.3$°K.; $p(C_2Cl_4) = 59.6$ mm. (bottom) $T = 418.8$°K.; $p(C_2Cl_4) = 60.1$ mm. +, corrected for the Draper–Benson effect according to Fig. 1.: ○, uncorrected.

$$C_2Cl_6 + Cl \longrightarrow C_2Cl_5 + Cl_2 \quad (5)$$
$$Cl + Cl + M \longrightarrow Cl_2 + M \quad (6)$$
$$Cl + C_2Cl_5 \longrightarrow C_2Cl_4 + Cl_2 \text{ (or } C_2Cl_6) \quad (7)$$
$$2C_2Cl_5 \longrightarrow C_2Cl_4 + C_2Cl_6 \quad (8)$$

Two chain breaking steps—radical/radical and atom/radical—determine the rate equation

$$v = I_a^{1/2}(Cl_2)k_3/[k_8 + k_7k_3(Cl_2)/k_2(C_2Cl_4) + k_7k_4/k_2(C_2Cl_4)]^{1/2} \quad (5)$$

Figure 2 shows the determination of the second term of equation 5, which at 393.3°K. would be overlooked if the correction for the Draper–Benson

effect is disregarded; at 418.8°K. a negative slope would be observed which is completely incomprehensible. Further the "corrected" results yield values for constants $k_3/k_8^{1/2}$ and $k_3(k_2/k_4k_7)^{1/2}$ giving nice linear logarithmic plots[12] *vs.* $1/T$ (from 360 to 465 and from 385 to 590°K.); the "uncorrected" results give a curvature at low temperatures as expected for this effect.

In fact these negative slopes and disagreements in Arrhenius plots called our attention to this effect.

To all our results on photochlorination reactions we now apply corrections using eq. 4 and $a_0 = 2$ cm. and calculating κ as described above.

Acknowledgments.—Thanks are due to the Centre National Belge de Chimie Physique Moléculaire and the Fonds National Belge de la Recherche Scientifique for financial assistance. Scholarships of the Institut pour l'Encouragement de la Recherche Scientifique dans l'Industrie et l'Agriculture (I.R.S.I.A.-Brussels) have permitted A. M. Mahieu-Van der Auwera and D. Van der Auwera to perform this research.

FISCHER–TROPSCH SYNTHESIS MECHANISM STUDIES. II. THE ADDITION OF RADIOACTIVE KETENE TO THE SYNTHESIS GAS

BY G. BLYHOLDER AND P. H. EMMETT

The Johns Hopkins University, Department of Chemistry, Baltimore, Maryland

Received October 27, 1959

When carbonyl labeled radioactive ketene is added to the extent of 0.7% of Fischer–Tropsch synthesis gas being passed over a singly promoted iron catalyst at 256° and one atmosphere, the hydrocarbon products are found to have a small activity which is directly proportional to the number of carbon atoms in the molecule. Similar results are obtained when 0.50% ketene is added to synthesis gas passed over a cobalt catalyst at 189° and one atmosphere. These results are interpreted as indicating that ketene, which has previously[1] been demonstrated to act as a chain initiator when added in a small percentage to Fischer–Tropsch synthesis gas, dissociates on the surface so that only the methylene part of the molecule functions as the chain initiator.

For a general introduction to the use of radioactive tracers in the study of the Fischer–Tropsch mechanism the reader is referred to the previous papers[1–5] on the addition of radioactive compounds to the synthesis gas. In the preceding paper,[1] ketene labeled with C^{14} in the methylene group when added in a small percentage to the synthesis gas was found to produce radioactive products which had an approximately constant radioactivity per mole. When 1:1 H_2:CO synthesis gas containing 2% ketene was passed over a singly promoted iron catalyst the products had about the same molar activity as the ketene. When 2:1 H_2:CO synthesis gas containing 0.25% ketene was passed over a cobalt catalyst the molar activity of the products was about one-third that of the ketene. These results led to the conclusion that the ketene was strongly adsorbed on both the iron and cobalt catalysts and acted as a chain initiator.

In order to check whether the ketene molecule behaved as a unit or split up when it acted as a chain initiator the experiments herein reported were performed. These experiments are similar to the previous ones except that the ketene is labeled in the carbonyl group rather than the methylene group. If the whole ketene molecule is the chain initiator the results of this experiment should be identical with the previous results. If the ketene molecule splits up before initiating a chain the results could be quite different.

(1) G. Blyholder and P. H. Emmett, THIS JOURNAL, **63**, 962 (1959).

(2) J. T. Kummer, H. H. Podgurski, W. B. Spencer and P. H. Emmett, *J. Am. Chem. Soc.*, **73**, 564 (1951).

(3) J. T. Kummer and P. H. Emmett, *ibid.*, **75**, 5177 (1953).

(4) W. K. Hall, R. J. Kokes and P. H. Emmett, *ibid.*, **79**, 2983 (1957).

(5) R. J. Kokes, W. K. Hall and P. H. Emmett, *ibid.*, **79**, 2989 (1957).

Experimental

The ketene was made by decomposing acetone over a hot wire in the previously described equipment. Acetone labeled with C^{14} in the 2-position was obtained from the Isotope Specialties Company. The ketene produced was purified by vacuum distillation and its purity checked by vapor phase chromatography. The ketene had an activity of 5000 counts per minute per cc. at S.T.P.

The same Fischer–Tropsch synthesis apparatus was used for these experiments as was the earlier reported ketene work.[1] The ketene was introduced into the synthesis gas stream by bubbling the mixture of carbon monoxide and hydrogen through liquid ketene immersed in an ethyl alcohol slush bath. The percentage ketene in the synthesis gas was determined by measuring the volume of liquid ketene in the trap before and after the run.

Synthesis products were analyzed on a vapor phase chromatography apparatus (Perkin–Elmer Model No. 154-B) using columns A and J. The radioactivity of the products was determined using a conventional Geiger counter with the previously described special cell.[1]

Runs were made on the two previously used catalysts. One catalyst (No. 613) is a reduced fused iron oxide. It is a singly promoted catalyst containing 1.80% SiO_2, 1.6% ZrO_2 and 0.58% Al_2O_3. The furnace was charged with 50 cc. of 10 to 20 mesh catalyst. The catalyst was reduced at 500° overnight with H_2 at a space velocity of 1000 $hr.^{-1}$. A 1:1 H_2:CO mixture containing 0.7% ketene was passed over the iron catalyst at 207 cc./min. for 5 hr. The average contraction was 18% with the furnace at 256°.

The cobalt catalyst (No. 89EE) whose preparation is described by Anderson[6] and co-workers is composed of cobalt, thoria, magnesia and kieselguhr in the ratio 100:6:12:200. The furnace was charged with 50 cc. of the pelletized catalyst. It was reduced at 400° overnight with a H_2 space velocity of 1000. A 5 hour run was made with 0.53% ketene added to the 2:1 H_2:CO synthesis gas which was passed over the catalyst at 210 cc./min. The contraction averaged 16% at 189°.

Results

In Table I is given the product distribution determined on the fractometer by directly running

(6) R. B. Anderson, W. K. Hall, H. Hewlett and B. Seligman, *ibid.*, **69**, 3114 (1947).

product gas collected just after the furnace. Since one complete product analysis required three separate chromatographic runs, one each for the fractions C_1 to C_3, C_3 to C_6 and C_6 to C_8, the samples to be run for each fraction were collected at 45 minute intervals. It was assumed that the product distribution did not change during the time between sample collections. The product distribution for both the cobalt and iron catalysts is seen to be shifted toward a greater number of low molecular weight products for the ketene runs relative to the control runs.

TABLE I

PRODUCT DISTRIBUTION IN RELATIVE MOLES

	Fe-cat.		Cobalt-cat.	
	No ketene	0.7% ketene	No ketene	0.53% ketene
CO_2	9.56	19.5	0.49	1.93
CH_4	3.5	7.0	11.0	33.0
C_2 total	1.20	2.4	0.59	1.53
Ethane	1.10	1.9	0.56	1.27
Ethylene	0.092	0.48	0.028	0.26
C_3 total	1.00	1.00	1.00	1.00
Propane	0.68	0.87	0.72	1.0
Propylene	.32	.13	.28	0.0
C_4 total	.79	.59	.91	.76
n-C_4 + iso-C_4	.29	.26	.68	.53
Butene-2	.50	.33	.23	.23
C_5 total	.33	.31	1.20	.67
n-C_5	.17	.12	0.72	.46
iso-C_5	.038	.026	.28	<.01
Pentene-2 + pentene-3	.12	.16	.20	.21
n-C_6	.07	.043	.50	.26
n-C_7			.46	.11
n-C_8			.29	

The radioactivity of the hydrocarbon products is shown in Figs. 1 and 2. The radioactive analysis was performed on the collected products after the run was completed. In the run over iron the CO and CO_2 after the furnace had activities of 40 and 63 counts per minute per cc. at S.T.P., respectively. In the cobalt run the CO and CO_2 activities were 55 and 40 c.p.m./cc., respectively.

Discussion

The most interesting feature of the results is the difference in the appearance of the radioactivity *vs.* carbon number plots for ketene labeled in the carbonyl group as compared with ketene labeled in the methylene group. When synthesis gas containing 2% of radioactive ketene (3000 c.p.m. per cc. with the C^{14} in the methylene group) was passed over an iron catalyst,[1] the plot of activity *vs.* number of carbon atoms (Fig. 3) indicated that at least two-thirds of the product molecule chains were initiated by ketene and that the activity per cc. of hydrocarbon increased about 200 to 300 counts per minute per cc. per carbon atom. The data in Table I indicate that for synthesis gas containing ketene the relative amount of light products is considerably increased over the amounts produced when no ketene is in the synthesis gas; this fact would result in the activity per mole of the C_2 and C_3 products being correspondingly high. When synthesis gas containing 0.25% ketene (3000 c.p.m. per cc., labeled in the methylene position) was passed over a cobalt catalyst the plot of activity *vs.* carbon number (Fig. 3) yielded the result that about 1/3 of the products were initiated by ketene and no increase in activity with carbon number was observable. In contrast to these results in the new experiments when synthesis gas containing 0.7% radioactive ketene (5000 counts per minute per cc.) labeled in the carbonyl group is passed over the same iron catalyst, the plot of activity *vs.* carbon number yields, if the data from C_4 to C_{10} are considered, a straight line which extrapolates to zero activity at zero carbon number and has a slope of 95 c.p.m. per cc.

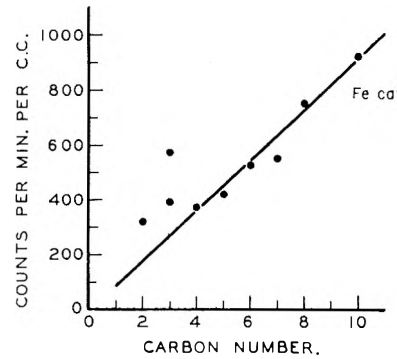

Fig. 1.—Radioactivity of hydrocarbons formed on adding 0.7% CH_2C^*O to 1:1 H_2:CO over a singly promoted iron catalyst.

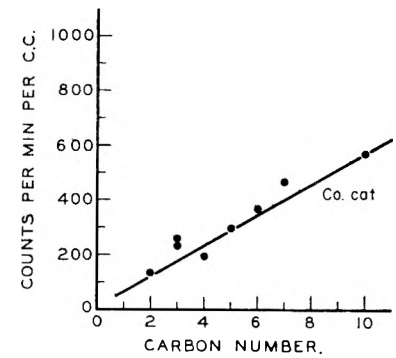

Fig. 2.—Radioactivity of hydrocarbons formed on adding 0.5% CH_2C^*O to 2:1 H:CO over a cobalt catalyst.

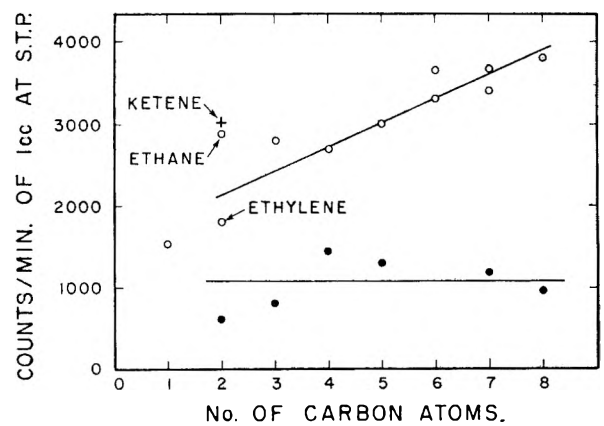

Fig. 3.—Radioactivity of hydrocarbons formed on passing 2% radioactive ketene (3,000 counts per minute per cc. labeled in the methylene group) in a 1:1 CO:H_2 mixture over an iron catalyst at 240° (open circles) and passing 0.25% methylene labeled radioactive ketene in a 2:1 H_2:CO mixture over a cobalt catalyst at 185° (solid circles).

per carbon number. Similarly with 0.50% radioactive ketene (5000 counts per minute per cc.), labeled in the carbonyl group in the synthesis gas passed over a cobalt catalyst, the straight line extrapolated through zero and has a slope of 56 counts per minute per cc. per carbon number.

The earlier experiments were interpreted as indicating that the ketene is strongly adsorbed on the surface and acts as a chain initiator. The new experiments refine this conclusion by giving evidence that the ketene molecule breaks up on the surface with the CH_2 group acting as a chain initiator.

This seems to be the first definite evidence that adsorbed CH_2 groups can serve as chain initiators for the synthesis of higher hydrocarbons.[7] The question therefore naturally arises as to whether any other interpretation of the results can reasonably be made. Only one complicating factor that could vitiate this conclusion in regard to CH_2 groups acting as chain initiators suggests itself. It is the possibility that CH_2C^*O and CO exchange rapidly either ahead of or at the entrance to the catalyst bed to form an equilibrium mixture of CH_2C^*O, C^*O, CH_2CO and CO. If this occurs, the ketene would be changed rapidly to an activity of only 69 c.p.m. per cc. in the iron runs and 78 counts per minute for cc. in the cobalt runs. Unfortunately, tests were not made of the activity of the ketene at various places along the catalyst bed so a conclusive answer to this possible complicating factor cannot be given. On chemical grounds such an exchange would not be expected because conditions severe enough to rupture the double bond in the ketene molecule and permit exchange would probably cause the ketene to decompose into more stable products.

Fortunately, one bit of direct information precludes the possibility of more than about 50% initial rapid exchange having taken place between CO and CH_2C^*O. The activity of the CO would have to be 69 counts per minute per cc. in the iron experiments, if complete exchange took place; it was actually 40 counts per minute. For cobalt, the exit CO would have had to be 78 counts; it was actually 55. Consequently it is certain that rapid exchange between CO and CH_2C^*O is not occurring to a sufficient extent to void the conclusion that the CH_2 group is primarily the chain initiator in forming higher hydrocarbons from CO and H_2.

(7) Fletcher and Gibson[8] have shown that in a gas mixture consisting of 47.5% C_2H_4, 47.5% H_2 and 5% radioactive CO (3650 c.p.m. per ml.) the hydrocarbon products at the C_4 level have an activity of 600 c.p.m. per ml. The activity increases at the rate of 550 counts per minute per ml. per carbon atom for the higher hydrocarbons. As the authors point out, the data indicate that the carbon atoms incorporated into the hydrocarbon chains appear to come both from CH_2 groups formed by dissociation of the ethylene and from carbon monoxide molecules. However, there is no indication in their work that the chain initiators are adsorbed CH_2 radicals rather than adsorbed C_2H_4 molecules.

(8) A. W. Fletcher and E. J. Gibson, Radioisotope Conference, 1954, Vol. II, p. 40.

One other possible complication should be mentioned. The addition of 0.5 to 0.7% ketene clearly influences the composition of products and may therefore be claimed to produce conditions not typical of regular Fischer–Tropsch synthesis. To avoid this difficulty experiments will be done in which only 0.01% tracer will be added, the radioactivity of the tracer being 50 to 100 times that for the ketene used in the present experiments.

The one remaining item to be discussed is the cause of the observed increase in activity of the hydrocarbons per carbon atom shown in Figs. 1 and 2. For iron, if one assumes that the average activity of the carbon monoxide is one half the exit value, then about 75 counts per minute per cc. per carbon atom must have come from the 0.7% of the carbonyl labeled radioactive ketene (5,000 c.p.m. per cc.). The fact that the plots of radioactivity *vs.* carbon number for the reaction over iron has a slope for both methylene labeled (Fig. 3) and carbonyl labeled ketene (Fig. 1) suggests that probably the ketene molecule itself builds into the chain sufficiently to give the observed slopes. Actually within a factor of about two the data for iron can be accounted for on this hypothesis. However, the slope with methylene labeled ketene (200 to 300 counts per minute per carbon atom, depending on whether one averages the points over the C_3–C_8 range or the C_4–C_8 range) is about twice as great as the slope that one would deduce from the run with carbonyl labeled ketene (Fig. 1). It seems probable therefore that some adsorbed CH_2 groups from ketene in addition to a few ketene molecules were building into the chains in both experiments even though most of the added carbon atoms were furnished by carbon monoxide in both experiments.

The observed activity of the CO_2 in the present experiments (63 c.p.m. per cc. compared to 40 c.p.m. per cc. of CO for iron, and 40 c.p.m. compared to 55 c.p.m. for CO for cobalt) suggest that CH_2C^*O molecules or possibly adsorbed C^*O of higher average activity than the gaseous CO at any point in the catalyst bed are involved in the formation of the radioactive carbon dioxide. The specific nature of such a reaction is not clear.

In the first article of this series an explanation of the high efficiency of adsorbed ketene in starting hydrocarbon chains on the catalyst surface was given in terms of the ketene being adsorbed by both a carbon and an oxygen atom. This may still be characteristic of the complex at the C_2 stage even though the present data suggest adsorbed CH_2 rather than adsorbed ketene as the chain initiator for the building up of hydrocarbons on the catalyst surface.

Acknowledgment.—The authors gratefully acknowledge financial support for this work under a contract from the Atomic Energy Commission, and the supplying of two recorders by the Leeds and Northrup Co.

AN EXTENSION OF SLATER'S HIGH PRESSURE UNIMOLECULAR RATE EXPRESSION TO SIMULTANEOUS REACTION COÖRDINATES[1]

BY EVERETT THIELE AND DAVID J. WILSON

Department of Chemistry, University of Rochester, Rochester 20, New York

Received September 2, 1959

Slater's classical expression for the high pressure rate of a unimolecular reaction is extended to the case where reaction is assumed to occur when two internal coördinates are simultaneously greater than a given pair of critical values. The pre-exponential factor is given by an energy-weighted average of the two Slater frequencies for the individual reaction coördinates. The results of this work are applied to cyclobutane.

Introduction

It was shown recently by Srinivasan and Kellner[2] that cyclobutane decomposes unimolecularly to ethylene with no migration whatsoever of hydrogen atoms. This suggests rather strongly that the reaction coördinate for cyclobutane involves either (1) the breaking of a single C–C bond to yield a diradical which subsequently decomposes, or (2) the simultaneous breaking of two C–C bonds on opposite sides of the ring. Slater's theory[3] leads one to expect a high pressure limit of the pre-exponential factor much smaller than the observed[4] value of 4×10^{15} sec.$^{-1}$ if the first coordinate mentioned above is applicable.[5] Slater's theory as it stands is not applicable to the simultaneous coördinates mentioned in case 2, and the effect on the pre-exponential factor of the requirement that two bonds be broken simultaneously was not immediately obvious to us.

We shall therefore extend Slater's theory for the high pressure limit of a unimolecular reaction to molecules in which two reaction coördinates must simultaneously each exceed some critical value. This will permit the further testing of Slater's harmonic classical model against the rather precise unimolecular rate data on cyclobutane at the high pressure limit. It might be pointed out that the failure to detect radicals during the decomposition of cyclobutane does not eliminate the possibility of the diradical mechanism mentioned above, since the diradical might well possess an extremely short lifetime and therefore not be detected by the methods employed.[6] As remarked above, however, Slater's theory applied to the diradical mechanism leads to unsatisfactory results.

There follows a brief resume of Slater's theory and an expression of one of Slater's results in terms of a Dirac δ-function; this is used in the following section on the extension of Slater's theory to models involving simultaneous reaction coördinates. The mathematical details of this last section are relegated to the Appendix.

Slater's Formulation.—Slater's theory[3] is based on the classical model of a vibrating polyatomic molecule in which reaction is assumed to occur when a particular internal coördinate (the reaction coördinate) attains a critical value q_r^0. If one approximates the kinetic and potential energy as quadratic forms, the vibrational motion of any coördinate q_r may be expressed as

$$q_r = \sum_{i=1}^{n} \alpha_{ri}\sqrt{\epsilon_i} \cos 2\pi(\nu_i t + \psi_i) \qquad (1)$$

where ν_i and ϵ_i are the frequency and energy of the i^{th} normal mode, and the α_{ri} can be determined by a normal mode analysis. Using an expression $(L(\alpha_{ri},\epsilon_i,\nu_i))$ for the frequency of zeros in a trigonometric sum of the type $q_r - q_r^0$, Slater formulates the high pressure rate constant as an average of L over a Boltzmann distribution in the normal mode energies. Thus

$$k_\infty = \int_0^\infty \cdots \int_0^\infty \frac{L(\alpha_{ri}, \epsilon_i, \nu_i)}{2} \prod_{i=1}^{n} \frac{\exp(-\epsilon_i/kT)\mathrm{d}\epsilon_i}{kT} \qquad (2)$$

where the factor of one-half arises from the fact that only zeros occurring when $\mathrm{d}q_r/\mathrm{d}t$ is positive are considered physically meaningful. Slater's final expression is

$$K_\infty = \bar{\nu}_r \exp[-(q_r^0)^2/\alpha_r^2 kT]$$
$$\bar{\nu}_r^2 = \sum_{i=1}^{n} \alpha_{ri}^2\nu_i^2/\alpha_r^2 \qquad (3)$$
$$\alpha_r^2 = \sum_{i=1}^{n} \alpha_{ri}^2$$

The quantity $(q_r^0)^2/\alpha_r^2$ represents the minimum energy necessary for q_r to reach q_r^0. The identification of q_r with a physically plausible reaction coördinate then determines the theoretical pre-exponential (or frequency) factor at the high-pressure limit.

Kac's formula can be derived with the aid of a Dirac δ function,[7] a device which we shall also find useful in the present work. Formally we may write for N, the number of times any bounded and continuous function q_r attains a value q_r^0 during a given interval $0 \leqslant t \leqslant T$

$$N = \Sigma \int \delta(q_r - q_r^0)|\mathrm{d}q_r|$$
$$\delta(x) = 0,\ x \neq 0 \qquad (4)$$
$$\int_{-\infty}^{\infty} \delta(x)f(x)\mathrm{d}x = f(0)$$

(1) This work was supported in part by a grant from the National Science Foundation.

(2) R. Srinivasan and S. Kellner, *J. Am. Chem. Soc.*, **81**, 5891 (1959).

(3) N. B. Slater, *Proc. Roy. Soc.* (*London*), **194A**, 112 (1948).

(4) C. T. Genaux, F. Kern and W. D. Walters, *J. Am. Chem. Soc.*, **75**, 6196 (1953).

(5) E. Thiele and D. J. Wilson, *Can. J. Chem.*, **37**, 1035 (1959).

(6) We are indebted to Professor W. D. Walters for a discussion on this point.

(7) The authors wish to thank Professor Frank P. Buff for pointing out this physically meaningful, and mathematically straightforward method of deriving Kac's formula. M. Kac, *Amer. J. Math.*, **65**, 609 (1943).

where the summation is over the branches of the multiple-valued function $t(q_r)$. Since q_r is a function of t, the frequency of zeros in the interval $0 \leqslant t \leqslant T$ is given by

$$\frac{N}{T} = \frac{1}{T}\int_0^T \delta(q_r - q_r^0)\left|\frac{dq_r}{dt}\right| dt \qquad (5)$$

Substituting the expression

$$\delta(u) = \frac{1}{2\pi}\int_{-\infty}^{\infty} e^{iuz}dz \qquad (6)$$

into eq. 5 leads to Kac's starting formula, which may be reduced to the form used by Slater by averaging over a uniform distribution in the phase angles ψ_i, (following the method of reference 8).

Simultaneous Reaction Coördinates.—We now wish to extend this formulation to the case where reaction is assumed to occur when two internal coördinates q_1 and q_2 (given by eq. 1) became simultaneously greater than a pair of critical values q_1^0 and q_2^0. (We shall refer to this situation as a critical configuration.) Quantities analogous to those previously defined will be designated by the same letter starred.

We can write the following formal expression for N^*, the number of times the critical configuration occurs during the interval $0 \leqslant t \leqslant T$

$$N^* = {}^1/_2 \Sigma \int S(q_1 - q_1^0)\delta(q_2 - q_2^0)|dq_2| + {}^1/_2 \Sigma \int S(q_2 - q_2^0)\delta(q_1 - q_1^0)|dq_1|$$
$$S(x) = 0,\ x < 0$$
$$S(x) = 1,\ x \geqslant 0 \qquad (7)$$

In examining the validity of this expression let us consider two ways in which a critical configuration

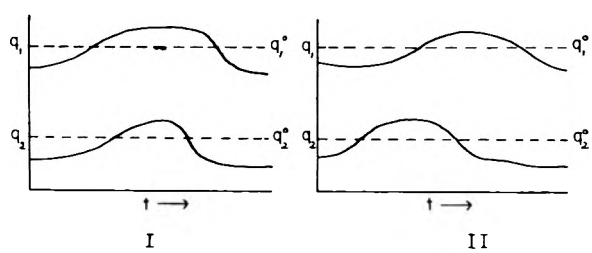

may occur. In case I, q_2 rises and falls past q_2^0 while q_1 is greater than q_1^0. The first integral in eq. 7 will have a value of two, while the second integral is zero, making N^* equal to one. In case II, q_1 rises above q_1^0 while q_2 is greater than q_2, and falls below q_1^0 after q_2 has fallen below q_2^0. Both integrals in eq. 7 will have a value of one and again N^* is equal to one. An interchange of subscripts clearly leaves the occurrence of critical configurations and the expression for N^* unchanged.

After converting N^* to an integral over t in the interval $0 \leqslant t \leqslant T$, we define the frequency L^* by averaging N^*/T over a uniform distribution of the phase angles.

$$L^* = \int_0^1 \cdots \int_0^1 \frac{N^*}{T}\, d\psi_1 \ldots d\psi_n \qquad (8)$$

Following Slater, we have for the high pressure rate constant

$$K_\infty^* = \int_0^\infty \cdots \int_0^\infty L^* \prod_{i=1}^{n} \frac{\exp(-\epsilon_i/kT)}{kT}\, d\epsilon_i \qquad (9)$$

(8) N. B. Slater, *Proc. Camb. Phil. Soc.*, **50**, 33 (1954).

The evaluation of expressions 8 and 9 will be discussed in the following section. With one simplifying approximation the result is

$$K_\infty^* = {}^1/_2 \sqrt{\frac{kT}{\pi}}\left[\frac{\bar{\nu}_1}{b_1} + \frac{\bar{\nu}_2}{b_2}\right]\exp(-E_0/kT)$$

$$\bar{\nu}_r^2 = \sum_{i=1}^{n} \alpha_{ri}^2\nu_i^2/\alpha_r^2,\ b_r^2 = E_0 - (q_r^0)^2/\alpha_r^2 \qquad (10)$$

$$\alpha_r^2 = \sum_{i=1}^{n} (\alpha_{ri})^2,\ r = 1, 2$$

$$\alpha_{12}' = \sum_{i=1}^{n} \alpha_{1i}\alpha_{2i}$$

$$E_0 = \frac{[\alpha_1^2(q_2^0)^2 + \alpha_2^2(q_1^0)^2 - 2\alpha_{12}'q_1^0q_2^0]}{\alpha_1^2\alpha_2^2 - (\alpha_{12}')^2} \qquad (10a)$$

The quantity E_0 can be interpreted as the minimum energy required for the occurrence of a critical configuration, and hence the minimum energy necessary for reaction. The previous result that $(q_r^0)^2/\alpha_r^2$ represents the minimum energy required for q_r to attain a value q_r^0, allows for a simple interpretation of b_1^2 and b_2^2 (see eq. 10a). Also from Slater's result as given by eq. 3, we see that $\bar{\nu}_1$ and $\bar{\nu}_2$ are the pre-exponential factors when either q_1 or q_2 is considered separately as the only reaction coördinate. The actual calculation of a pre-exponential factor by eq. 10 obviously requires the normal mode analysis required in Slater's theory, and also an assumption regarding the relative values of q_1^0 and q_2^0.

As a further comparison of eq. 10 with Slater's expression, let us consider the special case of equivalent simultaneous reaction coördinates, as might be expected in the decomposition of cyclobutane. That is, q_1^0 equals q_2^0, $\bar{\nu}_1$ equals $\bar{\nu}_2$, and α_1^2 equals α_2^2. Equation 10 then reduces to

$$k_\infty^* = \sqrt{\frac{kT}{\pi}}\frac{\bar{\nu}_1}{b_1}\exp(-E_0/kT) \qquad (11)$$
$$b_1^2 = \frac{E_0}{2}\left[1 - \frac{\alpha_{12}'}{\alpha_1^2}\right]$$

Taking a typical value for E_0/kT of 40, and assuming that b_1^2 equals $E_0/3$, we find that the pre-exponential factor has a value of $\bar{\nu}_1/6.5$.

For comparison with experimental values, where a temperature independent pre-exponential factor is assumed, we must multiply this value by $\sqrt{e}$. We therefore estimate that in general this model will predict pre-exponential factors of about one-fourth of the average of the two Slater frequencies involved.

The unimolecular decomposition of cyclobutane and a number of its derivatives have been investigated by Walters and co-workers.[4,9,10] In all cases a simultaneous breaking of opposite C–C bonds accounts most simply for the decomposition products observed, and for the absence of free radical effects. Pre-exponential factors range from 3×10^{14} sec.$^{-1}$ for cyclobutanone to 4×10^{15} sec.$^{-1}$ for cyclobutane. From the above estimate we

(9) (a) M. N. Das, F. Kern, T. D. Coyle and W. D. Walters, *ibid.*, **76**, 6271 (1954); (b) E. Wellman and W. D. Walters, *ibid.*, **79**, 1542 (1957).

(10) (a) G. Daignault and W. D. Walters, *ibid.*, **80**, 541 (1958); (b) M. N. Das and W. D. Walters, *Z. physik. Chem. (Frankfurt)*, **15**, 22 (1958).

see that this treatment cannot possibly account for these "high" pre-exponential factors if reaction coördinates dominated by low frequency C–C vibrations are used.

Appendix

Let us first consider the evaluation of L^*. Combining eq. 7 and 8, using expression 6 for the Dirac δ function, and substituting the following expression for the step function

$$S(u) = \frac{1}{2\pi}\int_{-\infty}^{\infty}\frac{e^{iuy}}{iy}\,dy + \frac{1}{2}$$

leads to an expression for L^* as the sum of four terms. Two of them are identical with Kac's formula, while the second pair of terms are of the same form, allowing the phase average integrations to be handled by again using the method of reference 3. This procedure leads to an expression for L^*

$$L^* = \frac{L(q_1)}{4} + \frac{L(q_2)}{4} - I_{12} - I_{21}$$

$$I_{12} = \frac{1}{8\pi^3}\int_{-\infty}^{\infty}\int_{-\infty}^{\infty}\int_{-\infty}^{\infty}\frac{\exp i(zq_2^0 + yq_1^0)}{iyx^2}\left[\prod_{i=1}^{n} J_0(\alpha_{2i}\sqrt{\epsilon_i}\,z + \alpha_{1i}\sqrt{\epsilon_i}\,y) - \prod_{i=1}^{n} J_0\{[(\alpha_{2i}\sqrt{\epsilon_i}\,z + \alpha_{1i}\sqrt{\epsilon_i}\,y)^2 + 4\pi^2\nu_i^2\alpha_{2i}^2\epsilon_i x^2]^{1/2}\}\right]dx\,dy\,dz$$

$$L(q_r) = \frac{1}{2\pi^2}\int_{-\infty}^{\infty}\int_{-\infty}^{\infty}\frac{\cos q_r^0 x}{y^2}\left[\prod_{i=1}^{n} J_0(\alpha_{ri}\sqrt{\epsilon_i}\,x) - \prod_{i=1}^{n} J_0(\alpha_{ri}\sqrt{\epsilon_i}\sqrt{x^2 + 4\pi^2\nu_i^2y^2})\right]dx\,dy \quad (12)$$

where I_{21} is defined by interchanging the subscripts 1 and 2 in the definition of I_{12}. $L(q_1)$ and $L(q_2)$ are Kac's expression for coördinates q_1 and q_2.

Using a bar to denote an average with respect to a Boltzmann distribution in the normal mode energies, we have on combining eq. 9 and 12

$$k_\infty^* = \frac{\bar{L}(q_1)}{4} + \frac{\bar{L}(q_2)}{4} - \bar{I}_{12} - \bar{I}_{21} \quad (13)$$

In evaluating $\bar{I}_{12}$ we invert the order of integration and use Weber's first exponential formula[11] to do the integrations with respect to the ϵ_1's. Introducing a new variable for z ($\xi = z + \alpha_{12}'y/\alpha_2^2$) reduces the ξ and x integrations to well known forms. Since the same integrations arise in Slater's theory (see ref. 3), we omit the details. The resulting expression for $\bar{I}_{12}$ is

$$\bar{I}_{12} = \bar{\nu}_2\exp[-(q_2^0)^2/\alpha_2^2kT]\cdot\int_{-\infty}^{\infty}\sin\left[\left(q_1^0 - \frac{\alpha_{12}'}{\alpha_2^2}q_2^0\right)y\right]\cdot\exp\left[-kT/4\left(\alpha_1^2 - \frac{(\alpha_{12}')^2}{\alpha_2^2}\right)y^2\right]dy/y \quad (14)$$

where the definitions given in (12) have been used. Using the formula (see ref. 12)

$$\mathrm{erf}(a) = \frac{1}{\pi}\int_{-\infty}^{\infty}\exp(-u^2/4a^2)\frac{\sin u}{u}\,du \quad (15)$$

where $\mathrm{erf}(a)$ denotes the error function, to evaluate the integral in (14), and the asymptotic expansion (see ref. 13)

$$\sqrt{\pi}[1 - \mathrm{erf}(u)] \cong \frac{e^{-u^2}}{u}\left(1 - \frac{1}{2u^2}\cdots\right) \quad (16)$$

we have, after dropping all terms but the first on the right in (16)

$$\bar{I}_{12} = \frac{\bar{\nu}_2}{2}\exp[-(q_2^0)^2/\alpha_2^2kT]\cdot\left[1 - \frac{\exp(-b_2^2/kT)}{\sqrt{\pi}\,b_2/\sqrt{kT}}\right] \quad (17)$$

I_{21} is again given by an interchange of subscripts 1 and 2. We shall also need Slater's results

$$\frac{\bar{L}(q_r)}{4} = \frac{\bar{\nu}_r}{2}\exp[-(q_r^0)^2/\alpha_r^2\,kT] \quad (18)$$

Combining (13), (17) and (18) gives expression (10) of the previous section.

It was also stated in the previous section that E_0 (defined in eq. 10a) could be interpreted as the minimum energy necessary for both q_1 and q_2 to reach q_1^0 and q_2^0. Consider the minimization of

$$E = \sum_{i=1}^{n}\epsilon_i$$

with the restrictive conditions that

$$q_r = \sum_{i=1}^{n}\alpha_{ri}\sqrt{\epsilon_i}\cos[2\pi(\nu_i t + \psi_i)] = q_r^0,\ r = 1,2$$

By a straightforward application of Lagrange's method of undetermined multipliers, we find

$$E_{\min} = \frac{(q_2^0)^2\sum_{i=1}^{n}\alpha_{1i}^2x_i^2 + (q_1^0)^2\sum_{i=1}^{n}\alpha_{2i}^2x_i^2 - 2q_1^0q_2^0\sum_{i=1}^{n}\alpha_{1i}\alpha_{2i}x_i^2}{\left(\sum_{i=1}^{n}\alpha_{1i}^2x_i^2\right)\left(\sum_{i=1}^{n}\alpha_{2i}^2x_i^2\right) - \left(\sum_{i=1}^{n}\alpha_{1i}\alpha_{2i}x_i^2\right)^2}$$

$$x_i = \cos[2\pi(\nu_i t + \psi_i)]$$

In order for the kinetic energy to be zero at the occurrence of a critical configuration, dq_i/dt, $i = 1, 2, \ldots n$, must be zero. Hence, all of the x_i's must have unit magnitude, reducing the above expression to E_0.

NOTE ADDED IN PROOF.—We are indebted to Professor N. B. Slater for the privilege of seeing his paper on this subject before publication, and for helpful criticism of our work.

(11) G. N. Watson, "Theory of Bessel Functions," University Press, Cambridge, 1952, p. 393.

(12) Erdelyi, Magnus, Oberhettinger and Tricomi, "Tables of Integral Transforms," Vol. I, McGraw-Hill Book Co., New York, N. Y., 1954, p. 73.

(13) E. Jahnke and E. Emde, "Table of Functions," Dover Publications Inc., New York, N. Y., 1945, p. 24.

SIMULTANEOUS REACTION COÖRDINATES IN TRANSITION STATE THEORY

BY N. B. SLATER

The University, Leeds, England

Received December 2, 1959

Thiele and Wilson's extension of unimolecular reaction rate theory to a pair of simultaneous reaction coördinates is treated by the method of the transition state, and a transmission coefficient is calculated.

Introduction

In the transition state model and in my "harmonic" model of gaseous unimolecular reactions,[1] a molecule dissociates when it passes through a critical internal configuration. This is represented by a reaction coördinate passing a critical value corresponding to the transition state. For some years it has been felt that some reactions might be due to two simultaneous distortions, perhaps in different parts of the molecule, or perhaps of contiguous interatomic distances. Thiele and Wilson[2] have solved this problem for the harmonic model by considering two reaction coördinates as sums of vibrations which have both to come sufficiently into phase to give together the two critical extensions. In effect, they do not look for exactly simultaneous extensions, but for the occurrence of a critical distortion of one coördinate when the other is already more than critically stretched.

This model appears unlike the transition state picture with its single reaction coördinate; but if we take the original view of a transition state rate as a flow through a critical surface, we shall find that simultaneous reaction coördinates can be handled quite simply from this point of view. This will be illustrated here merely for the classical harmonic model, although extensions to anharmonic models and one type of quantal theory will be seen to be possible.

Calculation of the Rate Constant

The internal configuration is described by n coördinates $q_1,\ldots,q_n$, such as stretches or contractions of interatomic distances, or linear combinations of these distances. If q_1 and q_2 are the "simultaneous reaction coördinates," with large critical values q_{10} (to be read as $q_{1,0}$ not q_{ten}) and q_{20}, then the molecule is assumed to dissociate if q_1 reaches q_{10} when $q_2 - q_{20}$ is positive, or if q_2 reaches q_{20} when $q_1 - q_{10}$ is positive.

In a high concentration at temperature T, the distribution over the gas of values of the q's and conjugate momenta will be effectively, as in non-dissociative equilibrium, proportional to $\exp(-H/\kappa T)$, where $H = V + T'$ is the sum of the molecular potential and kinetic energy functions. The first-order rate constant k is then the proportion of the phase-space distribution which flows out per second over the boundary indicated in Fig. 1. Thus

$$k \int e^{-H/\kappa T} = \int \dot{q}_1 e^{-H/\kappa T} + \int \dot{q}_2 e^{-H/\kappa T} \qquad (1)$$

where on the left side the integration is over $q_1,\ldots,p_n$ for the available phase-space of undissociated molecules; but on the right in $\int \dot{q}_1, \ldots$, we put $q_1 = q_{10}$ in H (omitting integration over q_1) and limit the ranges to have $q_2 \geqslant q_{20}$ and $\dot{q}_1 \equiv \partial H/\partial p_1 > 0$. In $\int \dot{q}_2, \ldots$, the roles of suffixes 1 and 2 are reversed.

The kinetic energy is of the form

$$T' = \tfrac{1}{2}\,\Sigma_1^n\Sigma g_{rs}p_r p_s = \tfrac{1}{2}\,\Sigma\Sigma a_{rs}\dot{q}_r\dot{q}_s \qquad (2)$$

where $\{g_{rs}\}$ is the matrix inverse of $\{a_{rs}\}$. If these matrices are effectively independent of the values of the q's, we can separate the coördinate and momentum (or velocity) integrations in equation 1, and write it in the more illuminating, but still very general, form

$$k = \tfrac{1}{2}\,v_1 \int_{q_{20}}^{(\infty)} P(q_{10}, q_2)\mathrm{d}q_2 + \tfrac{1}{2}\,v_2 \int_{q_{10}}^{(\infty)} P(q_1, q_{20})\mathrm{d}q_1 \qquad (3)$$

where $v_r \equiv \langle|\dot{q}_r|\rangle$ is the mean absolute velocity, as in (16) below, and $P(q_1, q_2)$ is the joint distribution of coördinates q_1 and q_2, namely

$$P(q_1, q_2) = \int\ldots\int e^{-V/\kappa T}\,\mathrm{d}q_3\ldots\mathrm{d}q_n \Big/ \int\ldots\int e^{-V/\kappa T}\,\mathrm{d}q_1\ldots\mathrm{d}q_n \qquad (4)$$

Attention is confined here to the harmonic approximation, in which V is a positive definite quadratic form

$$V = \tfrac{1}{2}\,\Sigma_1^n\Sigma b_{rs}q_r q_s \qquad (5)$$

and the ranges of integration in (4) may be taken as $(-\infty, \infty)$. To evaluate (4) we make a change from variables q_s to q_s' $(s = 3,4,\ldots,n)$, where

$$q_s = q_s' + (h_{22}h_{1s} - h_{12}h_{2s})q_1\eta^{-2} + (h_{11}h_{2s} - h_{12}h_{1s})q_2\eta^{-2} \qquad (6)$$

$$\eta^2 \equiv h_{11}h_{22} - h_{12}^2 \qquad (7)$$

$\{h_{rs}\}$ being the matrix inverse of $\{b_{rs}\}$. This gives for (5)

$$V = V' + \tfrac{1}{2}\,\Sigma_3^n\Sigma b_{rs}q_r'q_s' \qquad (8)$$

where

$$V' \equiv V'(q_1, q_2) = (h_{22}q_1^2 - 2h_{12}q_1q_2 + h_{11}q_2^2)/2\eta^2 \qquad (9)$$

The $q_3',\ldots,q_n'$ integrations in (4) now disappear, leaving

$$P(q_1, q_2) = (2\pi\kappa T\eta)^{-1}\,e^{-V'/\kappa T} \qquad (10)$$

It is convenient to bring in some energy parameters at this point. As the double sum in (8) is positive, the minimum or *dissociation energy*, at which q_1 and q_2 both have their critical values, is

$$E_0 = V'(q_{10}, q_{20}) = (h_{22}q_{10}^2 - 2h_{12}q_{10}q_{20} + h_{11}q_{20}^2)/2\eta^2 \qquad (11)$$

This is essentially larger than the separate mini-

(1) N. B. Slater, "Theory of Unimolecular Reactions," Cornell University Press, Ithaca, N. Y., 1959.

(2) E. Thiele and D. J. Wilson, THIS JOURNAL, **64**, 473 (1960). I am indebted to these authors for sending me a manuscript of their paper.

mum energies for q_1 to reach q_{10}, or q_2 to reach q_{20}, namely (ref. 1, p. 104)

$$E_{r0} = g_{r0}^2/2h_r^f \qquad (r = 1, 2) \tag{12}$$

The differences

$$\epsilon_{r0} = E_0 - E_{r0} \tag{13}$$

will appear in the calculation primarily in the form

$$\epsilon_{10} = (h_{11}g_{20} - h_{12}g_{10})^2(2h_{11}\eta^2)^{-1} \tag{14}$$

in which we shall assume the first bracket is positive; there is a similar form and assumption for ϵ_{20}.

The Integration.—A simple integration by "parts," using (10), (11), (14) and assuming $\epsilon_{10}/\kappa T$ is large, gives for the first integral in (3)

$$\int_{q_{20}}^{\infty} P(q_{10}, q_2)dq_2 = \frac{\exp(-E_0/\kappa T)}{2\pi\sqrt{(2h_{11}\epsilon_{10})}}\left\{1 - \frac{\kappa T}{2\epsilon_{10}} + \ldots\right\} \tag{15}$$

The mean velocity v_1 in (3), corresponding to the integral of $\dot{q}_1 \exp(-T'/\kappa T)$ in (1), is given by

$$^1/_2 v_1 = \int_0^{\infty} \dot{q}_1\, d\dot{q}_1 \int \ldots \int e^{-T'/\kappa T}\, d\dot{q}_2 \ldots d\dot{q}_n / \int \ldots \int e^{-T'/\kappa T}\, d\dot{q}_1 \ldots d\dot{q}_n \tag{16}$$

the unspecified ranges being $(-\infty, \infty)$. Hence (ref. 1, p. 104)

$$v_r = (2\kappa T' g_{rr}/\pi)^{1/2} \tag{17}$$

Finally, by (15) and (17) the rate constant (3) is

$$k = (2\sqrt{\pi})^{-1} e^{-E_0/\kappa T} \sum_{1,2} \bar{\nu}_r \beta_r (1 - \beta_r^2/2 + \ldots) \tag{18}$$

where

$$\beta_r^2 = \kappa T/\epsilon_{r0}, \qquad \bar{\nu}_r = (g_{rr}/h_{rr})^{1/2}/2\pi \tag{19}$$

and E_0 is as in (11).

The corresponding rate constants for dissociation at *one* critical extension $q_r = q_{r0}$ (r = 1 *or* 2) are

$$k_r = \bar{\nu}_r \exp(-E_{r0}/\kappa T) \tag{20}$$

Apart from the smaller exponential factor, the present rate constant k is essentially smaller because of the additional factors $\beta_r = (\kappa T/\epsilon_{r0})^{1/2}$.

Anharmonic modifications could be introduced in the potential in (4) as in the single reaction coördinate model (ref. 1, p. 125). The classical effects of isotopic substitution would still be given, however, by the changes in v_r or $\bar{\nu}_r$ (ref. 1, p. 122).

Comparison with Thiele and Wilson.—The parameters α_{ri} used by Thiele and Wilson are such that the transformation (ref. 1, p. 52)

$$q_r = \sum_{i=1}^{n} \alpha_{ri} Q_i \tag{21}$$

reduces the energy forms (5) and (2) to

$$V = \Sigma\, Q_i^2 \qquad T = \Sigma\, \dot{Q}_i^2/(2\pi\nu_i)^2 \tag{22}$$

so that a normal mode of frequency ν_i and energy ϵ_i has the form $Q_i = \sqrt{\epsilon_i}\cos 2\pi(\nu_i t + \psi_i)$. The q_r in (21) are then the sums of vibrations used by Thiele and Wilson. Relations between the α_{ri} and the present h_{rs} and g_r are (ref. 1, p. 54)

$$\sum_i \alpha_{ri}\alpha_{si} = 2h_{rs}, \qquad \sum_i \alpha^2{}_{ri}(2\pi\nu_i)^2 = 2g_{rr} \tag{23}$$

The first of these gives for their parameters

$$\alpha_r^2 \equiv \sum \alpha_{ri}^2 = 2h_{rr} \qquad \alpha_{12}' = \sum \alpha_{1i}\alpha_{2i} = 2h_{12} \tag{24}$$

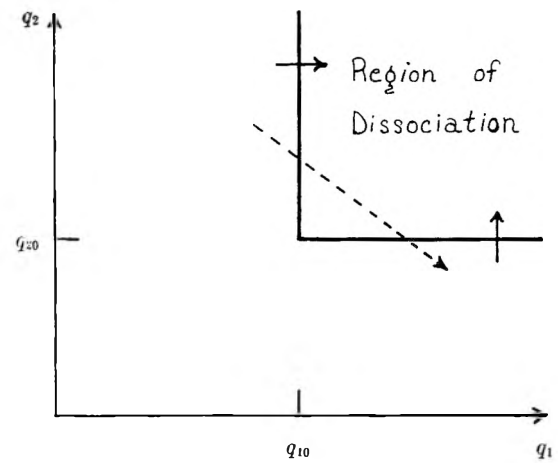

Fig. 1.—The critical boundary in phase space. The broken arrow is referred to in the last section of the paper.

so the energies E_0 and ϵ_{r0} of (11) and (13) are their E_0 and b_r^2. The relations (23) show also that $\bar{\nu}_r$, as defined in (19), is also

$$\bar{\nu}_r = (\Sigma\, \alpha^2{}_{ri}\nu_i^2/\alpha_r^2)^{1/2} \tag{25}$$

the mean frequency occurring in their formulas.

These comparisons identify the leading terms of (18) with the rate formula, equation 10 of Thiele and Wilson.

Bivariate Distributions.—These comparisons also suggest a more technically statistical approach to the harmonic model. The classical distribution $\exp\{-(V + T')/\kappa T\}$ indicates through (22) that the normal coördinates and velocities Q_i and $\dot{Q}_i$ have independent Gaussian distributions with variances

$$\langle Q_i^2\rangle = {}^1/_2\kappa T \qquad \langle \dot{Q}_i^2\rangle = {}^1/_2\kappa T \times 4\pi^2\nu_i^2 \tag{26}$$

Hence the bivariate distribution of q_1 and q_2, as the linear combinations (21) of the Q_i, is

$$P(q_1, q_2) = (2\pi\sigma')^{-1}\exp\{-(\sigma_2^2 q_1^2 - 2\sigma_{12}q_1q_2 + \sigma_1^2 q_2^2)/2\sigma'^2\} \tag{27}$$

where $\sigma'^2 \equiv \sigma_1^2\sigma_2^2 - \sigma_{12}^2$ and

$$\sigma_r^2 \equiv \langle q_r^2\rangle = \Sigma\, \alpha_{ri}^2 \langle Q_i^2\rangle \qquad \sigma_{12} \equiv \langle q_1 q_2\rangle = \Sigma\, \alpha_{1i}\alpha_{2i}\langle Q_i^2\rangle \tag{28}$$

Also in (3)

$$v_r = \langle|\dot{q}_r|\rangle = (2/\pi)^{1/2}\langle \dot{q}_r^2\rangle^{1/2} = (2/\pi)^{1/2}(\Sigma\, \alpha_{ri}^2\langle \dot{Q}_i^2\rangle)^{1/2} \tag{29}$$

We may now evaluate the rate constant (3) using the expressions (27)–(29). If in the result we substitute the classical means (26), we arrive at Thiele and Wilson's result directly in terms of their parameters. If, however, we replace the means (26) by those appropriate to a distribution of normal coördinates and momenta for quantum oscillators, we arrive at a quantum form of rate for simultaneous reaction coördinates. This is analogous to my quantum rate for a single reaction coördinate (ref. 1, Chapter 10), and rests on the same assumption that formulas of type (3) are valid as representing the phase-space flow of probability over a boundary for quantum oscillators.

A Transmission Coefficient

Looking back to the initial formulation of the rate constant, we may see that the corner at

(q_{10},q_{20}) in the critical surface in Fig. 1 suggests a modification which will be found equivalent to the introduction of a transmission coefficient.

Consider a dissociating molecule represented by a phase-space point crossing the boundary $q_1 = q_{10}$, with $\dot{q}_1$ positive and $q_2 - q_{20}$ positive but fairly small. If the point has $\dot{q}_2$ negative, it is likely soon to cross the boundary $q_2 = q_{20}$ downward (as shown by the broken arrow on the figure), corresponding to a recombination of the molecule. As much of the traffic toward dissociation will, from energy considerations, be in the neighborhood of the critical corner, this suggests that we should modify the integrals on the right of equation 1 by excluding negative values of $\dot{q}_2$ from $\int\dot{q}_1$ and of $\dot{q}_1$ from $\int\dot{q}_2$. This is equivalent to replacing $^1/_2v_r$ in (3) by $^1/_2v_r'$ where (compare (16))

$$^1/_2v_r' = \int_0^\infty \int_0^\infty \dot{q}_r P'(\dot{q}_1, \dot{q}_2)\mathrm{d}\dot{q}_1\mathrm{d}\dot{q}_2 \qquad (30)$$

$P'(\dot{q}_1,\dot{q}_2)$ being the joint distribution of the two velocities. This could be written down as a bivariate distribution as in the last section, or evaluated as the analog of (4) for velocities, with T' replacing V. In fact $P'(\dot{q}_1,\dot{q}_2)$ is given by (10) with the q_r and h_{rs} in (9) and (7) replaced by $\dot{q}_r$ and the g_{rs} of (2). This gives exactly for (30)

$$v_r' = {}^1/_2(2\kappa T g_{rr}/\pi)^{1/2}\{1 + g_{12}(g_{11}g_{22})^{-1/2}\} \qquad (31)$$

Comparing this with (17), we see that the rate constant (3), with v_r' for v_r, is again of the form (18) but with an extra factor or "transmission coefficient"

$$\chi = {}^1/_2\{1 + g_{12}(g_{11}g_{22})^{-1/2}\} \qquad (32)$$

If, for example, the critical coördinates are stretches of interatomic distances with q_2 relating different atoms from those in q_1, then in the kinetic energy matrix g_{12} is identically zero (ref. 1, p. 46). In this case the coefficient χ is exactly $^1/_2$. This is a not unexpected result, but a deeper investigation of transmission coefficients in this model would be of interest.

THE SOLUBILITY OF L-THYROXINE (Na) IN THE PRESENCE OF PHOSPHATE BUFFER AND OF NEUTRAL SALTS

BY HENRY E. EVERT

Department of Biochemistry, State University of New York, Downstate Medical Center, Brooklyn, N. Y.

Received November 4, 1959

L-Thyroxine (Na) was found to be soluble in phosphate buffer at *p*H 7.4, at 38° temperature and a range of ionic strength from 0.032–0.162, to the extent of 2.5–5.0 × 10^{-5} mole per liter. The addition of sodium chloride to the phosphate buffer solution at two initial ionic strengths of phosphate buffer (*i.e.*, at 0.032 and at 0.162) produced a change in the ionic atmosphere surrounding the central ion which resulted in an apparent "salting-in" and "salting-out" effect attributed to changes in the dipole moment of the molecule. Ultraviolet absorption spectra data indicated that thyroxine existed in the form of an intact molecule in the soluble phase and that an increased dissociation of the phenolic hydroxyl group with increased *p*H may be correlated with the increased solubility of thyroxine at a *p*H near 7.4.

Introduction

The extremely low solubility of thyroxine and related compounds in water has limited the study of their properties by conventional methods.[1] The early work of Kendall and Osterberg[2] and the later work of Winnek and Schmidt[3] demonstrated the relative insolubility of thyroxine and of thyroxine salts in water. It has become common laboratory practice to use the salt form or to solubilize thyroxine by the addition of alkali. The present study[4] with L-thyroxine (Na)[5] was prompted by the scarcity of quantitative data, particularly in the *p*H range 7.2 to 7.8 obtained at defined ionic strengths and at controlled temperature. A sensitive method was used to determine the soluble thyroxine which combines reduced pressure concentration with polarographic analysis.

(1) C. L. Gemmill, *Arch. Biochem. Biophys.*, **54**, 359 (1955).

(2) E. C. Kendall and A. E. Osterberg, *J. Biol. Chem.*, **40**, 265 (1919).

(3) P. S. Winnek and C. L. A. Schmidt, *J. Gen. Physiol.*, **19**, 773 (1935).

(4) A preliminary report was presented before the American Association of Biological Chemists at Atlantic City, N. J., in April, 1959. See *Federation Proc.*, **18**, 224 (1959).

(5) L-Thyroxine (Na) was obtained from the Nutritional Biochemicals Corporation, Cleveland, Ohio.

Methods

Stock solutions of phosphate buffer, 0.013 and 0.066 *M*, respectively, were prepared at definite *p*H values according to the method of Hastings and Sendroy.[6] The *p*H of the solutions was checked with a Beckman Model G *p*H Meter. In order to separate the thyroxine suspension into a soluble and an insoluble phase, 19.9 mg. of L-thyroxine (Na) was suspended in 125 ml. of phosphate buffer medium and after equilibration for one hour in a glass-stoppered flask placed in a thermostated water-bath at 25 or 35°, the suspension was filtered through a double thickness of Whatman No. 40 filter paper into a 300 ml. glass-stoppered round-bottom flask. The filtration was performed in a constant temperature–constant humidity cabinet. After concentrating the clear filtrate under reduced pressure at 35°, or below, to a volume of less than 10 ml., the residue was quantitatively transferred to a 10-ml. volumetric flask and diluted to 10 ml. with water. Aliquot portions (4 ml.) of the mixed suspension were placed in a 10-ml. volumetric flask and were analyzed polarographically. The supporting electrolyte[7] consisted of 1 ml. of *M* ammonium chloride, 1 ml. of *N* ammonium hydroxide, 0.25 ml. of 0.2% gelatin, 2.0 ml. of *n*-propyl alcohol diluted to 10 ml. with water. The polarograms were developed in the 5 μa. range on a Leeds and Northrup Electrochemograph, type E. The drop time of the Hg capillary in equimolar 0.1 *N* ammonium hydroxide

(6) A. B. Hastings and J. Sendroy, Jr., *J. Biol. Chem.*, **61**, 695 (1924).

(7) H. E. Evert, *Arch. Biochem. Biophys.*, **49**, 93 (1954).

and in 0.1 *M* ammonium chloride was 4.6 seconds. The mass of the Hg drops delivered per second was 1.55 mg.

The calibration data presented in Table I were obtained by dissolving 19.9 mg. of L-thyroxine (Na) in 25 ml. of 0.013 *M* phosphate buffer at *p*H 10.6. Aliquot portions (0–5 ml.) were introduced into a 10-ml. volumetric flask along with the supporting electrolyte. After dilution to 10 ml. with distilled water, the polarograms were obtained by the procedure described above.

TABLE I

TYPICAL CALIBRATION DATA USED FOR THE POLAROGRAPHIC DETERMINATION OF L-THYROXINE (Na)

Sum of combined wave heights, mm.	Concn. of L-thyroxine (Na) in polarographed soln. (concn. $\times 10^{-4}$ *M*)
7.6	1
15.9	2
25.2	3
30.7	4

Control experiments revealed that the filtration and reduced pressure concentration procedures produced no appreciable effect on the calibration. For example, when 19.9 mg. of L-thyroxine (Na) was dissolved in 125 ml. of buffer at *p*H 10.6 and after adjusting the *p*H to 7.4, followed by filtration and concentration, results identical with the procedure described above were obtained with the aliquot samples. The sum of the wave heights in mm. obtained in the P.V. range −0.9 to −2.0 bore a linear relation to the L-thyroxine (Na) present in the solution. An increase in phosphate buffer strength from 0.013 to 0.066 *M* did not alter the calibration data.

Results

Evidence for the presence of thyroxine in the soluble phase was obtained from ultraviolet absorption spectra of the concentrated filtrate (Fig. 1). The spectra were studied in the *p*H range 7.16 to 13.0 at a constant ionic strength of 0.284. A characteristic maximum was observed for thyroxine at 325 mμ.[1,8,9] The variation in the height of the absorbance curve at 325 mμ wave length with varied *p*H indicated the dissociation of the phenolic hydroxyl group to yield a phenoxide type ion. Based on this evidence for dissociation, the phenoxide ion is believed to be mainly responsible for the solubility of thyroxine in aqueous medium at a *p*H near 7.4.

Having established the presence of thyroxine in the concentrated filtrate, the results for the quantitative solubility of L-thyroxine (Na) are indicated in Figs. 2 and 3. In Fig. 2 the solubility of L-thyroxine (Na) in moles per liter $\times 10^{-5}$ is plotted as a function of the ionic strength at *p*H 7.4. The initial ionic strength due to the phosphate buffer, 0.013*M* was 0.032 and further increase in the ionic strength was produced by the addition of NaCl at *p*H 7.41 and at 38° temperature. Curve 1, Fig. 2, represents the effect of increased ionic strength brought about by increasing the phosphate buffer concentration. The maximum solubility occurred at 0.062 ionic strength. Starting with phosphate buffer having an ionic strength 0.032 at *p*H 7.4, an increase in ionic strength produced by the addition of NaCl produced an increase, followed by a decrease in solubility (curve 2, Fig. 2). It is of interest that approximately the same maximum level of solubility was observed in this case as was reached in curve 1, Fig. 2.

On the other hand, if one starts with a higher

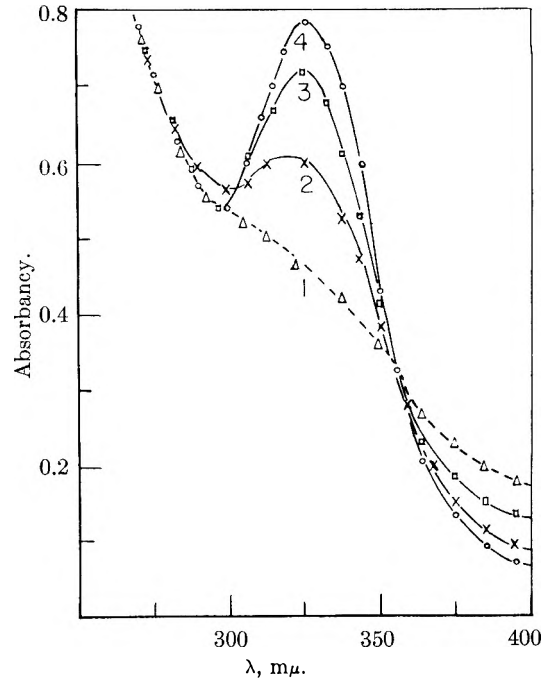

Fig. 1.—Ultraviolet absorption spectra of the concentrated filtrate which represents the soluble phase described under methods. The curves were obtained on a Beckman DU spectrophotometer at specified *p*H levels: curve 1, 7.16; curve 2, 8.32; curve 3, 10.95; and curve 4, 11.0 and above. The solutions contained: 6 ml. of concentrated filtrate; balanced proportions of NaCl and NaOH to give a constant ionic strength, 0.284, for each *p*H level; 1 ml. of *n*-propyl alcohol; and water (10 ml. final volume).

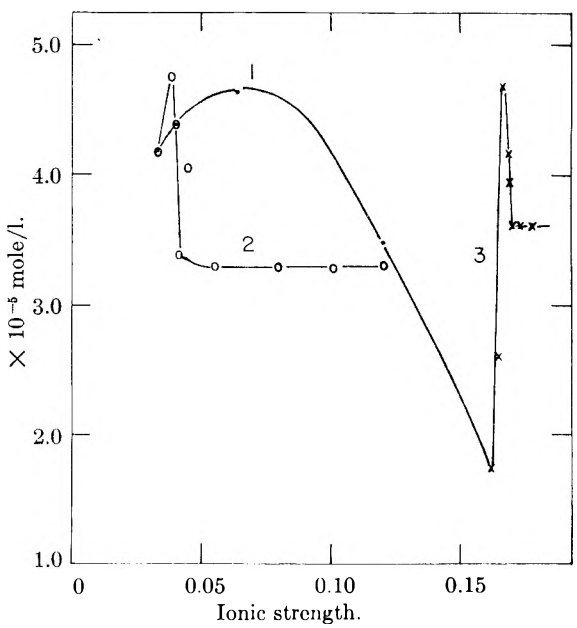

Fig. 2.—The effect of increased phosphate buffer concentration on the solubility of L-thyroxine (Na) in the presence of NaCl: curve 1, ionic strength increased by phosphate buffer only; curve 2, initial phosphate buffer concentration, 0.013 *M*, ionic strength, 0.032, plus added NaCl, *p*H 7.41, 38°; and curve 3, initial phosphate buffer concentration, 0.066 *M*, ionic strength, 0.162, plus added NaCl, *p*H 7.41, 38°.

(8) A. D. Marenzi and F. Villallonga, *Rev. soc. argentina biol.*, **17**, 270 (1941).

(9) D. B. Wetlaufer, J. T. Edsall and B. R. Hollingworth, *J. Biol. Chem.*, **233**, 1421 (1958).

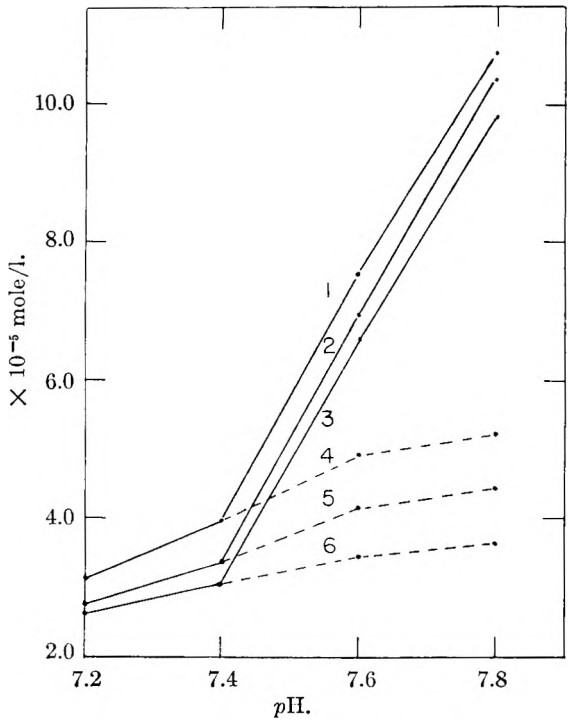

Fig. 3.—The effect of increased *p*H 7.2 to 7.8 on the solubility of L-thyroxine (Na) at 25 and 38° and at a constant ionic strength of 0.032 with phosphate buffer, plus added NaCl to give a further increase: curve 1, 38°, 0.032; curve 2, 38°, 0.037; curve 3, 38°, 0.040; curve 4, 25°, 0.032; curve 5, 25°, 0.037; and curve 6, 25°, 0.040.

phosphate buffer concentration, 0.066 *M*, (ionic strength, 0.162, *p*H 7.4, and 38° temperature), and the ionic strength is further increased by the addition of NaCl as shown in curve 3, Fig. 2, an increase followed by a decrease in the solubility of L-thyroxine (Na) was observed.

In Fig. 3, one observes the increase in solubility of L-thyroxine (Na) with an increase in temperature from 25 to 38°. A marked break in the curve was noted near *p*H 7.4 for curves at 38°. These observations correspond with those obtained with ultraviolet absorption spectra data (Fig. 1) and indicate that the dissociation of the phenolic hydroxyl group is associated with the observed solubility properties of thyroxine in alkaline solution.

Discussion

Pfeiffer and Würgler[10] and Euler and Rudberg[11] studied the effect of neutral salts on the solubility of many of the amino acids. Such studies yield considerable information concerning the activity of the molecule. It is well established that when a molecule in solution is surrounded by a neutral salt, an electrostatic influence is placed on the central ion which in turn disturbs the dipolar characteristics of the molecule. Since the solubility of a substance depends to a great extent on the electrical attraction between the solute and the solvent molecules, solubility properties are related to activity and to the binding capacity of the molecule. On the basis of the minute solubility of thyroxine in aqueous medium, in either the free or the salt form, it is apparent that thyroxine carries a relatively small charge compared to the size of the molecule. Similar characteristics have been observed for leucine, which likewise has a large hydrocarbon moiety and, therefore, does not dissolve readily in salt solutions.[10–12]

Ultraviolet spectra data (Fig. 1) indicate that a phenoxide ion is formed in alkaline solution. The formation of the phenoxide ion alters the dipolar characteristics of the thyroxine molecule to render it more soluble in the *p*H range under consideration, *i.e.*, 7.2–7.8.

The effect of placing thyroxine (Na) in solutions of increasing ionic strength (Fig. 2) produces what is akin to a "salting-in" and "salting-out" effect. A similar effect has been observed for other amino acids such as cystine[13] in the presence of neutral salts. Because of the small electrostatic charge carried by thyroxine in relation to the size of the molecule, the observed effects occur at very low ionic strengths.

Acknowledgments.—The author gratefully acknowledges the advice and support of Dr. Edward Muntwyler during the course of this work. Technical assistance was rendered by Mr. Ted Legett.

(10) P. Pfeiffer and J. Würgler, *Z. physiol. Chem.*, **133**, 180 (1924).

(11) H. V. Euler and K. Rudberg, *ibid.*, **140**, 113 (1924).

(12) J. T. Edsall, Chap. 16, pp. 871–952 in C. L. A. Schmidt, Editor, "The Chemistry of Amino Acids and Proteins," C. C Thomas, Springfield, Ill., 1938.

(13) T. L. McMeekin, E. J. Cohn and M. H. Blanchard, *J. Am. Chem. Soc.*, **59**, 2717 (1937).

TRACER DIFFUSION OF HYDROGEN ION IN AQUEOUS ALKALI CHLORIDE SOLUTIONS AT 25°

BY L. A. WOOLF[1,2]

Contribution from the Department of Chemistry, University of New England, Armidale, New South Wales, Australia

Received November 11, 1959

The tracer-diffusion coefficients of hydrogen ion have been obtained from diffusion measurements in 0.1–3.6 *M* potassium chloride, and 0.1–4.5 *M* sodium and lithium chloride solutions, respectively, as supporting electrolytes. The dependence of the tracer-diffusion coefficient on concentration of the supporting electrolyte is found to be greater than that of other univalent ions. Lithium chloride solutions are found to have an abnormal influence on hydrogen ion transport; an explanation is suggested in terms of the proton jump transport mechanism. Frames of reference for tracer diffusion are briefly mentioned.

Introduction

The transport properties of hydrogen ion are of interest in many branches of aqueous solution chemistry. A previous publication[3] described an application of the magnetically-stirred, porous-diaphragm cell[4] with which the tracer-diffusion coefficients of iodide ion were determined by a chemical method involving direct analysis[5] of iodide. The chemical method enables a fairly rapid and quite accurate (*ca.* 0.4%) determination of the tracer diffusion coefficients of particles which, while not possessing suitable properties for radiochemical analysis, can be studied readily by conventional analytical techniques. The normal hydrogen isotope ion is in this category since it is not radioactive and the less common isotopes, deuterium and tritium, are unsuitable for use in the usual radiochemical methods of studying tracer diffusion.

Tracer diffusion, and the somewhat erroneously termed self diffusion, measurements in solution, except those involving only solvent and tagged solvent molecules, are made in systems of more than two components. In other words tracer diffusion represents a limiting case of diffusion in systems of three or more components. A recent publication[6] has correlated tracer-diffusion data for Na^+ in aqueous KCl with diffusion coefficient measurements in the system H_2O–NaCl–KCl, with both solutes at finite concentrations. Thus the tracer diffusion work of this paper may be described as diffusion of hydrogen ion in the ternary system H_2O–MCl–HCl (where M = Na, K, Li) when the HCl is infinitely dilute.

Reference Frames for Tracer Diffusion.—Recent articles[7–9] have shown the importance of defining diffusion coefficients with respect to a definite reference frame. Those most commonly used are the solvent-, cell-, volume- and mass-fixed reference frames, respectively. Relationships between these various frames may be derived.[10] The volume-fixed reference frame can be identified with the cell frame so long as there is no appreciable bulk flow or volume change on mixing during diffusion.[11] In the limiting case of the diffusion in a multicomponent system of one component, whose concentration is close to infinite dilution, the diffusion coefficient of that component on the volume-, mass- and solvent-fixed frames of reference has the same magnitude. Therefore, in such systems, all tracer diffusion coefficients, including those of this article, which refer explicitly to the volume frame, refer equally, but implicitly, to the other reference frames, including the cell frame. It may be noted that the diaphragm cell method of studying diffusion evaluates diffusion coefficients on both the cell and volume-fixed reference frames so long as its theoretical requirements of no volume change on mixing and no bulk flow are satisfied.

Experimental

The diaphragm cells were of the magnetically stirred type described previously,[4] and were calibrated at approximately 200 hour intervals by the diffusion of 0.5 *M* potassium chloride solutions into water. All diffusion experiments were performed at 25 ± 0.01° in a water filled thermostat.

The preparation of solutions and the diffusion measurements are best described by considering a particular case: the tracer-diffusion of hydrogen ion in 1 *M* sodium chloride solutions. A small but known volume of concentrated, analytical reagent quality, hydrochloric acid was placed in a volumetric flask and the flask then filled with an approximately 1 *M* sodium chloride stock solution to obtain a solution about 0.1 *M* in hydrogen ion. An acid-free solution of the same final sodium chloride molarity as the acid solution was prepared in a similar manner by using an equal volume of water instead of acid in the volumetric flask; this solution was analyzed conductimetrically to give an accurate value of the concentration of the supporting electrolyte. The acid solution was used to fill the lower compartment of the diaphragm cell and allowed to diffuse into the acid-free solution in the upper compartment with the usual experimental technique [4] After a diffusion period of about 30 hours the experiment was concluded and the contents of the cell analyzed for hydrogen ion. Brom thymol blue was used as indicator for all the titrations, from which atmospheric carbon dioxide was excluded by passage of CO_2-free nitrogen. The hydrogen ion concentrations were measured by titrating with barium hydroxide solutions which had been standardized by titrations with samples of analytical reagent quality hydrochloric acid whose strength was known from conductance measurements. The titrations were made in duplicate with a reproducibility of 0.1% or better.

(1) Abstracted in part from a thesis submitted in partial fulfillment of the requirements of the University of New England for the degree of Doctor of Philosophy.

(2) Department of Chemistry, University of Wisconsin, Madison 6, Wisconsin.

(3) R. H. Stokes, L. A. Woolf and R. Mills, THIS JOURNAL, **61**, 1634 (1957).

(4) R. H. Stokes, *J. Am. Chem. Soc.*, **72**, 763 (1950).

(5) R. H. Stokes and L. A. Woolf, *Anal. Chem.*, **29**, 1883 (1957).

(6) I. J. O'Donnell and L. J. Gosting in "The Structure of Electrolytic Solutions," W. J. Hamer (Ed.), John Wiley and Sons, Inc., New York, N. Y., 1959, p. 160.

(7) R. P. Wendt and L. J. Gosting, THIS JOURNAL, **63**, 1287 (1959).

(8) L. J. Gosting, *Advances in Protein Chem.*, **11**, 429 (1956).

(9) G. J. Hooyman, *Physica*, **22**, 751 (1956).

(10) See, for example, ref. 7 where numerous references to such derivations are recorded.

(11) S. R. de Groot, P. de Mazur and J. Th. G. Overbeek, *J. Chem. Phys.*, **20**, 1825 (1952).

TABLE I[a]

TRACER-DIFFUSION COEFFICIENTS OF HYDROGEN ION IN AQUEOUS ALKALI CHLORIDE SOLUTIONS AT 25°

KCl				NaCl				LiCl			
C	D	D/D^0	k	C	D	D/D^0	k	C	D	D/D^0	k
0.1605	7.958	0.855	−22.86	0.1090	8.011	0.860	−36.38	0.08917	7.789	0.837	−52.65
0.4806	7.934	.852	− 9.705	.5418	7.473	.802	− 8.467	.4240	7.244	.778	−11.46
1.002	7.729	.830	− 5.556	.8124	7.053	.757	− 4.701	1.010	6.283	.674	− 1.611
1.016	7.675	.825	− 5.015	1.442	6.552	.704	− 1.859	1.311	5.606	.602	+ 0.1453
1.712	7.244	.778	− 2.332	2.271	5.726	.615	− 0.3199	1.586	5.298	.569	2.519
2.883	6.423	.690	+ 0.1363	3.570	4.316	.464	+ 1.687	2.974	3.662	.393	5.555
3.629	5.936	.638	0.2637	4.545	3.460	.372	2.668	4.590	2.109	.227	6.682

[a] Units: concentration C, mole/l.; tracer-diffusion coefficient D, cm.²/sec. × 10^5; slope k, cm.²/l./mole/sec. × 10^5.

Successive dilutions of the initial 0.1 M acid stock solution with the 1 M acid-free solution were made to give solutions for the lower compartment of the diaphragm cell which enabled the diffusion measurements to cover the initial acid concentration range 0.01–0.1 M (or, averaging the acid concentration over both compartments of the cell, 0.005–0.05 M). The apparent "diffusion coefficients" D' then were plotted against initial (lower compartment) acid concentration and extrapolated linearly to zero value on the abscissa. The limiting diffusion coefficient D thus determined was taken to be the tracer-diffusion coefficient of hydrogen ion in the 1 M sodium chloride solution. This procedure was repeated for each solution of the three supporting electrolytes NaCl, KCl and LiCl, respectively. The supporting electrolyte solutions were prepared from either analytical reagent quality salt, as in the case of the NaCl and KCl solutions, or from LiCl prepared by the method of Stokes and Stokes.[12] Doubly distilled water was used in the preparation of all solutions.

Results

The extrapolation of the "diffusion coefficients" D' measured in each supporting electrolyte solution at finite acid concentrations c' moles/l. of hydrogen ion to give the tracer coefficient D at $c' = 0$ can be represented by the equation $D' = D + kc'$. Both D' and k are complicated functions of the diffusion coefficients and thermodynamic terms specifying each H_2O-HCl-MCl system. In Table I the D and k values are listed for the various supporting electrolyte concentrations, C. The values of D/D^0 are also given since they allow a direct comparison of the present results with the tracer diffusion coefficients of other ions. Here the limiting tracer diffusion coefficient D^0 is defined by the Nernst equation $D^0 = (RT/F^2)\lambda^0_{H^+}$ where R, T and F are the gas constant, absolute temperature and the faraday, respectively, and $\lambda^0_{H^+}$ is the limiting equivalent conductance of hydrogen ion in water.[13]

Discussion

The extrapolation procedure for obtaining the tracer diffusion coefficients has been discussed previously.[3] Extension of the theory of diffusion in the diaphragm cell to include multicomponent diffusion with interacting solute flows enables a mathematical confirmation of the method.[14] It is hoped that the details will be presented in a future publication. Some of the theory, together with approximate values of one cross diffusion coefficient in the system water-pentaerythritol-sodium chloride, has been given by Kelly and Stokes.[15]

Unfortunately the diaphragm cell method cannot be used for diffusion measurements at electrolyte concentrations much less than 0.1 M[4]; *i.e.*, it cannot be used in the range where the Onsager limiting law[16] is applicable. Therefore, in the absence of theoretical descriptions of tracer diffusion at the supporting electrolyte concentrations of this work, we are necessarily limited to comparison of our tracer diffusion results with those for other ions in solutions of the same supporting electrolytes, and to intercomparisons between the results obtained in the three supporting electrolytes. This procedure illustrates certain features of the concentration dependence of the hydrogen ion tracer diffusion.

Previous publications[17,18] have shown the similarity of the tracer diffusion of the cations Na^+, Rb^+ and Cs^+, and the anions Cl^-, Br^- and I^-, respectively, in the same supporting electrolyte solutions. In Fig. 1 the results for hydrogen ion are compared with corresponding values for sodium ion[17-20] representing a typical univalent cation and iodide ion,[3,19] as a typical univalent anion. A comparison, using the Onsager slopes,[16] defined here by

$$D/D^0 = 1 - k_1\sqrt{C}$$

where C is the concentration of the supporting electrolyte in moles/l., shows that the predicted values of D/D^0 for hydrogen ion at 0.1 M agree to about 2% with experiment, which is better than the agreement observed with either of the other ions. However, the Onsager limiting law has, even at 0.1 M, been used for a concentration at which it should not theoretically apply. Therefore use of it for further predictions at even higher supporting electrolyte concentrations cannot be justified, and one can only observe that the disparity between the Onsager slope and the experimental curve becomes increasingly larger for hydrogen ion with increase in C than do the corresponding cases for sodium and iodide ions. Alternatively, if we ignore the comparison using the Onsager slopes, we may note that the hydrogen ion tracer diffusion varies more with the change in supporting electrolyte concentration than does the diffusion of either of the other ions.

The predominating influences on tracer diffusion for concentration ranges similar to those of this work have been attributed to the solution macro-

(12) J. M. Stokes and R. H. Stokes, THIS JOURNAL, **60**, 217 (1956).
(13) Robinson and Stokes, "Electrolyte Solutions," Butterworth's Scientific Publications, England, 1955, p. 454.
(14) L. A. Woolf, Ph.D. Thesis, University of New England, Armidale, N.S.W., 1959.
(15) Private communication, to be published.
(16) L. Onsager, *Ann. N. Y. Acad. Sci.*, **46**, 246 (1945).
(17) R. Mills, THIS JOURNAL, **61**, 1631 (1957); **63**, 1873 (1959).
(18) R. Mills and L. A. Woolf, *ibid.*, **63**, 2068 (1959).
(19) R. Mills, *ibid.*, **61**, 1258 (1957).
(20) R. Mills, *J. Am. Chem. Soc.*, **77**, 6116 (1955).

scopic viscosity η/η_0, or some factor of similar numerical magnitude.[3,17,21-24] Attempts to allow for it have generally been made graphically by plotting $(D/D^0)(\eta/\eta_0)$ or $D\eta/\eta_0$ against $\sqrt{C}$. The result for the alkali metal and halogen ions studied so far has been to bring the resulting curves closer together while overcorrecting[3,17] the initial values by reversing the order of the viscosity corrected curves in comparison to the position of the uncorrected plots, D/D^0 *vs.* $\sqrt{C}$. The noncoincidence of the curves may be attributable to specific effects of the supporting electrolytes, and other factors.[20,22,23] In Fig. 2 $(D/D^0)(\eta/\eta_0)$ *vs.* $\sqrt{C}$ has been plotted for the hydrogen ion results of Table I. While the three curves KCl, NaCl and LiCl have been brought appreciably closer, particularly the KCl and NaCl, than in the D/D^0 *vs.* $\sqrt{C}$ graph, their order is not completely reversed being (in order of increasing negative slope) NaCl, KCl, LiCl instead of LiCl, NaCl, KCl as would be expected by analogy with the result of the same procedure for sodium and iodide ions. The position of the LiCl curve suggests that some factor, in addition to that approximately measured by the first power of the macroscopic viscosity, has a strong influence on the hydrogen ion transport in those solutions. In the sodium and potassium chloride solutions the factors affecting the diffusion of hydrogen ion appear to be similar.

A possible explanation of this unusual result of the viscosity correction is forthcoming when the effect of lithium ions on water structures is considered in relation to the mechanism of proton transport in aqueous solutions. Liquid water may be pictured[25-27] as a continuously varying mixture of structures, consisting of tetrahedrally coordinated water molecules held together by hydrogen bonds, interspersed amongst non-structure water molecules. The commonly accepted mode of hydrogen ion movement in pure water, or aqueous solution, is by the proton-jump transport mechanism[28] which pictures the proton as progressively moving from one water molecule to another within a hydrogen bonded lattice structure rather than *via* non-structure molecules. The rate-determining step of the transport of protons is the rate of formation of hydrogen bonds at the edge of the hydration structure.[29] As a first approximation we therefore would expect solutes to have less effect on hydrogen ion transport than on ions moving by the usual transport mechanisms.

Brady and Krause[30] and Brady,[31] from analysis of X-ray data of concentrated solutions, have suggested certain effects of potassium and lithium ions in the water structures: potassium ion (and, presumably, sodium ion) is of comparable size to a water molecule and may enter substitutionally into a water structure without causing any breakdown or marked distortion; lithium ion, because of a larger charge-size ratio, causes a breakdown of the

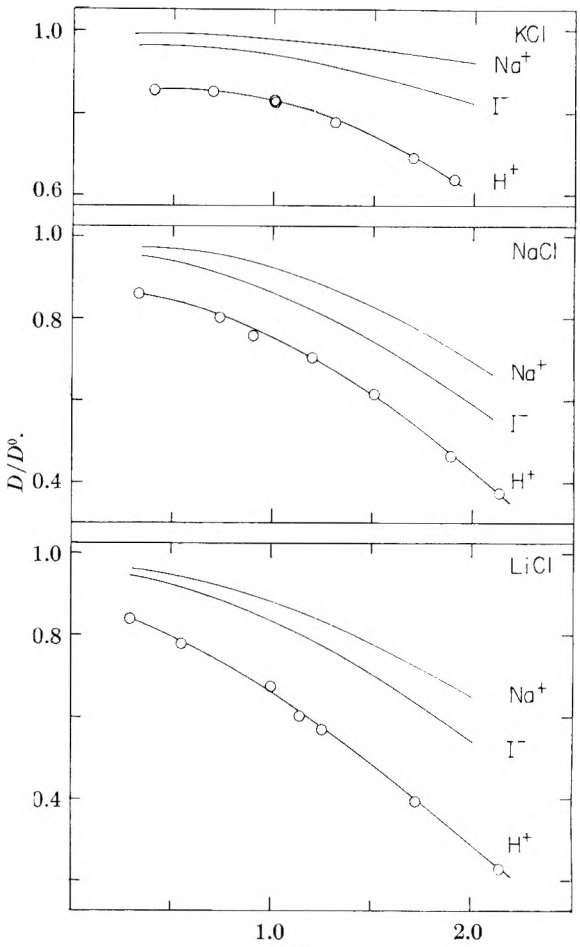

Fig. 1.—Na^+, I^- and H^+ tracer diffusion in KCl, NaCl and LiCl.

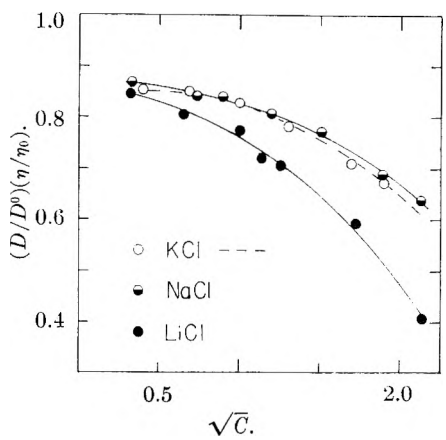

Fig. 2.—Viscosity product for H^+ tracer diffusion in KCl, NaCl and LiCl.

(21) J. E. Burkell and J. W. T. Spinks, *Can. J. Chem.*, **30**, 311 (1952).

(22) R. Mills and J. W. Kennedy, *J. Am. Chem. Soc.*, **75**, 5696 (1953).

(23) J. H. Wang, THIS JOURNAL, **58**, 686 (1954).

(24) R. Matuura and R. Shimozawa, *Mem. Fac. Sci. Kyushu University, Ser. C, (Chem.)*, **2**, 53 (1955).

(25) Ref. 13, chapter 1.

(26) *Disc. Faraday Soc.*, **24**, Part 3 (1957).

(27) J. A. Pople, *Proc. Roy. Soc., (London)*, **A205**, 163 (1951).

(28) A discussion of this mechanism and lists of many of the numerous articles on the subject may be found in: (a) ref. 26, (b) ref. 13, p. 116, (c) M. Eigen and L. deMaeyer in "The Structure of Electrolytic Solutions," W. Hamer, (Ed.), John Wiley and Sons, New York, N. Y., 1959, p. 64.

(29) Ref. 28 (c), p. 78; ref. 26, p. 190.

(30) G. W. Brady and J. T. Krause, *J. Chem. Phys.*, **27**, 304 (1957).

(31) G. W. Brady, *ibid.*, **28**, 464 (1958).

water structure at concentrations where, with potassium ion, the structure would predominate; the lithium ions and water molecules then reorient about the anions. If we may extend these ideas to the supporting electrolyte concentrations of this work a qualitative explanation is immediately obvious for the position of the LiCl curve in Fig. 2 and perhaps for the greater concentration dependence of the hydrogen ion tracer diffusion compared with other ions as shown in Fig. 1. The explanation may be stated briefly as follows: The tracer diffusion of hydrogen ion is affected not only by the usual processes influencing the tracer diffusion of other univalent ions, but may be additionally retarded by disruptions of the proton transport mechanism caused by the supporting electrolyte. This effect appears to be of particular importance in lithium chloride solutions.

It may be noted that values for the limiting conductance of hydrogen ion in several aqueous non-electrolyte solutions are available.[12,32,33] These data show that hydrogen ion is less hindered by the solution viscosity than are other univalent ions in the same solutions. This has been attributed to the proton jump mechanism being relatively unaffected by moderate concentrations of non-electrolytes. Comparison of the conductance data with the results of this paper (by use of Walden's rule and the Nernst equation) shows that hydrogen ion is considerably more retarded in the electrolyte solutions than in the non-electrolyte solutions of similar relative viscosities. This may be confirmatory evidence for the suggestions advanced in this paper of the influence of ions on proton transport in solution.

Acknowledgments.—It is a pleasure to acknowledge helpful discussions with Professor R. H. Stokes and Mr. F. J. Kelly of the University of New England, and criticism of the manuscript by Professor L. J. Gosting and Mr. R. P. Wendt of the University of Wisconsin.

(32) J. M. Stokes and R. H. Stokes, THIS JOURNAL, **62**, 497 (1958).
(33) B. J. Steel, J. M. Stokes and R. H. Stokes, *ibid.*, **62**, 1514 (1958).

THE SOLUBILITY, ACTIVITY COEFFICIENT AND HEAT OF SOLUTION OF SOLID XENON IN LIQUID ARGON[1]

BY W. H. YUNKER AND G. D. HALSEY, JR.

Department of Chemistry, University of Washington, Seattle 5, Washington

Received November 23, 1959

The liquid solutions of xenon in argon and krypton in argon and the solid solution of argon in xenon have been studied in the temperature range 84.0–87.5°K., using vapor pressure measurements. The solubility of Xe in Ar was found to be 4.14–5.01 ± 0.03 mole % Xe and the partial molar heat of solution of Xe in the infinitely dilute solution was found to be 632 ± 70 cal. per mole. For $\mu_{Xe} - \mu^0_{Xe} = RT \ln n_{Xe} + \alpha(1 - n_{Xe})^2$, α = 535 ± 58 cal. per mole. No saturation of Kr in Ar was reached in this region (up to 4.7%); α = 146 ± 30 cal. per mole. Argon was found to be less than 0.5% soluble in solid xenon.

Recently, work has been published from this Laboratory on solutions of rare gases dissolved in liquid argon and on solid solutions of rare gases. It seemed desirable to continue the study of solutions by considering the thermodynamics of a solid rare gas in liquid argon, *e.g.*, xenon and krypton. These systems represent some of the simplest examples of the solution in and saturation of a solvent by a solid solute.

Experimental

The experimental apparatus and technique was generally that of Karasz and Halsey,[2] but with certain changes.

The temperature of the solubility cell was maintained by liquid nitrogen under pressure up to three atmospheres (absolute). Use of liquid oxygen under reduced pressure was discontinued after it supported an electrical fire in the cell assembly. The cell and assembly was suspended in a thin wall (1 mm.) stainless steel can (4″ diameter and 28″ long) bolted to the underside of the brass plate to which the cell assembly was attached. The can was filled with liquid N_2 and surrounded with a dewar vessel. Pressure (hence temperature) was controlled by a 15 watt electrical spot heater, which was attached to the bottom of the stainless steel can, and a solenoid actuated exhaust valve, which was automatically operated from a vapor pressure thermometer. The vapor pressure thermometer was a copper-tipped glass tube which terminated directly below the cell in the liquid N_2. The solenoid valve was bypassed by a needle valve; another needle valve was on the exit side of the solenoid valve. This allowed a constant gas leak with an automatically regulated differential leak. The boiling of the liquid nitrogen acted to keep the liquid stirred. The cell was insulated with eight layers of "Scotch" #27 glass electrical tape, which maintained a seal through several cycles of starting and stopping the cryostat. Temperature fluctuation in the liquid nitrogen was regulated to a periodic (approx. 15 sec.) variation of ±0.1°, while the temperature fluctuation in the cell was ±0.005°K. (noted in the pure argon chamber adjacent to the solubility cell—this cell fluctuation could be reduced by using better insulation on the cell.) One cryostat filling lasted approximately eight hours.

Since the $P^0 - P$ readings were very sensitive to volatile impurities in the argon, especially at low concentrations, the vapor pressure of a small first fraction of distillate from a batch of purified argon was compared with the parent batch, and both with assay reagent argon, of less than 0.001% impurity. Maximum difference was always less than 0.015 cm. Most of this impurity would be removed with the first few fractions of argon as the concentration was increased, hence the last fractions were used to decrease the concentration.

Procedure.—All the solute gas for a run was condensed on the lower part of the cell first, then argon was added to fill the cell to about $^2/_3$ capacity. The mixture was shaken every few minutes for a period of several hours. This procedure assured that all the solute was transferred into the cell and that all the condensed solute was able to get into solution in the large amount of solvent at the beginning of the run. The extremely low vapor pressure of the solute

(1) Supported by contract AF 18(600)-987 with the Air Research and Development Command, U. S. Air Force.
(2) F. E. Karasz and G. D. Halsey, Jr., *J. Chem. Phys.*, **29**, 173 (1958).

at these temperatures prevented any detectable diffusion of it from the cell into the constant volume leg of the manometer system. Points were taken at successive removals of argon from the cell and checked by returning portions of argon to the cell. For each dose the temperature was adjusted to four standard settings. Randomization of the temperature and dose sequence acted as a check on equilibrium.

Thermodynamic Heat of Solution

We shall generally follow the treatment of Guggenheim.[3] For a substance in equilibrium between two phases, at constant pressure

$$\mu(T,n) = \mu'(T,n') \text{ and } d\mu(T,n) = d\mu'(T,n') \quad (1)$$

μ and n equal the partial molar free energy and mole fraction of the component in the respective phases, T is the temperature, the prime indicates the solid phase, and the unprimed the liquid. Hence

$$\left[\frac{\partial\mu}{\partial\, 1/T}\right]_n d\, 1/T + \left[\frac{\partial\mu}{\partial n}\right]_{1/T} dn = \left[\frac{\partial\mu'}{\partial\, 1/T}\right]_{n'} d\, 1/T + \left[\frac{\partial\mu'}{\partial n'}\right]_{1/T} dn' \quad (2)$$

Using

$$\mu = \bar{H} - T\bar{S} = \bar{H}' - T\bar{S}' = \mu' \quad (3)$$

in equation 2 gives

$$\left[\frac{\partial\mu}{\partial n}\right]_{1/T} dn + \left[\frac{\partial\mu'}{\partial n'}\right]_{1/T} dn' = -(\bar{H} - \bar{H}')\, T\, d\, 1/T = -\bar{L}_s T\, d\, 1/T \quad (4)$$

($\bar{L}_s$ is the partial molar heat of solution). We shall be concerned with the case of $n' = 1$, hence the second term on the l.h.s. of equation 4 equals zero.

If in the equation

$$\mu - \mu^0 = RT \ln n + \ln f \quad (5)$$

the activity coefficient is given by the expression $\ln f = \alpha (1 - n)^2/RT$, equation 4 becomes

$$\bar{L}_s = -R\left[1 - \frac{2\alpha n(1-n)}{RT}\right]\frac{d \ln n}{d\, 1/T} \quad (6)$$

From

$$\bar{H} = \frac{d\, \mu/T}{d\, 1/T} \quad (7)$$

the partial molar heat of solution at concentration n is

$$\bar{H} = \frac{d \ln f}{d\, 1/T} = \alpha(1-n)^2 \quad (8)$$

The partial molar heat of solution of the solid into an infinitely dilute solution, then, is

$$\bar{L}_s^0 = (\bar{H}_{sat} - \bar{H}') + (\bar{H}^0 - \bar{H}_{sat}) = \bar{L}_s + [\alpha - \alpha(1-n)^2] = \bar{L}_s + \alpha n(2-n) \quad (9)$$

Experimental Results

Xenon in Liquid Argon.—Since the partial pressure of xenon at this temperature is considerably less than 10^{-3} cm., the total pressure can be considered that of argon alone. A plot of $(P^0 - P)/P^0$ *vs.* n_{Xe} is shown in Fig. 1. For the portion of the isotherms below the saturation point, α (equation 5) was calculated for each experimental point. These α's were plotted as a function of concentration for each temperature. There is no detectable concentration dependence of α, the slight temperature dependence is within the probable error of the average over all measurements.

(3) E. A. Guggenheim, "Modern Thermodynamics," Methuen & Co. Ltd., London, 1933, p. 88.

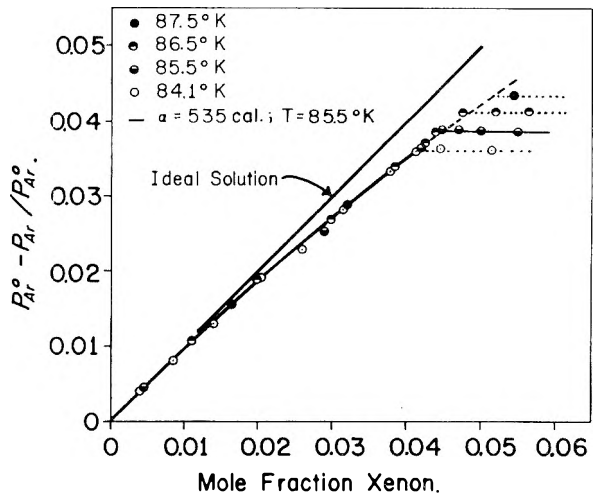

Fig. 1.—Vapor pressure lowering of liquid argon with increasing concentration of solute xenon. The horizontal portion indicates a saturated solution. The solid curved line is the isotherm for 85.5°K.

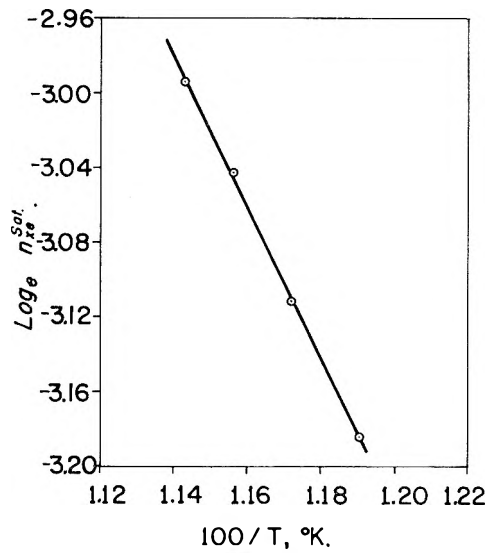

Fig. 2.—Ln n_{Xe}^{Sat} *vs.* $100/T$ °K.

Temp. (°K.)	α (cal./mole)
84.0	560 ± 55
85.5	536 ± 39
86.5	504 ± 39
87.5	504 ± 20
	Av. 535 ± 58

The isotherm at 85.5°K. generated by α_{av} is the curved line in Fig. 1. The straight line is the isotherm generated by Raoult's law.

The cell temperature changed very slowly with time as the liquid nitrogen level dropped (about 0.2°K. in eight hours). To test for equilibrium and to average measurements made at different temperatures, a plot of log $(P^0 - P)/P^0$ *vs.* $1/T$ was made. The points, taken under many combinations of elapsed time, temperature (reaching a point from higher or lower temperature), and concentration formed a good straight line. For each standard temperature, log $(P^0 - P)/P^0$ was changed to n_{Xe}^{sat} by use of the respective experimental isotherms. The slope of a ln n_{Xe}^{sat} *vs.* $1/T$ plot, Fig. 2, was -406.

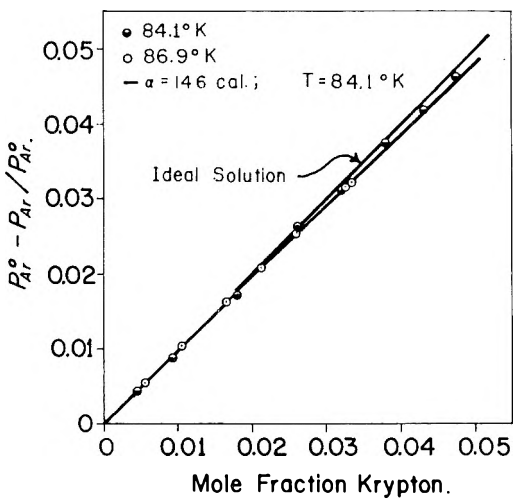

Fig. 3.—Vapor pressure lowering of liquid argon with increasing concentration of solute krypton. The solid curved line is the isotherm for 84.1°K.

Using α_{av}, and mean values for n_{Xe}^{sat} and T (0.0457 and 85.8°K., respectively) in equations 6 and 9, $\bar{L}_s^0 = 632 \pm 70$ cal. per mole.

Argon in Solid Xenon.—Singleton and Halsey[4] showed that Ar and Xe were insoluble in the solid phase at 78°K. Since the solubility would be expected to increase with temperature, it was necessary to check for a solid solution at these temperatures. This was done by condensing a relatively large amount of xenon in the cell, and adding a small amount of argon to it. Isotherms were determined in the same manner as the isotherms for the liquid solution. Results indicated a solubility of less than 0.5% Ar with no detectable temperature dependence.

If the solid phase is a solution of composition 0.5% Ar, its properties will follow an equation of the same form as the liquid solution and analogous solid solutions,[5,6] *i.e.*

$$\mu = \mu^0 + RT \ln n' + \beta(1 - n')^2 \qquad (10)$$

The complete form of equation 6 will be

$$\bar{L}_s = -R\left\{\left[1 - \frac{2\alpha n(1-n)}{RT}\right]\frac{d \ln n}{d\ 1/T} + \left[1 - \frac{2\beta n'(1-n')}{RT}\right]\frac{d \ln n'}{d\ 1/T}\right\} \qquad (11)$$

Assuming β to be of a magnitude comparable with analogous systems,[5,6] the term $2\beta(1 - n')/RT \ll 1$ and therefore need not be considered. This leaves d ln n'/d $1/T$ as the contributing factor. The magnitude of this term can be estimated by using the approximate solubility in the solid phase and the known separation of the isotherms under saturated conditions, on the $(P^0 - P)/P^0$ *vs.* n_{Xe} plot. If one assumes that $n_{Ar}^{sat} = 0.005$ at 84.1°K., then for d ln n'/d $1/T$ to be equal to 25 cal., n_{Ar}^{sat} would have to be in excess of 0.010 at 87.5°K. Such a condition is contradictory to the above experimental measurements. Therefore any contribution to the heat of solution from an impure solid phase is less than the experimental error.

Krypton in Liquid Argon.—A preliminary determination of two isotherms for the krypton–argon system was made in the manner described above. No detectable temperature dependence of α was found (within experimental error) as can be seen in Fig. 3. No saturated solution was found in the range measured (limited by the maximum pressure the apparatus could handle). This result is in agreement with the work of Heastie and Jones.[7] The average value of α was 146 ± 30 cal. per mole.

Conclusions

$\bar{L}_s^0$ depends on the heat of immersing xenon atoms in a liquid argon "atmosphere." This heat can be satisfactorily represented by a theoretical calculation using the Kirkwood-Müller formula[8] but the result is too sensitive to choice of lattice parameter to be of value. Since α is approximately equal to $\bar{L}_s^0$, the excess entropy of solution is essentially zero. The second virial coefficient for the solution $B(T)$, is α/RT. The argon–xenon(liquid) solution appears to be a very good example of a strictly regular solution,[9] in that within experimental error, the osmotic properties can be calculated from the heat of solution.

(4) J. H. Singleton and G. D. Halsey, Jr., THIS JOURNAL, **58**, 330 (1954).
(5) M. Freeman and G. D. Halsey, Jr., *ibid.*, **60**, 1119 (1956).
(6) J. F. Walling and G. D. Halsey, Jr., *ibid.*, **62**, 752 (1958).
(7) R. Heastie and G. O. Jones, *Nuovo Cimento*, **9**, suppl. #1, 365 (1958).
(8) A. Müller, *Proc. Roy. Soc. (London)*, **A154**, 624 (1936).
(9) E. A. Guggenheim, "Mixtures," Oxford University Press, London, 1952, p. 29.

A STUDY OF THE VOLATILE CHARACTERISTICS OF VARIOUS METAL β-DIKETONE CHELATES

BY EUGENE W. BERG AND JOSEPH T. TRUEMPER

Coates Chemical Laboratories, Louisiana State University, Baton Rouge, Louisiana

Received November 30, 1959

Vapor pressure–temperature data were determined for a series of metal β-diketone chelates. The ligand was varied by the systematic substitution of alkyl, fluorinated alkyl, aromatic, and heterocyclic groups in lieu of R and R′ in the formula

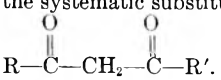

R—C—CH₂—C—R′. The molar heats of sublimation (vaporization) of these compounds were calculated from the vapor pressure–temperature data and used as the criterion for the degree of volatility as follows: the higher the molar heat of sublimation, the less volatile the compound. An attempt was made to relate compound volatility with the nature of the central metal atom and the structure of the ligand. The degree of volatility appeared to be related to the molecular symmetry and polarity of the molecule as follows: spherical molecules (given by a tetrahedral and octahedral arrangement of the metal coördination bonds) of the non-fluorinated compounds were more volatile than planar molecules. Substitution of the trifluoromethyl for the methyl group increased polarity and decreased volatility. The substitution of aromatic and heterocyclic groups for a methyl group apparently decreased volatility with increased polarity of the molecule.

The inner complexes formed between metallic ions and β-diketones are unusual in that they possess properties one normally associates with pure organic compounds. They can be insoluble in water, soluble in non-polar solvents, and volatile. The literature contains a number of reports which mention the volatile character of some metal chelates. Sidgwick[1] has collected a number of these references concerning the metal chelates of acetylacetone, acetoacetic ester, benzoylacetone and dibenzoylmethane. Other review sources[2–4] also contain similar references pertaining to the volatile character of some metal β-diketone chelates. Most of these references are quite sketchy and give little valuable information. Staniforth[5] investigated metal chelates of acetylacetone and other β-diketones to find compounds of greater volatility than the simple acetylacetonates. His approach was to replace hydrogen atoms in acetylacetone with fluorine and thereby increase the covalent character of the resulting compound. He was able to demonstrate that the fluorinated ligands produced chelates that were generally lower melting, thermally more stable, and more easily sublimed than the chelates formed with acetylacetone.

Wish and Bolomey[6] reported that the chelates of 2-thenoyltrifluoroacetone were not volatile under ordinary conditions. However, they reported that some could be sublimed at reduced pressures.

A survey of the literature failed to yield any comprehensive report of studies attempting to measure the degree of volatility of these chelates or correlating the available data with molecular structure. Consequently this study was undertaken. Vapor pressure–temperature curves were determined[7] for the chelates prepared from six different ligands and seven metal ions. The effect of the structure of the ligand on the volatility of the chelate was evaluated by the systematic substitution of alkyl, fluorinated alkyl, aromatic and heterocyclic groups *in lieu* of R and R′ in the β-diketone prototype

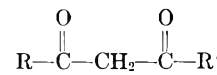

The ligands used are listed along with convenient abbreviations in Table I. The central metal atoms were beryllium(II), aluminum(III), manganese(II), iron(III), cobalt(II), nickel(II) and copper(II).

Size, shape and polarity of the molecules were considered as fundamental factors affecting volatility. Thus, it would seem reasonable that a correlation would exist between volatility and the nature of the central metal atom and the nature of the ligand. The directed coördination bonds of the metal contribute to the shape and polarity of the molecule. The number of these bonds dictates size by controlling the number of coördinating groups. Similarly, the structure of the ligand also affects the size, shape and polarity of the molecule.

Experimental

1. **Source of β-Diketones.**—Acetylacetone (Eastman Kodak), benzoylacetone (Mid-Continent Chemical Co.), and 2-thenoyltrifluoroacetone (University of California) were available commercially. These products were purified by distillation, recrystallization and sublimation, respectively. Acetyltrifluoroacetone, benzoyltrifluoroacetone and 2-furoyltrifluoroacetone were prepared by the method of Reid and Calvin.[8]

2. **Preparation of the Chelates.**—The following general method was used for the preparation of the chelates. The nitrate salt (except for beryllium as sulfate) of the metal was made up as a 5 weight % solution and buffered immediately before use by adding 5 g. of sodium acetate for every 100 ml. of solution. The buffered metal ion solution was shaken with an alcoholic solution of the ligand until reaction appeared complete. After precipitation the chelate was collected by filtration and treated according to the description below.

Tris-(acetylacetonato)-aluminum(III): the white precipitate was washed with water, recrystallized from ethanol and water and dried at 100°, m.p. 112° (reported[9,10] 112°).

(1) N. V. Sidgwick, "The Chemical Elements and Their Compounds," Vols. I and II, Oxford University Press, London, 1950.

(2) J. C. Bailar, Jr., "The Chemistry of the Coördination Compounds, Reinhold Publ. Corp., New York, N. Y., 1956.

(3) H. Diehl, *Chem. Revs.*, **21**, 39 (1937).

(4) W. C. Fernelius, "Inorganic Syntheses," Vol. II, McGraw-Hill Book Co., New York, N. Y., 1946.

(5) R. A. Staniforth, "Chelate Compounds of the Rare Earth Metals," Dissertation, Ohio State University, 1943.

(6) L. Wish and R. A. Bolomey, *J. Am. Chem. Soc.*, **72**, 4486 (1950).

(7) J. T. Truemper, "A Study of the Volatile Characteristics of Various Metal β-Diketone Chelate Compounds," Dissertation, Louisiana State University, 1959.

(8) J. C. Reid and M. Calvin, *J. Am. Chem. Soc.*, **72**, 2948 (1950).

(9) Fernelius, ref. 4, p. 32.

(10) Sidgwick, ref. 1.

TABLE I

β-DIKETONES INVESTIGATED

Common name	I.U.C. name	Abbreviation
Acetylacetone	2,4-Pentanedione	AA
Acetyltrifluoroacetone	1,1,1-Trifluoro-2,4-pentanedione	ATA
Benzoylacetone	1-Phenyl-1,3-butanedione	BA
Benzoyltrifluoroacetone	1-Phenyl-4,4,4-trifluoro-1,3-butanedione	BTA
2-Furoyltrifluoroacetone	1-(2-Furoyl)-4,4,4-trifluoro-1,3-butanedione	FTA
2-Thenoyltrifluoroacetone	1-(2-Thenoyl)-4,4,4-trifluoro-1,3-butanedione	TTA

Bis-(acetylacetonato)-beryllium(II): white, sublimed at 90° at 0.2 mm. of mercury, m.p. 108° (reported[9,10] 108°).

Bis-(acetylacetonato)-cobalt(II): washed with water and air dried. Sublimed (red) at 120° at 0.2 mm. of mercury. No melting points reported but sublimate identical to that described by Gach[11] with composition $Co(C_5H_7O_2)_2$.

Bis-(acetylacetonato)-copper(II): blue; recrystallized from benzene and dried at 110°, dec. above 230° (reported[5,10] dec. above 230°).

Tris-(acetylacetonato)-iron(III): red; sublimed at 80° at 0.2 mm. of mercury, m.p. 179° (reported[10] 179°).

Bis-(acetylacetonato)-manganese(II): prepared according to Emmert, *et al.*[12] The yellow hydrate dehydrated at 50° at reduced pressure to white compound; no m.p., sharp dec. below 290° (*Anal.* Calcd. for $MnC_{10}H_{14}O_4$: Mn, 21.70. Found: Mn, 21.70.)

Bis-(acetylacetonato)-nickel(II): the green precipitate was washed with ethanol and water and dried at 50° at 0.5 mm., dec. 230° (*Anal.* Calcd. for $NiC_{10}H_{14}O_4$: Ni, 22.85. Found: Ni, 22.85.)

Tris-(acetyltrifluoroacetonato)-aluminum (III): white; air dried and sublimed at 100° at 0.5 mm., m.p. 117° (reported[5] 117°).

Bis-(acetyltrifluoroacetonato)-beryllium(II): white; air dried and sublimed at 100° at 0.5 mm., m.p. 112° (reported[5] 112°).

Bis-(acetyltrifluoroacetonato)-copper(II): blue; recrystallized from benzene and dried at 110° at 0.5 mm., m.p. 200° (reported[5] 189°). (*Anal.* Calcd. for $CuC_{10}H_8O_4F_6$: Cu, 17.19. Found: Cu, 17.26.)

Tris-(acetyltrifluoroacetonato)-iron (III): red; recrystallized from petroluem ether and dried at 50° at 0.5 mm., m.p. 115°. (*Anal.* Calcd. for $FeC_{15}H_{12}O_6F_9$: Fe, 10.84. Found: Fe, 10.84.)

Bis-(acetyltrifluoroacetonato)-nickel(II): green; sublimed at 150° at 0.5 mm. (*Anal.* Calcd. for $NiC_{10}H_8O_4F_6$: Ni, 16.09. Found: Ni, 16.10.)

Tris-(benzoylacetonato)-aluminum(III): white; recrystallized from ethanol and dried at 110; m.p. 224–225° (reported[13] 217°) (*Anal.* Calcd. for $AlC_{30}H_{27}O_6$: Al, 5.28. Found: 5.26.)

Bis-(benzoylacetonato)-beryllium(II): white; recrystallized from benzene, washed with petroleum ether, and air dried or sublimed at 140° at 0.5 mm., m.p. 213° (reported[14] 211°).

Bis-(benzoylacetonato)-copper(II): blue; recrystallized from ethanol and water and dried at 110°, m.p. 197° (reported[15] 195–196°).

Bis-(benzoylacetonato)-cobalt(II): red; recrystallized from ethanol and dried at 50° at 0.5 mm., m.p. 181° (reported[16] 180°).

Tris-(benzoylacetonato)-iron(III): red; recrystallized from benzene and petroleum ether and dried at 50° at 0.5 mm., m.p. 222–224° (reported[17] 224–225°).

Bis-(benzoylacetonato)-manganese(II): yellow precipitate washed with ethanol and then ether and dried in nitrogen atmosphere at 90° for 6 hours at 0.5 mm., dec. above 140° (*Anal.* Calcd. for $Mn_{20}H_{18}O_4$: Mn, 14.56. Found: Mn, 14.52.)

Tris-(benzoyltrifluoroacetonato)-aluminum(III): white; recrystallized from benzene and petroleum ether and dried at 50°, m.p. 173–174°. (*Anal.* Calcd. for $AlC_{30}H_{18}O_6F_9$: Al, 4.012. Found: Al, 3.997.)

Bis-(benzoyltrifluoroacetonato)-beryllium(II): white; recrystallized from ethanol and dried at 50° at 0.5 mm., m.p. 143–144.° Commercial carbon, hydrogen and beryllium analyses gave erratic results.

Bis-(benzoyltrifluoroacetonato)-cobalt (II): yellow; recrystallized from alcohol and water and dehydrated at 85° at 0.2 mm., m.p. 158°. (*Anal.* Calcd. for $CoH_{12}O_4F_6$: Co, 12.04. Found: Co, 12.00.)

Bis-(benzoyltrifluoroacetonato)-copper(II): green; prepared by method of Reid and Calvin,[8] m.p. 241° (reported 243–244°).

Tris-(benzoyltrifluoroacetonato)-iron(III): red; recrystallized from petroleum ether and dried at 50° at 0.5 mm., m.p. 128–129.° (*Anal.* Calcd. for $FeC_{30}H_{18}O_6F_9$: Fe, 7.964. Found: Fe, 8.021.)

Bis-(benzoyltrifluoroacetonato)-manganese(II): yellow; recrystallized from ethanol and dehydrated at 85° at 0.5 mm., m.p. 129–130°. (*Anal.* Calcd. for $MnC_{20}H_{12}O_4F_6$: Mn, 11.32. Found: Mn, 11.36.)

Bis-(benzoyltrifluoroacetonato)-nickel(II): green; recrystallized from ethanol and benzene and dried at 55° at 0.5 mm. (*Anal.* Calcd. for $NiC_{20}H_{12}O_4F_6 \cdot 2H_2O$: Ni, 11.18. Found: Ni, 11.12.) Product dehydrated by heating at 175° for 6 hours at 0.5 mm., m.p. 223–224°. (*Anal.* Calcd. for $NiC_{20}H_{12}O_4F_6$: Ni, 12.00. Found: Ni, 12.05.)

Tris-(2-furoyltrifluoroacetonato)-aluminum(III): white; recrystallized from benzene and petroleum ether and dried at 50° at 0.5 mm., m.p. 204–205°. (*Anal.* Calcd. for $AlC_{24}H_{12}O_9F_9$: Al, 4.200. Found: Al, 4.216.)

Bis-(2-furoyltrifluoroacetonato)-beryllium(II): white; recrystallized from alcohol, and dried at 50° at 0.5 mm., m.p. 169–170°. Commercial carbon, hydrogen and beryllium analyses gave erratic results.

Bis-(2-furoyltrifluoroacetonato)-cobalt(II): yellow; recrystallized from ethanol and water and dehydrated at 88° at 0.5 mm. Compound darkened at 190° and melted at 215–220°. (*Anal.* Calcd. for $CoC_{16}H_8O_6F_6$: Co, 12.56. Found: Co, 12.51.)

Bis-(2-furoyltrifluoroacetonato)-copper(II): green; prepared by method of Reid and Calvin,[8] m.p. 227–228° (reported 226–228°).

Tris-(2-furoyltrifluoroacetonato)-iron(III): red; recrystallized from benzene and dried at 75° at 0.5 mm., m.p. 207–208°. (*Anal.* Calcd. for $FeC_{24}H_{12}O_9F_9$: Fe, 8.321. Found: Fe, 8.320.)

Bis-(2-furoyltrifluoroacetonato)-manganese(II): yellow; recrystallized from ethanol and water, air dried and dehydrated at 90° at 0.5 mm. for three hours. Orange; gradual melting 146–149°. (*Anal.* Calcd. for $MnC_{16}H_8O_6F_6$: Mn, 11.81. Found: Mn, 11.74.)

Bis-(2-furoyltrifluoroacetonato)-nickel(II): recrystallized from ethanol and water and dried at 50° at 0.5 mm., green. (*Anal.* Calcd. for $NiC_{16}H_8O_6F_6 \cdot 2H_2O$: Ni, 11.63. Found: Ni, 11.71.) The product was heated for four hours at 160° at 0.5 mm. Color changed from green to yellow, m.p. 293–296°. (*Anal.* Calcd. for $NiC_{16}H_{10}O_6F_6$: Ni, 12.52. Found: Ni, 12.61.)

Tris-(2-thenoyltrifluoroacetonato)-aluminum(III): white; recrystallized from ethanol and water and dried at 50° at 0.5 mm., m.p. 203–205°. (*Anal.* Calcd. for $AlC_{24}H_{12}O_6S_3F_9$: Al, 3.907. Found: Al, 3.880).

Bis-(2-thenoyltrifluoroacetonato)-beryllium(II): white; recrystallized from ethanol and dried at 50° at 0.5 mm., m.p. 169–170°. (*Anal.* Calcd. for $BeC_{16}H_8O_4S_2F_6$: C, 42.58; H, 1.786. Found: C, 41.28; 1.88. Commercial analysis for Be erratic.)

Bis-(2-thenoyltrifluoroacetonato)-cobalt(II): yellow; recrystallized from ethanol and dried at 50° at 0.5 mm. (*Anal.* Calcd. for $CoC_{16}H_8O_4S_2F_6 \cdot 2H_2O$: Co, 10.93. Found Co, 10.90.) Product dehydrated by heating for 3 hours at 100° and 0.5 mm. Compound darkens at 200° and changes from solid to dark liquid at 215°. (*Anal.* Calcd. for $CoC_{16}H_8O_4S_2F_6$: Co, 11.76. Found: Co, 11.69.)

Bis-(2-thenoyltrifluoroacetonato)-copper(II): green; prepared by method of Reid and Calvin,[8] m.p. 242–243° (reported 242–243°).

(11) F. Gach, *Monatsh.*, **21**, 106 (1900).

(12) B. Emmert, H. Gsottschneider and H. Stanger, *Ber.*, **69B**, 1319 (1936).

(13) E. C. Baly and C. H. Desch, *J. Chem. Soc.*, **87**, 773 (1905).

(14) H. S. Booth and D. G. Pierce, THIS JOURNAL, **37**, 59 (1933).

(15) W. Wislicenus and W. Stoeber, *Ber.*, **35**, 545 (1902).

(16) C. Musante, *Gazz. chim. ital.*, **76**, 123 (1946).

(17) W. Wislicenus and W. Stoeber, *Ber.*, **35**, 550 (1902).

Tris-(2-thenoyltrifluoroacetonato)-iron(III): red; recrystallized from petroleum ether and dried at 50° at 0.5 mm., m.p. 159–160°. (*Anal.* Calcd. for $FeC_{24}H_{12}O_6S_3F_2$: Fe, 7.763. Found: Fe, 7.700.)

Bis-(2-thenoyltrifluoroacetonato)-manganese(II): recrystallized from ethanol and water and dehydrated by heating for three hours at 90° and 0.5 mm. Color changed from yellow to orange, m.p. 177–179°. (*Anal.* Calcd. for $MnC_{16}H_8O_4S_2F_6$: Mn, 11.05. Found: Mn, 11.10.)

Bis-(2-thenyltrifluoroacetonato)-nickel(II): recrystallized from ethanol and water and dried at 100° at 0.2 mm., compound green. (*Anal.* Calcd. for $NiC_{16}H_8O_4S_2F_6 \cdot 2H_2O$: Ni, 10.72. Found: Ni, 10.80.) Compound dehydrated by heating for five hours at 180° at 0.5 mm. Color changed to yellow; gradual melting 291–295°. (*Anal.* Calcd. for $NiC_{16}H_8O_4S_2F_6$: Ni, 11.49. Found: Ni, 11.52.)

3. Vapor Pressure–Temperature Measurements.—Vapor pressure–temperature data were obtained by utilizing a technique proposed by Smith and Menzies[18] and modified by Booth and Halbedel.[19] Samples showing a temperature hysteresis were discarded and fresh runs were made at lower maximum temperatures until no hysteresis was observed. Thermal decomposition thus limited the upper temperatures studied. Exact decomposition temperatures at reduced pressures were not determinable. Some of the compounds decomposed at such low temperatures that only a limited amount of data was collected. In such instances the calculation of the molar heat of vaporization or sublimation must be considered as only approximate.

A check of the method for measuring vapor pressure at various temperatures was made by measuring the vapor pressure of mercury and of benzoic acid. For pressures below 4 mm. an error of ±0.05 mm. was observed and for pressures up to 600 mm. an error of ±1 mm. was estimated. The precision for the range of pressures covered with the cathotometer was ±0.02 mm. The precision for the range of pressures over which the manometer was used was ±1 mm.

The plot of the logarithm of the vapor pressure *vs.* 1/T was done in accordance with the Clausius–Clapeyron equation for determining the molar heats of vaporization.

Discussion

Representative plots of the vapor pressure *vs.* the reciprocal of the absolute temperature for various chelates are given in Figs. 1 and 2 to illustrate the linearity of such data. The molar heats of sublimation of some chelates are given in Table II. An evaluation of the data indicates that certain molecular factors are determinative with regard to the magnitude of the molar heat of sublimation but these factors cannot be sharply divided according to the nature of the metal and the structure of the ligand. Rather, the factors involve the consequences of an interplay of these two items.

TABLE II

MOLAR HEATS OF SUBLIMATION (KCAL.) OF SOME β-DIKETONE CHELATE COMPOUNDS[a]

Spatial arrangement	Metal	Ligand AA	ATA	BA	BTA	FTA	TTA
Octahedral	Al	4.58	9.56	(4.90)	13.2	...	11.1
	Fe	4.67	20.8	(2.68)	8.56	(14.3)	11.1
Tetrahedral	Be	8.51	7.28	4.71	(3.93)	7.78	...
Planar	Ni	16.5	(8.14)	10.1	(0.915)	4.51	5.95
	Co	15.0	...	(22.9)	...	...	(4.24)
	Cu	..	12.1	...	...	3.53	...

[a] Values in parentheses considered approximate; ..., insufficient data for calculation.

Tetrahedral and octahedral arrangements of the coördination bonds of the metal result in the formation of roughly spherical molecules. Planar molecules result from the four coplanar arrangement of the coördination bonds of the metal. It is assumed that the tetra-coördinated chelates of Co(II), Ni(II) and Cu(II) are planar.

Non-fluorinated chelates whose central metal atoms possess octahedral or tetrahedral configurations have lower molar heats of sublimation than those with planar configurations. This can be explained by the fact that planar molecules can pack more closely in layers in the solid state than the spherically shaped molecules. Thus more energy would be required to place the planar molecules into

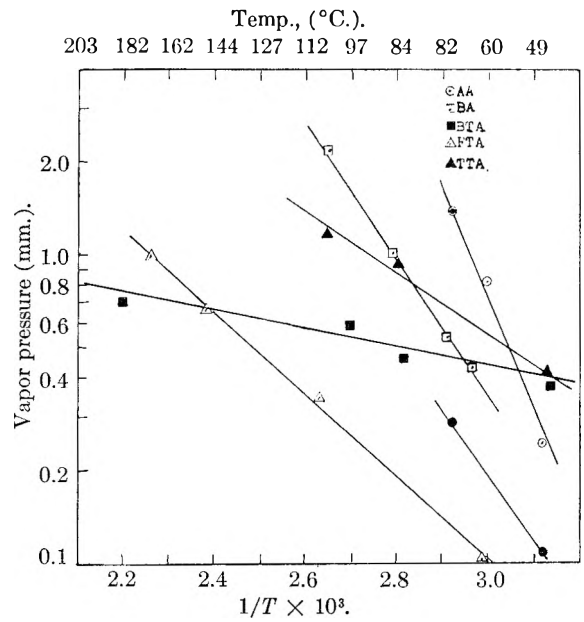

Fig. 1.—Vapor pressure *vs.* $1/T$ for some β-diketone chelate compounds of nickel(II).

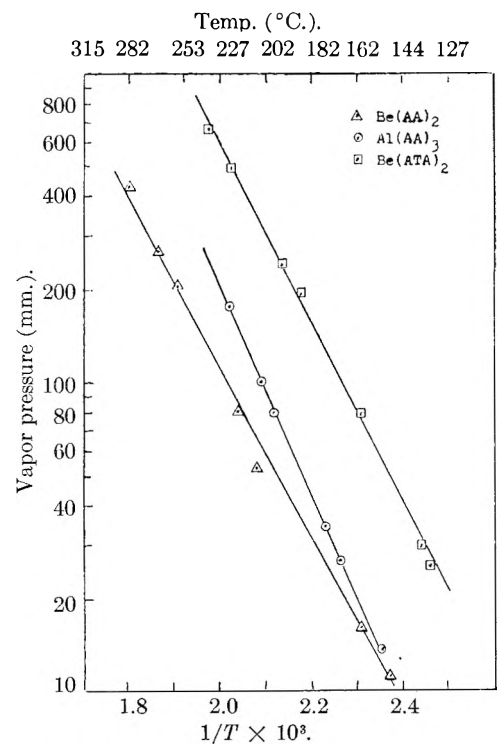

Fig. 2.—Vapor pressure *vs.* $1/T$ for some molten β-diketone chelate compounds of aluminum(III) and beryllium(II).

(18) A. Smith and A. Menzies, *J. Am. Chem. Soc.*, **32**, 1412 (1910).
(19) H. S. Booth and H. S. Halbedel, *ibid.*, **68**, 2652 (1946).

the gaseous state and they would have the higher molar heat of sublimation.

In the case of the fluorinated compounds, the planar configuration results in a lower heat of sublimation. This can be explained by the fact that the trifluoromethyl group can give rise to a polarization phenomenon and to the formation of dipoles. A comparison of the chelates of acetylacetone with acetyltrifluoroacetone and benzoylacetone with benzoyltrifluoroacetone shows that trifluoromethylation increased the molar heat of sublimation for iron and aluminum compounds and reduced it for beryllium and nickel compounds.

Though not conclusive, some indication of the contributions made by dipole interactions can be obtained from the data. When there was an octahedral arrangement of the coördination bonds, the molar heats of sublimation were higher. All such arrangements result in having at least one trifluoromethyl group opposing a non-polarizing group along a line drawn approximately through the centers of these groups and the central metal atom. The opposing arrangement forms a dipole and the dipolar molecules attract one another in the crystalline state and require more energy to be vaporized. This could explain the higher molar heat of sublimation for the fluorinated compounds of iron and aluminum compared to the corresponding non-fluorinated compounds. In the tetrahedral arrangement around the beryllium atom, it is possible that the polar groups are arranged so that no dipoles are created. The trend in the observed molar heats of sublimation indicates that the arrangement did not create dipoles. Rather, the lower molar heats of sublimation indicate that a repulsion of the molecules was operative. In the planar arrangement, it is possible to arrange the polar groups either *cis* or *trans*. In the former case, a dipolar molecule would result and in the latter a non-polar molecule. The lower molar heat of sublimation for the nickel compound indicates that the *trans* arrangement was preferred and that repulsion of the molecules was also likely.

When aromatic and heterocyclic groups were substituted for a methyl group in the ligand, two distinct orders were observed for increasing heats of sublimation. For the compounds of aluminum, cobalt and manganese, the heats of sublimation increased in the order of substitution: methyl, thenyl, phenyl and furyl. One exception to this order was the methyl group in the cobalt compounds. For the compounds of beryllium, iron, nickel and copper the order was phenyl, thenyl, furyl and methyl. Two exceptions were the methyl group in the beryllium compounds and the furyl group in the nickel compounds. The second order happens to be the same as the order of decreasing aromatic character of the substituent group which suggests that greater resonance in the compounds results in a more even electronic distribution in the molecule and a lower dipole moment. Thus it would appear that varying degrees of resonance contribution to the molecule would result in a series of increasing heats of sublimation in the order of substitution of phenyl, thenyl, furyl and methyl. The above explanation leaves the compounds of aluminum, cobalt and manganese and the methyl compound of beryllium and the furyl compound of nickel in an anomalous position.

An approximate order of thermal stability (Table III) was established from the temperatures

TABLE III

ORDER OF THERMAL STABILITY OF SOME β-DIKETONE CHELATE COMPOUNDS ARRANGED ACCORDING TO THE METAL ATOM

Ligand	Metal						
AA	Be	Al	Fe	Co	Ni		Cu and Mn
BA	Be	Fe	Ni	Co and Al			Cu and Mn
ATA	Be and Al	Cu	Ni	Fe			Co and Mn
BTA	Ni	Cu	Be	Al	Fe and Mn		Co
FTA	Ni	Be	Cu	Mn	Fe	Co	Al
TTA	Fe	Al	Ni	Co	Mn	Cu	Be

at which decomposition was suspected. There was some resemblance of the general order, when arranged by the metal atoms, to the order of stabilities in solution that was found for a large number of chelate compounds, this order being: copper, beryllium, iron, nickel, cobalt and manganese.[20] Several other generalizations were possible. Aluminum and beryllium compounds were among the more stable ones and manganese among the less stable. Trifluoromethylation increased the thermal stability of the nickel and copper compounds but decreased the stability of the iron and cobalt compounds with one exception, tris-(2-thenoyltrifluoroacetonato)-iron(III).

An exceptionally stable set of hydrated compounds were encountered. These were the dihydrates of bis-(benzoyltrifluoroacetonato)-, bis-(2-furoyltrifluoroacetonato)- and the bis-(2-thenoyltrifluoroacetonato)-nickel(II) compounds. Dihydrates of the compounds of manganese and cobalt were also encountered, but analyses indicated that these were successfully dehydrated at 60° at reduced pressures. Presumably, the acetylacetone, benzoylacetone and acetyltrifluoroacetone compounds of nickel were also dihydrates.

Acknowledgment.—This contribution[21] was supported in part by the Celanese Corporation of America.

(20) Bailar, ref. 2, p. 179.

(21) Presented in part at Southwest Regional Meeting of American Chemical Society, San Antonio, Dec., 1958.

THE MECHANISM AND KINETICS OF THE DEHYDRATION OF CALCIUM HYDROGEN PHOSPHATE DIHYDRATE

BY J. G. RABATIN, R. H. GALE AND A. E. NEWKIRK

Luminescent Materials Laboratory, Lamp Metals & Components Department, General Electric Company, 1099 Ivanhoe Road, Cleveland 10, Ohio

Received December 14, 1959

The dehydration of $CaHPO_4 \cdot 2H_2O$ in dry air, humid air, and at various pressures of N_2 was studied by means of thermogravimetric, differential thermal and X-ray diffraction methods. It was found that in humid air or at three or more atmospheres of N_2 the dehydration is catalyzed by moisture and proceeds in a single reaction at 135° or lower to form anhydrous $CaHPO_4$. In the absence of moisture the reaction is complex involving several changes including formation of an amorphous phase. This phase persists on further heating even after the formation of $Ca_2P_2O_7$ at 430° until recrystallization occurs at 530°.

Introduction

In 1948, Boullé[1] noted that thermogravimetric analyses indicated stepwise dehydration of $CaHPO_4 \cdot 2H_2O$ between 100 and 225° in dry air. Vol'fkovich and Urosov[2] have found by differential thermal analysis that at vapor pressures of water between 25 and 100 mm. the dehydration occurred in three steps at 100–110°, 127–142° and 172–175°. Boullé and duPont[3] have also found that the dehydration proceeds similarly *in vacuo*. More recently Boullé and duPont[4] have reported that the anhydrous $CaHPO_4$ obtained by heating $CaHPO_4 \cdot 2H_2O$ in humid air shows well-defined crystals and more distinct X-ray diffraction patterns compared to the dry air dehydrated product.

The present investigation was undertaken to clarify further the mechanism and kinetics of the dehydration of $CaHPO_4 \cdot 2H_2O$ both in dry air and in a humid atmosphere. The unique effect of pressure of dry gases on the dehydration mechanism of $CaHPO_4 \cdot 2H_2O$ also was studied.

Experimental

Thermogravimetric Analyses (TGA).—A pen-recording Chevenard type thermobalance was used for the TGA studies. A heating rate of 5° per minute was used for all analyses except those performed at constant temperature. The performance characteristics of the Chevenard thermobalance have been evaluated recently.[5] A special vacuum and pressure thermobalance[6] was used for the pressure TGA studies.

A sample size of 0.5 g. was used for all runs. The thermobalances have a sensitivity of ±0.2 mg. For humid air dehydration studies, a steam generator was used at a steam flow of 20 to 40 cc. per minute. This flow rate had no measurable effect on the furnace temperature because of heat capacity of the furnace and fast recovery of the heating circuit.

The results are reported in the figures as weight per cent. change as a function of temperature or time.

Differential Thermal Analysis (DTA).—The DTA studies were performed by means of a pressure and vacuum DTA apparatus constructed at this Laboratory.[7] The heating rate was 7° per minute for all runs. Calcined Al_2O_3 was used as the inert reference material. The sample size was about 0.4 to 0.6 g. packed into a cylindrical cavity of $^1/_2$" depth and $^1/_{16}$" diameter. The thermocouple was Pt–Pt/10% Rh, No. 32 wire with the junctions centered in the alumina and sample cavities. The temperature scale is reproducible to ±2° and the endothermic and exothermic peaks are reproducible to ±3°. Additional information on DTA may be found in a recent text.[8]

X-Ray Diffraction Studies.—The X-ray diffraction patterns were obtained by means of a GE XRD-5 apparatus using Cu Kα radiation. The phases identified according to the ASTM X-Ray Powder Data File are reported on Table I.

Density Measurements.—The absolute densities were measured with a 10 ml. pycnometer at 27.5° using butyl acetate as the liquid medium. The values are reproducible to ±0.1 g./cc.

Kinetic Studies.—Some kinetic data were obtained by direct analysis of the thermobalance curves made at constant temperature. Reproducibility as determined by making several runs at each temperature was ±0005 $min.^{-1}$ for the first-order velocity constants. For the other data reported a special vacuum oven was used. With the oven set at 130°, samples were introduced and the chamber evacuated. Then the desired pressure of steam was built up rapidly. The samples were held for various times and then air quenched. The kinetic data obtained from the rate curves were reproducible to ±0.005 $min.^{-1}$

Materials.—The $CaHPO_4 \cdot 2H_2O$ for these experiments was a special electronic grade product used in phosphor manufacture. The % impurities are less than those found in reagent grade $CaHPO_4$. The Fisher Sub Sieve Sizer average particle diameter was 2.2 μ.

Results

In the diagrams, Figures 1-2, corresponding DTA and TGA thermograms were placed on the same graph for ease in comparing results. The convention is used that an exothermic reaction is indicated by an upward deflection of the DTA curve from the baseline (shown as a broken horizontal line) and an endothermic reaction by downward deflection. Typical TGA and DTA curves for the dehydration of $CaHPO_4 \cdot 2H_2O$ in dry air show (Fig. 1) characteristic endotherm peaks at 135, 155 and 195°. The TGA curve shows a sharp change in slope at about 180°, but cannot be resolved into three distinct reactions corresponding to the DTA peaks. The formation of $Ca_2P_2O_7$ occurs between 360–450° as indicated by an endotherm peaking at 430° and a corresponding 4.8% weight loss on the TGA curve (theory 5.2%). The difference in weight loss may be explained by chemical analysis for $Ca_2P_2O_7$ according to the method of Gee and Dietz,[9] which shows 3–5% $Ca_2P_2O_7$ in the air dehydrated product for dehydration temperatures as low as 170°. A characteristic exotherm appearing at 530° (where no weight loss

(1) A. Boullé, *Compt. rend.*, **226**, 1617 (1948).

(2) S. I. Vol'fkovich and V. V. Urosov, *Izvest. Akad. Nauk SSSR, Otdel Kim. Nauk*, **4**, 341 (1951).

(3) A. Boullé and M. duPont, *Compt. rend.*, **240**, 860 (1955).

(4) A. Boullé and M. duPont, *ibid.*, **241**, 42 (1955).

(5) E. L. Simons, A. E. Newkirk and I. Aliferis, *Anal. Chem.*, **29**, 48 (1957).

(6) J. G. Rabatin and C. S. Card, *ibid.*, **31**, 1089 (1959).

(7) J. G. Rabatin and C. S. Card, *J. Electrochem. Soc.*, **104**, 68c (1957).

(8) W. J. Smothers and Yao Chiang, "Differential Thermal Analysis," Chemical Publishing Co., Inc., New York, N. Y., 1958.

(9) A. Gee and V. R. Dietz, *Anal. Chem.*, **25**, 1320 (1953).

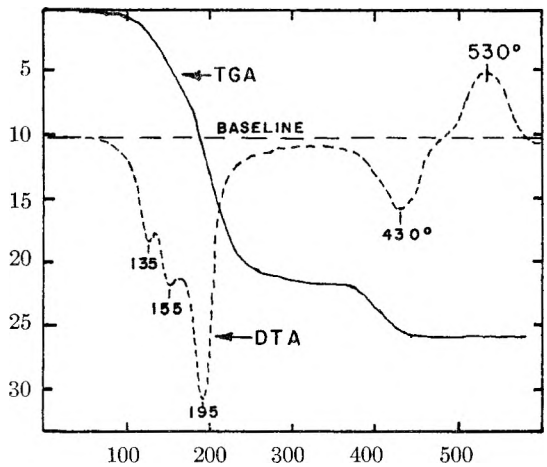

Fig. 1.—$CaHPO_4 \cdot 2H_2O$ dehydration in dry air.

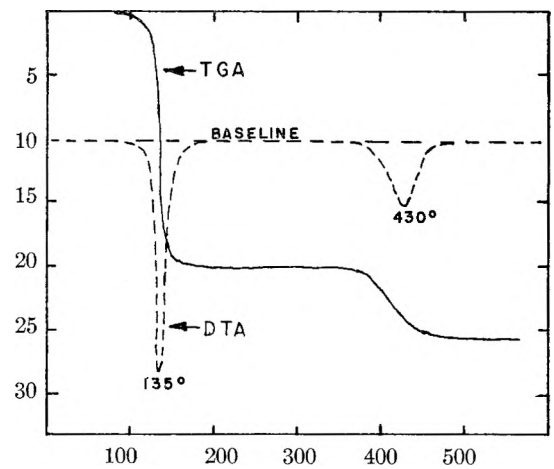

Fig. 2.—$CaHPO_4 \cdot 2H_2O$ dehydration in humid air.

or gain occurs) must be attributed to some physical change as will be brought out later.

The DTA and TGA curves reproduced in Fig. 2 for the dehydration of $CaHPO_4 \cdot 2H_2O$ in a humid atmosphere show a single sharply peaking endotherm at 135° in contrast to 3 peaks found in the dry air dehydrations (Fig. 1). The TGA curve shows a rapid weight loss of 20.2% between 120 and 160° compared to a theoretically expected weight loss of 20.9% for complete removal of hydrate water. The DTA curve shows an endotherm peaking at 430° but unlike the air dehydration (Fig. 1) no exotherm appears.

Dry CO_2 and N_2 were substituted for dry air for the studies on the effect of pressure on the dehydration mechanism. At one atmosphere N_2 or CO_2 the TGA and DTA results were identical to the dry air dehydration as shown in Fig. 1. At 3 atmospheres N_2 (or CO_2) the DTA curves are similar to the humid air dehydration results shown in Fig. 2 except that the endotherm at 135° is split into a very sharp peak at 132° and a broader endotherm at 148°. At 25 atmospheres N_2 the sharp endotherm has shifted to 112° and the broad endotherm remained relatively invariant at 150°. At intermediate pressures the sharp peak falls between these temperatures, with the peak temperatures approximately inversely proportional to the pressures.

The TGA curve for 3 atmospheres N_2 shows a weight loss of 20.6% between 100 and 200° similar to the humid air dehydration (Fig. 2). For higher pressures the thermobalance showed a shift to higher temperatures for the weight loss due to the increase in the boiling point of water and a decrease in the vaporization rate of water. Thus it could not be used to show the rate of release of crystal water which was faster than the vaporization rate of free water at these pressures.

In humid air the loss of hydrate water proceeds rapidly according to the first-order reaction with a velocity constant of 0.11 $min.^{-1}$ at 130°. On the other hand, in dry air the dehydration is much slower with the total amount of hydrate water lost dependent on the temperature. For instance, at 130°, about $1/2$ of the hydrate water is lost even after many hours of heating. Thus evaluation of the reaction kinetics of the dry air dehydration was possible for only the initial phase of the reaction. Using first-order equations also for dry air dehydrations, the velocity constant was 0.009 $min.^{-1}$ at 130°.

Because of the dependency of the reaction kinetics on the presence of moisture, a study was made on the effect of various partial pressures of water vapor on the reaction rates. The vacuum oven technique described in the experimental section was used, although accurate data could not be obtained below pressures of 0.05 atmosphere of water vapor. The velocity constants were determined at 130° for several pressures. *In vacuo*, the velocity constant is close to that for dry air (0.009 $min.^{-1}$). The results show a direct dependency on the dehydration to the vapor pressure up to about 0.2 atmosphere, after which the rate is constant at about 0.11 $min.^{-1}$.

Attempts to identify new phases by the X-ray diffraction method were unsuccessful. The actual phases present were identified by use of the ASTM X-Ray Powder Data File and by reference to the work of McIntosh and Jablonski.[10] These results together with the absolute densities are listed in Table I.

TABLE I

X-RAY AND DENSITY DATA FOR THE PRODUCTS OF $CaHPO_4 \cdot 2H_2O$ DEHYDRATION

Dehydration procedure	Dehydration temp., °C.	Absolute density	Phases by X-ray
Dry air	170	2.33-2.40	$CaHPO_4 \cdot 2H_2O$ + $CaHPO_4$ (weak)
1 atm. N_2	170	2.31	$CaHPO_4 \cdot 2H_2O$ + $CaHPO_4$ (weak)
3 atm. N_2	135	2.81	$CaHPO_4$
25 atm. N_2	110	2.82	$CaHPO_4$
Humid air	135	2.82	$CaHPO_4$

In dry air most of the $CaHPO_4 \cdot 2H_2O$ X-ray diffraction lines were present even after heating at 250°, although the weight loss indicated all of the dihydrate water should have been lost. These lines were of low intensity and broadened indicating poor crystallinity. Weak anhydrous $CaHPO_4$ lines were also present but did not intensify even at 400° where the $Ca_2P_2O_7$ begins to form. An amorphous phase could be seen under microscope examination. At 3 atmospheres or more N_2 and in humid air, the

(10) A. D. McIntosh and N. L. Jablonski, *Anal. Chem.*, **28**, 1424 (1956).

X-ray diffraction patterns of the dehydration products showed sharp, intense lines of anhydrous $CaHPO_4$.

Discussion

The dehydration of $CaHPO_4 \cdot 2H_2O$ in humid air (Fig. 2) is susceptible to a straightforward interpretation. On heating in the presence of sufficient water, the dihydrate decomposes according to equation 1

$$CaHPO_4 \cdot 2H_2O \longrightarrow CaHPO_4(S) + 2H_2O(g) \quad (1)$$

yielding a step in the TGA curve and the 135° peak in the DTA curve. On further heating, the anhydrous salt remains stable to just below 400°, then decomposes according to equation 2 yielding a second step in the TGA curve and the 430° DTA peak.

$$2CaHPO_4(S) \longrightarrow Ca_2P_2O_7(S) + H_2O(g) \quad (2)$$

The weight loss for each step is near that expected. When the dihydrate is dehydrated at 135° in humid air, the anhydrous $CaHPO_4$ formed gives a sharp X-ray pattern and has a density of 2.82, somewhat less than the ideal value of 2.92.[11]

If we consider next the dehydration under nitrogen pressure, there are three new features to be explained: (1) the lowering of the temperature of the 135° DTA peak with increased pressure; (2) the appearance of a 148° DTA peak; and (3) the shift of the TGA curve to higher temperatures with increased pressure. The differences can be accounted for by reactions 3 and 4. The liquid water would, of course, tend to be saturated with $CaHPO_4$.

$$CaHPO_4 \cdot 2H_2O \longrightarrow CaHPO_4(S) + 2H_2O(l) \quad (3)$$

$$H_2O(l) \longrightarrow H_2O(g) \quad (4)$$

We would expect liquid water to form under nitrogen pressure for two reasons; first the nitrogen would cut down the rate of diffusion of water away from the sample, and second since the atmosphere is relatively static, the higher pressure of water vapor near the sample would tend to reduce the rate of evaporation. The presence of liquid water would serve to increase the rate of reaction. Also the rate of heat transfer would be increased between the sample and the crucible. On all these grounds, we would expect reaction 3 to occur at lower temperatures, the higher the N_2 pressure and thus the 135° DTA peak would move toward lower temperatures approaching the equilibrium temperature of 36° as a limit.[12] The TGA curve, of course, detects only weight losses, and since water will evaporate more slowly the greater the nitrogen pressure, we observe a shift of the TGA curve to higher temperatures. The 148° DTA peak may be accounted for as simply the evaporation of water (equation 4). Similar effects have been noted by Borchardt and Daniels[13] and by Reisman and Karlak[14] with other hydrates. The formation of anhydrous $CaHPO_4$ with a good sharp X-ray diffraction pattern and a density of 2.82 by heating at 110° under 25 atmospheres N_2 serves to confirm this picture.

The dehydration of $CaHPO_4 \cdot 2H_2O$ in dry air presents a most complex picture relative to the first two cases discussed above. The presence of 3 endotherms at 135, 155 and 195° may be explained as follows. Since prolonged heating of $CaH_2PO_4 \cdot 2H_2O$ in dry air at 135° results in only about $1/2$ of the hydrate water lost, it can be assumed that the 135° endotherm results from the reaction

$$CaHPO_4 \cdot 2H_2O \longrightarrow CaHPO_4 \cdot xH_2O + (2 - x)H_2O(l) \quad (5)$$

where x is about 0.9 to 1.2 moles of H_2O.

The second endotherm is less easily explained but may be due to the boiling off of the water released from the hydrate. The 195° endotherm results from further release of the hydrate water according to reaction 6

$$CaHPO_4 \cdot xH_2O \longrightarrow \text{amorphous } CaHPO_4 + xH_2O \quad (6)$$

The X-ray diffraction pattern of the amorphous $CaHPO_4$ resembles the original $CaHPO_4 \cdot 2H_2O$ pattern. On continued heating the X-ray diffraction lines become less intense and the absolute densities remain close to the values for $CaHPO_4 \cdot 2H_2O$. According to X-ray diffraction data at 475° this amorphous phase remains even after weight loss data (Fig. 1) show that $Ca_2P_2O_7$ should be present. At 600° the X-ray diffraction data shows the presence of crystalline γ-$Ca_2P_2O_7$. Thus the exotherm at 530° results from the reaction

$$Ca_2P_2O_7 \text{ (amorphous)} \longrightarrow \gamma\text{-}Ca_2P_2O_7 \text{ (crystalline)} \quad (7)$$

The same γ-form of $Ca_2P_2O_7$ results regardless of the dehydrating conditions.

Acknowledgments.—The authors wish to express their appreciations to Dr. Dallas T. Hurd and to Mr. Clyde S. Card for their valuable discussions and comments.

(11) G. MacLennan and C. A. Beevers, *Acta Cryst.*, **9**, 579 (1955).

(12) H. Bassett, *J. Chem. Soc.*, 2949 (1958).

(13) H. J. Borchardt and F. Daniels, THIS JOURNAL, **61**, 917 (1957).

(14) A. Reisman and J. Karlak, *J. Am. Chem. Soc.*, **80**, 6500 (1958).

NOTES

THE STANDARD HEATS OF FORMATION OF THE ION PAIRS CdI^+ AND ZnI^+

By D. W. Anderson, G. N. Malcolm and H. N. Parton

University of Otago, Dunedin, New Zealand

Received October 1, 1959

Austin, Matheson and Parton[1] have reported values of the thermodynamic properties of some of the complex ions formed in aqueous solutions of lead and cadmium halides. Calorimetric enthalpies of formation were reported for the lead halide complex ions of type PbX^+, but not for the corresponding cadmium halide complexes. Approximate enthalpies of formation for the latter species were calculated from the heat of dilution measurements of Robinson and Wallace.[2]

We present here the result of a calorimetric determination of the enthalpy of formation of the complex ion CdI^+ which is in satisfactory agreement with the calculated value. The result of a similar measurement for the ion ZnI^+ is also reported.

The results were obtained by measuring the heat effects produced by the hundred-fold dilution of a potassium iodide solution firstly with 0.054 *m* $Cd(ClO_4)_2$ and secondly with a perchloric acid solution of such concentration that the final mixtures had the same ionic strength (I). These two dilution processes may be represented as

$$KI(m') \xrightarrow{0.054\ m\ Cd(ClO_4)_2} KI(0.01\ m'). \quad \text{Ionic strength } I_1 \cdot Q_1 \text{ cal.} \quad (1)$$

$$KI(m') \xrightarrow{HClO_4\ (m'')} KI(0.01\ m'). \quad \text{Ionic strength } I_1 \cdot Q_2 \text{ cal.} \quad (2)$$

If it is assumed that the difference between Q_1 and Q_2 is due entirely to the formation of complex ions, which in cadmium iodide solutions may be of the form CdI^+, CdI_2, CdI_3^-, CdI_4^{2-}, then

$$\Delta Q = Q_1 - Q_2 = [CdI^+]\Delta H_1 + [CdI_2]\Delta H_2 + [CdI_3^-]\Delta H_3 + [CdI_4^{2-}]\Delta H_4 \quad (3)$$

In this equation $[CdI^+]$, etc., are the numbers of gram moles of the various complex ions in the final solution, and ΔH_1, etc., are the molar enthalpies of formation of the complex ions at the particular ionic strength of the solution. The concentrations of the complex ions can be calculated from the association constants of the complexes and the concentrations of cadmium and iodide ions. It has been pointed out by Young and Jones[3] that the reported values of the association constants for complexes such as CdI_3^- and CdI_4^{2-} may be considerably in error because of lack of information concerning the values of the activity coefficients. But if the concentration of the cadmium ions in the solution is made several times greater than that of the iodide ions the concentrations of CdI_3^- and CdI_4^{2-} will be extremely small since the values of the association constants of these species which have so far been published are all small.[4] Under these circumstances the last two terms in equation 3 may be neglected. The values of ΔH_1 and ΔH_2 then can be calculated from at least two equations of this simplified form.

Experimental

Apparatus.—The dilution experiments were performed in a calorimeter of about one-liter capacity similar to that described by Young and Vogel.[5] The potassium iodide solution was contained in a thin-walled glass bulb of about 10 ml. capacity and was mixed with 990 ml. of surrounding solution by breaking the bulb with the blade of the stainless steel stirrer. The temperature change caused by the heat of reaction was measured by means of two thermistors connected in opposite arms of an a.c. bridge, and was compared both before and after the breaking of the bulb with the temperature change produced by a measured amount of heat generated electrically in a Nichrome wire heater. The heating current of about 0.3 ampere was measured by means of a potentiometer and a one ohm standard resistance. The heating period of about four minutes was measured with a one-tenth second stop-watch. A minimum temperature change of 0.001° could be detected by the change in resistance of the thermistors, which corresponded to a heat change of 1 calorie in the system. The calorimeter was completely immersed in a thermostat at 25 ± 0.01°.

The calorimeter was tested by measuring the heat of dilution of a sodium chloride solution. The results of this test are given in Table I.

Table I

The Heat of Dilution of NaCl Solution from 2.97 to 0.0297 *m* at 25°

Moles of NaCl	ΔH (measured), cal.	$\Delta H_{dil.}$/mole of NaCl, cal.
2.802×10^{-2}	9.580	342
2.795×10^{-2}	9.412	337
2.787×10^{-2}	10.180	365
2.817×10^{-2}	9.467	336

Mean = 345 cal. mole^{-1}

The heat absorbed for the one-hundredfold dilution of a 2.97 *m* sodium chloride solution is given in the tables of the National Bureau of Standards[6] as 348 cal.mole^{-1}.

Materials.—A.R. Chemicals were used throughout the work. All stock solutions were made up by weight. Stock solutions of cadmium and zinc perchlorates were prepared by dissolving known weights of the oxides in a calculated amount of 60% A.R. perchloric acid. The concentration of the cadmium perchlorate solution was calculated from the weight of oxide used, but the concentration of the zinc perchlorate solution was determined by analysis.

(1) J. M. Austin, R. A. Matheson and H. N. Parton, "The Structure of Electrolytic Solutions," edited by W. J. Hamer, John Wiley and Sons, New York, N. Y., 1959.

(2) A. L. Robinson and W. E. Wallace, *Chem. Revs.*, **30**, 195 (1942).

(3) T. F. Young and A. C. Jones, *Ann. Rev. Chem.*, **3**, 285 (1952).

(4) "Stability Constants, Pt. II," Chem. Soc. (London) Special Publication No. 7, 1958, p. 120.

(5) T. F. Young and O. G. Vogel, *J. Am. Chem. Soc.*, **54**, 3034 (1932).

(6) "Selected Values of Chemical Thermodynamic Properties," Natl. Bur. Standards Circ. No. 500, 1952.

Results

CdI†.—The results of the dilution experiments represented by equation 1 are shown in Table II.

TABLE II

THE HEAT (Q_1) OF THE REACTION

$$KI(m') \xrightarrow{0.054\ m\ Cd(ClO_4)_2} KI(.01\ m'),\ \text{Ionic strength } 0.3$$

m'	Moles of KI × 10^3	Q_1, cal.
1.00	10.11	−17.7
	10.05	−18.0
	10.07	−17.5
0.50	4.78	−10.2
	4.80	−11.1
	4.76	−10.0
0.25	2.31	− 5.3
	2.32	− 5.5
	2.33	− 4.8
	2.32	− 4.8

The heats of dilution of the potassium iodide solution with perchloric acid were too small to be detected with the apparatus. With a more sensitive calorimeter Austin[1] obtained a value of −52.35 cal. mole^{-1} for the one hundredfold dilution of 1 *m* potassium iodide with perchloric acid, from which it can be calculated that the heat of reaction (Q_2) in equation 2 would in all cases be less than 3% of Q_1. Consequently the value of ΔQ for use in equation 3 is given with sufficient accuracy by Q_1 in Table I.

The concentrations of the various ions in each solution were calculated by a method of successive approximations outlined by Riley and Gallafent.[7] The values taken for the association constants at 25° and zero ionic strength were 287[1] for CdI^{+1}, and 43, 12 and 12.6 for CdI_2, CdI_3^- and CdI_4^{2-}, 287[1] respectively.[8] These constants were corrected to the particular ionic strengths of the solutions by the equation of Davies.[9] The ionic strength of the solutions was found to be 0.3. From these calculations and the results in Table II the following equations of the form of equation 3 were obtained.

$$-17.7 = 8.4 \times 10^{-3}\,\Delta H_1 + 3.3 \times 10^{-4}\,\Delta H_2 + 3 \times 10^{-6}\,\Delta H_3 + 5 \times 10^{-8}\,\Delta H_4 \quad (4)$$

$$-10.4 = 4.2 \times 10^{-3}\,\Delta H_1 + 7.5 \times 10^{-5}\,\Delta H_2 + 4 \times 10^{-7}\,\Delta H_3 + 3 \times 10^{-9}\,\Delta H_4 \quad (5)$$

$$-5.1 = 2.2 \times 10^{-3}\,\Delta H_1 + 2.0 \times 10^{-5}\,\Delta H_2 + 5 \times 10^{-8}\,\Delta H_3 + 2 \times 10^{-10}\,\Delta H_4 \quad (6)$$

In these equations the coefficients of ΔH_3 and ΔH_4 are negligible. From (4) and (5), ignoring ΔH_3 and ΔH_4, $\Delta H_1 = -2780$ cal.mole^{-1} and $\Delta H_2 = 17{,}200$ cal.mole^{-1}. Substituting the value of ΔH_2 in equation 6 gives $\Delta H_1 = -2470$ cal.mole^{-1}. The mean of the two values of ΔH_1 is −2625 cal.mole^{-1}. This value was corrected to zero ionic strength by the formula[1]

$$\Delta H_1^0 = \Delta H_1 + \frac{3RT^2}{2}\left(\frac{1}{D} \times \frac{dD}{dT} + \frac{1}{T}\right) \ln \frac{K_1}{K_1^0}$$

where ΔH_1^0 is the standard heat of formation and D is the solvent dielectric constant. The correction term amounted to 230 cal.mole^{-1} so that $\Delta H_1^0 = -2395 \pm 300$ cal.mole^{-1} at 25°. The value obtained for ΔH_2 is not reliable as the amount of CdI_2 formed in the solutions was extremely small.

ZnI†.—The heat change during the one hundredfold dilution of 0.01 mole of 1 *m* KI with 0.05 *m* $Zn(ClO_4)_2$ was found to be less than 1 caloric.

Discussion

Matheson[1] has calculated the standard heat of formation of CdI^+ from heat of dilution data. His value of -2050 ± 300 cal.mole^{-1} is in agreement with the value obtained in this work.

The result of the experiment with zinc perchlorate and potassium iodide is in keeping with the conclusion of Sillén and Liljequist[10] that the association constants for ZnI^+, ZnI_2 and ZnI_3^- are all very small.

(10) L. G. Sillén and B. Liljequist, *Svensk Kem. Tid.*, **56**, 85 (1944).

THE DIFFUSION COEFFICIENTS OF Pb^{210} AND Cl^{36} IN MOLTEN $PbCl_2$ FOR THE TEMPERATURE RANGE 510–570°[1]

BY GERALD PERKINS, JR., R. B. ESCUE, JAMES F. LAMB[2] AND TROY H. TIDWELL[2]

Department of Chemistry, North Texas State College, Denton, Texas

Received October 5, 1959

For molten salts, values of the self-diffusion coefficient (*i.e.*, the diffusion coefficient measured during the interdiffusion of isotopes) give information of interest for the understanding of transport phenomena and some insight into the structure of the melt. Such measurements have been made and reported for a number of salts containing only univalent ions,[3-6] but when the present work was begun, such was not the case for salts of higher valence type; although, subsequently, values have been reported for the self-diffusion coefficient of zinc in molten zinc bromide.[7]

As a start toward consolidating and extending the reported physical data for molten salt systems, an investigation of such systems was begun in this Laboratory. Lead chloride was chosen early as one of the salts to be studied, for its properties made it convenient, considerable data were already reported for the molten state, and a controversy had arisen concerning the nature and values of the transport numbers, with conflicting values reported for these quantities.[8,9] There was even

(1) The work reported in this paper is part of a continuing project initiated under a Frederick G. Cottrell Grant and continued under a series of grants from the Robert A. Welch Foundation.

(2) Robert A. Welch Foundation Research Fellows.

(3) E. Berne and A. Klemm, *Z. Naturforschg.*, **8a**, 400 (1953).

(4) E. R. Van Artsdalen, D. Brown, A. S. Dworkin and F. J. Miller, Jr., *J. Am. Chem. Soc.*, **78**, 1772 (1956).

(5) (a) A. Z. Borucka, J. O'M. Bockris and J. A. Kitchener, *J. Chem. Phys.*, **24**, 1282 (1956); (b) *Proc. Roy. Soc. (London)*, **A241**, 554 (1957).

(6) A. S. Dworkin and R. B. Escue, ORNL Chem. Ann. Prog. Rep., June 20, 1957, p. 72.

(7) L. E. Wallin and A. Lunden, *Z. Naturforschg.*, **14a**, 262 (1959).

(8) H. Bloom and N. J. Doull, THIS JOURNAL, **60**, 620 (1956).

(9) F. R. Duke and R. W. Laity, *J. Am. Chem. Soc.*, **76**, 4046 (1954); THIS JOURNAL, **59**, 549 (1955).

(7) H. L. Riley and V. Gallafent, *J. Chem. Soc.*, **152**, 521 (1932).

(8) R. G. Bates and W. C. Vosburgh, *J. Am. Chem. Soc.*, **60**, 137 (1938).

(9) C. W. Davies, *J. Chem. Soc.*, 2093 (1938).

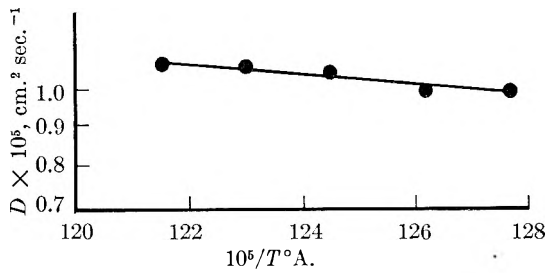

Fig. 1.—The diffusion coefficient of Pb^{210} in molten $PbCl_2$.

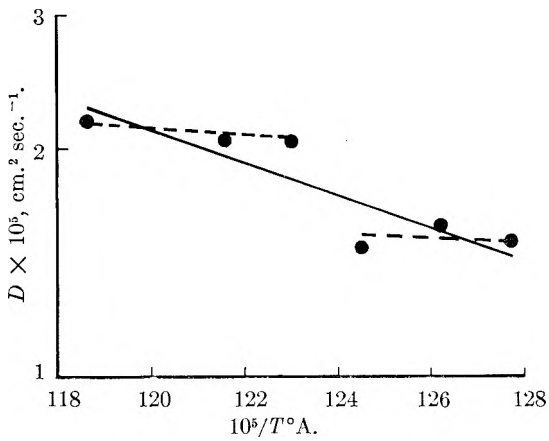

Fig. 2.—The diffusion coefficient of Cl^{36} in molten $PbCl_2$.

some indication of polymorphism in the liquid.[10] The work reported herein is part of the larger investigation of molten lead chloride systems, but it is reported at this time because of the possible novelty of the results.

Experimental Procedure

The necessary data were collected by the "capillary method" of Anderson and Saddington.[11] Active material contained within a capillary was allowed to diffuse for a measured time into a large volume of inactive material of identical chemical composition. From the fraction of active material remaining in the capillary, together with the capillary length and the time of diffusion, a calculation of the diffusion coefficient was made. The coefficients for Pb^{210} and Cl^{36} were obtained in separate experiments employing only the single active species in each instance.

The inactive lead chloride was prepared from reagent-grade salt without further purification except for removal of water. This was accomplished by maintaining the salt under vacuum at a temperature of about 400° for several hours, while periodically flooding the container with hydrogen chloride to minimize hydrolysis of the lead chloride.

Pb^{210} was introduced into one portion of the $PbCl_2$ and Cl^{36} into a second portion. Expired-radon needles were pulverized and refluxed for several hours with a concentrated solution of $PbCl_2$. When the exchange had reached equilibrium, the solution was filtered, crystallized, refiltered, washed and dried, with a final vacuum drying as already described. Cl^{36} was introduced by a similar exchange between $PbCl_2$ and active HCl.

Groups of Pyrex capillaries, all about 25 mm. in length and selected with identical inside diameters of about 0.5 mm., were filled from a reservoir of active material by means of a micro-pipet. The capillaries, reservoir and pipet were contained within a transparent, argon-blanketed furnace constructed of Vycor tubing. Manipulation of the pipet was effected by means of an external, three-dimensional adjustment. The capillaries were filled at a temperature slightly below that at which the diffusion was to take place so that no contraction would occur and the entire capillary length would be filled with active salt when immersed. When filled, the capillaries were transferred rapidly to the diffusion furnace. Throughout the filling and during the diffusion, the capillaries, in clusters of four, were suspended by means of a Vycor rod. In the diffusion furnace this assembly floated freely within a centering sleeve.

The diffusion furnace contained the reservoir of inactive salt. This reservoir was completely enclosed and argon-blanketed and was stirred by means of a Pyrex-covered magnetic bar. The stirrer operated at approximately 60 r.p.m. The temperature was maintained constant within maximum limits of ±1° with most of the fluctuation falling within ±0.5°. The capillaries were lowered into this bath and kept there for about 48 hours. After removing and crushing the capillaries they were quantitatively extracted by refluxing with an appropriate solvent. Aqueous ammonium acetate was used for the recovery of Cl^{36} and an aqueous mixture of nitric acid and silver nitrate for the Pb^{210}. The resulting solution was filtered and diluted to a prescribed volume before counting.

The initial activity of any given capillary was obtained by multiplying its length by the initial activity per unit length established from several capillaries of identical cross section. These were measured, filled and treated in all respects the same as the diffusion set, except that the time of immersion was only a few minutes (to ensure thermal equilibrium). The ratio of final activity to calculated initial activity gave the fraction of active material remaining in the capillary at the end of the experiment.

Results

In Table I are shown, for both Pb^{210} and Cl^{36}, the average values of the diffusion coefficients obtained at each temperature, together with the average deviations of the measurements.

TABLE I

THE DIFFUSION COEFFICIENTS OF Pb^{210} AND Cl^{36} IN PURE $PbCl_2$

T, °C.	$D \times 10^5$, cm.^{2} sec.$^{-1}$ Pb^{210}	Cl^{36}
510	0.98 ± 0.01	1.51 ± 0.15
520	0.98 ± .06	1.58 ± .22
530	1.06 ± .04	1.49 ± .04
540	1.07 ± .07	2.06 ± .02
550	1.08 ± .04	2.07 ± .02
570		2.13 ± .14

Since diffusion is a kinetic phenomenon, it is expected that the diffusion coefficient may be represented by a rate equation of the form

$$D = A \exp(-\Delta H^*/RT)$$

in which ΔH^* represents an activation energy for diffusion. In all previously reported work the data for molten salts have fit this relationship very well. Accordingly, the data of Table I are again shown in Figs. 1 and 2, in which D has been plotted on a logarithmic scale against the reciprocal of the absolute temperature. For Pb^{210} the values indicate a linear relationship and the best straight line, obtained by means of least squares calculations, has the equation

$$D = 9.28 \times 10^{-5} \exp(-3503/RT)$$

The value of 3503 cal. for the activation energy has a standard error of ±155 cal. For Cl^{36} the values appear more scattered. The best straight line through the points has the form

$$D = 3.68 \times 10^{-3} \exp(-8576/RT)$$

Here the value of 8576 cal. for ΔH^* has a standard error of ± 325 cal. It can be seen that, for Cl^{36}, the values seem to be grouped very nearly along two approximately horizontal lines and these have been indicated by dashed curves.

(10) V. T. Slavyanskii, *Doklady Akad. Nauk*, **68**, 1077 (1947).

(11) J. S. Anderson and K. Saddington, *J. Chem. Soc.*, Suppl. 381 (1949).

Discussion

The results obtained for Pb^{210} appear to be normal as compared with the behavior of other cations in molten salts. The results obtained for Cl^{36}, if we accept the least-squares straight line, also appear normal. The activation energies closely approximate those found for NaCl (5a), whose ions have about the same relative radii. On the other hand, the transference numbers calculated from the measured values of D will have values of about 0.5 as contrasted to the widely accepted, measured value of about 0.7 for the chloride ion in molten $PbCl_2$.[12] Of course, diffusion and conductance need not proceed by similar mechanisms and this is indicated by the fact that the conductance calculated from the Nernst–Einstein equation, utilizing the measured values of D, significantly exceeds reported values. This has been a general experience with molten salts.[4,5]

If, as seems possible from Fig. 2, there is an abrupt change in diffusion coefficient in the neighborhood of 540° then the behavior is different from that of any ion yet reported. Slavyanskii[10] has suggested polymorphism in molten $PbCl_2$ and his data indicate an abrupt change in slope in the vicinity of 545° when a viscosity Φ scale is plotted against temperature.

A further search of the literature shows other evidence to support the idea of an abrupt change in some properties of the melt at about 540°. A graphical reinterpretation of the viscosity data of Prasad[13] supports Slavyanskii. The same reference shows lead bromide to be normal. The surface-tension data of Lorenz and Kaufler[14] when plotted against temperature show an abrupt change at about 535°. Similar data reported by Dahl and Duke[15] fail to cover this exact region but otherwise compare with the data of Lorenz and Kaufler. No comparable data for other lead salts could be found, but it has been suggested by many authors that surface tension should be a linear function of temperature,[16] and so it has proven for other molten salts.

Such evidence, although meager, leads us to accept the possibility of the discontinuity shown in Fig. 2. This does not necessarily indicate polymorphic behavior in molten lead chloride. The possibility of reaction with the glass vessel cannot be overlooked. Pyrex softens in the temperature range under discussion and molten $PbCl_2$ readily attacks the glass at these temperatures in the presence of oxygen. However, oxygen was scrupulously excluded from the apparatus and, furthermore, the data of Prasad[13] indicate normal behavior for lead bromide, which would also be expected to attack the glass. In addition, the diffusion coefficient of Pb^{210} shows no apparent abnormality.

Conductance data[17] show some abnormality in the region of 540° but no discontinuity. A mechanism can be proposed, however, which might account for such conflicting behavior. If we picture lead chloride, in the vicinity of the melting point, as an equilibrium mixture of free ions and fragmentary residues of the crystalline lattice, a lattice in which the divalent lead is held more tightly than the chlorine, then we can assume that an increase in temperature will bring about an increase in the number of free ions, a decrease in the size and number of the lattice residues, and an expansion among the atoms still composing the lattice. A continued expansion of the lattice will eventually allow relatively free movement of the chloride ions through the framework of the lead atoms. At the temperature at which this movement becomes sterically possible there would be a discontinuous increase in the diffusion coefficient of the chloride ion.

Conductance would mainly involve the free ions, and these would be replenished from the lattice residues as discharge at the electrodes shifted the equilibrium between the ions and the lattice-bound atoms. A preliminary examination of the dimensions of the lead chloride crystal[18] indicates that the density change observed in going from the melting point to the vicinity of 540° would be approximately sufficient to allow passage of the chloride ion through the lattice, particularly if the expansion were mainly in two dimensions. This is not improbable when it is observed that the interatomic distances are significantly smaller in one dimension.

With or without the discontinuity, the data indicate a larger diffusion coefficient for the larger ion. This is counter to the results obtained for molten salts containing only univalent ions, but entirely in accord with the results obtained in ionic crystals containing divalent ions. Presence of intermediate ions, such as $PbCl^+$, might explain this behavior, but evidence for the presence of such ions is conflicting. Work now in progress in this Laboratory should provide additional data for clarification of the mechanism of diffusion in molten $PbCl_2$ and further discussion will be reserved until these or other data are available.

(12) G. J. Janz, C. Solomon and H. J. Gardner, *Chem. Revs.*, **58**, 461 (1958).

(13) B. Prasad, *Phil. Mag.*, **16**, 263 (1933).

(14) R. Lorenz and F. Kaufler, *Ber.*, **41**, 3727 (1908).

(15) J. L. Dahl and F. R. Duke, THIS JOURNAL, **62**, 1498 (1958).

(16) J. R. Partington, "An Advanced Treatise in Physical Chemistry," Vol. II, Longmans, Green and Co., New York, N. Y., 1951, p. 140.

(17) H. Bloom and E. Heymann, *Proc. Roy. Soc. (London)*, **A188**, 392 (1947).

(18) H. Braekken, *Z. Krist.*, **83**, 222 (1932).

COPPER(I) COMPLEXES OF 4,4′,6,6′-TETRAMETHYL-2,2′-BIPYRIDINE

BY ROBERT H. LINNELL AND DOROTHY MANFREDI

Department of Chemistry, University of Vermont, Burlington, Vermont

Received October 30, 1959

The preparation of 4,4′,6,6′-tetramethyl-2,2′-bipyridine (t.bipy.) has been described previously[1] and its formation of a Cu(I) complex briefly studied by Smith.[2] The present work reports the formation of Cu(t.bipy.) and Cu(t.bipy.)$_2$ complexes as well as the pK_a of the t.bipy.

(1) R. H. Linnell, *J. Org. Chem.*, **22**, 1691 (1957).

(2) G. F. Smith, *Anal. Chim. Acta*, **16**, 401 (1957).

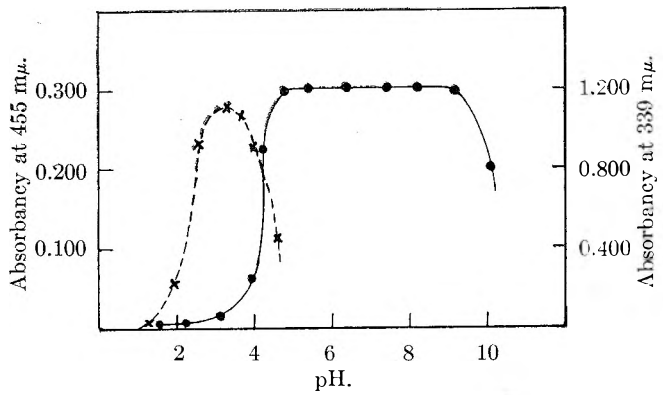

Fig. 1.—4.50 × 10^{-4} molar Cu(I) and 4.50 × 10^{-4} molar t.bipy. in 10% EtOH and 0.10 ionic strength: ———, 455 mμ; - - -, 339 mμ.

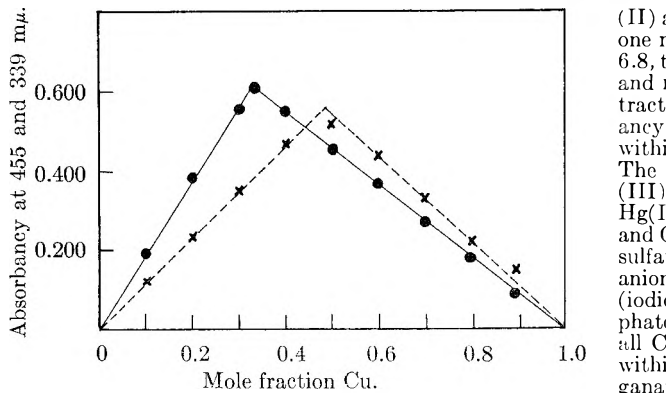

Fig. 2.—Cu(I) + t.bipy. 8.00 × 10^{-4} molar in 10% EtOH and 0.10 ionic strength: ———, 455 mμ; - - - 339, mμ.

Experimental

The t.bipy. was prepared as previously described[1] and had a m.p. 144° (cor.). The reagents in general were of A.C.S. reagent grade. Standard Cu solutions were made from Cu shot dissolved in HNO_3–H_2SO_4.

The solubility of t.bipy. at 25° was found to be 1.67 mg./l. in water, 200 mg./l in 10% EtOH (by volume) and 400 mg./l. in 95% EtOH. For the work reported here, final concentrations of 10% EtOH were used and a stock 0.0025 *M* t.bipy. 40% EtOH solution was adopted. Isoamyl and ethyl alcohols were redistilled on a Todd column. A Beckman DU spectrophotometer with standard tungsten and hydrogen light sources was used; the silica cells were matched with distilled water and suitable corrections applied. A Beckman model H2 *p*H meter was used with Beckman No. 20037 and 20051 electrodes. All solutions were made to a constant ionic strength of 0.10 by the addition of NaCl.

Solutions were prepared with *p*H values from 1.0–10.0 (HCl, HOAc–NaOAc, NH_4OAc HBO_2–$NaBO_2$) with constant ionic strength of 0.10 in 10% EtOH, with Cu^{++} 4.50 × 10^{-5} mole/l., t.bipy. 4.50 × 10^{-4} mole/l. and 1 ml. of 5% hydroxylamine hydrochloride solution in 100 ml. total volume. The colored complex had maximum absorbancy at 455 mμ; a plot of absorbancy at 455 mμ *vs.* *p*H is shown in Fig. 1. A shoulder in the spectrum at 339 mμ suggested a 1:1 complex; absorbancy at 339 mμ *vs.* *p*H also is shown in Fig. 1.

Aqueous solutions of the t.bipy.–Cu(I) complex changed with time, the 455 mμ absorbancy decreasing and the 339 mμ absorbancy increasing; this change was shown to be due to CO_2 uptake and decrease in *p*H rather than to air oxidation. Isoamyl alcohol extracts did not change in absorbancy with time.

The formulas of the complexes were determined by Job's[3] method, using a blank containing identical concentrations of all species present with the omission of the t.bipy. The total concentration of Cu + t.bipy. was kept constant at 8.00 × 10^{-4} mole/l., and the ionic strength maintained at 0.10 with NaCl in 10% EtOH solution. Measurements were made at *p*H 6.8 and 455 mμ, and at *p*H 2.6 and 339 mμ. All absorbancies were measured on isoamyl alcohol extracts. The results are shown in Fig. 2.

Samples containing Cu in concentrations from 5.0 × 10^{-6} to 1.00 × 10^{-5} mole/l. were treated with a threefold excess of t.bipy. (over that for Cu(t.bipy.)$_2$), NH_3 to a *p*H 5.8, one ml. 5% hydroxylamine hydrochloride (in 100 ml. total vol.) and the colored complex extracted with isoamyl alcohol. It was found that one extraction quantitatively removed the complex. The absorbancy at 455 mμ was linear with concentration with a molar absorptivity of 8100. These same isoamyl alcohol extracts were stable with time and absorbancies one month later checked within ±1% of the original values.

The influence of a number of common ions on the Cu(I)-t.bipy. complex was investigated. Standard solutions were prepared containing 0.1 mg. of Cu(II) and 10 mg. of foreign ion (as nitrate or chloride salts), one ml. hydroxylamine hydrochloride, NH_3 to adjust *p*H to 6.8, t.bipy, in threefold excess, NaCl to ionic strength of 0.10. and made to 50 ml. and 10% EtOH. The solutions were extracted once with 10 ml. of isoamyl alcohol and the absorbancy measured at 455 mμ. The absorbancies were in all cases within 2% of the value for Cu–t.bipy. without the foreign ion. The cations investigated were Li, Na, K, Mg, Ca, Ba, Cr(III), Mn(II), Fe(III), Fe(II), Ni(II), Ag, Zn, Cd, Hg(II), Hg(I), Al, Sn(IV), Sn(II), Pb(II), As(V), As(III), Co(II) and Co(III). It was shown that the anions chloride, nitrate, sulfate, acetate and perchlorate do not interfere. Those anions which form insoluble Cu(I) salts in isoamyl alcohol (iodide, thiocyanate, cyanide, thiosulfate, sulfide and phosphate) require 2–4 extracts with isoamyl alcohol to remove all Cu(I) from the aqueous solution and give absorbancies within 2% of the correct value. Oxidizing anions (permanganate, chlorate and ferricyanide) do not interfere if sufficient excess hydroxylamine is added. Competitive chelation of Cu(I) with t.bipy. and ammonium tartrate, sodium citrate and sodium malonate was investigated using the same Cu–t.bipy. standard and technique, substituting 1.0 mg. of the hydroxy acid for the foreign ions mentioned above. After making a small correction for the Cu present in the hydroxy acids, one extraction with isoamyl alcohol yielded absorbancy values within 2% of the correct value.

For ultraviolet solution spectra of t.bipy. we assume the equilibrium

$$BH^+ \rightleftharpoons B + H^+ \qquad B = \text{t.bipy.}$$

$$K_a = \frac{a_B a_{H^+}}{a_{BH^+}} = \frac{\gamma_B}{\gamma_{BH^+}} \times \frac{c_B}{c_{BH^+}} \times a_{H^+}$$

$$pK_a = pH + \log \gamma_{BH^+} + \log c_{BH^+}/c_B$$

We take γ_B = 1.00 and calculate log γ_{BH^+} = −0.13 from Debye–Hückel using 0.10 ionic strength and a dielectric constant of 73 for our 10% EtOH at 21°.[4] The term log c_B/c_{BH^+} is determined spectrophotometrically[5] as log $(\epsilon_{BH^+} - \epsilon)/(\epsilon - \epsilon_B)$ where ϵ = molar absorptivity of buffered solution containing BH^+ and B; ϵ_{BH^+} = molar absorptivity of BH^+. The value of pK_a determined from 14 measurements over the wave length region 2350–3050 Å. was 4.54 ± 0.08 (standard deviation) at 21° in 10% EtOH. By comparison we redetermined pK_a for 2,2′-bipyridine and found 3.95 ± 0.05 under the same conditions. Literature values[6] for the 2,2′-bipyridine (concentration K) are 4.44 (in H_2O, 0.10 ionic strength) and 4.12 (20% EtOH, 0.10 ionic strength) at 20°.

Discussion

The experimental results indicate the t.bipy. forms two complex ions with Cu(I)

(1) Cu(I) + t.bipy. $\rightleftharpoons$ Cu(t.bipy.)$^+$

(3) P. Job, *Compt. rend.*, **180**, 928 (1925).

(4) H. S. Harned and B. B. Owen, "The Physical Chemistry of Electrolytic Solutions," 3rd ed., Reinhold Publ. Corp., New York, N. Y., 1958.

(5) L. Flexser, L. Hammett and A. Dingwall, *J. Am. Chem. Soc.*, **57**, 2103 (1935).

(6) A. P. Krumholz, *ibid.*, **73**, 3487 (1951).

(2) $Cu(t.bipy.)^+ + t.bipy. \rightleftharpoons Cu(t.bipy.)_2^+$

At *p*H values 2.6–4.0 the 1:1 complex predominates, and under these conditions most of the t.-bipy. would be in cationic form. Above *p*H 4.5 the $Cu(t.bipy.)_2^+$ complex forms essentially quantitatively, when t.bipy:Cu is 2.0 or more. Above *p*H 9.3 the 1:2 complex is no longer stable. The presence of four methyl groups in t.bipy. gives an increased basic character, a specific chelating action with Cu and decreased water solubility (increased ease of extraction in organic solvents such as isoamyl alcohol) compared to the parent 2,2′-bipyridine. The $Cu(t.bipy.)_2^+$ complex is extremely stable in isoamyl alcohol and the t.bipy. reagent is very specific for Cu(I) and would be of value in analysis.

Acknowledgment.—Support of the Research Corporation is gratefully acknowledged.

HEATS OF SOLUTION OF AMMONIUM, POTASSIUM AND SODIUM IODATES AND OF SODIUM BROMATE; HEAT OF REACTION OF IODINE PENTOXIDE WITH AQUEOUS HYDROXIDE

BY JESSE G. SPENCER, JR.,[1] AND LOREN G. HEPLER[2]

Cobb Chemical Laboratory, University of Virginia, Charlottesville, Virginia

Received October 31, 1959

As part of an investigation of the thermodynamic properties of compounds containing halogens in the +5 oxidation state, these solution and reaction heats have been determined

$$NH_4IO_3(c) = NH_4^+(aq) + IO_3^-(aq) \quad (1)$$
$$NaIO_3(c) = Na^+(aq) + IO_3^-(aq) \quad (2)$$
$$KIO_3(c) = K^+(aq) + IO_3^-(aq) \quad (3)$$
$$NaBrO_3(c) = Na^+(aq) + BrO_3^-(aq) \quad (4)$$
$$I_2O_5(c) + 2OH^-(aq) = 2IO_3^-(aq) + H_2O \quad (5)$$

Experimental

The high-precision solution calorimeter employed in these investigations has been described in detail.[3,4] All heats of reaction or solution were determined at 25.0 ± 0.3° in 950 ml. of solution.

Chemicals. Potassium Iodate.—Mallinckrodt analytical grade KIO_3 was recrystallized once and oven-dried at 120°. Two samples, I and II, were prepared.

Sodium Iodate.—Fischer reagent grade $NaIO_3$ was recrystallized once and oven-dried at 100°. Two samples, I and II, were prepared.

Sodium Bromate.—J. T. Baker C.P. $NaBrO_3$ was recrystallized once and oven-dried at 92°.

Ammonium Iodate.—One-hundred milliliters of a 20% (by weight) Merck reagent NH_4NO_3 solution was added to a solution containing 14.0 g. of Mallinckrodt analytical grade KIO_3 in 200 ml. of water maintained at 45°. The solution was cooled to 0°, decanted, and the precipitated NH_4IO_3 was collected in a büchner funnel. The crude product was recrystallized twice. Qualitative tests for potassium and nitrate were negative. The product was divided into samples I and II. Sample I was dried at 100° in an oven and II was dried over P_2O_5 in a desiccator. Each sample was analyzed by titrating with thiosulfate the iodine liberated after addition of excess iodide.[5] Sample I was found to be 98.77% NH_4IO_3 and sample II was found to be 99.41% NH_4IO_3.

Iodine Pentoxide.—Iodide pentoxide (I_2O_5) was prepared by dehydrating iodic acid (HIO_3) to constant weight at 185 ±5°.[6] The iodic acid had been prepared previously according to the method of Palmer.[7] The first sample of I_2O_5 had a light flesh color; the second, although tinted, was more nearly white. A third sample, prepared by mixing portions of the first two and leaching with CCl_4, was the color of the second sample. Our I_2O_5 was entirely soluble in water and no free iodine was indicated by starch. The three samples were analyzed by thiosulfate titration[5] and found to be 99.9, 100.0 and 99.9% I_2O_5.

Results

Heats of solution of $NH_4IO_3(c)$, $NaIO_3(c)$, $KIO_3(c)$ and $NaBrO_3(c)$ (equations 1–4) are given in Tables I–IV. We have used heats of dilution of $NaIO_3(aq)$[8] and $KIO_3(aq)$[9] with data in Tables II and III to calculate the standard heats of solution of $NaIO_3(c)$ and $KIO_3(c)$. Heats of dilution of $NH_4IO_3(aq)$ and $NaBrO_3(aq)$ have been estimated from heats of dilution of various 1:1 electrolytes[9] and used with data in Tables I and IV to calculate standard heats of solution of $NH_4IO_3(c)$ and $NaBrO_3(c)$.

TABLE I

HEATS OF SOLUTION OF $NH_4IO_3(c)$

Sample	Moles $NH_4IO_3 \times 10^3$/950 ml.	ΔH_1(kcal./mole)
I	6.6490	7.63
I	13.346	7.63
II	11.969	7.61
II	10.026	7.63

TABLE II

HEATS OF SOLUTION OF $NaIO_3(c)$

Sample	Moles $NaIO_3 \times 10^3$/950 ml.	ΔH_2(kcal./mole)
I	3.6246	4.85
II	6.5099	4.87
I	6.6483	4.79
I	10.382	4.85

TABLE III

HEATS OF SOLUTION OF $KIO_3(c)$

Sample	Moles $KIO_3 \times 10^3$/950 ml.	ΔH_3(kcal./mole)
II	5.4903	6.66
I	7.7655	6.66
I	7.8496	6.63
I	9.5253	6.65
I	10.208	6.66

Heats of reaction of $I_2O_5(c)$ with excess $OH^-(aq)$ (equation 5) are given in Table V. The initial concentration of KOH was such that the hydroxide concentration after each run did not exceed 0.013 *M*. We have estimated heats of dilution for this reaction from heats of dilution of KOH(aq) and $KIO_3(aq)$[9] and have used these estimated heats

(1) Fellow of the Southern Fellowship Fund of the Council of Southern Universities.

(2) Alfred P. Sloan Research Fellow.

(3) R. L. Graham and L. G. Hepler, *J. Am Chem. Soc.*, **78**, 4846 (1956).

(4) C. N. Muldrow, Jr., and L. G. Hepler, *ibid.*, **79**, 4045 (1957).

(5) I. M. Kolthoff and E. B. Sandell, "Textbook of Quantitative Inorganic Analysis," The Macmillan Co., New York, N. Y., 1952, p. 594.

(6) A. King, "Inorganic Preparations," D. Van Nostrand Co., New York, N. Y., 1936, p. 64.

(7) W. G. Palmer, "Experimental Inorganic Chemistry," The University Press, Cambridge, 1954, pp. 470–472.

(8) E. Lange and A. L. Robinson, *Z. physik. Chem.*, **A148**, 97 (1930).

(9) F. Rossini, *et al.*, "Selected Values of Chemical Thermodynamic Properties," Circular 500, National Bureau of Standards, 1952.

TABLE IV

HEATS OF SOLUTION OF $NaBrO_3$(c)

Moles $NaBrO_3 \times 10^3$/950 ml.	ΔH_4(kcal./mole)
9.3488	6.47
11.5846	6.46
15.7812	6.48
11.402	6.45[a]
15.885	6.47[a]
19.157	6.46[a]

[a] Values were obtained by Mr. M. M. Birky of this Laboratory. Mr. Birky's work was done on a twice-recrystallized sample which had been oven-dried at 100° for several hours.

with the data in Table V to calculate the standard heat of reaction 5.

TABLE V

HEATS OF REACTION OF I_2O_5(c) WITH SOLUTIONS OF KOH

Sample	Moles $I_2O_5 \times 10^3$/ 950 ml.	Moles KOH $\times 10^3$/ 950 ml.	ΔH_5(kcal./mole I_2O_5)
I	3.7850	1.999	−26.39
I	4.9985	1.999	−26.52
I	3.9051	1.999	−26.36
II	5.1491	2.499	−26.34
II	4.2295	1.999	−26.38
III	3.0487	1.499	−26.45

All of the standard heats of solution (equations 1–4) and reaction (equation 5) are given in Table VI. Our estimates of *total* uncertainties, including uncertainties in compound purity, experimental heat determinations and heats of dilution, indicated by ±, are also given in Table VI.

TABLE VI

STANDARD HEATS OF SOLUTION AND REACTION

Equation number	Substance	ΔH^0(kcal./mole)
1	NH_4IO_3(c)	7.62 ± 0.12
2	$NaIO_3$(c)	4.83 ± .06
3	KIO_3(c)	6.63 ± .05
4	$NaBrO_3$(c)	6.43 ± .06
5	I_2O_5(c) + $2OH^-$(aq)	−26.4 ± .2

Discussion and Calculations

While this research was in progress, Russian workers[10] reported heats of solution of NH_4IO_3(c) in agreement with our values; therefore further attempts to prepare very pure NH_4IO_3(c) were abandoned.

We know of no prior determinations of heats of solution of $NaIO_3$(c) or $NaBrO_3$(c). Heats of solution of KIO_3(c) ranging from 5.57 to 6.78 kcal./mole have been reported.[11] We know of no prior determinations of the heat of reaction of I_2O_5(c) with excess OH^-(aq).

The entropy[9,12] and solubility[13] of KIO_3(c) are known. We have taken the activity coefficient of KIO_3(aq) in saturated solution to be equal to that of $KBrO_3$(aq)[14] at the same concentration. The standard free energy of solution of KIO_3(c) is 1670 cal./mole as calculated from the solubility and activity coefficient and has been combined with entropies of KIO_3(c) and K^+(aq)[9] and our standard heat of solution to give 28.4 cal./deg. mole for the standard partial molal entropy of IO_3^-(aq).

We have calculated the standard partial molal entropy of BrO_3^-(aq) to be 38.7 cal./deg. mole from the solubility,[13] entropy[9,12] and heat of solution[15] of $KBrO_3$(c) and activity coefficient[14] of $KBrO_3$(aq) in saturated solution. The solubility[13] of $NaBrO_3$(c) and the activity coefficients[16] for saturated solution lead to a standard free energy of solution of $NaBrO_3$(c) of −110 cal./mole. We have used this free energy with our standard heat of solution of $NaBrO_3$(c), the entropy of Na^+(aq)[9] and the entropy of BrO_3^-(aq) calculated above to obtain 31.1 cal./deg. mole for the standard entropy of $NaBrO_3$(c) at 298.15°K.

Acknowledgment.—We are grateful to M. M. Birky for assistance with some of the calorimetric measurements and to the Southern Fellowship Fund and the Alfred P. Sloan Foundation for financial support.

(10) A. F. Kapustinsky, A. A. Shidlovsky and U. S. Shidlovskaya, *Izvestiya Akademy Nauk SSSR*, No. 4, 385 (1958).

(11) F. R. Bichowsky and F. D. Rossini, "The Thermochemistry of the Chemical Substances," Reinhold Publ. Corp., New York, N. Y., 1936.

(12) J. E. Ahlberg and W. M. Latimer, *J. Am. Chem. Soc.*, **56**, 856 (1934).

(13) A. Seidell, "Solubilities of Inorganic and Metal Organic Compounds," D. Van Nostrand, New York, N. Y., 1940.

(14) J. H. Jones, *J. Am. Chem. Soc.*, **69**, 2066 (1947).

(15) H. C. Mel, W. L. Jolly and W. M. Latimer, *ibid.*, **75**, 3827 (1953).

(16) J. H. Jones and H. R. Froning, *ibid.*, **66**, 1672 (1944).

LIMITING CONDUCTANCES OF HYDROCHLORIC ACID AND HYDROGEN ION IN AQUEOUS GLYCEROL SOLUTIONS AT 25°

BY L. A. WOOLF[1,2]

Contribution from the Department of Chemistry, University of New England, Armidale, New South Wales, Australia

Received November 11, 1959

The data in this note supplement previously published results for the conductance of hydrochloric acid and hydrogen ion in aqueous sucrose and mannitol solutions[3–5] by providing values in 5, 10 and 20% glycerol solutions.

Experimental

Analytical reagent quality glycerol was diluted with doubly-distilled water (specific conductance 1–2 × 10^{-6} ohm^{-1} $cm.^{-1}$) to prepare several stock solutions slightly more concentrated than the desired values of 5, 10 and 20%, respectively. These were each passed through a mixed bed ion-exchange resin.[5] Then the concentration of each solution was obtained by comparing the measured density with values from the literature.[6] The literature data gave specific gravities calculated from weighings not corrected for air buoyancy (a correction which is unnecessary below a 30% glycerol concentration). For the purposes of the present work the specific gravities were converted to densities taking 0.99707 g./ml. as the density of water at 25°. The density–composition data thus obtained were fitted, for each of several ranges of composition, by the

(1) Presented, in part, in a thesis submitted in partial fulfillment of the requirements of the University of New England for the degree of Doctor of Philosophy.

(2) Department of Chemistry, University of Wisconsin, Madison 6, Wisconsin.

(3) J. M. Stokes and R. H. Stokes, THIS JOURNAL, **60**, 217 (1956).

(4) J. M. Stokes and R. H. Stokes, *ibid.*, **62**, 497 (1958).

(5) B. J. Steel, J. M. Stokes and R. H. Stokes, *ibid.*, **62**, 1514 (1958).

(6) M. Sheely, *Ind. Eng. Chem.*, **24**, 1060 (1932).

method of least squares to equations $P = ad - b$, where a and b were constants, d the density in g./ml. and P was the weight per cent. of glycerol defined by

$$P = \frac{\text{wt. of glycerol}}{\text{wt. of glycerol + wt. of water}} \times \frac{100}{1}$$

A stock solution of 0.8 M hydrochloric acid was prepared by dilution of the analytical reagent. An accurate value of its concentration was obtained from conductance measurements using the data of Owen and Sweeton[7] and Shedlovsky.[8]

The standardized glycerol stock solutions were suitably diluted with either water or the 0.8 M acid to obtain the solutions which were used in the conductance measurements. These dilutions and the conductance measurements are most readily described by considering an actual case, say 10% glycerol: Part of a glycerol stock solution was diluted with water to prepare a water–glycerol solution of $P = 10$. Another portion of the same stock solution was diluted with the 0.8 M acid to give a water–glycerol–acid solution also of $P = 10$ (it should be noted that for these ternary solutions P is not the weight per cent. of glycerol in the total solution, but only of the water–glycerol part). This solution was successively diluted with the binary solution of the same P value to enable the conductance measurements to cover the range 0.008–0.1 M acid concentration at $P = 10$.

This process of preparing binary and ternary solutions having the same P values and using the binary to dilute the ternary solution was repeated at least twice for each of the three concentrations $P = 5$, 10, and 20, respectively. All weighings were referred to vacuum. The 5, 10 and 20% water–glycerol solutions had densities and viscosities agreeing to 0.05% or better with the literature values,[6] and had specific conductances of about 2×10^{-6} ohm^{-1} cm.$^{-1}$. To find the molarity of the acid in the glycerol–acid–water solutions the difference in density between the binary and ternary solutions at the same value of P had to be known and was assumed to be a linear function of the acid concentration expressed as

$$\text{wt. percentage} = \frac{\text{wt. of HCl} \times 100}{\text{wt. of HCl + wt. of glycerol + wt. of water}}$$

For this purpose the increase in density caused by 1% of hydrochloric acid was taken as 0.00493 g./ml. at 25°.

The conductance measurements were made in an oil thermostat at 25 ± 0.002° in the usual manner[3,4] and the resistances extrapolated to infinite frequency. The values of the equivalent conductances at each glycerol concentration were extrapolated to zero acid concentration by the method of Robinson and Stokes.[9] Use of the $\dot{a}$ parameter for hydrochloric acid in water[10] gave a satisfactory extrapolation in all the glycerol solutions.

Results

The limiting equivalent conductances of hydrochloric acid Λ^0 and of hydrogen ion λ^0 in the three glycerol solutions are given in Table I. Transference numbers, obtained from the literature,[5] were used to calculate the limiting ionic conductances. The maximum experimental error in Λ^0 is estimated as 0.08%. The relative fluidity η_0/η is given for each solution; the value of η is that measured here, and η_0 is taken as 0.893 centipoise.

Discussion

The remarks made by previous authors[4,5,11] regarding conductance measurements for hydrochloric acid in sucrose and mannitol solutions at 25° seem to apply also to glycerol. As before hydrogen ion is the least affected of the univalent ions by the solution viscosity, and its mobility lies closer to the Walden's rule value than to its value in pure water.[5] The viscosity of the glycerol solutions appears to be somewhat more effective than that of sucrose or mannitol solutions in retarding hydrogen ion. This has been interpreted for other ions[5] as due to the hydration characteristics of either the glycerol molecules or the ion being considered.

TABLE I

LIMITING EQUIVALENT CONDUCTANCE OF HYDROCHLORIC ACID[a] AND HYDROGEN ION[b] IN 5, 10 AND 20% GLYCEROL SOLUTIONS AT 25°

	5%	10%	20%
Λ^0	388.9	353.3	283.9
R	0.912	0.829	0.666
λ^0	319.3	290.2	234.0
r	0.913	0.830	0.669
η_0/η	0.884	0.774	0.579

[a] Λ^0 in cm.^{2} (Int. ohm)$^{-1}$ g. equiv.$^{-1}$; $R = \Lambda^0$ (in glycerol solution)/Λ^0 (in water). [b] λ^0 in cm.^{2} (Int. ohm)$^{-1}$ g. equiv.$^{-1}$; $r = \lambda^0$ (in glycerol solution)/λ^0 (in water).

(7) B. B. Owen and F. H. Sweeton, *J. Am. Chem. Soc.*, **63**, 2811 (1941).

(8) T. Shedlovsky, *ibid.*, **54**, 1411 (1932).

(9) Robinson and Stokes, "Electrolyte Solutions," Butterworth, *Sci. Publ.*, London, England, 1955, p. 150.

(10) Ref. 9, p. 148.

(11) In ref. 4, Table I, the entries obtained by this author for hydrochloric acid in 20% sucrose should read $\Lambda^\circ = 287.4$, $R = 0.674$; and in Table IV of reference 5 the values for hydrogen ion in 20% sucrose should read $\lambda^\circ = 239.2$ and $R = 0.684$.

EXCHANGE OF RADIOCHLORINE BETWEEN MOLECULAR CHLORINE AND CARBON TETRACHLORIDE[1]

BY IRVING M. PEARSON AND CLIFFORD S. GARNER

Department of Chemistry, University of California, Los Angeles 24, California

Received October 31, 1959

In 1937 Rollefson and Libby[2] reported no significant exchange ($t_{1/2} > 7$ hr.) when solutions of Cl_2 (37-min. Cl^{38} label) in CCl_4 were exposed to ultraviolet light for 30 min. at room temperature (enough light absorbed to dissociate all Cl_2 molecules present four times). Later Downs[3] found no appreciable exchange in a solution of Cl_2 (310,000-yr. Cl^{36} label) in CCl_4 kept in the dark for one week at room temperature (single experiment). Recently Schulte[4] reported significant Cl_2–CCl_4 exchange (Cl^{36} label) under the influence of Co^{60} γ rays, ultraviolet, sunlight, and even in the dark at room temperature. His samples were contaminated with relatively large percentages of HCl and presumably a radioactive organochloride impurity (probably formed by attack of Cl_2 on hydrocarbon grease in his vacuum system).

Because of the limitations of the previous studies on the dark exchange and because we were interested in its effect on another exchange being studied, we have investigated the Cl_2–CCl_4 exchange in the dark and in sunlight over long time intervals in systems of high relative purity and at least 100 times more concentrated in Cl_2 than Schulte's exchange solutions. We have shown that radioactive organochloride impurities have an appreciable effect on the apparent exchange.

(1) Supported by U.S. Atomic Energy Commission under Contract AT(11-1)-34, Project No. 12.

(2) G. K. Rollefson and W. F. Libby, *J. Chem. Phys.*, **5**, 569 (1937).

(3) J. J. Downs, Ph.D. Thesis, Florida State University, Aug. 1954, p. 35.

(4) J. W. Schulte, *J. Am. Chem. Soc.*, **79**, 4643 (1957).

TABLE I

Cl_2–CCl_4 EXCHANGE IN CCl_4 SOLUTION AT 22–35°

Illum.	Exchange time, days	(Cl_2), M	Net c.p.m.[a] in Cl_2	Net c.p.m.[a] in CCl_4: before dist.	after dist.	$10^{11}k$, $M^{-1/2}$ sec.$^{-1}$	$10^{11}kb$ M^{-1} sec.$^{-1}$
Dark	0	0.149	3209 ± 46	2.8 ± 0.9	0.9 ± 1.2		
	48	.174	4650 ± 56	3.5 ± 0.8	2.1 ± 1.1	0.9	2.2
	211	.184	3520 ± 39	5.3 ± 1.0	2.5 ± 0.8	0.3	0.6
Light[b]	28	.181	4059 ± 43	24.0 ± 1.0	22.4 ± 1.1	18	42
	123	.241	5803 ± 56	141 ± 2	133 ± 2	21	42
Dark[c]	...	.0014	...	...	...	120	3200
Light[c]	...	.0008	...	...	...	940	34000

[a] Error given is the standard deviation computed from combining the net statistical counting error with an estimate of the aliquot error. [b] Sunlight plus fluorescent room lights; times exclude the dark intervals (*ca.* 40% of total time) since the dark exchange is much slower. [c] Data of Schulte[4]; dark run at 23°, "light" run at 5–16° in "sunlight."

Experimental

Radioactive Chlorine.—Chlorine-36 (310,000-yr. half-life) was obtained as 2.7 *f* HCl from the Oak Ridge National Laboratory. Tests showed that the radioactivity was present as Cl^- of very long half-life. Matheson tank Cl_2 was purified initially by the method of Downs and Johnson,[5] then passed through an evacuated $Mg(ClO_4)_2$ drying tube in a Pyrex bulb on a high-vacuum system, frozen with liquid N_2, pumped on, and traces of HCl removed by surrounding the bulb with a *n*-pentane slush-bath at −130° (vapor pressures of Cl_2 and HCl are *ca.* 0.2 and 20 mm., respectively) and connecting to an evacuated trap at −196°. The purified Cl_2 was labeled by high-temperature equilibration[5,6] with labeled AgCl precipitated from the labeled HCl and dried and fused *in vacuo* to remove water. The labeled Cl_2 was repurified by the above fractionation procedure, then kept frozen in a bulb on the high-vacuum system, except when being transferred, in order to minimize attack on the high-temperature-grade Halocarbon grease in the stopcocks and joints.

Carbon Tetrachloride.—J. T. Baker "Analyzed" CCl_4 was purified by the method of Wallace and Willard,[7] except that in the initial step the saturated solution of Cl_2 in CCl_4 was irradiated with a 10-watt ultraviolet immersion source for one week. The purified CCl_4 (b.p. 76.8°) was stored in a graduated Pyrex bulb attached to the high-vacuum system. Other chemicals were reagent grade.

Exchange Runs.—Known amounts of labeled Cl_2 were condensed at −196° into graduated 12-ml. Pyrex tubes (previously baked out and evacuated) and the solid pumped on and fractionated at −130° as described above. Purified CCl_4 was distilled onto the Cl_2 (in the dark except for occasional brief examination with a flashlight), the mixtures pumped on at −196°, fractionated at −130°, cooled to −196° and the tubes sealed off by torch at a constriction while open to a high vacuum. The mixtures were thawed to room temperature. One solution as processed at once as a "zero-time" sample. Two others were kept in the dark at room temperature for 48 and 211 days, respectively, and the remaining two were exposed for these same times to sunlight during the days and to laboratory fluorescent light for *ca.* 16 hours per day.

After the indicated time, the contents of each tube was frozen with liquid N_2, the tube tip broken off and the tube inserted quickly into a g.s. flask containing 100 ml. of 0.1 *f* air-free KI, the flask stoppered and the contents stirred until the CCl_4 had thawed. The liberated I_2 was titrated with standard $Na_2S_2O_3$ to a starch end-point. Trace amounts of HCl were then determined by titration with standard base. Each analyzed mixture was acidified slightly with HNO_3, and the phases separated for radioassay.

Dithizone and $SnCl_2$ spot tests[8] made on the "zero-time" mixture gave negative tests for Hg(I) and Hg(II) (chlorides of which might have formed by Cl_2 reacting with traces of Hg vapor in the high-vacuum system, and which could conceivably exchange with CCl_4); a control test showed that 0.4 μg. of Hg(II) could have been detected in the *ca.* 15-g. exchange solution.

Radioactivity Determinations.—A 10-ml. aliquot of each aqueous phase was dip-counted with a G-M tube, and the net activity of each entire aqueous phase calculated. Each entire CCl_4 phase was dried for one day over $Mg(ClO_4)_2$ (Drierite for the "zero-time" sample), filtered, diluted to 10 ml. with inactive CCl_4, dip-counted, distilled, then the distillate volume measured and the distillate diluted with inactive CCl_4 to 10 ml. for dip-counting. Statistical counting errors were kept below 2% standard deviation. The usually very small radioactivity from any potassium salts present was corrected for by determining all background rates, usually *ca.* 24–28 counts per minute (c.p.m.), on solutions identical in composition with those being measured except for the absence of radiochlorine. Coincidence corrections were less than 1%. Counting rates in CCl_4 were converted to an "aqueous" basis by use of a factor of 1.03 empirically determined. The mean standard deviation from the mean of the total c.p.m. per mole of Cl_2 in the five exchange solutions was only 0.8%.

Results and Discussion

Neither our measurements nor those of earlier investigators establish the exchange rate law. If, in analogy with the Br_2–CCl_3Br exchange[9] in the gas phase and in liquid CCl_4 solution at *ca.* 100–220°, the Cl_2–CCl_4 exchange rate is assumed to be given by $R = k(Cl_2)^{1/2}(CCl_4) = kb^{1/2}a$, k may be calculated from

$$R = -[8ab/(4a + 2b)t] \ln (1 - F) \quad (1)$$

$$F = (4a + 2b)x/4ay_0 \quad (2)$$

where R is the constant rate of exchange of Cl atoms (active plus inactive) between CCl_4 and Cl_2 in gram-atoms $l.^{-1}$ $sec.^{-1}$ in a given run, F is the fraction exchange, and x and y_0 are the net c.p.m. of the initially inactive CCl_4 at time t and of the Cl_2 at zero time, respectively. Values of k given in Table I are based on "after-distillation" x values. Table I also gives the bimolecular rate constant k_b obtained from equations 1 and 2 for the assumption $R = k_b(Cl_2)(CCl_4)$, since if the exchange is not of order 3/2 it may well be second order. Rows 6 and 7 of Table I give Schulte's results for comparison.

The reduction in activity of the CCl_4 phase on distillation may arise from an organochloride impurity formed by reaction of Cl_2 with Halocarbon grease used in the stopcocks of the high-vacuum system (such a "grease chloride" deliberately produced under more favorable conditions in control experiments was quantitatively left behind when CCl_4 was distilled off of solutions of the "grease chloride"). However, the small per cent. reduction of activity on distillation shown in rows 4 and 5 of Table I suggests that there was little organochloride impurity present and that the

(5) J. J. Downs and R. E. Johnson, *J. Am. Chem. Soc.*, **77**, 2098 (1955).

(6) Ref. 3, p. 10.

(7) C. H. Wallace and J. E. Willard, *ibid.*, **72**, 5275 (1950).

(8) F. Feigl, "Qualitative Analysis by Spot Test," Elsevier Publishing Co., N.Y., 3rd English ed., 1946, pp. 49–51.

(9) A. A. Miller and J. E. Willard, *J. Chem. Phys.*, **17**, 168 (1949).

greater per cent. reduction in our other runs was probably due to accidental contamination of the CCl_4 phase with traces of the highly active aqueous phase or some other radiocontaminant. The high relative purity of the exchange system may be inferred also from the fact that the equivalents of HCl found was only 0.4–0.7% of the equivalents of Cl_2 (in contrast to 7 and 15% in Schulte's two runs). The HCl can arise from Cl_2 attacking H_2O or stopcock grease in the system. Unpublished experiments we have made on the HCl^*–CCl_4 exchange under comparable conditions indicate that it would contribute less than 1% based on the upper limits for our specific dark exchange rates. For the latter dark exchange we may take $k \leqslant 3 \times 10^{-11}$ liter$^{1/2}$ mole$^{-1/2}$ sec.$^{-1}$ and $k_b \leqslant 8 \times 10^{-11}$ liter mole^{-1} sec.$^{-1}$ as conservative upper limits at room temperature, values approximately two orders of magnitude smaller than those based on Schulte's data, assuming no change in mechanism over the concentration range involved. The exchange is faster in sunlight.

A solution of labeled Cl_2 in CCl_4 was deliberately passed through a Halocarbon-greased stopcock; a white radioactive "grease-chloride" residue[10] was left upon distilling off the CCl_4 and Cl_2. Dissolution of the residue in CCl_4, followed by immediate treatment by Schulte's procedure with aqueous KI and dip-counting of the separated aqueous and CCl_4 phases showed that *ca.* 80% of the activity entered the CCl_4 phase, where it can be mistakenly ascribed to Cl_2^*–CCl_4 exchange if the CCl_4 phase is not distilled. The effect of a possible CCl_4–"grease chloride" exchange may be inferred from data on a separate solution of labeled Cl_2 in CCl_4 (known to contain "grease chloride") kept in sunlight plus room fluorescent light for *ca.* 2 months and in the dark for another month. This solution was treated with KI, then titrated with $Na_2S_2O_3$ for Cl_2 determination (0.00441f in Cl_2), KIO_3 added, a $Na_2S_2O_3$ titration made for HCl determination (0.00743 f in HCl, presumably a measure of the "grease chloride" formed), and finally the separated phases dip-counted. The net c.p.m. in the CCl_4 phase before and after distillation were 108 ± 2 and 55 ± 1, respectively, corresponding to (108–55)/108, or 49%, of the activity of the undistilled CCl_4 fraction as "grease chloride." These CCl_4 activities may be compared with those, namely, 6.9 ± 0.1 c.p.m. before and 6.5 ± 0.1 c.p.m. after distillation, obtained by normalizing the Cl_2 activity of the fifth experiment of Table I (roughly comparable conditions, but with much greater relative purity) to that of the above experiment. The much greater activity of 55 c.p.m. for our "contaminated" system, relative to the 6.5 c.p.m. for our much purer system, suggests that the former activity may arise largely from exchange between CCl_4 and active "grease chloride." Since the percentage of HCl and presumably of "grease chloride" is much greater in Schulte's runs and since his CCl_4 phases were not distilled, his exchange rates in the dark and in sunlight are high. Exchange of "grease chloride" with CCl_4 could be enhanced by the ultraviolet and γ-irradiation in his work, so it is possible that even those runs may be affected somewhat.

The very small exchange rates in the Cl_2–CCl_4 system found in our study indicate that this exchange is probably of negligible significance in most, if not all, studies of dark and sunlight-induced exchanges of Cl_2 and anhydrous chlorides in CCl_4 reported in the literature.

(10) Cl_2 also attacks hydrocarbon (Apiezon), Dow-Corning high-vacuum silicone, and glycerol-based greases.

THE SYSTEM LITHIUM HYDRIDE–LITHIUM FLUORIDE

BY CHARLES E. MESSER AND JOHN MELLOR

Contribution No. 263 from the Department of Chemistry, Tufts University, Medford 55, Massachusetts

Received November 9, 1959

Lithium hydride and lithium fluoride both have the same face-centered cubic-sodium chloride type crystal structure, with lattice constants of 4.083[1] and 4.027 Å.,[2] respectively, differing by only 1.4%. Tobolsky[3] has shown that for alkali halide salt pair systems where the lattice constants differ by 5% or less, solid solutions in all proportions, stable at room temperature, are formed.

However, Zintl and Harder[4] found two phases at room temperature in a mixture of 27 mole % LiF in LiH, cooled from the melt under hydrogen.

Hence, the system LiH–LiF was investigated by thermal analysis and X-ray crystallography to determine the conditions of solid solution formation at and below the melting point.

Experimental

Materials.—Lithium hydride was made by direct synthesis from the elements in the freezing point sample bomb at 1 atmosphere pressure and 725°. The lithium metal was "low sodium" grade, obtained from the Maywood Chemical Works, Maywood, New Jersey, trimmed of its oxide-nitride coating in an argon-filled drybox, and weighed under argon. The hydrogen was purified by passage over hot uranium.

Lithium fluoride was obtained from the Optovac Company, North Brookfield, Mass. It was used in the form of transparent cleavings from optical grade crystal fragments.

Thermal Analysis.—The apparatus was that used in earlier work in this Laboratory on the lithium–lithium hydride system,[5] with modifications to adapt the measuring circuit to temperatures up to 875°. The working thermocouple was calibrated: (a) against a standard which had been calibrated against fixed points, and (b) in place in the sample bomb by means of the known freezing point of lithium fluoride, 848 ±1°.[6]

The full composition range was covered, in steps of 5 mole % from 0–30 mole % LiF, and in steps of 10% from 40–100% LiF. All samples were run under 1 atmosphere of hydrogen pressure, except pure LiF which was run under argon. Cooling and warming runs were made at each composition, at rates of temperature change of about 1.5°/min. just before the onset of freezing or melting, respectively.

All samples were annealed for at least one hour before each run. At each composition, the sample was annealed overnight at about 50° below the melting point before one of the warming runs, the results agreeing within experimental error with runs of shorter annealing time.

(1) E. Staritzsky and D. J. Walker, *Anal. Chem.*, **28**, 1955 (1056).

(2) H. E. Swanson and E. Tatge, "Standard X-ray Diffraction Patterns," Natl. Bureau Standards, Circ. 539, U. S. Gov't. Print. Office, Washington 25, D. C., Vol. 1, 1953, pp. 61–62.

(3) A. V. Tobolsky, *J. Chem. Phys.*, **10**, 187 (1942).

(4) E. Zintl and A. Harder, *Z. physik. Chem.*, **B14**, 265 (1931).

(5) C. E. Messer, E. B. Damon, P. C. Maybury, J. Mellor and R. A. Seales, THIS JOURNAL, **62**, 220 (1958).

(6) T. B. Douglas and J. L. Dever, *J. Am. Chem. Soc.*, **76**, 4826 (1954).

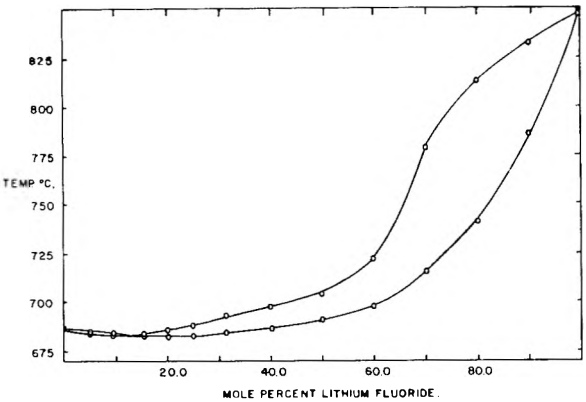

Fig. 1.—The system lithium hydride–lithium fluoride.

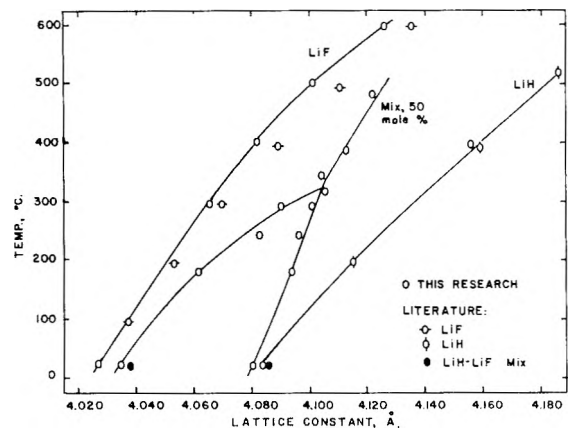

Fig. 2.—Lithium hydride–lithium fluoride.

Up to 30 mole % LiF, solidus and liquidus temperatures from warming and cooling runs agreed well, with precisions of about 0.3–0.5°. From 40–90 mole % LiF, the precision was 1–2°, and for the solidus points only the warming runs gave consistent values.

The lithium hydride melted over a range of about 2.0°, and the lithium fluoride over 2.6°, due to impurity premelting effects plus imperfect heat transfer. All observed solidus temperatures were corrected upwards by an amount interpolated between these values.

X-Ray Crystallography.—The apparatus of Goon, Mason and Gibb[7] designed to obtain powder photographs of specimens at high temperatures and pressures, was used. The samples were run under 1 atmosphere of argon in a beryllium capillary.

Pure lithium hydride, pure lithium fluoride, and a mixture recovered from the 60 mole % LiF thermal analysis sample, were run at temperatures from 25 to 600°. The mixture, which had been stored under argon, was thoroughly ground, with mixing, in the drybox. A small portion was loaded into the capillary, and a larger portion subjected to analysis by hydrogen evolution with water followed by titration of the resulting alkali. The results indicated the sample to be 50.0 ± 0.5 mole % LiF. Since the agreement of the titration and the hydrogen evolution results indicated no alkali in the sample, the change in composition is attributed to phase segregation in the cooling and removal of the thermal analysis sample.

In the lithium fluoride runs the exposure was for 3.5 hours, and in the lithium hydride and most of the mixture runs it was 5 hours. For the mixture runs at 321, 395 and 490°, the exposure was for 7 hours, with oscillation of the capillary. The mixture was annealed for one hour at each temperature before exposure, and cooled to room temperature between runs. The consistency of the results showed no influence of the thermal treatment, indicating satisfactory approach to equilibrium within these times.

(7) E. J. Goon, J. T. Mason and T. R. P. Gibb, Jr., *Rev. Sci. Instr.*, **28**, 342 (1957).

Interpretation of Diffraction Patterns.—Interpretation was confined to the back reflection region of the spectrum because the small lattice constant difference between LiH and LiF demanded high resolution.

In LiH and LiF, the 331, 420, 422 and 511 lines were observed at each temperature. The first three of these are the most intense in the higher order portion of the published spectra of LiH[4] and LiF[2]. The 400 line was observed in most LiF patterns, but was masked by a beryllium line for LiH.

In the mixture patterns, the same four reflections were also prominent. At and below 295°, two lines appeared for certain sets of indices, indicating the possible presence of two phases. At and above 321°, each type of line appeared only once. The lines were faint, but their positions could be read well enough to give the lattice constant to ± 0.001 Å. for the 511 lines and to ±0.005 Å. for the 331 lines.

On each pattern the lattice constants were extrapolated to $\cos^2\theta = 0$ by the method of Bradley and Jay.[8]

Results

Equilibrium solidus and liquidus temperatures are shown in Table I and Fig. 1. The system exhibits solid solution formation in all proportions, with a minimum at 13.0 ± 0.5 mole % LiF and 682.0 ± 0.5°, only 4.5° below the melting point of pure LiH.

The freezing point of LiH was 686.4°, 1.4° below the previous value.[5] Since the freezing curves of this research were as sharp as those of the earlier research,[5] the difference is attributed to absolute error in the temperature measurements.

The appearance of the thermal analysis samples on cooling was glassy and opaque, as described by Zintl and Harder.[4] They were easily removed from the sample bomb and pulverized, in contrast with pure LiH and LiF. Thus, a phase change on cooling is indicated.

TABLE I

THE SYSTEM LITHIUM HYDRIDE–LITHIUM FLUORIDE SOLID–LIQUID EQUILIBRIUM

Mole % LiF	Liquidus, °C.	Solidus, °C.	Mole % LiF	Liquidus, °C.	Solidus, °C.
0.00	686.4	686.4	39.95	698.0	686.7
5.06	685.0	683.8	50.01	704.4	691.7
9.44	684.2	683.1	59.99	722.4	698.4
15.42	684.1	682.6	70.06	778.5	715.6
20.05	685.6	683.1	80.01	802.0	741.0
25.03	688.6	683.5	90.09	832.4	786.8
31.46	693.4	685.0	100.00	848.0	848.0

Crystallographic.—The results are shown in Fig. 2. The agreement with known values is good for LiH and LiF at 25°. At 400°, the lattice constant of LiH is 0.003 Å. lower than that of Zalkin.[9] For LiF, the lattice constants differ increasingly at higher temperatures from those predicted from the dilatometric data of Eucken and Dannöhl[10] and Sharma,[11] which agree excellently with each other.

In the mixture at 25°, two lattice constants were well defined. The results agree fairly well with those of Zintl and Harder,[4] which have been corrected for impurity error as suggested by Zalkin.[9] The existence of two phases in the system at 25° is confirmed.

(8) A. J. Bradley and A. H. Jay, *Proc. Phys. Soc. (London)*, **44**, 563 (1932).

(9) A. Zalkin, Report UCRL-4239, November 16, 1953.

(10) A. Eucken and W. Dannöhl, *Z. Elektrochem.*, **40**, 814 (1934).

(11) S. Sharma, *Proc. Indian Acad. Sci.*, **32A**, 268 (1950).

At 185, 248 and 295°, only one lattice constant—the larger or hydride phase value—was precisely defined, the smaller or fluoride phase constant being defined by the extrapolation to $\cos^2\theta = 0$ of only two points.

At and above 321°, only one lattice constant was defined. The possibility of a critical solution temperature between 295 and 321° is thus demonstrated.

Discussion

In the mixture at 25°, the lattice constant of the hydride phase was shifted very little from the pure LiH, while that of the fluoride was shifted considerably in the direction of the hydride. This indicates appreciable solubility of hydride in fluoride, but very little of fluoride in hydride. The lattice energy of the fluoride is greater than that of the hydride,[12] so that the latter would gain in stability by dissolving somewhat in the fluoride.

At the critical temperature, the lattice constant is the mean of the values for the components within experimental error, as would be given by Vegard's law for the 50% mixture. At higher temperatures, the deviation from Vegard's law becomes increasingly negative. Studies on quenched samples of alkali halide solid solutions in general indicate positive deviations from Vegard's law.[13-16] However, no equilibrium determinations of lattice constants at high temperature seem to be in the literature for these systems.

The lithium hydride–lithium fluoride system differs from the alkali halide systems in that the fluoride and hydride anions differ considerably in polarizability, and the lithium–hydrogen and lithium–fluorine bonds differ in degree of covalent character. The systems silver chloride–sodium chloride[17] and silver chloride–lithium chloride[18] are analogous in these respects. Both show extensive solid solution formation at the melting point, and unmixing of the solid solutions on cooling. There is definitely a critical solution temperature in the sodium chloride system between 400 and 500°, but such a temperature cannot be defined in the lithium chloride system due to sluggishness of diffusion.

In the system AgCl–NaCl, the lattice constants at 25°[19] differ by 1.4%, the same value as in the lithium hydride–lithium fluoride system. The instability of room temperature solid solutions in these systems despite the small lattice constant difference must thus be dependent upon the effects of the polarizability and bonding differences.

Acknowledgments.—The authors are indebted to Dr. E. J. Goon for helpful advice and criticism in the crystallographic work.

(12) J. Sherman, *Chem. Revs.*, **11**, 93 (1932).

(13) J. E. Nickels, M. A. Fineman and W. E. Wallace, THIS JOURNAL, **53**, 625 (1949).

(14) W. T. Barrett and W. E. Wallace, *J. Am. Chem. Soc.*, **76**, 366 (1954).

(15) J. S. Wollam and W. E. Wallace, THIS JOURNAL, **60**, 1654 (1956).

(16) E. T. Teatum and N. O. Smith, *ibid.*, **61**, 697 (1957).

(17) M. B. Panish, F. F. Blankenship, W. R. Grimes and R. F. Newton, *ibid.*, **62**, 1325 (1958).

(18) M. B. Panish R. F. Newton, W. R. Grimes and F. F. Blankenship, *ibid.*, **63**, 668 (1959).

(19) R. W. G. Wyckoff, "Crystal Structures," Chap. III, Table, Interscience Publishers, Inc., New York, N. Y., 1948, p. 11.

This research was sponsored by the U. S. Atomic Energy Commission, Contract AT(30-1)1410.

MECHANISM OF OZONE PRODUCTION BY THE MERCURY SENSITIZED REACTION OF OXYGEN[1]

BY ROBERT J. FALLON, JOSEPH T. VANDERSLICE AND EDWARD A. MASON

Institute for Molecular Physics, University of Maryland, College Park, Maryland

Received November 13, 1959

Recently, there have been discussions in the literature concerning the mechanism for the production of ozone from oxygen by mercury photosensitization.[2-4] It is generally accepted that these reactions are important

$$Hg^*(^3P_1) + O_2(X^3\Sigma_g^-) \longrightarrow Hg(^1S_0) + O_2^* \quad (1)$$

$$O_2^* + O_2 \longrightarrow O_3 + O \quad (2)$$

The energy transferred in process (1) is 4.88 e.v. Discussion has centered around the nature of the excited oxygen molecule, O_2^*. The present note makes use of some recently determined[5] potential curves for O_2 to propose a mechanism for production of the O_2^* which appears to reconcile the main features of the various points of view.

Volman[2] has concluded from work carried out earlier[6] that the O_2^* is in a vibrationally excited $^1\Sigma_g^+$, $^1\Delta_g$ or $X^3\Sigma_g^-$ state (see Fig. 1). This conclusion was based on the fact that the ozone production was increased by the presence of foreign gases, the order of effectiveness being He>Ar>N_2>CO_2. Volman argued that in order to explain the difference in ozone production between added He and Ar, the O_2^* had to be formed in a highly excited vibrational state (either $^1\Sigma_g^+$, $^1\Delta_g$, or $X^3\Sigma_g^-$) so that the results could be explained by the difference in rates of vibrational deactivation. If the O_2^* corresponded to any of the highly excited electronic states, in particular the $A^3\Sigma_u^+$, it is difficult to explain the relative effects of added He and Ar.

Gill and Laidler[3] argued that if O_2^* were formed in a high vibrational level, the foreign gases would readily cause vibrational deactivation, and no overall increase in rate would be observed, which they felt was apparent from an analysis of Volman's experiments.[6] They claimed that if the higher electronically excited $A^3\Sigma_u^+$ state were formed, then deactivation would occur only with difficulty, and hardly at all for the inert gases. Another argument used by Gill and Laidler was that the most probable mechanism for (1) is one involving the least net loss of total electronic energy; *i.e.*, the electronic energy transferred from the Hg* would all go into electronic energy in the O_2^* and not into vibrational energy. The $A^3\Sigma_u^+$ state satisfies this requirement.

(1) This research was supported in part by the National Aeronautics and Space Administration.

(2) D. H. Volman, *J. Chem. Phys.*, **24**, 122 (1956).

(3) E. K. Gill and K. J. Laidler, *Can. J. Chem.*, **36**, 79 (1958).

(4) D. H. Volman, E. K. Gill and K. J. Laidler, *J. Chem. Phys.*, **30**, 589 (1959).

(5) J. T. Vanderslice, E. A. Mason and W. G. Maisch, *J. Chem. Phys.*, in press.

(6) D. H. Volman, *J. Am. Chem. Soc.*, **76**, 6034 (1954).

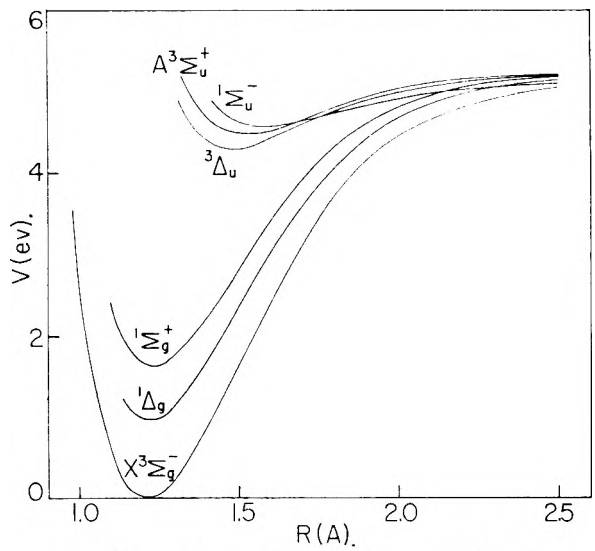

Fig. 1.—Potential energy curves for O_2.

Finally, Volman, Gill and Laidler[4] mention that the original work of Volman[6] could be misinterpreted because of the possibility that the concentration of $Hg(^3P_1)$ is greater at the higher flow rates, this effect being more or less independent of the flowing gas. They claim that it is perhaps more likely that the foreign gases retard the production of ozone, but suggest that the $A^3\Sigma_u^+$ state may still be the one involved. The difficulty remains, however, in explaining the relative effects of He and Ar.

The purpose of this note is to show that excitation to one of the higher electronic states ($A^3\Sigma_u^+$, $^1\Sigma_u^-$, $^3\Delta_u$) as proposed by Gill and Laidler is still consistent with the relative effects of the added gases. This can be shown by means of some recently determined[5] potential curves for the various states of O_2. These curves are based as nearly as possible on experimental data and are shown in Fig. 1. The point of interest in the present connection is that the curves for both the $^1\Delta_g$ and the $^1\Sigma_g^+$ states cross the curve for the $^1\Sigma_u^-$ state. The first crossing occurs 4.96 e.v. above the lowest vibrational level of the $X^3\Sigma_g^-$ state, and the second at 4.88 e.v. Both of these crossing points are uncertain by about ± 0.1 e.v., but the analysis indicates that the curves definitely do cross. There is another uncertainty in the position of the $^1\Sigma_u^-$ curve, the one shown in Fig. 1 being based on a particular assignment for the lower vibrational levels. If another proposed assignment is used, the $^1\Sigma_u^-$ curve lies lower, and the crossing points also lie slightly lower. Further details are given in reference 5.

Let us suppose that the initial excitation of O_2 is to any of the $A^3\Sigma_u^+$, $^1\Sigma_u^-$, or $^3\Delta_u$ states. All of these transitions satisfy the correlation rules given by Shuler[7] for non-linear complexes. They also satisfy Gill and Laidler's argument for the least net change in electronic energy being the most probable. They would also be more probable, according to the Franck–Condon principle, than a transition to a vibrationally excited lower electronic state since much less change in internuclear distance is involved. Since the cross section for quenching of $Hg(^3P_1)$ by O_2 is so large,[8] the process must occur readily, and this would seem unlikely if a large change in the internuclear distance of the quenching molecule had to occur. If these transitions are assumed correct, then the question arises as to how to explain the effects of the added gases. Examination of the curves shown in Fig. 1 suggests a plausible explanation. As mentioned previously, both the $^1\Delta_g$ and $^1\Sigma_g^+$ curves cross the $^1\Sigma_u^-$ curve at an energy around 4.9 e.v. above the lowest vibrational level of the $X^3\Sigma_g^-$ state. A pressure-induced radiationless transition from the $^1\Sigma_u^-$ to the $^1\Delta_g$ state is permitted and probably happens on nearly every collision at these pressures.[9] A similar transition to the $^1\Sigma_g^+$ state is forbidden by the rule $+ \leftarrow|\rightarrow -$. If the O_2^* ends up in the $^1\Delta_g$ state, then the effects of the foreign gases can be explained, as is discussed below.

We wish first to discuss the initial transition to the $A^3\Sigma_u^+$, $^1\Sigma_u^-$, or $^3\Delta_u$ state. In order to explain the effect of foreign gases, the molecules must get from any of these states over into the $^1\Delta_g$ *via* the $^1\Sigma_u^-$ state, since it is the only one crossed. This can happen if the initial transition goes directly to the $^1\Sigma_u^-$. It can also happen if the initial transition is to the $^3\Delta_u$ and then the two pressure-induced steps occur: $^3\Delta_u \rightarrow {}^1\Sigma_u^- \rightarrow {}^1\Delta_g$. These pressure-induced transitions are permitted by Zener's rules,[9] but the transition $A^3\Sigma_u^+ \rightarrow {}^1\Sigma_u^-$ is not because of the rule $+ \leftarrow|\rightarrow -$. We would therefore conclude that of the three upper states, the $^3\Delta_u$ or the $^1\Sigma_u^-$ are the most likely ones involved in the reaction, with the $^1\Sigma_u^-$ being the most probable since it has a vibrational level lying exactly 4.88 e.v. above the lowest vibrational level of the $X^3\Sigma_g^-$ state.[5] Another reason why we would expect the $^3\Delta_u$ to be less important than the $^1\Sigma_u^-$ is that in the region where one might expect the transition $^3\Delta_u \rightarrow {}^1\Sigma_u^-$ to occur, the nuclei are moving quite rapidly, making the transition less likely.[10] Also, Wigner claims that on the basis of spin conservation the formation of a singlet state is three times more probable than the formation of a triplet state.[11] Finally, if the curve for the $^1\Sigma_u^-$ state really does lie beneath the curves of both the $^3\Delta_u$ and $A^3\Sigma_u^+$ states, the only state that can be involved in the reaction is the $^1\Sigma_u^-$. The $A^3\Sigma_u^+$ state is probably not involved since its curve does not seem to cross either the $^1\Sigma_g^+$ or the $^1\Delta_g$ curve in the appropriate region.

If the initially excited oxygen ends up in the $^1\Delta_g$ state with an energy of 4.88 e.v., the explanation of the relative effects of the foreign gases on the rate of ozone production is essentially that proposed by Volman.[2] Reaction (2) is endothermic by 4.06 e.v., requiring the O_2^* to have at least this energy to make the reaction go. Vibrational deactivation of this O_2^* from a high energy of 4.88

(7) K. E. Shuler, *J. Chem. Phys.*, **21**, 624 (1953).

(8) H. S. W. Massey and E. H. S. Burhop, "Electronic and Ionic Impact Phenomena," Oxford University Press, London, England, 1952, p. 422.

(9) C. Zener, *Proc. Roy. Soc.* (*London*), **140**, 660 (1933).

(10) K. J. Laidler, "The Chemical Kinetics of Excited States," Oxford University Press, London, England, 1955, p. 31.

(11) J. R. Bates, *J. Am. Chem. Soc.*, **54**, 569 (1932).

e.v. to less than 4.06 e.v. would quench the reaction. The difference in the quenching for the different foreign gases is explained by their different effectiveness in producing vibrational deactivation.[2] Unfortunately, little of quantitative significance can be said on this point for two reasons. First, vibrational deactivation appears to be quite sensitive to traces of certain impurities, especially water.[12] Second, experimental information on vibrational deactivation of O_2 comes from sound dispersion measurements, in which the lower vibrational levels of the $X^3\Sigma_g^-$ state are involved and not the upper ones of the $^1\Delta_g$ state.

Cross sections in Å.^{2} for quenching of $Hg(^3P_1)$ by the gases in question are[8]: He, ~ 0; Ar, ~ 0; N_2, 6.0; O_2, 62–70; CO_2, 11.1. N_2 and CO_2 could therefore also decrease the reaction rate by decreasing the concentration of $Hg(^3P_1)$ as well as by deactivating the vibrationally excited $O_2(^1\Delta_g)$.

In conclusion, we wish to suggest that the O_2* which occurs in the process is likely to be a molecule in the $^1\Sigma_u^-$ state which passes over into the $^1\Delta_g$ state by pressure-induced predissociation. This mechanism satisfies the main arguments given by Gill and Laidler and also satisfies Volman's points on the effect of foreign gases. Further experimental work would be most valuable.

Acknowledgment.—The authors wish to thank Professor B. de B. Darwent for helpful discussions and comments.

(12) J. C. McCoubrey and W. D. McGrath, *Quart. Revs.*, **11**, 87 (1957).

DENSITIES OF SOLID SALTS AT ELEVATED TEMPERATURES AND MOLAR VOLUME CHANGE ON FUSION

BY J. O'M. BOCKRIS, A. PILLA AND J. L. BARTON

John Harrison Laboratory of Chemistry, University of Pennsylvania, Philadelphia, Penna.

Received November 19, 1959

Data[1-3] for the molar volume change on fusion of simple inorganic salts are sparse and discrepant; those for the bulk densities of solid salts at elevated temperatures have not been reported. Knowledge of the change of volume on fusion is of use as a basis for the evaluation of structural models for the liquid pure electrolytes[4]; that of densities indicates changes in crystal structure in the solid which must be known before interpretation of the structural implications of the volume change on fusion can be evaluated.[5]

Here, a high temperature gas densitometer is described, which has been used to measure the expansion of a solid salt from room temperature to just below the melting point. As the solid densities at room temperature and the liquid densities over a range of temperatures near to the melting point are generally available, the molar volume change on fusion ΔV_f may be obtained.

(1) G. J. Landon and A. R. Ubbelohde, *Trans. Faraday Soc.*, **52**, 647 (1956).

(2) H. Schinke and F. Sauerwald, *Z. anorg. allgem. Chem.*, **287**, 313 (1956).

(3) M. A. Bredig and J. W. Johnson, ORNL-1940 p. 19.

(4) J. O'M. Bockris and N. E. Richards, *Proc. Roy. Soc.* (*London*), **241**, 44 (1957).

(5) E. A. Moelwyn-Hughes, "Physical Chemistry," Pergamon Press, London, 1957, p. 728–735.

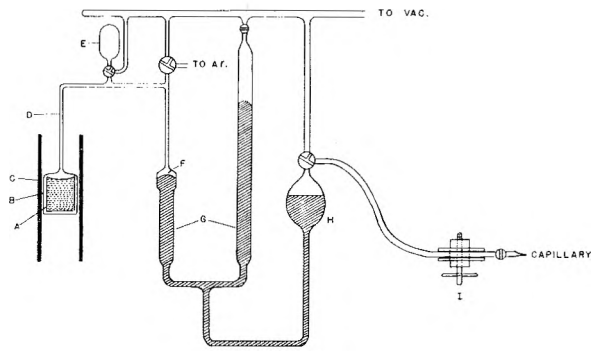

Fig. 1.

Experimental

The measurements consist of the determination as a function of temperature of the free volume inside a vessel containing a known weight of salt in a platinum crucible. A constant volume manometer (temperature T_r and containing gas of volume v_r) is connected by a capillary of negligible volume to the salt container situated inside a furnace at temperature T_f. A calibration bulb of known volume v_b may be connected to the system, or to a vacuum line by a two-way stopcock. The free volume in the salt container, v_f, is obtained from the change in pressure in the system when it is connected to the evacuated calibration bulb. If p_1 and p_2, respectively, are the pressures in the system before and after the expansion, it can be shown that

$$v_f = \frac{T_f}{T_r}\left\{\frac{p_2}{p_1 - p_2} v_b - v_r\right\} \qquad (1)$$

v_b is obtained by weighing; and v_r is determined by measuring the change of pressure in the system with the capillary sealed off just above the level of the furnace.

The change in v_f with temperature is due to the combined expansions of the Vycor vessel, platinum crucible and the salt. Thus, at any temperature t the density of the salt, ρ_t, may be calculated from the expression

$$\frac{1}{\rho_t} = \frac{1}{\rho_{tr}} + \frac{\Delta v_v - \Delta v_c - \Delta v_f}{W} \qquad (2)$$

where W is the weight of the salt, ρ_{tr} is its density at room temperature; Δv_v, Δv_c and Δv_f are the changes in volume between room temperature, t_r, and temperature t of the Vycor vessel, the platinum crucible and v_f, respectively.

Δv_v is calculated from the total internal volume of the Vycor vessel using the expansion coefficient 8.0×10^{-7}. Δv_c is calculated from the weight of the crucible using the density values of Shartsis and Spinner.[6] Usually, $(\Delta v_v - \Delta v_c)$ is about 4% of Δv_f.

The crucible A (Fig. 1) is 36 mm. o.d., 50 mm. high, 1 mm. thick. The Vycor vessel, B, encases the crucible to within *c.*2 mm. so that expansion of the salt reduces the free volume by a significant fraction. The volume v_f is about 25 cc. and the salt volume about 40 cc. The capillary D between the vessel and the constant volume manometer G is 1 mm. i.d., v_r is about 8.5 cc. The calibration bulb E of 15 cc. reduces the pressure by a factor of about one half.

The furnace is water jacketed and its winding (Kanthal A-1) is tapped at six points to allow a temperature uniformity of $\pm 0.1°$ to be obtained in the region of the container (surrounded by Al_2O_3). The temperature is measured to $\pm 0.2°$.

The molten salt is introduced through an orifice in B into A, after the latter has been sealed into B.

The apparatus is evacuated with the sample at room temperature, and then filled with Ar purified by passage through Na–K. Determinations of v_f are made at a series of temperatures, the highest being about 10° below the melting

(6) L. Shartsis and S. Spinner, *J. Research Natl. Bur. Standards*, **46**, 176 (1951).

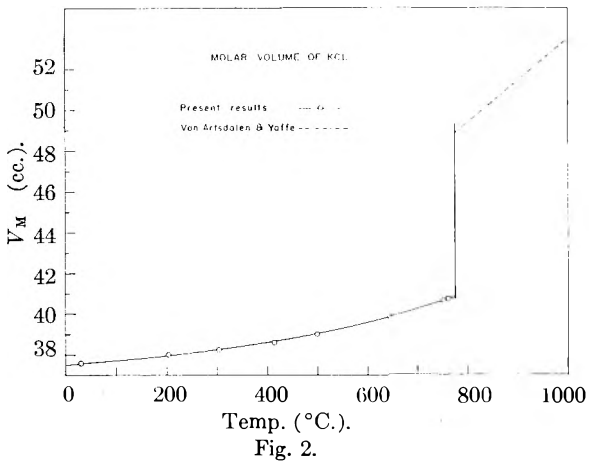

Fig. 2.

point. At each temperature, three measurements are made using different initial pressures in the range 300–700 mm.

Fine adjustment in pressure measurement is made by applying pressure to the tubing with the adjustable clamp I until the needle F just touches the mercury surface. Pressure measurements are reproducible to ±0.05 mm. and v_f measurements at a given temperature to ±0.1%. In general it is found about 1 min. is required for equilibration after expansion and about 45 min. for equilibration after change in temperature.

To test for the presence of cavities in the sample as normally prepared, it was melted *in situ* and allowed to cool slowly from the bottom upward. Values of v_f obtained before and after the re-freezing agreed to within the normal experimental error (±0.3%).

The form of the apparatus is similar to that employed by Nachtrieb and Clement.[7] The procedure, however, involves no measurements with the salt in the molten state so that difficulties which arise from the solubility of Ar in the fused salt are avoided. Moreover, it is unnecessary to apply vacuum to the salt at elevated temperatures, thus avoiding clogging of the capillary.

Results

From room temperature densities[8] and the measured expansivities these equations were found for density of the solid salts

$$\rho_{KCl} = 1.985 - 5.459 \times 10^{-5} t - 1.836 \times 10^{-7} t^2 \quad (\pm 0.001 \text{ g. cc.}^{-1})$$

$$\rho_{NaCl} = 2.168 - 1.267 \times 10^{-4} t - 1.754 \times 10^{-7} t^2 \quad (\pm 0.002 \text{ g. cc.}^{-1})$$

where t is the temperature in °C. Hence, the molar volumes of the solid at the melting point, V_s, may be calculated and compared with those obtained from the corresponding density data for the liquids[9] to give the molar expansion on fusion ΔV_f. Values of ΔV_f expressed as a fraction of the solid molar volume are given, together with the values obtained by other investigators, in Table I.

Figure 2 shows the variation of molar volume of KCl from room temperature to above the melting point.

Attempts to measure ΔV_f from the change in pressure over the melting point were not successful. The apparent changes were 30–50% lower than those found by other methods. The discrepancy can be accounted for by a solubility of Ar in the liquid salts concerned of about 10^{-8} mole cc.$^{-1}$. Grimes, *et al.*,[12,13] have shown that the solubility of noble gases in various molten salt systems is of this order. The method might thus be adapted to the measurement of gas solubilities in molten salts.

TABLE I

$\Delta V_f/V_s$ % NaCl	$\Delta V_f/V_s$ % KCl	Method
25.58 ± 0.07	20.20 ± 0.05	Present measurements
22.8 ± .7	16.8 ± .5	Linear expansion[10]
30.0	23.0	Not specified[11]
25.0 ± .5	17.3 ± .5	Crystallization pycnometry[2]
23.2 ± 2.0	17.5 ± 2.0	Extrapolated density data[3]
	21.0 ± 0.5	Crystallization pycnometry[1]

Acknowledgment.—Thanks are due to the Atomic Energy Commission, Contract No. At30-1-1769, for financial support of this work.

(7) N. H. Nachtrieb and N. Clement, THIS JOURNAL, **62**, 747 (1958).

(8) "International Critical Tables," Vol. 3, McGraw-Hill Book Co., New York, N. Y., 1928, p. 43.

(9) I. S. Yaffe and E. R. Van Artsdalen, THIS JOURNAL, **60**, 1125 (1956).

(10) A. Eucken and E. Dannohl, *Z. Elektrochem.*, **40**, 814 (1934).

(11) A. Eucken, *Z. angew. Chem.*, **55**, 163 (1942).

(12) W. R. Grimes, N. V. Smith and G. M. Watson, THIS JOURNAL, **62**, 862 (1958).

(13) M. Blander, W. R. Grimes, N. V. Smith and G. M. Watson, *ibid.*, **63**, 1164 (1959).

THE EFFECT OF ALKANOLS ON MALONIC ACID

BY LOUIS WATTS CLARK

Contribution from the Department of Chemistry, Saint Mary of the Plains College, Dodge City, Kansas

Received November 30, 1959

When malonic acid is placed in contact with a nucleophilic solvent at a suitable temperature it decomposes into acetic acid and carbon dioxide. To date this reaction has been studied kinetically in 41 polar liquids comprising representatives of 13 homologous series.[1] These studies have amply confirmed the mechanism of the reaction proposed by Fraenkel and co-workers,[2] namely, the formation, prior to cleavage, of a transition complex involving coördination between the electrophilic carbonyl carbon atom of the malonic acid and the unshared pair of electrons on the nucleophilic atom of the solvent molecule. In addition these studies have contributed to a better understanding of the electron properties of the solvent molecules.

Although the reaction has been studied previously in several hydroxy compounds, namely, four monocarboxylic acids,[3] one phenol,[4] one alicyclic alcohol[1], and one aromatic alcohol[1], it has not been studied in any of the aliphatic alcohols. Because of the unique position of the alkanols in the family of polar liquids it was deemed advisable to investigate the reaction in several representatives of this group in order to fill this hiatus. The present paper describes the results of kinetic studies carried out in this Laboratory on the decarboxylation of malonic acid in six aliphatic alco-

(1) L. W. Clark, THIS JOURNAL, **64**, in press (1960), and previous papers in this series.

(2) G. Fraenkel, R. L. Belford and P. E. Yankwich, *J. Am. Chem. Soc.*, **76**, 15 (1954).

(3) L. W. Clark, THIS JOURNAL, **64**, 41 (1960).

(4) L. W. Clark, *ibid.*, **62**, 1468 (1958).

hols, namely, *n*-butyl alcohol, *n*-amyl alcohol, *n*-hexyl alcohol, isoamyl alcohol, diisobutylcarbinol and 2-ethylhexanol-1. This brings the total number of polar liquids in which this reaction has been studied to 47 and the total number of homologous groups to 14.

Experimental

Reagents.—(1) Reagent Malonic Acid, 100.0% Assay, was used in these experiments. (2) Solvents: All the alkanols used in this research were reagent grade or highest purity chemicals. Each sample of each solvent was distilled at atmospheric pressure directly into the dried reaction flask immediately before the beginning of each decarboxylation experiment.

Apparatus and Technique.—The kinetic experiments were conducted in a constant-temperature oil bath (±0.05°) by the technique previously described.[5] Temperatures were determined by means of a thermometer calibrated by the U. S. Bureau of Standards. In each experiment a 0.1857-g. sample of malonic acid (the amount required to produce 40.0 ml. of CO_2 at STP on complete reaction) was introduced in the usual manner into the reaction flask containing a weighed sample of solvent saturated with dry CO_2 gas.

Results

Kinetic experiments were carried out in each solvent over approximately a 20° temperature interval. Duplicate experiments were conducted at each temperature. Generally the reaction failed to yield more than 95% of the theoretical volume of CO_2, due, undoubtedly, to a very slow esterification reaction proceeding simultaneously with the more rapid decarboxylation reaction. Straight lines invariably were obtained over the first 75% of the reaction when log $(a - x)$ was plotted against t (where a is the maximum theoretical volume of CO_2 evolved, and x the volume evolved in time t). Variation in the ratio of solvent to solute had no appreciable effect upon the rate of reaction. The quantity of solvent generally used was approximately 50 ml.

In Table I are listed the average values of the apparent first-order rate constants for the reaction in the various solvents at each temperature studied, as calculated from the slopes of the experimental logarithmic plots. The parameters of the Eyring equation are shown in Table II. Data for the decarboxylation of malonic acid in *n*-butyric acid and in water, reported in the literature, are included for comparison.

Table I

Apparent First-order Rate Constants for the Decarboxylation of Malonic Acid in Several Aliphatic Alcohols

Solvent	Temp., °C. cor.	$k \times 10^4$, sec.$^{-1}$
n-Butyl alcohol	102.54	1.38 ± 0.01[a]
	112.54	3.62 ± .01
	122.50	9.08 ± .03
Iso-amyl alcohol	105.78	1.93 ± .03
	115.50	4.86 ± .04
	125.40	11.93 ± .04
n-Amyl alcohol	110.19	3.66 ± .01
	119.06	4.86 ± .03
	131.23	16.66 ± .04
n-Hexyl alcohol	103.81	1.50 ± .01
	113.40	3.63 ± .02
	122.60	8.17 ± .02
2-Ethylhexanol-1	110.89	3.42 ± .02
	118.11	6.33 ± .02
	126.04	12.22 ± .04
Diisobutylcarbinol	106.77	2.08 ± .03
	115.50	4.43 ± .04
	120.21	6.59 ± .02
	125.40	10.08 ± .03

[a] Average deviation.

Table II

Kinetic Data for the Decarboxylation of Malonic Acid in Several Liquids

Solvent	ΔH^*, kcal.	ΔS^*, e.u.	$\Delta F^*_{100°}$ kcal.	$k_{10} \times 10^4$ sec.$^{-1}$
(1) *n*-Butyl alcohol	27.2	− 4.4	28.8	1.07
(2) Isoamyl alcohol	27.1	− 4.5	28.8	1.07
(3) *n*-Amyl alcohol	26.0	− 7.6	28.84	1.02
(4) *n*-Hexyl alcohol	26.0	− 7.6	28.84	1.02
(5) 2-Ethylhexanol-1	24.8	−10.4	28.7	1.23
(6) Diisobutylcarbinol	24.8	−10.7	28.8	1.07
(7) *n*-Butyric acid[3]	32.3	+ 2.5	31.4	0.03
(8) Water[6]	30.1	− 0.4	30.2	0.16
(9) Aniline[7]	26.9	− 4.5	28.6	1.41

Discussion of Results

If an alkyl group is substituted for one of the hydrogen atoms on the water molecule it will increase the electron density on the oxygen atom due to its positive inductive effect. Since an increase in the attraction between two reagents lowers the ΔH^* of the reaction,[8] it would be predicted, therefore, that the ΔH^* of the decomposition of malonic acid would be less in the alcohols than in water. This is seen to be the case for all the alcohols listed in Table II.

If an acyl group is substituted for one of the hydrogen atoms in the water molecule it will decrease the electron density on the oxygen atom. It would therefore be expected that the ΔH^* of the reaction would be less in the alkanoic acids than in water. That this is the case is seen by comparing lines 7 and 8 of Table II. As regards the effective negative charge on the oxygen atom, therefore, water occupies an intermediate position between the alcohols and the acids.

The ΔH^* for the reaction in *n*-butyl alcohol is about 3 kcal. less than in water. For the reaction in *n*-butyric acid ΔH^* is 2.2 kcal. higher (lines 1, 7 and 8 of Table II). Another way of looking at the data is to observe that the ΔH^* of the reaction is about 5 kcal. greater in *n*-butyric acid than in *n*-butyl alcohol, indicative of the strong electron-withdrawing effect of the double bond O atom substituted for the two hydrogens on the No. 1 carbon atom of the alcohol.

Although water is more associated than the alcohols, the alcohol monomers are larger than that of water. It is not surprising to find, therefore, that the ΔS^* of the reaction is less in the alcohols than in the water. As the number of carbon atoms of the alcohol increases, and as branching becomes

(5) L. W. Clark, *ibid.*, **60**, 1150 (1956).
(6) G. A. Hall, Jr., *J. Am. Chem. Soc.*, **71**, 2691 (1949).
(7) L. W. Clark, This Journal, **62**, 79 (1958).
(8) K. J. Laidler, "Chemical Kinetics," McGraw-Hill Book Co., Inc., New York, N. Y., 1950, p. 138.

more extensive, a progressive decrease in the ΔS^* of the reaction takes place (lines 1 to 6 of Table II). The ΔH^* of the reaction decreases also as the inductive effect of the substituents increases. There is very little change in ΔH^* on going from butanol-1 to 3-methylbutanol-1 (lines 1 and 2 of Table II). However, on going from 1-butanol to 1-pentanol ΔH decreases by about 1 kcal. (lines 1 and 3 of Table II). Again no further change in ΔH^* takes place on going to 1-hexanol (line 4). When an ethyl group is substituted on the No. 2 carbon atom of 1-hexanol, however, the ΔH of the reaction decreases again by about 1 kcal. (lines 4 and 5 of Table II). When an isobutyl group is substituted on the No. 1 carbon atom of isoamyl alcohol ΔH decreases by about 2 kcal. (lines 2 and 6 of Table II).

Interestingly enough, at 100°, the apparent first-order rate constant for the reaction differs but little in the various alcohols studied, despite the range in size from 4 to 9 carbon atoms. In each case, on passing from the more simple to the more complex molecules, the disadvantage imposed by steric hindrance is almost entirely compensated for by the advantage accruing from the lowering of ΔH, with the result that the ΔF^* of the reaction remains practically unchanged in all six solvents.

On going from *n*-butyric acid to 1-butanol ΔS^* decreases by about 7 e.u. (lines 1 and 7 of Table II). This result is in harmony with the fact that the "supermolecule" of the associated alcohol is made up of three or four monomers, whereas that of the acid consists of the dimer.[9] The increase in ΔS^* of about 3 e.u. on going from water to the acid (lines 7 and 8) also is in line with the fact that although the water molecule is considerably smaller than that of the acid, the associated complex of water contains many more monomers than does that of the acid.

For the reaction in *n*-butyl alcohol, isoamyl alcohol and aniline the Eyring parameters are very nearly equal (see lines 1, 2 and 9 of Table II). This circumstance suggests that the electron and steric properties of these three liquids are closely parallel.

In compounds of the ammonia and water systems containing the same types of substituents the nitrogen is more basic in the Lewis sense than is the oxygen (the oxygen atom is smaller than nitrogen and its nucleus contains one more proton than nitrogen). This situation may be reversed, however, if compounds containing different types of substituents are considered. In aniline the strong I-effect of the resonating aromatic nucleus greatly reduces the electron density on the nitrogen atom, whereas in *n*-butyl and isoamyl alcohols the $^+$I effect of the alkyl groups increases the electron density on the oxygen atom. It is not too surprising, therefore, to discover that the ΔH^* of the reaction is about the same in these three liquids—in other words, that they are about equally basic in the Lewis sense. At 100°, malonic acid decomposes in aniline only 1.3 times as fast as in the two alcohols. This suggests that for other reactions which proceed in alcohols and amines by the same mechanism as the malonic acid decomposition, *e.g.*, acylation,[10] the rate of reaction at a given temperature should be nearly the same in aniline, *n*-butyl alcohol and isoamyl alcohol, and also the Eyring parameters should be nearly equal for the three liquids.

When two alkyl groups are joined to the carbinol group, or are in close proximity to it, their combined inductive effects may cause the electron density on the oxygen atom to exceed that on the nitrogen atom in aniline, as revealed by the fact that the ΔH of the reaction is lower in such liquids than it is in aniline (lines 5, 6 and 9 of Table II).

Acknowledgments.—The support of this research by the National Science Foundation, Washington, D. C., is gratefully acknowledged.

(9) W. Hückel, "Theoretical Principles of Organic Chemistry," Vol. II, Elsevier Publishing Co., New York, N. Y., 1958, p. 325 *et seq.*

(10) R. Q. Brewster, "Organic Chemistry," 2nd edition, Prentice-Hall, Inc., New York, N.Y., 1953, pp. 204 and 558.

BEHAVIORS OF C–D STRETCHING BANDS IN POLYETHYLENE-d_4 TEREPHTHALATE

BY AKIHISA MIYAKE

Central Research Laboratories, Toyo Rayon Co., Otsu, Shiga, Japan

Received November 16, 1959

The dichroism of the C–H stretching bands in drawn samples of polyethylene terephthalate does not agree with expectation. In spite of the parallel orientation of the polymer chain with respect to the direction of drawing,[1-4] two bands at 2970 and 2910 cm.$^{-1}$ assigned to the aliphatic C–H stretching vibrations show parallel dichroism.[5,6] This parallel dichroism which is opposite to the predicted perpendicular dichroism, has been explained as a result of the overlapping of vibrations of *trans* and *gauche* ethylenedioxy (OCH_2CH_2O) groups.[7,8] The *gauche* ethylenedioxy groups in the amorphous region of the polymer may achieve completely different orientations with respect to the direction of drawing. The dichroism of the C–H stretching bands may be determined by these *gauche* ethylenedioxy groups.

In order to settle this point more definitely, C–D stretching bands of polyethylene-d_4 terephthalate have been re-investigated using a LiF prism. Previous investigation of this polymer has only been done by the low dispersion NaCl prism.[8]

In quenched samples of polyethylene-d_4 terephthalate, there appear three bands attributable to C–D stretching vibrations at 2260, 2200 and 2130 cm.$^{-1}$. On crystallizing the samples by heating, two new bands appear at 2275 and 2175 cm.$^{-1}$ (Fig. 1). On the basis of a previously established relation between the crystalline bands and the rotational isomerism for this polymer,[7,9] these two

(1) R. G. J. Miller and H. A. Willis, *Trans. Faraday Soc.*, **49**, 433 (1953).

(2) C. Y. Liang and S. Krimm, *J. Chem. Phys.*, **27**, 327 (1957).

(3) R. Daubney, C. Bunn and C. Brown, *Proc. Roy. Soc. (London)*, **A226**, 531 (1954).

(4) W. J. Dulmage and A. L. Geddes, *J. Polymer Sci.*, **31**, 499 (1958).

(5) G. J. Weston, *Chemistry & Industry*, 604 (1954).

(6) M. C. Tobin, THIS JOURNAL, **57**, 1392 (1945).

(7) D. Grime and I. M. Ward, *Trans. Faraday Soc.*, **54**, 959 (1958).

(8) A. Miyake, *J. Polymer Sci.*, **38**, 497 (1959).

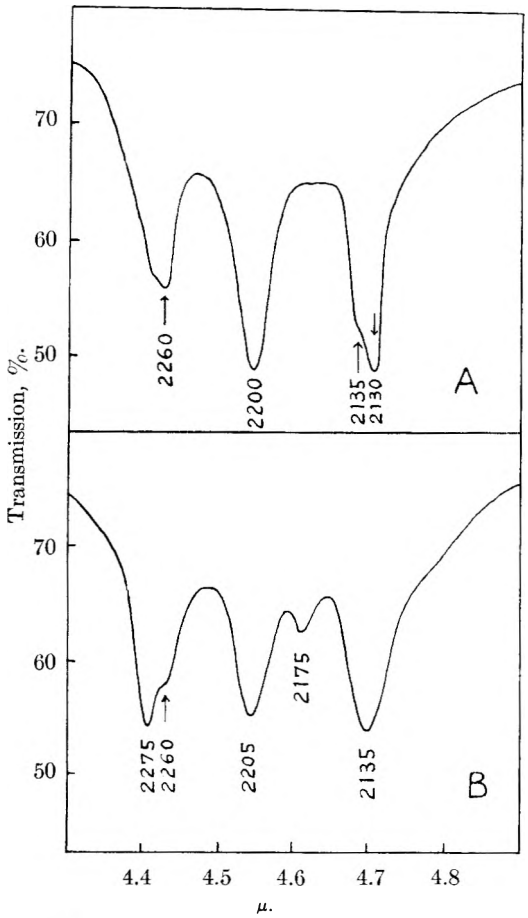

Fig. 1.—C–D stretching bands of polyethylene-d_4 terephthalate: (A) quenched; (B) annealed.

bands can be attributed to the C–D stretching vibrations of ethylenedioxy groups which exist in the *trans* form, while three bands observed in quenched samples can be attributed to ethylenedioxy groups in the *gauche* form. The lowest C–D bands of the *gauche* form seem to be composed of two vibrations. The reason for the shift of its peak on crystallization is not clear.

(9) A. Miyake, *J. Polymer Sci.*, **38**, 479 (1959).

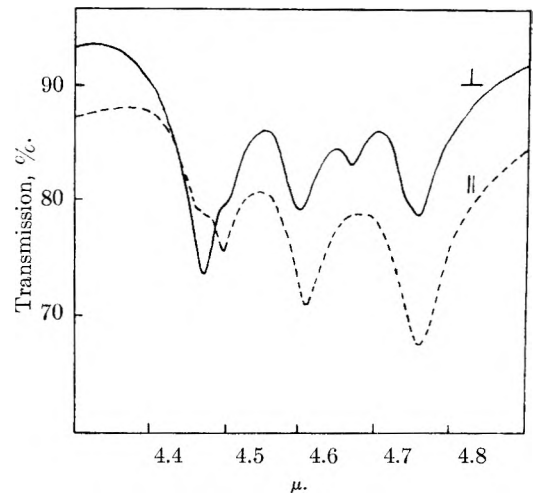

Fig. 2.—Dichroisms of the C–D stretching bands.

Now, in an oriented and annealed sample, the two crystalline bands at 2275 and 2175 cm.$^{-1}$ apparently show perpendicular dichroism which is in agreement with the parallel orientation of the chain. On the other hand, three bands attributed to the *gauche* form show parallel dichroism (Fig. 2). Thus these results give confirmation for the interpretation of the C–H stretching bands of polyethylene terephthalate referred to above.

Since the symmetric stretching, antisymmetric stretching and wagging modes of a CH_2 group have mutually perpendicular transition moments, Liang and Krimm[10] have cast doubt on assigning the CH_2 wagging vibration to a parallel band at 1345 cm.$^{-1}$ in polyethylene terephthalate. However, from the results obtained in polyethylene-d_4 terephthalate, it seems almost certain that perpendicular C–H stretching bands of the *trans* form lie buried under the *gauche* bands, and hence the parallel band at 1345 cm.$^{-1}$ can now be reasonably assigned to a CH_2 wagging mode of *trans* ethylenedioxy groups.

Experimental

The samples are the same as those in a previous research.[8] The infrared absorption measurement were carried out by a Perkin-Elmer Model 21 spectrometer with a LiF prism.

(10) C. Y. Liang and S. Krimm, *J. Chem. Phys.*, **27**, 1437 (1957).

COMMUNICATION TO THE EDITOR

THE MERCURY-SENSITIZED RADIOLYSIS AND PHOTOLYSIS OF METHANE[1]

Sir:

The radiation chemistry of pure methane[2] and the argon and krypton sensitized radiolysis of methane[3] have been described recently. These investigations were interpreted in terms of an ion-molecule mechanism based originally upon mass spectrometer studies.[4] We have undertaken the study of the radiation chemistry of methane in the presence of an almost six-fold excess of mercury vapor so that charge transfer reactions of the type

$$CH_4^+ + Hg \longrightarrow CH_4 + Hg^+ \qquad (1)$$

should effectively scavenge hydrocarbon molecule ions which survive neutralization. Although quantitative data are not available for equation

(1) This work was performed under the auspices of the U. S. Atomic Energy Commission.

(2) F. W. Lampe, *J. Am. Chem. Soc.*, **79**, 1055 (1957).

(3) G. G. Meisels, W. H. Hamill and R. R. Williams, Jr., THIS JOURNAL, **61**, 1456 (1957).

(4) (a) D. O. Schissler and D. P. Stevenson, *J. Chem. Phys.*, **24**, 926 (1956); (b) G. G. Meisels, W. H. Hamill and R. R. Williams, Jr., *ibid.*, **25**, 790 (1956).

(1), cross-sections for asymmetric charge transfer are generally of the same order of magnitude as those quoted for ion-molecule reactions.[5] Furthermore, the energy dissipated in the mercury vapor (approximately seventy times the energy dissipated in the methane) can be transferred to the methane by chemical reactions such as

$$CH_4 + Hg\ (^3P_1) \longrightarrow CH_3 + H + Hg \qquad (2)$$

for which cross-section data are readily available.[6] Excited ions and multiply-charged ions should be effectively degraded to excited atomic states of mercury and singly-charged mercury ions by collision with atomic mercury.

We have investigated the radiolysis of methane in the presence and absence of mercury at 260°. The electron source was a 4.5 Mev. electron beam from a microwave linear accelerator. Square wave, 50 milliampere pulses, 5 microseconds in duration, bombarded the Pyrex reaction vessel through a window in an aluminum block oven. For comparison we also investigated the mercury-sensitized photolysis of methane at 260°. In each experiment the methane pressure was 10 mm. measured at 25°. In the radiolysis experiment in the presence of mercury, excess liquid mercury was added to the reaction vessel; in the photolysis experiment sufficient mercury was added to effect a 20 mm. mercury vapor pressure at 260°.

A typical set of analyses for the major products is shown in Table I. These represent the percentage yield of each gas in the reaction vessel after bombardment. Unreacted methane constitutes the remainder of the sample. Analyses of the products by gas chromatography and by mass spectrometry confirm their identification. The gross features of the product distribution are identical. The products from photolysis exhibit a somewhat larger proportion of higher hydrocarbons, especially neopentane, than is formed in either of the radiolysis experiments at 260°. The rapid build-up of higher hydrocarbons in photolysis probably is due to the high local concentrations of free radicals near the surface of the quartz reaction vessel.

The efficiency with which mercury transfers its excitation to methane is seen by comparing the first two columns in Table I. Although the CH_4–Hg radiolysis was exposed to about 11% of the dose to which the CH_4 radiolysis was exposed, the actual decomposition is greater in the former. This indicates that about 13% of the total energy absorbed by the mercury vapor is effective, a figure which seems too high to be attributed to appreciable energy transfer from excited mercury ions and multiply-charged mercury ions. Therefore, it appears probable that equation (2) and similar chemical quenching reactions account for most of the energy transfer to methane and hydrocarbon products. Thus, this mechanism of energy transfer is expected to accelerate free radical reactions in the CH_4–Hg radiolysis experiment.

TABLE I

METHANE RADIOLYSIS AND PHOTOLYSIS—TYPICAL ANALYSES[a]

Dose[b] / Product	7.2×10^4 e⁻ at 260°, %	8.1×10^3 Hg + e⁻ at 260°, %	[c] Hg + $h\nu$ at 260°, %	10.8×10^4 e⁻ at 25°, %
Hydrogen	3.94	4.37	4.83	4.49
Ethane	1.26	2.10	1.48	1.62
Propane	.41	.47	.27	.31
n-Butane	.05	.05	.02	.05
Isobutane	.10	.14	.13	.05
Neopentane	.12	.12	.58	.03
Isopentane	.04	.03	.02	.03
Neohexane	.03	.04	.09	.05
Heptane	.01	.01	.02	.01
Ethylene	.15	.20	.08	.04
Isobutene	.03	.02	.02	.03
Isopentene	.01	.01	.01	...

[a] Product yields expressed as per cent. of total gas. [b] Total number of 50 milliampere, square-wave electron pulses, 5 microseconds in duration. [c] Irradiated for four minutes using three four-watt low pressure mercury lamps.

The photolysis products must of necessity be described by processes not involving ions. The product distributions in the radiolysis and photolysis are quite similar. Mercury vapor, expected to behave as an ion-scavenger and free radical promoter, did not affect the nature or essential distribution of products. Therefore we conclude that ion–molecule reactions are not necessary to account for the radiolysis of methane at 260°. Thus we cannot agree with the statement that free radical reactions cannot account for the formation of propane, butane, and pentane in the radiolysis of methane.[3] Recently, Yang and Manno[7] have reported that 85% of the ethane and propane and 100% of the higher products arise from a free radical mechanism at 25°. Assuming a free radical process activation energy of 8 kcal./mole and zero activation energy for non-free radical processes, the latter need account for less than 0.1% of the higher radiolysis products at 260°. Our experimental results are in accord with this conclusion. We are undertaking a more complete study of these systems.

LAWRENCE RADIATION LABORATORY
UNIVERSITY OF CALIFORNIA
BERKELEY, CALIFORNIA
GILBERT J. MAINS
AMOS S. NEWTON

RECEIVED FEBRUARY 25, 1960

(5) S. B. Karmopatro and T. P. Das, *J. Chem. Phys.*, **29**, 240 (1958).

(6) K. J. Laidler, "Chemical Kinetics of Excited States," Oxford University Press, New York, N. Y., 1955.

(7) K. Yang and P. J. Manno, *J. Am. Chem. Soc.*, **81**, 3507 (1959).

You MAY reproduce material from CA

under certain conditions . . .

Many subscribers to CHEMICAL ABSTRACTS find it of distinct value to reproduce material from CA for limited internal or external use.

Unfortunately this is done all too often without permission of the American Chemical Society, the copyright holder.

The ACS *does* allow subscribers to CHEMICAL ABSTRACTS to reprint from this publication. However, there is a fee for this service if more than an occasional abstract is reproduced.

This fee is essential to the support of CHEMICAL ABSTRACTS. In 1960 it will cost approximately $2.5 million to produce this publication. Therefore, income from every available source must be sought. If unlicensed reproduction for internal distribution is permitted to flourish, the need for additional subscriptions to CHEMICAL ABSTRACTS by those doing the reproducing is lessened. If the reproduction is done for external distribution—a company's technical bulletin for distribution to customers, for example—the recipient of the bulletin may not enter a subscription to CHEMICAL ABSTRACTS which he otherwise would need.

Lost subscriptions increase the price each of you must pay for yours.

If you wish to reproduce material the following fees must be paid:

CURRENT ABSTRACTS

Right to use abstracts, $750

Reprinting charge, $3.00 per 1000 abstract-impressions, obtained by multiplying number of abstracts by print order.

NONCURRENT ABSTRACTS

Right to use abstracts, $300

Reprinting charge, $2.00 per 1000 abstract-impressions, obtained by multiplying number of abstracts by print order.

The right-to-use abstracts fee is annually recurring and must be paid before reproduction is undertaken. Current material is material reproduced from the current volume at any time during the volume year. If both current and noncurrent abstracts are to be used, the $750 right-to-use current abstracts fee must be paid.

If you wish to use this service, direct your inquiry to: **Business Manager, American Chemical Society, 1155 Sixteenth St., N.W., Washington 6, D. C.**